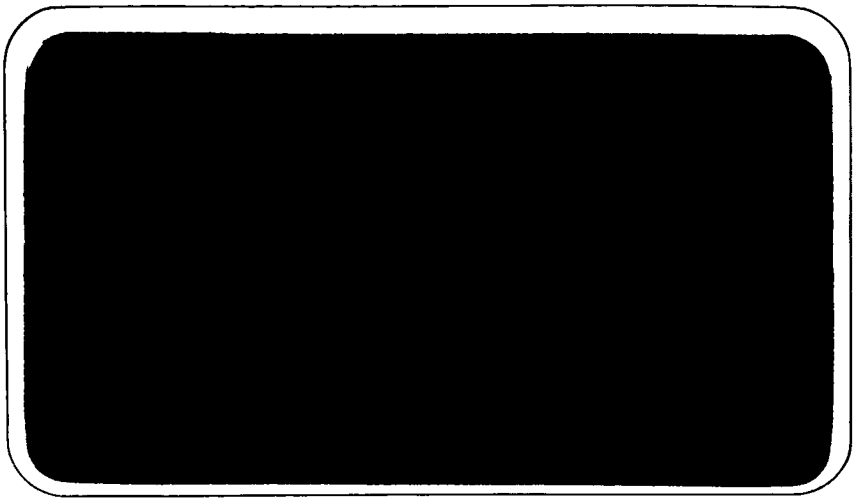

GPO PRICE $ _____

OTS PRICE(S) $ _____

Hard copy (HC) $6.00

Microfiche (MF) $1.50

Westinghouse

ELECTRIC CORPORATION

1750E

VOLUME V
ANALYTICAL SUPPLEMENT
(Appendixes to Volume III)

Compilation Report
for
ADVANCED SPACEBORNE DETECTION, TRACKING, AND NAVIGATION SYSTEMS STUDY AND ANALYSIS

NAS 8 - 11205

July 1964

Presented to

GEORGE C. MARSHALL SPACE FLIGHT CENTER
Huntsville, Alabama

By

WESTINGHOUSE DEFENSE AND SPACE CENTER
Aerospace Division
Baltimore, Maryland

TABLE OF CONTENTS

TABLE OF CONTENTS (Continued)

APPENDIX B (Continued)

APPENDIX C
LUNAR PARKING AND DESCENT ORBITS

APPENDIX D
LUNAR LANDING ANALYSES

TABLE OF CONTENTS (Continued)

APPENDIX D (Continued)

APPENDIX E
LUNAR ASCENT

TABLE OF CONTENTS (Continued)

LIST OF ILLUSTRATIONS

LIST OF ILLUSTRATIONS (Continued)

APPENDIX D (Continued)

LIST OF ILLUSTRATIONS (Continued)

LIST OF TABLES

APPENDIX A

SYNOPSIS OF MATHEMATICAL TECHNIQUES

1. INTRODUCTION

The application of recursive minimum variance data smoothing to orbital navigation and the use of adjoint techniques in powered trajectory control analysis have received considerable attention in recent literature. A great deal of insight into these topics has been provided in a number of excellent articles, but due to space limitations which are unavoidable in published literature, interesting and explanatory details are omitted from the text. As a result many readers who are unfamiliar with the subject must accumulate information slowly from several sources using different nomenclature and notation.[1]

The purpose of this presentation is to consolidate the information pertinent to this seemingly complex area of analysis and to organize the concepts for application to space navigation and guidance as defined below. It will be emphasized at the outset that no originality is claimed in any of the derivations or interpretations which have been included; the entire presentation consists of restatements of other authors' works. In addition, the accompanying bibliography does not constitute a complete survey of applicable literature; it is felt, however, that any reader who follows the articles referenced herein will naturally be led to further developments in his particular area of interest.

For the purposes of this study the functions under consideration for analysis are defined as follows:

> Navigation - The estimation of position and velocity from observations which contain unknown random errors

---

[1] Although the matrix relations needed for this development are discussed in some detail herein, a basic acceptance of vector and matrix algebra is necessary as well as a fundamental understanding of orbital motion and probability.

Guidance - The determination, based upon navigation results, of the maneuvers necessary to bring an orbiting vehicle to its desired destination

The theory of guidance and navigation is presented here as a detailed study of the interrelations between various types of error which tend to degrade the performance:

Deviation of space vehicle from a known reference trajectory

Uncertainty in the position and velocity of the vehicle

Navigation measurement errors

Maneuvering errors

These latter two items, which can be considered as the ultimate sources of error, are reasonably characterized by Gaussian statistics. To enhance the evaluation of these errors, the development leads to a linear mathematical model of the actual dynamic system. Although admittedly this step is taken in order to capitalize upon existing analytical techniques, it should be kept in mind that successful applications of the linearization theory have been made.

The presentation is kept as brief as the depth of the subject matter will allow. For the sake of brevity, certain restrictions are placed upon the scope:

The effects of bias errors upon minimum variance orbital navigation have not been taken into account, and only "scalar" navigation measurements are considered; i.e., it is assumed that only one observable can be measured at a particular instant of time. (These restrictions do not apply to the powered trajectory analysis).

Supporting mathematical theorems of secondary importance are simply stated and referenced without rigorous proof.

No detailed discussion of the origin of the differential equations of motion was felt necessary; it is sufficient to note that the acceleration vector of a vehicle can be described by simple Newtonian mechanics. Similarly, the equations relating navigation measurements to vehicle geometry are treated in general form.

Although these restrictions render this presentation somewhat less self-sufficient, they enhance the overall coherence for expository purposes. The analytical extensions suggested by these restrictions can be found in the applicable literature.

2. CHARACTERIZATION OF TRAJECTORIES

A central feature in the implementation of the guidance and navigation functions is the selection of terms used to define the vehicle flight path. In this subsection trajectory characterization is described as a choice between various transformations of the equations of motion and the constants of integration pertinent to each form of the equations.

The equations of motion for a space vehicle in their most basic form express the effects of forces (e.g., gravitation, thrust) upon accelerations in space. It follows that the motion of the vehicle can be expressed as a second-order vector differential equation. In the most general case the vectors are three-dimensional, a forcing function is present, and the equations are nonlinear.

As a special case of this general condition, an example of a three-dimensional vector differential equation without a forcing function is the expression for a Keplerian orbit in a fixed rectangular coordinate system:

$$\frac{d^2\underline{R}}{dt^2} + \frac{\mu}{r^3}\,\underline{R} = 0 \qquad (1)$$

where ($\underline{R}$) is a cartesian vector of length (r) between the instantaneous vehicle position and the center of gravitation and (μ) is the gravitational constant of the central force field. For any complete set of initial conditions

$$\underline{R}_o = \underline{R}(t_o) = \begin{bmatrix} R_{01} \\ R_{02} \\ R_{03} \end{bmatrix} \quad ; \quad \underline{V}_o = \frac{d\underline{R}}{dt}(t_o) = \begin{bmatrix} V_{01} \\ V_{02} \\ V_{03} \end{bmatrix} \qquad (2)$$

there exists a unique orbit which satisfies equation 1. There are, however, alternative ways of defining a unique orbit. As a first example, the vector differential equation might be rewritten in another coordinate system to facilitate integration. In fact, the transformation of equations of motion into generalized coordinates and the determination of the corresponding constants of integration is a science in itself. Examples of alternative parameters which could be used to define an orbit are

Two position vectors separated by a fixed time interval or eccentric anomaly

The semimajor axis, eccentricity, inclination, longitude of the ascending node, argument of the perigee, and mean anomaly at epoch time

Various nonsingular (Ref. 1) combinations of these basic orbital elements

To explain this last example, it is noted that the perigee is undefined for a circular orbit and the ascending node is undefined for an equatorial orbit. In spite of these singularities, it is possible to use combinations of the basic elements to define meaningful orbit equations that are applicable to all conditions.

Selection of orbit-defining parameters fixes the type of computations needed for characterization of vehicle motion; the prescribed navigation calculations are slanted toward the determination of these parameters, which in turn are used to compute the vehicle position and velocity at a specified time of interest. Significantly, a nonsingular solution to equation 1 is expressible (Ref 2) in terms of the cartesian position and velocity vector components (R_{kj} and V_{kj} respectively) at a given epoch time (t_k):

$$R_i(t_m) = R_{mi}(R_{k1}, R_{k2}, R_{k3}, V_{k1}, V_{k2}, V_{k3}; t_m - t_k) \; ; \; i = 1, 2, 3 \qquad (3)$$

$$V_i(t_m) = V_{mi}(R_{k1}, R_{k2}, R_{k3}, V_{k1}, V_{k2}, V_{k3}; t_m - t_k); \; i = 1, 2, 3 \qquad (4)$$

where the vectors

$$\underline{R}_m = \underline{R}(t_m) = \begin{bmatrix} R_{m1} \\ R_{m2} \\ R_{m3} \end{bmatrix} \; ; \; \underline{V}_m = \underline{V}(t_m) = \begin{bmatrix} V_{m1} \\ V_{m2} \\ V_{m3} \end{bmatrix} \qquad (5)$$

represent the solution of equation 1 at time (t_m). Immediately this suggests the possibility of using the position and velocity vector components themselves as the trajectory parameters. This procedure provides direct dynamic transformations and facilitates the estimation updating process. Immediately after a measurement or a velocity impulse, the updated (and, in the case of a measurement, improved) observed position and velocity vectors can replace the previous estimate.

Ref. 1 Cohen C. J. and E.C. Hubbard, A Nonsingular Set of Orbit Elements, NWL Report No. 1756.

Ref. 2 Pines S., H. Wolf, D. Woolston, and R. Squires, Goddard Minimum Variance Orbit Determination Program, Goddard Space Flight Center Report No. X-640-62-191.

The above approach typifies the state variable formulation of dynamic systems. As applied to the case at hand, this formulation calls for the definition of a six-dimensional state vector:

$$\underline{X}_m \triangleq \underline{X}(t_m) \triangleq \begin{bmatrix} X_{m1} \\ X_{m2} \\ X_{m3} \\ X_{m4} \\ X_{m5} \\ X_{m6} \end{bmatrix} \triangleq \begin{bmatrix} R_{m1} \\ R_{m2} \\ R_{m3} \\ V_{m1} \\ V_{m2} \\ V_{m3} \end{bmatrix} \tag{6}$$

and the symbolic representation of the equations of motion (equations 3 and 4) are written as

$$X_i(t_m) = X_{mi}(X_{k1}, X_{k2}, \ldots, X_{k6}; t_m - t_k); \; i = 1, 2, \ldots, 6 \tag{7}$$

At any given time, then, the position and velocity vector components form a set of six state variables, constituting a six-dimensional state vector which defines a unique orbit without any singularities in the mathematical expressions.

This basic approach can now be extended to nonhomogeneous systems. When a forcing function is present, equation 1 is replaced by:

$$\frac{d^2\underline{R}}{dt^2} + \frac{\mu}{r^3}\underline{R} = \underline{F} \tag{8}$$

where

$$\underline{F} = \begin{bmatrix} F_1(t) \\ F_2(t) \\ F_3(t) \end{bmatrix} \tag{9}$$

defines a time-varying force vector in three-dimensional space.

According to a fundamental mathematical principle, any n^{th} order, x-dimensional matrix differential equation can be transformed into a first-order differential equation in nx dimensions; it follows that equation 8 can be rewritten in terms of state variables as:

$$\frac{d}{dt}\left\{X_i(t)\right\} = \dot{X}_i\left\{X_1(t), X_2(t). \ldots, X_6(t), F_1(t), F_2(t), F_3(t); t\right\}; \quad i = 1, 2, \ldots, 6 \tag{10}$$

Although in general no closed-form solution exists for this expression, it is always possible to obtain a unique numerical solution for any specific forcing function and initial conditions.[2] Suppose, for example, that the state vector is known at some time (t_m); its derivative at time (t_m) can be computed from equation 10:

$$\frac{d}{dt}\left\{X_i(t)\right\}\Bigg|_{t = t_m} = \dot{X}_{mi}\left\{X_{m1}, X_{m2}, \ldots, X_{m6}, F_{m1}, F_{m2}, F_{m3}; t_m\right\}; \quad i = 1, 2, \ldots, 6 \tag{11}$$

and the state vector at a short time later, dt, can be computed as:

$$X_{m+1} = \underline{X}_m + (dt)\dot{\underline{X}}_m; \; dt = t_{m+1} - t_m \tag{12}$$

Combination of the last two expressions results in a recursive relation for the state variables:

$$X_i(t_{m+1}) = X_{m+1,i}\,(X_{m1}, X_{m2}, \ldots, X_{m6}, F_{m1}, F_{m2}, F_{m3}; dt) \quad i = 1, 2, \ldots, 6 \tag{13}$$

It should be emphasized that this analysis is not limited to any specific coordinate system. The relationships derived herein exist (at least in numerical form) for any complete nonsingular set of independent state variables which can be used to define the motion.

3. PREPARATION FOR USAGE OF SYSTEM EQUATIONS

Given exact values of a set of parameters which define a unique flight path, it is a simple matter to compute the exact value which any observable (e.g., instantaneous altitude, orientation of instantaneous local vertical with reference to a known reference, doppler shift of radar return from a beacon) will have at any point along the path. The inverse of this operation - i.e., determination of the flight path from actual observations (which constitutes the navigation problem) - is not quite so simple; the major obstacles to this task arise from the following two points:

In general, the observations are not simultaneous. The trajectory parameters, therefore, cannot be expressed as explicit functions of quantities available from navigation data. Precise determination of the flight path would require the solution of a set of simultaneous nonlinear equations, including not

---

[2] The discussion of numerical integration applies not only to the case in which the forcing function is an independent variable, but also to the closed loop situation, when the vector ($\underline{F}_m$) is an implicit time function, which must be computed from observed state variables according to a prescribed guidance law.

only the relations between state and observables, but also the expressions describing the dynamic state variations as a function of time.

A significant amount of error will in general be present in the navigation measurements. Therefore, in order to determine the flight path accurately, a relatively large number of navigation measurements must be taken, and the data must be averaged in some manner to reduce the influence of measurement errors.

The necessity for solving high order systems of equations which involve various nonlinear and transcendental relationships must be avoided, at least for practical reasons. Furthermore, the concept of an exact solution to these equations has little meaning in an actual case because:

Inevitably, some random error will remain after all navigation measurements have been processed.

There is no exact mathematical model of any existing gravitational field; even the gravitational constants are not known exactly.

When the number of measurements exceeds the minimum required to define a unique trajectory, the complete set of equations, taken literally, is inconsistent.

The relationships used to transform navigation data into trajectory information, then, must be approximations based upon known geometric and dynamic equations. An excellent opportunity for approximation is afforded by the existence of a known reference trajectory; the physical relationships between the observables and the flight path parameters, expressed as Taylor series expansions about this reference, converge rapidly for neighboring trajectories. In fact, for small deviations from the reference, the first order term alone provides a reasonable approximation to the expression of a physical law. With this expedient, the equations relating an observable (Y_m) to the instantaneous state at time (t_m) are written in terms of differential corrections.

$$y_m \triangleq \delta Y_m \doteq \sum_{i=1}^{6} \frac{\delta Y_m}{\delta X_{mi}} x_{mi} \tag{14}$$

where:

$$\underline{x}_m \triangleq \delta \underline{X}_m \triangleq \begin{bmatrix} x_{m1} \\ x_{m2} \\ x_{m3} \\ x_{m4} \\ x_{m5} \\ x_{m6} \end{bmatrix} \tag{15}$$

is defined as the deviation of the six-dimensional state vector from its reference value at time (t_m). It is convenient to arrange the measurement derivatives into a 1 x 6 row vector:

$$\underline{H}_m \triangleq \begin{bmatrix} h_{m1} & h_{m2} & h_{m3} & h_{m4} & h_{m5} & h_{m6} \end{bmatrix}; \; h_{mi} \triangleq \frac{\partial Y_m}{\partial X_{mi}} \tag{16}$$

so that equation 14 can be written as:

$$y_m = \underline{H}_m \underline{x}_m \tag{17}$$

The same procedure is applicable to the equations of motion; for example, from equation 7 it follows that:

$$x_{mi} = \sum_{j=1}^{6} \frac{\partial X_{mi}}{\partial X_{kj}} x_{kj}; \; i = 1, 2, \ldots, 6 \tag{18}$$

or in matrix form:

$$\underline{x}_m = \left[\frac{\partial \underline{X}_m}{\partial \underline{X}_k} \right] \underline{x}_k \tag{19}$$

where the quantity in square brackets is the symbolic form of a 6 x 6 matrix of partial derivatives, representing the transition in the state vector deviations from time (t_k) to (t_m). For a Keplerian orbit, all elements of this matrix are directly obtainable through differentiation of the six expression indicated by equation 7,[3/] with all derivatives being evaluated on the reference orbit.

[3/] Vector solutions to the Keplerian orbit are derived in Ref. 2.

To apply the same technique to the nonhomogeneous case, equation 11 can be approximated as:

$$\dot{\underline{x}}_m = \left[A_m\right] \underline{x}_m + \left[B_m\right] \underline{f}_m \tag{20}$$

where the $[A]$ and $[B]$ matrices are defined symbolically[4] as:

$$\left[A_m\right] \triangleq \left[\frac{\partial \dot{\underline{X}}_m}{\partial \underline{X}_m}\right] \tag{21}$$

and

$$\left[B_m\right] \triangleq \left[\frac{\partial \dot{\underline{X}}_m}{\partial \underline{F}_m}\right] \tag{22}$$

In all cases of interest for this study, the thrust vector variation ($\underline{f}_m$) is determined by the application of a guidance law to the observed state vector deviation ($\hat{\underline{x}}_m$) thus:

$$\underline{f}_m = \left[S_m\right] \hat{\underline{x}}_m = \left[S_m\right] (\underline{x}_m - \tilde{\underline{x}}_m) \tag{23}$$

where ($\tilde{\underline{x}}_m$) is the error in the observed state. (The 3 x 6 time-varying guidance law matrix $[S_m]$ is exemplified in Section 6 of this appendix.) Combination of this expression with equation 20 yields:

$$\dot{\underline{x}}_m = \left[A'_m\right] \underline{x}_m - \left[D_m\right] \tilde{\underline{x}}_m \tag{24}$$

where:

$$\left[D_m\right] \triangleq \left[B_m\right]\left[S_m\right] \tag{25}$$

and:

$$\left[A'_m\right] = \left[A_m\right] + \left[D_m\right] \tag{26}$$

The approximations preparatory to the evolution of a data processing scheme are now complete. Both the dynamic state variations as a function of time and the equations relating observables to the instantaneous state have been expressed as linear relationships with coefficients that are known (i.e., obtainable by numerical evaluation of solutions to the reference trajectory in equations). The linearity of equations 17, 19, and 22 promises a

---

[4] It follows from the dimensions of $\underline{X}$ and $\underline{F}$ that $[A_m]$ is a 6 x 6 matrix and $[B_m]$ is a 6 x 3 matrix. Clearly these can be considered as known quantities, since all matrix elements can be computed directly by evaluating the derivatives of the nonlinear equations of motion at time (t_m) on the reference trajectory.

straightforward navigation computing procedure and, as explained in the next section, affords an extremely valuable technique for dealing with random errors.

4. CHARACTERIZATION OF RANDOM VARIABLES

In preceding sections it has been recognized that the navigation measurements contain random errors. It is readily seen that these errors will lead to discrepancies in the observed state and consequently in the computed thrust vector correction deemed necessary to trim the flight path. This error in the apparent desired thrust, combined with the effects of imperfect engine control, will in turn cause the trajectory to deviate from the intended course. The effects of these errors, propagated through the appropriate transformations, are naturally at the center of attention in this analysis. As a starting point in illustrating these transformations it is of interest to consider the influence of trajectory deviations upon the true value of an observable.

From the definitions of y, $\underline{x}$, and $\underline{H}$ in the preceding section, equation 17 is written in the equivalent form[5/]

$$y = h_1 x_1 + h_2 x_2 + \ldots + h_6 x_6 \tag{27}$$

Assuming for the moment that the state vector deviation components are normally distributed with zero mean;[6/] i.e.:

$$p_i(x_i) = \frac{1}{\sqrt{2\pi}\,\sigma_i} \exp\left\{\frac{-x_i^2}{2\sigma_i^2}\right\}; \quad i = 1, 2, \ldots, 6 \tag{28}$$

and recalling that the coefficients h_i are deterministic (i.e., nonrandom; obtainable from evaluation of partial derivatives along the reference trajectory), it follows from a basic statistical principle that the weighted sum of the random variables in equation 27 must also be a normally distributed random variable with zero mean. To complete the definition for the probability distribution of y, therefore, all that remains is to derive an expression for its variance. It is informative to approach this problem gradually,

---

5/ The time-dependence subscript (m) is tentatively omitted for clarity of this development.

6/ Although this is a reasonable assumption, it is subject to justification later in this section.

starting with the special case (to be generalized later in this subsection) in which all of the variables x_i are statistically independent; i.e. [7]

$$\rho_{ij} \triangleq \frac{\text{av}\{x_i x_j\} - [\text{av}\{x_i\}]\ [\text{av}\{x_j\}]}{\sigma_i \sigma_j} = 0, \quad i \neq j \tag{29}$$

For the case in which all variables x_i have zero mean, equation 29 reduces to:

$$\overline{x_i x_j} \triangleq \text{av}\{x_i x_j\} = 0, \quad i \neq j \tag{30}$$

and the square of equation 27,

$$y^2 = \sum_{i=1}^{6} h_i^2 x_i^2 + 2 \sum_{\substack{i=1 \\ i \neq j}}^{6} \sum_{j=1}^{6} h_i h_j x_i x_j \tag{31}$$

when averaged, does not contain any nonzero cross products:

$$\overline{y^2} = \sum_{i=1}^{6} h_i^2 \overline{x_i^2} \tag{32}$$

Since for any random variable (z):

$$\overline{z^2} \equiv (\bar{z})^2 + \sigma_z^2 \tag{33}$$

equation 30 leads to the relation:

$$\sigma_y^2 = \sum_{i=1}^{6} h_i^2 \sigma_i^2 \tag{34}$$

It follows that the probability density function for (y) is:

$$p(y) = \frac{1}{\sqrt{2\pi \sum_{i=1}^{6} h_i^2 \sigma_i^2}} \exp\left\{ \frac{-y^2}{2 \sum_{i=1}^{6} h_i^2 \sigma_i^2} \right\} \tag{35}$$

[7] Equation 29 is actually a condition of pairwise linear independence only. For Gaussian random variables, however, this automatically assures complete statistical independence.

This equation can also be derived in a more general form from the joint probability density function

$$p(x_1, x_2, \cdots, x_6) = \frac{1}{(2\pi)^3 \prod_{i=1}^{6} (\sigma_i)} \exp\left\{-\frac{1}{2} \sum_{i=1}^{6} \frac{x_i^2}{\sigma_i^2}\right\} \tag{36}$$

which follows directly from equation 28 and the multiplicative law for joint probabilities of independent random variables. For this purpose it is convenient to define a covariance matrix for the vector $(\underline{x})$, in which the i, j, element is the mean product $(\overline{x_i x_j})$:

$$N = \operatorname{cov}\left\{\underline{x}, \underline{x}\right\} \triangleq \operatorname{av}\left\{\underline{x}\,\underline{x}^T\right\} = \begin{bmatrix} \overline{x_1^2} & \overline{x_1 x_2} & \cdots & \overline{x_1 x_6} \\ \overline{x_2 x_1} & \overline{x_2^2} & & \\ \vdots & & \ddots & \vdots \\ \overline{x_6 x_1} & & \cdots & \overline{x_6^2} \end{bmatrix} \tag{37}$$ [8/]

For the particular case being considered, $[N]$ is a diagonal matrix with the (i, i) element equal to the variance σ_i^2. In this case it is obvious that equation 36 can be written as:

$$p(\underline{x}) = \frac{1}{(2\pi)^3 \left|[N]\right|^{1/2}} \exp\left\{-\frac{1}{2}\, \underline{x}^T N^{-1}\, \underline{x}\right\} \tag{38}$$

where $\left|[N]\right|$ and (N^{-1}) represent the determinant and the inverse of N respectively. The advantage of writing the function in this form is that equation 38 is not restricted to special conditions of zero mean and independence between pairs x_i, x_j. To illustrate the utility of the covariance matrix formulation, it is noted that the statistical properties of y can be determined

---

[8/] The superscript (T) is used to denote the transpose of vectors and matrices. It should be noted that, when a column vector is postmultiplied by its transpose, the resulting square matrix is symmetric.

from the state variable deviations in a single step, merely from linear transformation (equation 17) and the definition of a covariance matrix[9]:

$$\overline{y^2} = \text{cov}\left\{y, y\right\} \triangleq \text{av}\left\{yy^T\right\} = \text{av}\left\{(\underline{H}\,\underline{x})\,(\underline{H}\,\underline{x})^T\right\} = \text{av}\left\{\underline{H}\,\underline{x}\,\underline{x}^T\,\underline{H}^T\right\} \quad (39)$$

Since $\underline{H}$ is deterministic, it can be taken out of the averaging operation:

$$\overline{y^2} = \underline{H}\,\text{av}\left\{\underline{x}\,\underline{x}^T\right\}\underline{H}^T \quad (40)$$

As a further example of linear statistical transformations through the covariance matrix, it follows from equation 19 that:

$$N_m \triangleq \text{cov}\left\{\underline{x}_m, \underline{x}_m\right\} = \text{av}\left\{\Phi(t_m, t_k)\,\underline{x}_k\,\underline{x}_k^T\,\Phi^T(t_m, t_k)\right\} \quad (41)$$

where $\left[\Phi(t_m, t_k)\right]$ is defined as the state transition matrix symbolized in equation 19. Again, since this is a deterministic matrix, equation 41 becomes:

$$N_m = \Phi(t_m, t_k)\,N_k\,\Phi^T(t_m, t_k) \quad (42)$$

The 6 x 6 covariance matrix can be envisioned as a partioned array of four 3 x 3 matrices:

$$N = \begin{bmatrix} N^{(1)} & N^{(2)} \\ N^{(3)} & N^{(4)} \end{bmatrix} \quad (43)$$

in which the submatrices $\left[N^{(1)}\right]$ and $\left[N^{(4)}\right]$ are the position and velocity error covariance matrices respectively. It should be noted that the diagonal elements of these submatrices are defined as mean squared components of error. For an orthogonal coordinate system, then, two significant relationships become clear:

---

[9] The scalar y can be thought of as a degenerate 1 x 1 vector or as a degenerate matrix, for which the properties of vectors and matrices still hold true. For example,

a. The covariance "matrix" of y is a 1 x 1 matrix with a single element equal to the mean squared value.
b. The "transpose" of y is equal to the product of the transposes of $\underline{H}$ and $\underline{x}$, multiplied in reverse order.

The trace - i.e., the sum of the diagonal terms - of $\left[N^{(1)}\right]$ is the total mean squared position error.

The trace of $\left[N^{(4)}\right]$ is the total mean squared velocity error.

Another important property of the trace arises in regard to coordinate rotations. Physically, the total mean squared error is obviously independent of the coordinate system used to define that error. Mathematically, the trace of a matrix is invariant under a similarity transformation (Ref. 3).

Assume that it is desirable to express the position error in a new coordinate system by means of a rotation matrix $\left[W\right]$:

$$(\Delta \underline{R})_k = \left[W\right] (\delta \underline{R})_k \tag{44}$$

The statistics of the error, expressed in the new coordinates, become

$$\text{cov}\left\{(\Delta \underline{R})_k, (\Delta \underline{R})_k\right\} = W \text{ cov}\left\{(\delta \underline{R})_k, (\delta \underline{R})_k\right\} W^T = W \left[N_k^{(1)}\right] W^T \tag{45}$$

Equation 43 defines a similarity transformation[10]. As applied to guidance and navigation, it is often used to reexpress the position or velocity errors at some point in terms of horizontal, vertical, and transverse components.

As another illustration of error coordinate transformations, it is instructive to consider the principal axes of error. To elaborate on this point, consider the possibility that a unit vector $\underline{U}$ exists such that, for an n x n symmetric error matrix $\left[P\right]$, the matrix transformation leaves the direction of the vector unchanged; i.e.:

$$\left[P\right] \underline{U} = \lambda \underline{U} \tag{46}$$

Ref. 3 Goldstein, Classical Mechanics, London: Addison-Wesley 1950, p. 105

[10] As defined in Ref. 3, the similarity transformation is made through premultiplication by the transformation matrix and postmultiplication by its inverse. Since, however, $\left[W\right]$ is a rotation matrix, its transpose and its inverse are identical.

where (λ) is a real scalar. Actually, for any n x n symmetric matrix, there are n orthogonal vectors which conform to this equation. To illustrate the existence of a set of "eigenvalues," λ_i, and corresponding "eigenvectors," $\underline{U}_i$, equation 46 is written for a 3 x 3 P-matrix as:

$$\begin{bmatrix} p_{11} - \lambda_i & p_{12} & p_{13} \\ p_{21} & p_{22} - \lambda_i & p_{23} \\ p_{31} & p_{32} & p_{33} - \lambda_i \end{bmatrix} \begin{bmatrix} u_{1i} \\ u_{2i} \\ u_{3i} \end{bmatrix} = \underline{O}, \quad i = 1, 2, 3 \tag{47}$$

where (u_{ji}) is the j^{th} component of the i^{th} eigenvector.

The above expression will hold when the determinant of the matrix on the left vanishes. This condition leads to a cubic equation in λ_i; the three roots of this cubic are the eigenvalues. 11/

The vectors $\underline{U}_i$ can be interpreted geometrically as a set of principal axes for an ellipsoid. Their directions are found as follows: In equation 47 replace u_{1i}, u_{2i}, and u_{3i} by x, y, and z respectively, and from the nine scalar equations implied by equation 47, select the following three:

$$(p_{11} - \lambda_1)\, x + p_{12}\, y + p_{13}\, z = 0 \tag{48}$$

$$p_{21}\, x + (p_{22} - \lambda_2)\, y + p_{23}\, z = 0 \tag{49}$$

$$p_{31}\, x + p_{32}\, y + (p_{33} - \lambda_3)\, z = 0 \tag{50}$$

Each of these equations represents a plane. The intersection of each pair of planes will be a straight line in the direction of an eigenvector. The three eigenvectors will be mutually orthogonal.

11/ In ref. 3 it is shown that all eigenvalues of any hermitian matrix (and therefore of any symmetric matrix) are real, and the eigenvectors form an orthogonal set. It sometimes happens that the cubic eigenvalue equation has multiple roots; the solution for the eigenvector set is not unique in this case. The fact remains, however, that it is always possible to find a real orthogonal set of eigenvectors and a corresponding set of real eigenvalues satisfying equation 46.

As applied to the navigation problem, the significance of the principal axis transformation lies in the insight it provides into the state vector uncertainties. For example, suppose that the uncertainty covariance matrix at time t_k;

$$P_k \triangleq \text{av}\left\{ \underset{\sim}{x}_k \underset{\sim}{x}_k^T \right\} \tag{51}$$

is extrapolated by the familiar linear transformation to an intended measurement time (t_m):

$$P_m = \Phi(t_m, t_k)\, P_k \Phi^T(t_m, t_k) \tag{52}$$

and this extrapolated matrix is partitioned into four 3 x 3 submatrices:

$$P_m \equiv \begin{bmatrix} P_m^{(1)} & P_m^{(2)} \\ P_m^{(3)} & P_m^{(4)} \end{bmatrix} \tag{53}$$

As an example of the utility of the principal axis transformation, consider the case in which the largest eigenvalue of $\left[P_m^{(1)} \right]$ happens to correspond with the instantaneous vertical direction of an orbiting vehicle at time t_m; this would indicate that an altitude measurement would be particularly helpful. More generally, the eigenvectors of $\left[P_m^{(1)} \right]$ and $\left[P_m^{(4)} \right]$ could be used to select the position-sensitive and velocity-dependent measurements respectively, which contain the most significant information at any given measurement time.

It is now clear that the linearized models of trajectory dynamics and measurement geometry have provided powerful tools for analyzing transformations of statistical variables. The merits of linearization are further illustrated in the following subsections, in which the navigation and guidance techniques are expressed in terms of straightforward linear transformations. Since, therefore, <u>all</u> transformations of the random errors encountered in the entire analysis can be linearized, and since the ultimate sources of error (i.e., measurement and thrust errors) are Gaussian with zero mean, 12/

12/ Actually, this comment applies only for an ensemble of missions, for which the average bias errors must vanish. The effects of bias errors upon orbital navigation, as previously explained, are out of the scope of this presentation. Bias effects in powered flight are discussed in Section 6.

it follows that the state variable deviation x_{mi} and uncertainty $\tilde{x}_{mi}$ errors at any time t_m are similarly characterized, and their statistics are completely defined by the covariance matrices $\left[N_m\right]$ and $\left[P_m\right]$ respectively.

Thus far orbital (unpowered) and powered flight have been treated simultaneously in this presentation and certain characteristics applicable to both trajectory types have been explored to prepare a suitable mathematical representation for analysis. From this point on powered and unpowered flight are analyzed separately because of differences in methods of applying the analytical model. In the sections to follow, mathematical techniques are described which illustrate:

- Transformation of navigation measurement data into accurate trajectory estimates
- Transformation of observed trajectory deviations into guidance commands
- Corruption of these processes by navigation and guidance errors
- Effects of navigation and guidance transformations upon error statistics

For both orbital and powered flight, then, the techniques to be explained will serve to describe both the physical system and an analytical method of evaluating its performance.

5. APPLICATION OF ANALYTICAL MODEL TO ORBITAL FLIGHT

As applied to flight paths which are essentially free-fall trajectories (with the possible exception of an occasional impulsive velocity change), the foregoing problem formulation leads readily to useful techniques for orbital navigation and guidance. The development of these techniques and the performance analysis of systems utilizing the techniques are treated in this subsection.

To demonstrate the task to be performed in processing the navigation measurements as a preparation for orbital guidance, it is convenient to postulate the flight of a space vehicle in a given gravitational field:

At time t_A an attempt is made to inject a vehicle by a velocity impulse [13] into a free fall trajectory nominally characterized by a given initial state $\underline{X}_o$.

[13] The subscripts A and o are used to distinguish between conditions before and after the impulse respectively.

However, because of departures from the nominal initial position (which of course cannot be corrected by a velocity impulse) and because of uncertainties in the actual initial state, combined with thrusting errors, the actual vehicle trajectory will not coincide with either the originally prescribed nominal orbit or the orbit defined by the estimated state immediately after injection. To provide compensation for these errors, a plan is devised whereby an impulsive thrust correction will be determined for application at a prescribed time of orbital correction, t_E. Determination of the thrust command is to be based upon the estimated state at time t_E, computed from the observed orbit after all navigation data have been processed.

5.1 Navigation Data Processing by Least Squares

One possible scheme for processing the measured data is the least squares method, which is conveniently illustrated by the following example.

Suppose that a large number M of measurements is prescribed and, in addition to the nominal value Y_m of the observable at each measurement time t_m, the matrices $\left[\underline{H}_m \right]$ and $\left[\Phi(t_m, t_o) \right]$ defined in equations 17 and 19 respectively are computed from the nominal orbit. It is convenient to combine equations 17 and 19 into the expression

$$y_m = \underline{C}_m \underline{x}_o$$

where the row vector $\left[\underline{C}_m \right]$ is the product (54)

$$\underline{C}_m = \underline{H}_m \Phi(t_m, t_o) \quad (55)$$

With all M measurements taken into account, there are M simultaneous linear equations which can be combined into the matrix relation

$$\underline{y} = C \underline{x}_o \quad (56)$$

where $[C]$ is a (M x 6) matrix with the m^{th} row defined by equation 55 and $\underline{y}$ is an M x 1 vector of deviations from nominal measurement values.

If only six measurements were taken, the initial state vector deviation could be computed from these measurements merely by inverting equation 56. Obviously, however, this is inferior to a scheme whereby a larger number of measurements is taken in the same total time duration and the results are averaged. In this case the matrix $[C]$ is not square and before inversion

can take place the basic equation must be multiplied by the transpose of $[C]$:

$$[C]^T \underline{y} = \left[C^T C\right] \underline{x}_o \tag{57}$$

The matrix product $\left[C^T C\right]$ is always square, and

$$\hat{\underline{x}}_o = \left[C^T C\right]^{-1} C^T \hat{\underline{y}} \tag{58}$$

Here, in writing the observed state vector deviations as an explicit function of known quantities, the circumflex is used to illustrate the degradation caused by measurement errors. The true value of an observable (Y_m') cannot be measured without the inclusion of an error (a_m):

$$\hat{y}_m = Y_m' - Y_m + a_m = y_m + a_m \tag{59}$$

Theoretically, with a sufficient number of measurements, the effects of these errors will be minimized due to averaging. Thus it would appear that a simple and accurate solution has been found for the initial state and therefore for the entire orbit. This method, however, is subject to difficulties in extrapolation over extended time durations and furthermore is critically dependent upon two conditions:

The vehicle must be sufficiently close to its reference state so that equations 17 and 19 are accurate.

It must be possible to obtain an accurate inversion.

Unfortunately, satisfaction of the first requirement does not at all guarantee the second; equation 58 is subject to errors incurred in matrix inversion. The matrix $\left[C^T C\right]$ approaches singularity (i.e., its determinant approaches zero) as the total time encompassing the measurements increases. (Ref. 2)

To circumvent the difficulties present in the least squares process, modifications of the basic technique have been developed. It has been shown (Ref.4)

Ref. 4 Magness, T.A. and J.B. McGuire, Comparison of Least Squares and Minimum Variance Estimates of Regression Parameters, Ann. Math. Stat., Vol 33, June 1962, P. 462 A-24

that at best the weighted least squares method is equivalent to the minimum variance (also referred to as the Markov and as the maximum likelihood) technique. For linear systems the minimum variance method is optimum from a statistical standpoint. As its name implies, it minimizes the rms error in the estimated position and velocity. This technique will now be described.

5.2 Navigation Data Processing by Minimum Variance

In a paper by R. E. Kalman, (Ref. 5) the minimum variance formulation has been derived in recursive form. As applied to the navigation problem at hand, this technique provides a completely updated estimate of the vehicle state after each measurement. This is done by extrapolating the most recent [14] estimate, $\underline{\hat{x}}_{m-1}$, to determine the predicted state vector deviation $\underline{x}_m^{(-)}$ immediately before the (m^{th}) measurement

$$\underline{x}_m^{(-)} = \Phi(t_m, t_{m-1})\, \underline{\hat{x}}_{m-1} \tag{60}$$

and correcting this estimate by means of a linear transformation of the new data point:

$$\underline{\hat{x}}_m = \underline{x}_m^{(-)} + \underline{K}_m \left[\hat{y}_m - y_m^{(-)} \right] \tag{61}$$

where $\left[y_m^{(-)} \right]$ is the predicted measurement deviation

$$y_m^{(-)} \triangleq \underline{H}_m \underline{x}_m^{(-)} \tag{62}$$

The weighting vector $\underline{K}_m$, to be derived in this section, can be regarded as an error distributor which attributes the measurement deviation to each possible cause in accordance with the a priori sensitivity of the measurement

---

[14] For the first measurement the vector $\underline{\hat{x}}_{m-1} = \underline{\hat{x}}_o$ is the observed deviation from nominal state immediately after the impulsive injection. For subsequent measurements the vector $\underline{\hat{x}}_{m-1}$ is the observed deviation from nominal state immediately after the last measurement.

Ref. 5 Kalman, R.E., A New Approach to Linear Filtering and Prediction Problems, Trans. ASME, Series D., Jour. Basic Engr., Vol 82, No. 1, March 1960, pp. 35-45.

to that cause and the theoretical capability of the weighted state vector correction to reduce the rms uncertainty in the estimate. This distribution is achieved by combining the effects of the measurement sensitivities with the statistical behavior of the measurement errors and of the state vector uncertainties in the determination of the optimum weighting coefficients. All that is required for this purpose is a knowledge [15] of the measurement error variance (which may in general vary from one measurement to the next) and of the initial state vector uncertainty covariance matrix $\left[P_o\right]$. The ensuing derivation, then, will include a procedure for updating the P-matrix as well as an expression for $\underline{K}_m$.

The derivation of the optimum weighting vector (Ref. 8) begins with a combination of equations 17, 59, 61, and 62:

$$\hat{\underline{x}}_m = \underline{x}_m^{(-)} + \underline{K}_m \underline{H}_m \left[\underline{x}_m - \underline{x}_m^{(-)}\right] + \underline{K}_m \alpha_m \tag{63}$$

From the definition of $\tilde{\underline{x}}_m$:

$$\tilde{\underline{x}}_m \triangleq \underline{x}_m - \hat{\underline{x}}_m \tag{64}$$

---

[15] Actually, as demonstrated in Ref. 6, an approximation to the true measurement error statistics will suffice. Also, the adoption of a pessimistic diagonal initial uncertainty covariance matrix will provide a conservative result. Since final errors are reasonably insensitive to initial errors (Ref. 7) the results will not be too pessimistic.

Ref. 6 Gunckel, T.L., Orbit Determination Using Kalman's Method, Journal of the Institute of Navigation, Vol. 10 No. 3, Autumn, 1963.

Ref. 7 McLean, J.D., S.F. Schmidt, and L.A. McGee Optimal Filtering and Linear Prediction Applied to Midcourse Navigation System for the Circumlunar Mission, NASA TN D-1208, 1961.

Ref. 8 Battlin, R.H., A Statistical Optimizing Navigation Procedure for Space Flight, ASRJ, Vol. 32, No. 11, Nov. 1962, pp. 1681-1696.

it follows that the error in the updated estimate is:

$$\underline{\tilde{x}}_m = \left[I_{66} - \underline{K}_m \underline{H}_m\right] \left[\underline{x}_m - \underline{x}_m^{(-)}\right] - \underline{K}_m a_m \qquad (65)\ \underline{16/}$$

which could be written in terms of a prediction error $\left[\underline{\tilde{x}}_m^{(-)}\right]$ as:

$$\underline{\tilde{x}}_m = \left[I_{66} - \underline{K}_m \underline{H}_m\right] \underline{\tilde{x}}_m^{(-)} - \underline{K}_m a_m \qquad (66)$$

It is permissible to postmultiply each side of this equation by its transpose and take the expected value. This leads to equation 67 in which, on the right side, the cross products involving (a_m) and $\left[\underline{\tilde{x}}_m^{(-)}\right]$ vanish: $\underline{17/}$

$$\text{av}\left\{\underline{\tilde{x}}_m \underline{\tilde{x}}_m^T\right\} = \left[I_{66} - \underline{K}_m \underline{H}_m\right] \text{av}\left\{\underline{\tilde{x}}_m^{(-)} \left[\underline{\tilde{x}}_m^{(-)}\right]^T\right\} \left[I_{66} - \underline{H}_m^T \underline{K}_m^T\right] + \underline{K}_m Q_m \underline{K}_m^T \qquad (67)$$

where

$$Q_m \triangleq \text{av}\left\{a_m^2\right\} \qquad (68)$$

If

$$P_m^{(-)} \triangleq \text{av}\left\{\underline{\tilde{x}}_m^{(-)} \left[\underline{\tilde{x}}_m^{(-)}\right]^T\right\} \qquad (69)$$

equation 67 can be written as:

$$P_m = \left[I_{66} - \underline{K}_m \underline{H}_m\right] P_m^{(-)} \left[I_{66} - \underline{H}_m^T \underline{K}_m^T\right] + \underline{K}_m Q_m \underline{K}_m^T \qquad (70)$$

It will now be explained that to optimize the weighting vector, a value must be found for $\left[\underline{K}_m\right]$ which will minimize the trace of $\left[P_m\right]$. Consider a

---

$\underline{16/}$ The notation $\left[I_{jj}\right]$ is used to denote a j^{th} order identity matrix consisting of 1's in the principal diagonal and zeroes elsewhere.

$\underline{17/}$ The prediction prior to the measurement is obviously independent of a_m and, as previously explained, all random variables in this analysis have zero mean.

partitioned form of the above expression in which all (6 x 6) matrices are rewritten in terms of (3 x 3) partitions; e.g.:

$$\left[P_m\right] \equiv \begin{bmatrix} P_m^{(1)} & P_m^{(2)} \\ P_m^{(3)} & P_m^{(4)} \end{bmatrix} \tag{71}$$

$$\left[I_{66}\right] \equiv \begin{bmatrix} I_{33} & O_{33} \\ O_{33} & I_{33} \end{bmatrix} \tag{72}$$ [18/]

and the (6 x 1) vectors are partitioned as

$$\left[\underline{K}_m\right] \equiv \begin{bmatrix} \underline{K}_m^{(1)} \\ \underline{K}_m^{(2)} \end{bmatrix} \quad ; \quad \left[\underline{H}_m\right] = \left[\underline{H}_m^{(1)} \quad \underline{H}_m^{(2)}\right] \tag{73}$$

With equation 70 written in partitioned form it is readily seen that $\left[P_m^{(1)}\right]$ is independent of $\left[\underline{K}_m^{(2)}\right]$ and that $\left[P_m^{(4)}\right]$ is independent of $\left[\underline{K}_m^{(1)}\right]$. It follows that when $\left[\underline{K}_m\right]$ is selected to minimize the trace of the 6 x 6 P-matrix, it is automatically ensured that the individual traces of the position uncertainty and the velocity uncertainty covariance matrices are minimized separately.

The trace of the covariance matrix is minimized by means of the variational technique, a vectorial counterpart to the familiar minimum-maximum problem of elementary differential calculus. To apply this technique to equation 70, the vector $\left[\underline{K}_m\right]$ is replaced by $\left[\underline{K}_m + \delta\underline{K}_m\right]$, and the first order residual covariance $\left[\delta P_m\right]$ is found by subtracting the result from equation 70, neglecting all terms of second order in δ. It can readily be verified that the result is:

18/ The notation $\left[O_{ij}\right]$ is used to denote a (ixj) matrix in which all elements are zero.

$$\left[\delta P_m\right] = \delta \underline{K}_m \underline{H}_m P_m^{(-)} \left[I_{66} - \underline{H}_m^T \underline{K}_m^T\right]$$
$$+\left[I_{66} - \underline{K}_m \underline{H}_m\right] P_m^{(-)} \underline{H}_m^T \delta \underline{K}_m^T \tag{74}$$
$$- \delta \underline{K}_m Q_m \underline{K}_m^T - \underline{K}_m Q_m \delta \underline{K}_m^T$$

It will be noted that each pair of consecutive terms on the right of this expression is a transpose pair; i.e., since:

$$P_m^{(-)} \equiv \left[P_m^{(-)}\right]^T \tag{75}$$

for any symmetric matrix, then

$$\delta \underline{K}_m \underline{H}_m P_m^{(-)} \left[I_{66} - \underline{H}_m^T \underline{K}_m^T\right] = \left\{\left[I_{66} - \underline{K}_m \underline{H}_m\right] P_m^{(-)} \underline{H}_m^T \delta \underline{K}_m^T\right\}^T \tag{76}$$

and

$$\delta \underline{K}_m Q_m \underline{K}_m^T = \left[\underline{K}_m Q_m \delta \underline{K}_m^T\right]^T \tag{77}$$

From the definition of a trace, it follows that the trace of a matrix is equal to that of its transpose, and from equation 74

$$\text{trace}\left\{\delta P_m\right\} = 2 \cdot \text{trace}\left\{\left[I_{66} - \underline{K}_m \underline{H}_m\right] P_m^{(-)} \underline{H}_m^T \delta \underline{K}_m^T - \underline{K}_m Q_m \delta \underline{K}_m^T\right\} \tag{78}$$

In order that the trace of $\left[P_m\right]$ be a minimum, the following conditions must hold: the total residual error must vanish for an arbitrary nonzero variation in the weighting vector, or

$$\text{trace}\left\{\delta P_m\right\} = 0; \delta \underline{K}_m \neq \underline{O}_{61} \tag{79}$$

From equation 78 then:

$$\left[I_{66} - \underline{K}_m \underline{H}_m\right] P_m^{(-)} \underline{H}_m^T - \underline{K}_m Q_m = \underline{O}_{61} \tag{80}$$

or

$$\underline{K}_m = P_m^{(-)} \underline{H}_m^T \left[\underline{H}_m P_m^{(-)} \underline{H}_m^T + Q_m\right]^{-1} \tag{81}$$

It is now convenient to write equation 70 as:

$$P_m = \left[I_{66} - \underline{K}_m \underline{H}_m\right] P_m^{(-)} - P_m^{(-)} \underline{H}_m^T \underline{K}_m^T + \underline{K}_m \left[\underline{H}_m P_m^{(-)} \underline{H}_m^T + Q_m\right] \underline{K}_m^T \tag{82}$$

Combination of the last two expressions yields:

$$P_m = \left[I_{66} - \underline{K}_m \underline{H}_m\right] P_m^{(-)} \tag{83}$$

This completes Battin's derivation (Ref. 8); the minimum variance data processing scheme is defined by equations 61, 81, and 83. The merits of this technique are:

The acquisition of an optimum updated state vector estimate after each measurement is obviously preferable to waiting for the accumulation of several data points.

The recursive nature of the computations implies a lenient storage capacity requirement for the minimum variance computer.

The type of computations necessary for data processing is simple (e.g., no large matrix inversions are necessary).[19/]

The continuous updating procedure affords an opportunity to minimize the error due to linearization by computing all partial derivative matrix elements from the updated estimate.

This last point was advocated early (Ref. 2, 9) in the development of minimum variance orbital navigation. To implement this procedure, the

---

19/ The order of the inversion indicated in equation 81 is equal to the number of simultaneous measurements, whereas with weighted least squares the order of the required inversion is equal to the total number of navigation measurements.

Ref. 9 Smith, G.L., S.F. Schmidt and L.A. McGee, Application of Statistical Filter Theory to the Optimal Estimation of Position and Velocity on Board a Circumlunar Vehicle, NASA TR R-135, 1962.

extrapolation of equation 60 is replaced by equation 7 with the components of the estimated state vector $\underline{\hat{X}}_{m-1}$ used to predict the state $\underline{X}_m^{(-)}$. The state vector $\underline{\hat{X}}_{m-1}$ is also used to compute the transition matrix $\left[\Phi(t_m, t_{m-1})\right]$ for extrapolating the P-matrix, and the predicted state vector $\underline{X}_m^{(-)}$ is used to compute both the predicted measurement $Y_m^{(-)}$ and its partial derivatives $\underline{H}_m$. The weighting vector is computed as usual from equation 81, and equation 61 is replaced by:

$$\underline{\hat{X}}_m = \underline{X}_m^{(-)} + \underline{K}_m (\hat{Y}_m - Y_m^{(-)}) \tag{84}$$

where $(\hat{Y}_m)$ is the measured value of the observable. Thus as the estimate converges toward the actual orbit, the linearized analytical model also gains in accuracy.

From the general nature of the foregoing analysis it can be concluded that the recursive minimum variance navigation scheme is as versatile as it is powerful. It is not surprising, therefore, that a variety of successful applications have been reported in the literature.

5.3 End Point Guidance With a Fixed Arrival Time (Ref. 7)

Given an observed or predicted position at a specified time and a desired position at some later time, there are several methods of guiding the flight to the intended destination. A thorough analysis, or even a thorough discussion, of available techniques is out of the scope of this presentation. However, to provide a concrete example of linearization theory applied to guidance, the implementation of one possible approach and the corresponding tools for analysis will be described.

The fixed time-of-arrival (FTOA) end-point guidance law specifies that at a given time (t_A) of thrust, an impulsive velocity vector increment[20/] $(\underline{f}_A)$ is to counteract the apparent deviations from a particular desired trajectory in order to reestablish the reference position at a specified future time t_E. For an observed deviation of $\underline{\hat{x}}_A$ immediately before the impulsive injection at time t_A, equation 19 gives the resulting uncorrected deviation at time t_E:

$$\underline{x}_E^{(U)} = \Phi(t_E, t_A)\, \underline{\hat{x}}_A \tag{85}$$

20/ The velocity impulse may be purely corrective or, more generally, may be an adjustment to a preplanned injection command.

which can be written symbolically as

$$\begin{bmatrix} \delta \underline{R}_E^{(U)} \\ \delta \underline{V}_E^{(U)} \end{bmatrix} = \begin{bmatrix} \Phi_E^{(1)} & \Phi_E^{(2)} \\ \Phi_E^{(3)} & \Phi_E^{(4)} \end{bmatrix} \begin{bmatrix} \delta \hat{\underline{R}}_A \\ \delta \hat{\underline{V}}_A \end{bmatrix} \tag{86}$$

The apparent future position deviation at time t_E can be brought to zero by means of a corrective impulse $\underline{f}_A$ such that

$$\begin{bmatrix} \underline{O}_{31} \\ \delta \underline{V}_E \end{bmatrix} = \begin{bmatrix} \Phi_E^{(1)} & \Phi_E^{(2)} \\ \Phi_E^{(3)} & \Phi_E^{(4)} \end{bmatrix} \begin{bmatrix} \delta \hat{\underline{R}}_A \\ \delta \hat{\underline{V}}_A + \underline{f}_A \end{bmatrix} \tag{87}$$

It is readily seen that the predicted end point position error can be brought to zero by a correction to the nominal injection command:

$$\underline{f}_A = [G] \hat{\underline{x}}_A \tag{88}$$

where the 3 x 6 guidance law matrix is defined in partitioned form as:

$$[G] = - \left[(\Phi_E^{(2)})^{-1} \Phi_E^{(1)} \quad I_{33} \right] \tag{89}$$

This completes the illustration of the FTOA end-point guidance technique, in which the observed state is used to determine a corrective impulse. All that remains is a description of the corresponding statistical transformations of state vector deviations arising from navigation and thrust control errors:

The actual deviation immediately after thrust is:

$$\underline{x}_o = \underline{x}_A + \begin{bmatrix} \underline{O}_{31} \\ G \hat{\underline{x}}_A \end{bmatrix} - \underline{c}_A \tag{90}$$

where $\underline{c}_A$ is a 6 x 1 vector composed of the vehicle state error introduced by imperfect engine control. Since the position component of this error is zero

for an impulsive thrust, the covariance matrix of engine error can be written in the form:

$$\text{cov}\left\{\underline{c}_A, \underline{c}_A\right\} = \begin{bmatrix} O_{33} & O_{33} \\ O_{33} & \Gamma_{(eng)} \end{bmatrix} \tag{91}$$

Using the definitions:

$$\underset{\sim}{\underline{x}}_A \triangleq \underline{x}_A - \hat{\underline{x}}_A \tag{92}$$

and introducing a 6 x 6 guidance matrix to facilitate further manipulations,

$$\left[G_A\right] \triangleq \begin{bmatrix} O_{36} \\ G \end{bmatrix} \tag{93}$$

equation 90 can be written as:

$$\underline{x}_o = \left[G_A + I_{66}\right] \underline{x}_A - \left[G_A\right] \underset{\sim}{\underline{x}}_A - \underline{c}_A \tag{94}$$

Multiplying each side of this equation by its transpose and taking averages,

$$\begin{aligned} N_o = &\left[G_A + I_{66}\right] N_A \left[G_A + I_{66}\right]^T - \left[G_A + I_{66}\right] \text{cov}\left\{\underline{x}_A, \underset{\sim}{\underline{x}}_A\right\} G_A{}^T \\ &- G_A \,\text{cov}\left\{\underline{x}_A, \underset{\sim}{\underline{x}}_A\right\} \left[G_A + I_{66}\right]^T + G_A P_A G_A{}^T \\ &+ \text{cov}\left\{\underline{c}_A, \underline{c}_A\right\} \end{aligned} \tag{95}$$

Since[21]

$$\text{cov}\left\{\underline{x}_A, \underset{\sim}{\underline{x}}_A\right\} = \text{cov}\left\{\left(\hat{\underline{x}}_A + \underset{\sim}{\underline{x}}_A\right), \underset{\sim}{\underline{x}}_A\right\} = O_{33} + P_A \tag{96}$$

equation 95 can be rearranged as:

$$N_o = \left[G_A + I_{66}\right]\left[N_A - P_A\right]\left[G_A + I_{66}\right]^T + P_A + \text{cov}\left\{\underline{c}_A, \underline{c}_A\right\} \tag{97}$$

---

[21] As explained in Ref. 7, the minimum variance estimate $\left[\hat{\underline{x}}\right]$ at any time is uncorrelated with the error $\left[\underset{\sim}{\underline{x}}\right]$ in that estimate.

which is the final expression for the state vector deviation covariance matrix after an impulsive thrust command.

6. APPLICATION OF LINEARIZED ANALYSIS TO POWERED FLIGHT

In the following two subsections a powerful technique for use in linearized analyses of systems described by nonlinear differential equations is applied to two problems pertaining to powered flight: guidance logic determination and error analysis. The key to the technique is the introduction of a set of differential equations, termed the adjoint differential equations, which are related to the homogeneous portion of the linearized differential equations describing the system. Manipulation of the combined sets of equations can be made to yield valuable information applicable to both guidance law determination and evaluation of the effects of random and nonrandom errors on system performance.

It should be noted that the problems discussed herein can be solved by straightforward operations involving only the original set of differential equations. The advantage of introducing the set of adjoint equations lies primarily in the greater ease and speed with which the desired information can be obtained.

6.1 Application of Adjoint Analysis to Guidance Law Determination

The first problem discussed is to determine a set of guidance equations which can be used during powered flight. These equations are used to compute acceleration commands which will move the vehicle to the desired terminal position even though it is initially displaced from the desired trajectory.

The solution proceeds in two steps. First, the terminal errors which would result if no correction were made to the reference acceleration program are estimated. (These errors are the result of the fact that the vehicle is not on the reference trajectory.) Then deviations from the reference accelerations are postulated which are constant over the remaining time of flight, and the magnitudes of these deviations required to compensate for selected components of the estimated terminal error are computed. (All terminal state errors cannot be removed because there are in general only half as many independent control quantities as there are state variables.)

The starting point for this investigation is the set of linearized differential equations describing vehicle motion which have been introduced previously (equation 20):

$$\dot{\underline{x}} = [A]\,\underline{x} + [B]\,\underline{f} \tag{98}$$

(Here the subscript m has been dropped, but all quantities remain continuous functions of time.) Recall that $\dot{\underline{x}}$, $\underline{x}$, and $\underline{f}$ are vectors composed of deviations from the reference state and force vectors respectively, while $[A]$ and $[B]$ are matrices of partial derivatives evaluated using reference values of $\underline{X}$ and $\underline{F}$. Throughout this discussion, $\underline{x}$ and $\dot{\underline{x}}$ are considered to be 6 x 1 column vectors, and $\underline{f}$ is considered to be a 3 x 1 column vector.

Given this information, there exists a set of linear differential equations closely related to the homogeneous part of equation 98. These equations, termed the adjoint differential equations, are defined below (see Ref. 10):

$$[\dot{\Lambda}] = -[A]^T[\Lambda] \tag{99}$$

Matrices $[\dot{\Lambda}]$ and $[\Lambda]$ are both 6 x 6 square matrices.

To make use of these additional equations, proceed in the following manner. Premultiply equation 98 by $[\Lambda]^T$, and equation 99 by $\underline{x}^T$:

$$[\Lambda]^T \dot{\underline{x}} = [\Lambda]^T [A]\, \underline{x} + [\Lambda]^T [B]\, \underline{f} \tag{100}$$

$$\underline{x}^T[\dot{\Lambda}] = -\underline{x}^T [A]^T[\Lambda] \tag{101}$$

Transpose both sides of equation 101:

$$[\dot{\Lambda}]^T \underline{x} = -[\Lambda]^T [A]\, \underline{x} \tag{102}$$

and sum equations 100 and 102:

$$[\Lambda]^T \dot{\underline{x}} + [\dot{\Lambda}]^T \underline{x} = [\Lambda]^T [B]\, \underline{f} \tag{103}$$

However,

$$[\Lambda]^T \dot{\underline{x}} + [\dot{\Lambda}]^T \underline{x} = \frac{d\left\{[\Lambda]^T \underline{x}\right\}}{dt}$$

Therefore equation 108 becomes:

$$\frac{d\left\{[\Lambda]^T \underline{x}\right\}}{dt} = [\Lambda]^T [B]\, \underline{f} \tag{104}$$

Ref. 10 Leitmann, G., Optimization Techniques with Application to Aerospace Systems, New York; Academic Press, 1962, P. 218

The left-hand side of equation 104 is a perfect differential, so that the integral of this expression with respect to time over the interval $t = t_m$ to $t = t_f$ can be written:

$$\left[\Lambda\ (t_f)\right]^T \underline{x}\ (t_f) - \left[\Lambda\ (t_m)\right]^T \underline{x}\ (t_m) = \int_{t_m}^{t_f} \left[\Lambda\right]^T \left[B\right] \underline{f}\ dt \qquad (105)$$

for

$$t_o \leq t_m < t_f$$

where t_f is the end time of the reference trajectory, t_o is the start time of the reference trajectory, generally set equal to zero, and t_m is any time within the indicated interval. For ease in handling, the time arguments are indicated by subscripts as in previous sections. Thus:

$$\left[\Lambda_f\right]^T \underline{x}_f - \left[\Lambda_m\right]^T \underline{x}_m = \int_{t_m}^{t_f} \left[\Lambda\right]^T \left[B\right] \underline{f}\ dt \qquad (106)$$

Before the set of adjoint differential equations (expression 99) can be solved specifically, additional information, usually in the form of initial conditions on the matrix $[\Lambda]$, is required. In this analysis, however, specification of the elements of $[\Lambda_f]$ (the terminal conditions on the matrix $[\Lambda]$) is found to be more useful. To understand the reason, refer to the first term on the left-hand side of equation 106. The components of the vector $\underline{x}_f$ are linearized estimates of the terminal state variable deviations caused by state deviations existing at time t_m and force vector deviations in the interval $t_m \leq t < t_f$. The analytical goals are to predict the uncorrected value of $\underline{x}_f$ (i.e., the terminal state vector deviation which would exist if $\underline{f}$ were zero), and then to determine what constant value of $\underline{f}$ in the interval $t_m \leq t < t_f$ will reduce the terminal deviations to zero. The first goal is most easily achieved if $[\Lambda_f]^T$ is the identity matrix $[I_{66}]$.[22/] (The vector $\underline{x}_f$ is then

---

22/ One is free to specify n arbitrary constants of integration for n first-order linear differential equations.

directly available from equation 106. Substituting the selected value of $\left[\Lambda_f\right]^T$ into equation 103 yields:

$$\underline{x}_f = \left[\Lambda_m\right]^T \underline{x}_m + \int_{t_m}^{t_f} \left[\Lambda\right]^T \left[B\right] \underline{f}\, dt \tag{107}$$

Note that the second goal as stated is to determine what constant value of $\underline{f}$ over the interval will reduce $\underline{x}_f$ to zero. Thus the vector $\underline{f}$ that is of interest is constant over the integration interval and can be taken out of the integrand. This quantity is denoted $\underline{f}_m$ since it is the value of $\underline{f}$ computed at $t = t_m$:

$$\underline{x}_f = \left[\Lambda_m\right]^T \underline{x}_m + \left\{\int_{t_m}^{t_f} \left[\Lambda\right]\left[B\right]\, dt\right\} \underline{f}_m \tag{108}$$

although it would be desirable, it is not possible to find a value of $\underline{f}_m$ that will make all six elements of $\underline{x}_f$ zero. This is obvious from examination of equation 108, since to do so requires the inversion of the matrix:

$$\left[B'_m\right] \triangleq \int_{t_m}^{t_f} \left[\Lambda\right]\left[B\right] dt \tag{109}$$

which is not square. However, if equations 108 and 109 are combined in partitioned form, it is possible to write a third-order matrix equation from which a value of $\underline{f}_m$ that will make any three elements of $\underline{x}_f$ equal to zero can be determined. The appropriate partitioning is shown in equation 110:

$$\begin{bmatrix} \underline{x}_f^{(1)} \\ \underline{x}_f^{(2)} \end{bmatrix} = \begin{bmatrix} \left[\Lambda_m\right]^{(1)} \left[\Lambda_m\right]^{(2)} \\ \left[\Lambda_m\right]^{(3)} \left[\Lambda_m\right]^{(4)} \end{bmatrix} \begin{bmatrix} \underline{x}_m^{(1)} \\ \underline{x}_m^{(2)} \end{bmatrix} + \begin{bmatrix} \left[B'_m\right]^{(1)} \\ B'^{(2)}_m \end{bmatrix} \underline{f}_m \tag{110}$$

where

$\underline{x}_f^{(1)}$, $\underline{x}_f^{(2)}$; $\underline{x}_m^{(1)}$, $\underline{x}_m^{(2)}$, and $\underline{f}_m$ are 3 x 1 column vectors

$\left[\Lambda_m\right]^{(1)}$, $\left[\Lambda_m\right]^{(2)}$, $\left[\Lambda_m\right]^{(3)}$, $\left[\Lambda_m\right]^{(4)}$, $\left[B_m'\right]^{(1)}$ and $\left[B_m'\right]^{(2)}$

are 3 x 3 square matrices.

Writing the expression for $\underline{x}_f^{(1)}$ resulting from equation 109 and setting $\underline{x}_f^{(1)}$ equal to zero results in the following equation, which is easily solved for $\underline{f}_m$:

$$\underline{O}_{31} = \begin{bmatrix} \left[\Lambda_m\right]^{(1)} \\ \left[\Lambda_m\right]^{(3)} \end{bmatrix}^T \begin{bmatrix} \underline{x}_m^{(1)} \\ \underline{x}_m^{(2)} \end{bmatrix} + \left[B_m'\right]^{(1)} \underline{f}_m \tag{111}$$

Therefore:

$$\underline{f}_m = -\left[\left[B_m'\right]^{(1)}\right]^{-1} \begin{bmatrix} \left[\Lambda_m\right]^{(1)} \\ \left[\Lambda_m\right]^{(2)} \end{bmatrix}^T \underline{x}_m$$

$$\triangleq \left[S_m\right] \underline{x}_m \tag{112}$$

Note that any three of the six state variables can be made to appear in $\underline{x}_f^{(1)}$ merely by rearranging the original matrix expression, equation 98.

The matrix $\left[\Lambda\right]$ must be known as a function of time to obtain the value of matrix $\left[S\right]$ as a function of time. This matrix can be evaluated by numerical integration of equation 99. Since final rather than initial conditions are specified on the elements of matrix $\left[\Lambda\right]$, the indicated integration must proceed backwards in time from t_f toward t_o. Recall that $\left[\Lambda(t_f)\right] = \left[\Lambda_f\right]$ is specified to be a 6 x 6 identity matrix.

All quantities required to compute elements of the matrix $\left[S_m\right]$ at any and all times in the interval $t_o \leq t < t_f$ are evaluated on the reference trajectory. Hence this matrix can be precomputed and stored on board the spacecraft. Then at any time t_m in the powered phase of flight, the commanded deviations in $\underline{F}$, denoted $\underline{\hat{f}}_m$, are determined from the expression:

$$\underline{\hat{f}}_m = \left[S_m\right] \underline{\hat{x}}_m \tag{113}$$

where $\underline{\hat{x}}_m$ is the vector of observed deviations in $\underline{X}$ at time t_m. This completes the derivation of the guidance law based on adjoint analysis. This form of guidance is seen to be a linear predictive guidance concept; that is, the guidance law expressions (equations 113) are linear, and control is based on predicted values of the terminal deviations.

6.2 Application of Adjoint Analysis to Sensor Error Evaluation.

This subsection illustrates the application of adjoint analysis techniques to the problem of evaluating the effects on performance of system errors, which were not previously considered. The measure of performance employed is the vector of terminal state deviations, $\underline{x}_f$. The source of error to be investigated is the vehicle navigation sensor system which determines the estimated value of $\underline{x}$, denoted $\underline{\hat{x}}$, upon which acceleration commands are based. When sensor errors are present, $\underline{\hat{x}}$ is not equal to $\underline{x}$; rather:

$$\underline{\hat{x}} = \underline{x} - \underline{\tilde{x}} \tag{114}$$

where $\underline{\tilde{x}}$ is the observation error vector.

To begin the analysis, return to equations 98, which are the linearized equations of motion.

$$\dot{\underline{x}} = \left[A\right] \underline{x} + \left[B\right] \underline{\hat{f}} \tag{115}$$

Quantity $\underline{\hat{f}}$ is the computed command force vector which is determined by using the observed state variable deviations, $\underline{\hat{x}}$, in the guidance law which is to be employed. In practice the actual guidance law equations can be derived in a variety of ways, perhaps emperically, and they can be either linear or nonlinear. However, this discussion deals with a linearized model of the actual vehicle guidance and control system in which the guidance law is represented by the linear matrix equation:

$$\hat{\underline{f}} = \left[S \right] \hat{\underline{x}}$$
$$= \left[S \right] \left\{ \underline{x} - \tilde{\underline{x}} \right\} \tag{116}$$

where the matrix $\left[S \right]$ can be thought of as a matrix of partial derivatives evaluated on the reference trajectory.

In addition, the components of the state vector used in the guidance law (equation 116) are quite often not physical quantities which can be observed directly on board the spacecraft. When this is the case, an additional navigational task is to compute an estimated value of $\underline{x}$ on the basis of the observed value of $\underline{y}$, the vector of observables, the physical quantities which can be measured directly. Vector $\underline{y}$ is the actual deviation of $\underline{Y}$ from the reference value. It is assumed that during powered flight, sufficient observables are used to allow estimation of the vehicle state at any time on the basis of observed information available at that time. The expressions used to perform the estimation of the vehicle state from the observables, termed navigation equations, here, are in general nonlinear geometrical relations and are represented functionally as:

$$\underline{X} = \underline{g} \left(\underline{Y} \right) \tag{117}$$

In the linearized system model the navigation equations take the form

$$\hat{\underline{x}} = \left[G \right] \hat{\underline{y}} \tag{118}$$

where $\left[G \right]$ is a matrix of partial derivatives, relating deviations in $\underline{X}$ to deviations in $\underline{Y}$ evaluated on the reference trajectory, and $\hat{\underline{y}} = \underline{y} - \tilde{\underline{y}}$ where $\tilde{\underline{y}}$ is the vector of sensor errors. Then:

$$\hat{\underline{x}} = \underline{x} - \tilde{\underline{x}} = \left[G \right] \underline{y} - \left[G \right] \tilde{\underline{y}} \tag{119}$$

Since $\underline{x} = \left[G \right] \underline{y}$; and $\tilde{\underline{x}} = \left[G \right] \tilde{\underline{y}}$ in the linearized system, equation 118 can be written in the form:

$$\hat{\underline{x}} = \underline{x} - \left[G \right] \tilde{\underline{y}} \tag{120}$$

Substituting equation 120 into 116 and the result into 115 yields:

$$\dot{\underline{x}} = \left[A' \right] \underline{x} - \left[B' \right] \tilde{\underline{y}} \tag{121}$$

where

$$[A'] \triangleq [A] + [B][S]$$

$$[B'] \triangleq [B][S][G]$$

The equations adjoint to the homogeneous part of equation 121 are:

$$[\dot{\Lambda}] = -[A']^T [\Lambda] \tag{122}$$

Following a procedure identical to that outlined in subsection 6.1 leads to the following equation:

$$\frac{d\{[\Lambda]^T \underline{x}\}}{dt} = -[\Lambda]^T [B'] \tilde{\underline{y}} \tag{123}$$

Equation 123 is next integrated with respect to time over the entire trajectory, since the error inputs of interest exist during the entire flight. If t_o is set equal to zero, this yields:

$$[\Lambda_f]^T \underline{x}_f - [\Lambda_o]^T \underline{x}_o = -\int_o^{t_f} [\Lambda]^T [B'] \tilde{\underline{y}}\, dt \tag{124}$$

As before, we are free to specify the value of $[\Lambda]$ at some time, and it is again convenient to set $[\Lambda_f]$ equal to the identity matrix, since the terminal deviation vector, $\underline{x}_f$, is of primary interest. This makes the terminal deviation vector caused by initial deviations from the reference flight path, $\underline{x}_o$, and by navigation sensor errors during flight, $\tilde{\underline{y}}$, directly available from equation 124. In this particular analysis, which is aimed at evaluating the effects of sensor errors, terminal errors caused by initial deviations are not of interest, so that $\underline{x}_o$ is set equal to zero. It can be seen that this will not in any way affect the determination of sensor error effects as determined by the integral on the right-hand side of equation 121. The following expression results from the preceding considerations:

$$\underline{x}_f = -\int_o^{t_f} [\Lambda]^T [B'] \tilde{\underline{y}}\, dt \tag{125}$$

Two types of error are of interest: bias errors and random fluctuation errors. Bias errors are time-invariant over the performance of any single mission but random over the ensemble of possible missions. Random errors, on the other hand, fluctuate randomly during the course of any given member of the ensemble of missions. It is assumed that the random components of sensor error to be discussed are samples of white [23] stationary Guassian noise with zero mean values. To distinguish between the two types of sensor error, $\tilde{\underline{y}}$ is thought of as the sum of two components, $\tilde{\underline{y}}_b$ and $\tilde{\underline{y}}_n$, representing bias and random errors respectively.

$$\tilde{\underline{y}} = \tilde{\underline{y}}_b + \tilde{\underline{y}}_n \tag{126}$$

Letting $\tilde{\underline{y}}_n$ equal zero leads to rapid conclusion of the analysis of bias errors. Since $\tilde{\underline{y}}_b$ is constant over the mission, it can be removed from the integrand of equation 125.

$$\underline{x}_{fb} = \left\{ - \int_o^{t_f} \left[\Lambda \right]^T \left[B' \right] \, dt \right\} \tilde{\underline{y}}_b \tag{127}$$

$$\underline{x}_{fb} = \left[K_b \right] \tilde{\underline{y}}_b \tag{128}$$

where $\left[K_b \right]$ is a matrix of sensitivity coefficients evaluated by performing the integration indicated in equation 127.

The analysis of random errors is more complicated, since $\tilde{\underline{y}}_n$ is a randomly varying function of time. The function $\tilde{\underline{y}}_n$ (t) cannot be known explicitly; however, it can be described in a statistical sense. Since $\tilde{\underline{y}}_n$ has been stated to be white noise, the mean squared value of $\tilde{\underline{y}}_n$ is not defined. However, each of the elements of $\tilde{\underline{y}}_n$ can be characterized by its power spectral density. The spectral density of $\tilde{y}_{qn}$, defined as W_{qn} is constant

---

[23] Nonwhite noise can be handled by assuming that the desired spectral distribution is generated by passing white noise through a suitable linear shaping filter (Ref. 11). The shaping filter is then included in the system described by the linearized equations of motion.

Ref. 11 Laning, J.H. and R.H. Battin, Random Processes in Automatic Control, New York; McGraw-Hill, 1956.

over the range of frequencies $-\infty < f < +\infty$. Also defined is the auto-correlation function of $\tilde{y}_{qn}$ which is denoted $R_q(\tau)$ and is equal to:

$$R_q(\tau) = \text{av}\left\{ \tilde{y}_{qn}(\tau)\, \tilde{y}_{qn}(t+\tau) \right\} ; \; q = 1, \; 2, \; \ldots Q \tag{129}$$

where Q is the total number of observables. In addition, random errors in each of the observables are assumed to be independent; that is,

$$\text{av}\left\{ \tilde{y}_{pn}(t_1)\, \tilde{y}_{qn}(t_2) \right\} = 0 \tag{130}$$

for $p \neq q$ and for any values of t_1 and t_2. Another method of obtaining $R_q(\tau)$ is the use of the Wiener-Khintchine relationship, which states:

$$R_q(\tau) = \frac{1}{2} \int_{-\infty}^{\infty} W_q(f)\, e^{j2\pi f\tau}\, df \tag{131}$$

$$= \frac{W_{qn}}{2} \int_{-\infty}^{\infty} e^{j2\pi f\tau}\, df = \frac{W_{qn}}{2}\, \delta(\tau)$$

where $\delta(\tau)$ is a Dirac delta function at $\tau = 0$.

The preceding information is useful in the further analysis of equation 125 with $\underline{\tilde{y}}_b$ set to zero:

$$\underline{x}_{fn} = -\int_{o}^{t_f} \left[\Lambda\right]^T \left[B'\right] \underline{\tilde{y}}_n\, dt \tag{132}$$

The quantity $\underline{x}_{fn}$ is a random variable which can only be discribed in terms of statistical averages. It is clear that the average value of $\underline{x}_{fn}$ is zero, since the average value of $\underline{\tilde{y}}_n$ is zero. Of greater significance, as explained in section 4, is the covariance matrix of $\underline{x}_{fn}$ which is denoted $\left[N_f\right]$ are defined:

$$\left[N_f\right] \triangleq \text{av}\left\{ \underline{x}_{fn}\, \underline{x}_{fn}^T \right\} \tag{133}$$

Substituting equations 132 into 133 yields:

$$\left[N_f \right] = \text{av} \left\{ \int_o^{t_f} \int_o^{t_f} \left[D(t_1) \right] \tilde{\underline{y}}_n(t_1) \, \tilde{\underline{y}}_n(t_2)^T \left[D(t_2) \right]^T dt_1 \, dt_2 \right\} \tag{134}$$

where

$$\left[D \right] \triangleq \left[\Lambda \right]^T \left[B' \right] \tag{135}$$

The averaging process in equation 134 can be moved inside the integrand:

$$\left[N_f \right] = \int_o^{t_f} \int_o^{t_f} \left[D(t_1) \right] \text{av} \left\{ \tilde{\underline{y}}_n(t_1) \, \tilde{\underline{y}}_n(t_2)^T \right\} \left[D(t_2) \right]^T dt_1 \, dt_2 \tag{136}$$

The quantity $\text{av} \left\{ \tilde{\underline{y}}_n(t_1) \, \tilde{\underline{y}}_n(t_2) \right\}$ is seen to be zero when $t_1 \neq t_2$ and equal to $\left[Q(t_1) \right]$, the covariance matrix of $\tilde{\underline{y}}_n$, when $t_1 = t_2$:

$$\left[Q(t_1) \right] \triangleq \text{av} \left\{ \tilde{\underline{y}}_n(t_1) \, \tilde{\underline{y}}_n(t_1)^T \right\} \tag{137}$$

The off-diagonal terms of $\left[Q(t_1) \right]$ are zero by equation 130, while the diagonal elements are given by equation 129:

$$\left[Q(\tau) \right] = \frac{1}{2} \left[W_n \right] \delta(\tau) \tag{138}$$

where

$$\left[W_n \right] \triangleq \begin{bmatrix} W_{1n} & 0 & \cdots & 0 \\ 0 & W_{2n} & \cdots & 0 \\ \vdots & & \ddots & \\ 0 & 0 & & W_{Qn} \end{bmatrix} \tag{139}$$

and

$$\tau = t_1 - t_2$$

Thus equation 136 can be written (Ref. 11):

$$\left[N_f\right] = \frac{1}{2} \int_o^{t_f} \left[D(t_1)\right] \left[W_n\right] \left[D(t_1)\right]^T dt_1 \tag{140}$$

It is the diagonal terms of $\left[N_f\right]$ that are of particular interest. They are the mean squared values of the terminal deviations of each of the state variables. Define:

$\underline{\sigma}_{fn}^2$ as a column vector made up of the diagonal elements of $\left[N_f\right]$. The p^{th} element of $\underline{\sigma}_{fn}^2$ is equal to av $\left\{(\underline{x}_\rho)_{fn}^2\right\}$.

$\underline{W}_n$ as a column vector made up of the diagonal terms of matrix $\left[W_n\right]$.

$$\underline{W}_n \triangleq \begin{bmatrix} W_{1n} \\ W_{2n} \\ \vdots \\ W_{Qn} \end{bmatrix} \tag{141}$$

Subject to these definitions, it can be shown by expanding equation 140 that,

$$\underline{\sigma}_{fn}^2 = \left[K_n\right] \underline{W}_n \tag{142}$$

where $(k_{pq})_n$, the general element of (K_n), is defined as:

$$(k_{pq})_n = \frac{1}{2} \int_o^{t_f} \left\{ d_{pq}(t_1) \right\}^2 dt_1 \tag{143}$$

Quantity $d_{pq}(t_1)$ is the pq^{th} element of $\left[D(t_1)\right]$.

Matrix $\left[K_n\right]$ is therefore a matrix of sensitivity coefficients which can be used to estimate the mean squared terminal error components caused by random sensor errors as characterized by the average power spectral density

associated with the noise input to each sensor. The value of $\left[\Lambda(t_1)\right]$ is obtained by numerical integration backward in time from $t = t_f$ with $\left[\Lambda(t_f)\right]$ specified to be the identity matrix. Matrix $\left[B'(t_1)\right]$ in equation 121 is evaluated using the reference values of $\underline{X}(t_1)$ and $\underline{F}(t_1)$. Thus it can be seen that all the information required to compute the matrix $\left[K_n\right]$ is available.

In conclusion, sensitivity coefficient matrices have been derived which can be used to estimate the effects of both bias and random sensor errors on terminal state deviations.

APPENDIX B

MIDCOURSE PHASE

In this appendix the equations for midcourse guidance are derived. The mathematical notations used are listed below.[1]

$\underline{x}(t)$	6-component state vector whose components are ΔX, ΔY --- $\Delta \dot{Z}$
$F(t)$	6x6 matrix used in writing linearized equations of motion
$\Phi(t, t_o)$	6x6 transition matrix which relates deviations at t to deviations at t_o
I_{ii}, O_{ij}	i-by-i and i-by-j unit and null matrices respectively
f_{ij}, ϕ_{ij}	Components of $F(t)$ and $\Phi(t, t_o)$ matrices
ζ	Angle between star sightline and planet center
$\underline{S}$	Unit vector along star sightline
a, b, c	Components of $\underline{S}$ (star direction cosines)
X, Y, Z	Spacecraft position components in earth-centered coordinates
X_m, Y_m, Z_m	Moon position components in earth-centered coordinates
$H(t)$	Matrix relating measurement deviations to state deviations
$\underline{R}$	Position vector
R	Range
θ	Half-subtense angle of visible disc of planet

---

[1] This list does not include the notation used in Sections 2 and 9, which in many cases conflicts with the notation used in other sections.

$\underline{H}$	Vector from spacecraft to horizon
r	Planet radius
ζ_h	Angle between star direction and near horizon
ζ_f	Angle between star direction and far horizon
$E\{\ \}$	Expected value
$\hat{\underline{x}}(t)$	Estimated value of $\underline{x}(t)$
$\tilde{\underline{x}}(t)$	Error in estimate of $\underline{x}(t)$
$\underline{\Delta \tilde{V}}$	6-vector, whose three position components are zero and whose three velocity components are the errors in measuring the velocity correction
P	Covariance matrix of estimation errors
N	Covariance matrix of deviations from the nominal trajectory
G	Matrix relating corrected state to estimated state
$\underline{x}_Q$	Error in implementing the velocity correction (6-vector whose three position components are zero)
S	Subsidiary variable in Section 4; 6x6 covariance matrix of velocity correction errors in Section 5
S'	3x3 covariance matrix of velocity correction error
$\dot{X}_Q$	3-vector consisting of errors in implementing velocity corrections
σ_k^2	Variance of errors in magnitude of applied correction velocity
σ_κ^2	Variance of errors in percentage thrust error in velocity corrections
σ_e^2	Variance of errors in timing of correction thrust
σ_γ^2	Variance of errors in pointing direction of velocity corrections
$\lvert \dot{X}_{QT} \rvert$	Magnitude error in applied correction
μ_e, μ_m	Gravitational constants of earth and moon
ψ_o	Angle from moon's ascending line of nodes to the earth-moon line at t_o

T	Orbital period of moon
ϕ	Inclination of lunar orbit plane to earth's equator
$K(t_k)$	Weighting vector
Q	Measurement variance
k_i	Standard deviation of reference point error on earth (k_1) and moon (k_2)
σ^2	Variance of optical instrument errors
σ_R^2	Variance of ranging errors
V	Covariance matrix of velocity corrections
$A_1(t_k)$, $A_2(t_k)$	Upper 3x3 submatrices of $\Phi(t_A, t_k)$ (Section 6)
G'	3x6 matrix relating state deviations to correction commands
u, Δv	RMS correction velocity
r	RMS position deviation from nominal
v	RMS velocity deviation from nominal
$\tilde{r}$	RMS position estimation error
$\tilde{v}$	RMS velocity estimation error
$\Sigma\Delta v$	Total of rms correction velocities in flight
$T(t_k)$	Target uncertainty at t_k
r_t	RMS position uncertainty at target
v_t	RMS velocity uncertainty at target
M	Rotation matrix from XYZ coordinates to downrange-crossrange-altitude coordinates
$\Delta\zeta$	Angle measurement error
V_s	Magnitude of spacecraft velocity
Δt	Error in timing a measurement
R_L	Range from spacecraft to some surface reference point
ξ	Angle between sightline to reference point and vehicle velocity vector
σ_ζ	RMS measurement error due to timing, landmark, and instrument uncertainties

$\sigma_L, \sigma_I, \sigma_T$	RMS errors due to timing, instrument, and landmark uncertainties
$E(t)$	Matrix of partials of vehicle accelerations with respect to astrodynamic constants
$\underline{e}$	3-vector of astrodynamic uncertainties
$\underline{y}(t)$	Measurement vector
$\underline{n}(t)$	Noise on each measurement
$\underline{w}(t)$	State of dynamic measurement noise process
$\underline{u}(t)$	Gaussian input to noise process
$\Gamma(t)$	Matrix relating state of noise process to measurement noise
$W(t)$	Matrix related to noise process
$\underline{x}^*(t)$	Augmented state vector, composed of $\underline{x}(t)$, $\underline{e}(t)$ and $\underline{w}(t)$
$*$	Refers to augmented matrices and vectors in general
$M(t)$	Matrix which relates observations to augmented state vector
Φ_w	Transition matrix of noise process (Section 8)
A_1, A_2	Time constants of measurement noise
R_{em}	Earth-moon distance
$\Delta\mu_m, \Delta R_{em}, \Delta\mu_e$	Errors in astrodynamic constants
$\Delta\underline{\tilde{x}}_m$	Error in estimation of moon's state (in earth coordinates)
$\underline{\tilde{x}}_m$	Error in estimation of vehicle state after transformation in lunar coordinates
$\underline{a}, \underline{d}, \underline{c}$	Unit vectors in coordinate system defined by nominal altitude, downrange, and crossrange directions at periselenum
$\underline{r}_e$	Position error 3-vector at periselenum
e_x, e_y, e_z	Components of $\underline{r}_e$ in X, Y, Z directions
e_a, e_d, e_c	Components of $\underline{r}_e$ in $\underline{a}$, $\underline{d}$, $\underline{c}$ directions
M'	The 3 x 3 matrix required to rotate position errors from XYZ coordinates into $\underline{adc}$ coordinates
$\underline{v}_e$	Velocity error 3-vector at periselenum

$\underline{\varepsilon}_e$ Periselenum error 6-vector composed of $\underline{r}_e$ and $\underline{v}_e$

P_a P matrix in adc coordinates

1. COMPUTATION OF TRANSITION MATRICES

In this section the computation of the transition (Φ) matrices is derived. These transition matrices relate state deviations at some time (t) to state deviations at some initial time t_o.

In paragraph 2.3.1.2 of Volume III, the linearized equations of motion are written in matrix form:

$$\dot{\underline{x}}(t) = F(t)\underline{x}(t) \tag{1}$$

where $\underline{x}(t)$ is the 6-vector of state deviations (ΔX, ΔY..... $\Delta \dot{Z}$).

It is well known (Ref. 1) that the solution of equation 1 is given by:

$$\underline{x}(t) = \Phi(t, t_o)\underline{x}(t_o) \tag{2}$$

where $\Phi(t, t_o)$ is the 6 x 6 matrix defined by:

$$\frac{d\Phi(t, t_o)}{dt} = F(t)\Phi(t, t_o) \tag{3}$$

where

$$\Phi(t_o, t_o) = I_{66} \tag{4}$$

for all t_o.

Writing equation 3 in expanded form,

$$\begin{bmatrix} \dot{\phi}_{11} & \dot{\phi}_{12} & - & - & - & \dot{\phi}_{16} \\ \dot{\phi}_{21} & - & - & - & - & - \\ - & - & - & - & - & - \\ - & - & - & - & - & - \\ - & - & - & - & - & - \\ \dot{\phi}_{61} & - & - & - & - & - \end{bmatrix} = \begin{bmatrix} f_{11} & f_{12} & - & - & - & f_{16} \\ f_{21} & - & - & - & - & - \\ - & - & - & - & - & - \\ - & - & - & - & - & - \\ - & - & - & - & - & - \\ f_{61} & - & - & - & - & f_{66} \end{bmatrix} X \begin{bmatrix} \phi_{11} & \phi_{12} & - & - & - & \phi_{16} \\ \phi_{21} & - & - & - & - & - \\ - & - & - & - & - & - \\ - & - & - & - & - & - \\ - & - & - & - & - & - \\ \phi_{61} & - & - & - & - & \phi_{66} \end{bmatrix} \tag{5}$$

Ref. 1. Bellman, R. E., Introduction to Matrix Analysis, New York: McGraw-Hill, 1960.

where

$$\left.\begin{array}{l} \phi_{11}(0) = 1 \qquad \phi_{ij}(0) = 0,\ i = j \\ \phi_{22}(0) = 1 \\ | \\ | \\ | \\ | \\ | \\ \phi_{66}(0) = 1 \end{array}\right\} \tag{6}$$

Writing out equation 5,

$$\begin{aligned} \dot{\phi}_{11} &= f_{11}\phi_{11} + f_{12}\phi_{21} + - - - - f_{16}\phi_{61} \\ \dot{\phi}_{21} &= f_{21}\phi_{11} + f_{22}\phi_{21} + - - - \quad f_{26}\phi_{61} \\ &- \quad - \qquad - \qquad - \\ &- \quad - \qquad - \qquad - \\ &- \quad - \qquad - \qquad - \\ \dot{\phi}_{61} &= f_{61}\phi_{11} + f_{62}\phi_{12} + - - - \quad f_{66}\phi_{61} \end{aligned} \tag{7}$$

where $\phi_{11}(0) = 1$ and $\phi_{1j}(0) = 0$ for $j \neq 1$. Simultaneous solution of equation 7 with these initial conditions will yield the quantities ϕ_{11}, ϕ_{21} - - - ϕ_{61}.

The other five columns of the matrix $\Phi(t, t_o)$ can be generated in similar fashion, except that for the second column, $\phi_{22}(0) = 1$ and $\phi_{2j}(0) = 0$ for $j \neq 2$ and so on.

It should be kept in mind that the elements of the F(t) matrix (f_{ij}) are in general time-varying, since F(t) is given by

$$F(t) = \begin{bmatrix} 0 & 0 & 0 & 1 & 0 & 0 \\ 0 & 0 & 0 & 0 & 1 & 0 \\ 0 & 0 & 0 & 0 & 0 & 1 \\ \partial f_{1}/\partial x & \partial f_{1}/\partial y & \partial f_{1}/\partial z & 0 & 0 & 0 \\ \partial f_{2}/\partial x & \partial f_{2}/\partial y & \partial f_{2}/\partial z & 0 & 0 & 0 \\ \partial f_{s}/\partial x & \partial f_{3}/\partial y & \partial f_{3}/\partial z & 0 & 0 & 0 \end{bmatrix} \quad (8)$$

where the partials $\partial f_{1}/\partial x$, etc are evaluated along the reference trajectory. Thus, in the computer program used in this study, each column of the Φ matrices was developed by simultaneous solution of both the linearized equations 7 and the nonlinear differential equations of motion (equations 84 through 86).

2. APPLICATION OF KALMAN'S RESULTS TO SPACE NAVIGATION

In paragraph 2.3.1.3 of Volume III, it was stated that equations 2-20 through 2-22 were solutions to the problem of making a minimum variance estimate of a trajectory based on noisy observations and an initial estimate. It was stated that these equations were Kalman's. However, since the exact problem formulation and notation used by Kalman in Ref. 2 and that used in this report (and Ref. 3) are different, this section presents a precise derivation of equations 2-20 through 2-22 in order to bridge the notation gap.

Kalman's results are as follows. Given a dynamic model represented by the following equations:

$$\underline{x}(t+1) = \Phi(t+1, t)\,\underline{x}(t) + u(\underline{t}) \quad (9)$$

$$\underline{y}(t) = M(t)\underline{x}(t) \quad (10)$$

where $\underline{u}(t)$ is an independent Gaussian random process of n-vectors with zero mean, $\underline{x}(t)$ is an n-vector, $\underline{y}(t)$ is a p-vector ($p \leq n$), $\Phi(t+1, t)$ and $M(t)$ are n x n and p x n matrices respectively whose elements are nonrandom functions of time.

Ref. 2 Kalman, R. E., A New Approach to Linear Filtering and Prediction Problems, Jour. of Basic Engr., March 1960, pp. 35-45.

Given observed $\underline{y}(t_o) \ldots\ldots \underline{y}(t)$, find the estimate $\underline{x}^*(t_1/t)$ of $\underline{x}(t_1)$ which minimizes the expected loss. The results derived in Ref. 2 in equations 21, 28, 29 and 30 are listed below.

$$\underline{x}^*(t+1 \mid t) = \Phi^*(t+1 \mid t)\underline{x}^*(t \mid t-1) + \Delta^*(t)\underline{y}(t) \tag{11}$$

$$\Delta^*(t) = \Phi(t+1, t)P^*(t)M'(t)\left[M(t)P^*(t)M'(t)\right]^{-1} \tag{12}$$

$$\Phi^*(t+1, t) = \Phi(t+1, t) - \Delta^*(t)M(t) \tag{13}$$

$$P^*(t+1) = \Phi^*(t+1, t)P^*(t)\Phi'(t+1, t) + q(t) \tag{14}$$

where $q(t) = E\left\{u(t)u'(t)\right\}$

Also, as Kalman shows, P^* can be written

$$P^*(t+1) = \Phi(t+1, t)\left[P^*(t) - P^*(t)M'(t)(M(t)P^*(t)M'(t))^{-1} \text{ times } P^*(t)M(t)\right]\Phi'(t+1, t) + q(t) \tag{15}$$

Equations 11 through 15 are all written in Kalman's notation in which (') is a transpose and $\underline{x}^*$ indicates the optimal estimate of $\underline{x}$. Converting this notation to that used in paragraph 2.3.1.3, of Volume III where $(\ )^T$ denotes a transpose, $\hat{\underline{x}}$ an optimal estimate, and denoting the observation times t_k, t_{k-1} ..... etc,

$$\hat{\underline{x}}(t_{k+1} \mid t_k) = \Phi^*(t_{k+1}, t_k)\hat{\underline{x}}(t_k \mid t_{k-1}) + \Delta^*(t_k)y(t_k) \tag{16}$$

$$\Delta^*(t_k) = \Phi(t_{k+1}, t_k)P^*(t_k)M^T(t_k)\left\{M(t_k)P^*(t_k)M^T(t_k)\right\}^{-1} \tag{17}$$

$$\Phi^*(t_{k+1}, t_k) = \Phi(t_{k+1}, t_k) - \Delta^*(t_k)M(t_k) \tag{18}$$

$$P^*(t_{k+1}) = \Phi(t_{k+1}, t_k)\left\{P^*(t_k) - P^*(t_k)M^T(t_k)\left[M(t_k)P^*(t_k)M^T(t_k)\right]^{-1} \text{ times } P^*(t_k)M(t_k)\right\}\Phi^T(t_{k+1}, t_k) + Q(t_k) \tag{19}$$

Ref. 3 Smith, G. L., S. F. Schmidt, and L. A. McGee, Application of Statistical Filter Theory to Optimal Estimation of Position and Velocity on Board a Circumlunar Vehicle, NASA Ames, NASA TR R-135, 1962.

Now, define the following:

$$K(t_k) = P^*(t_k)M^T(t_k)\left\{ M(t_k)\ P^*(t_k)M^T(t_k) \right\}^{-1} \tag{20}$$

Substituting into equations 16 through 19,

$$\hat{\underline{x}}(t_{k+1}\,|\,t_k) = \Phi^*(t_{k+1}, t_k)\hat{\underline{x}}(t_k, t_{k-1}) + \Phi(t_{k+1}, t_k)\,K(t_k)\underline{y}(t_k) \tag{21}$$

$$\Delta^*(t_k) = \Phi(t_{k+1}, t_k)\,K(t_k) \tag{22}$$

$$\Phi^*(t_{k+1}, t_k) = \Phi(t_{k+1}, t_k) - \Phi(t_{k+1}, t_k)K(t_k)M(t_k) \tag{23}$$

$$P^*(t_{k+1}) = \Phi(t_{k+1}, t_k)\left[P^*(t_k) - K(t_k)P^*(t_k)M(t_k)\right]\Phi^T(t_{k+1}, t_k) \tag{24}$$

$$+\,Q(t_k)$$

Now equation 23 can be substituted in equation 21, and equation 22 is no longer necessary, so that:

$$\hat{\underline{x}}(t_{k+1}\,|\,t_k) = \left[\Phi(t_{k+1}, t_k) - \Phi(t_{k+1}, t_k)K(t_k)M(t_k)\right]\hat{\underline{x}}(t_k\,|\,t_{k-1}) \tag{25}$$

$$+\,\Phi(t_{k+1}, t_k)K(t_k)\underline{y}(t_k)$$

$$K(t_k) = P^*(t_k)M^T(t_k)\left\{M(t_k)P^*(t_k)M^T(t_k)\right\}^{-1} \tag{26}$$

$$P^*(t_{k+1}) = \Phi(t_{k+1}, t_k)\left\{P^*(t_k) - K(t_k)P^*(t_k)M(t_k)\right\}\Phi^T(t_{k+1}, t_k) \tag{27}$$

$$+\,Q(t_k)$$

Rearranging equation 25,

$$\hat{\underline{x}}(t_{k+1} \mid t_k) = \Phi(t_{k+1}, t_k)\hat{\underline{x}}(t_k \mid t_{k-1}) + \Phi(t_{k+1}, t_k)K(t_k)\left[y(t_k) - M(t_k)\hat{\underline{x}}(t_k \mid t_{k-1}) \right] \quad (28)$$

The transition matrix $\Phi(t_{k+1}, t_k)$ is used to translate the optimal estimate $\hat{\underline{x}}$ from t_k to t_{k+1}. Therefore the optimal estimate of $\underline{x}(t_k)$ including the observation at t_k is given by

$$\hat{\underline{x}}(t_k \mid t_k) = \hat{\underline{x}}(t_k \mid t_{k-1}) + K(t_k)\left[\underline{y}(t_k) - M(t_k)\hat{\underline{x}}(t_k \mid t_{k-1}) \right] \quad (29)$$

Since $\hat{\underline{x}}(t_k \mid t_{k-1}) = \Phi(t_k, t_{k-1})\hat{\underline{x}}(t_{k-1} \mid t_{k-1})$

$$\hat{\underline{x}}(t_k \mid t_k) = \Phi(t_k, t_{k-1})\hat{\underline{x}}(t_{k-1} \mid t_{k-1}) + K(t_k)\left[y(t_k) - M(t_k)\Phi(t_k, t_{k-1})\hat{\underline{x}}(t_{k-1} \mid t_{k-1}) \right] \quad (30)$$

Equations 26, 27 and 30 specify the recursion process. Letting $\hat{\underline{x}}(t_k/t_k)$ be denoted by $\hat{\underline{x}}(t_k)$ and writing equations 26, 27, and 30 in terms of the "augmented" state notation used in paragraph 2.3.1.3, Volume III:

$$\hat{\underline{x}}^*(t_k) = \Phi^*(t_k, t_{k-1})\hat{\underline{x}}^*(t_{k-1}) + K^*(t_k)\left\{ y(t_k) - M(t_k)\Phi^*(t_k, t_{k-1})\hat{\underline{x}}(t_{k-1}) \right\} \quad (31)$$

$$K^*(t_k) = P^*(t_k)M^T(t_k)\left\{ M(t_k)P^*(t_k)M^T(t_k) \right\}^{-1} \quad (32)$$

$$P^*(t_{k+1}) = \Phi(t_{k+1}, t_k)\left\{P^*(t_k) - K(t_k)M(t_k)P^*(t_k)\right\}\Phi^T(t_{k+1}, t_k) \quad (33)$$

$$+ Q^*(t_{k+1}, t_k)$$

$$Q^*(t_{k+1}, t_k) = \int_{t_k}^{t_{k+1}} \Phi_n(t_{k+1}, t_k)\, E\left\{\underline{u}_n(\tau)\underline{u}_n^T(\tau)\right\}\Phi_n^T(t_{k+1}, t_k)d\tau \quad (34)$$

3. DERIVATION OF RELATIONS BETWEEN STATE VARIABLES AND OBSERVABLES

In this section the relations between the state variables X, Y..... $\dot{Z}$ and the observables are derived for various types of measurements.

3.1 Angle Between Planet Center and Star Direction

Figure 1, illustrates the situation in which each observation consists of the measurement of the angle ζ between some star direction and the center of the earth or moon.

When the angle ζ to the center of the earth (ζ_e) is measured and the measurements are being referenced to an earth-centered inertial coordinate system, then H, the matrix of partials of ζ_e with respect to the state variables is developed as follows:

$$H = \left[\frac{\partial \zeta_e}{\partial x} \quad \frac{\partial \zeta_e}{\partial y} \quad \frac{\partial \zeta_e}{\partial z} \quad 0 \quad 0 \quad 0\right] \quad (35)$$

Let $\underline{R}_e = X\underline{i} + Y\underline{j} + Z\underline{k}$ be the position vector of the vehicle in earth coordinates and $\underline{S} = a\underline{i} + b\underline{j} + c\underline{k}$ be the unit vector representing the star direction.

Then

$$\zeta_e = \cos^{-1}\left(\frac{\underline{R}_e \cdot \underline{S}}{|\underline{R}_e||\underline{S}|}\right) = \cos^{-1}\left(\frac{\underline{R}_e \cdot \underline{S}}{R_e}\right) \quad (36)$$

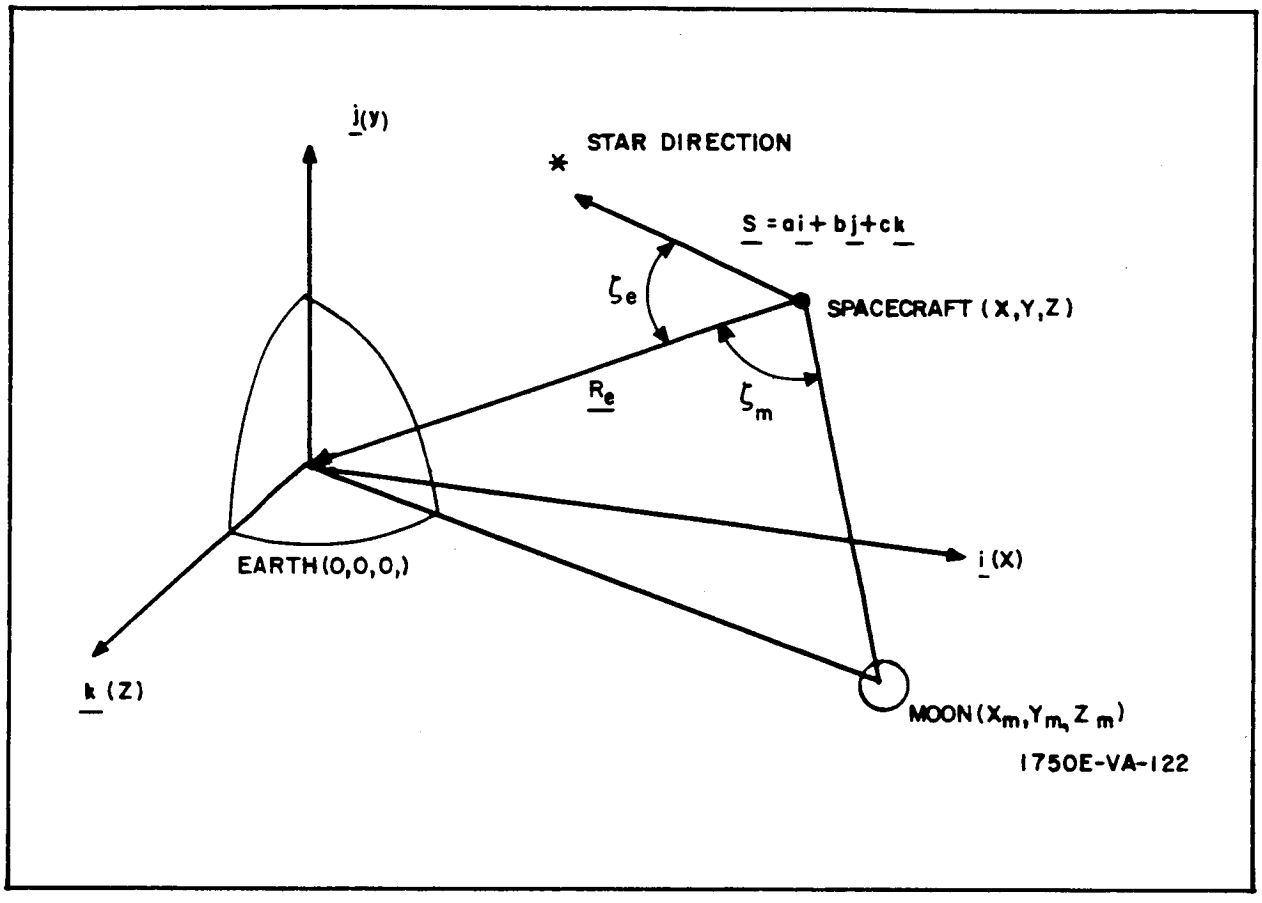

Figure 1. Geometry of Earth-Star Measurement

$$\zeta_e = \cos^{-1}\left(\frac{-aX + bY + cZ}{R_e}\right) = \cos^{-1} d_e \tag{37}$$

$$\frac{\partial \zeta_e}{\partial X} = -\frac{1}{\sqrt{1 - d_e^2}}\left(\frac{\partial d_e}{\partial X}\right) \tag{38}$$

Therefore

$$\left.\begin{aligned} \frac{\partial \zeta_e}{\partial X} &= \frac{aR_e + Xd_e}{R_e^2\sqrt{1 - d_e^2}} \\ \frac{\partial \zeta_e}{\partial Y} &= \frac{bR_e + Yd_e}{R_e^2\sqrt{1 - d_e^2}} \\ \frac{\partial \zeta_e}{\partial Z} &= \frac{cR_e + Zd_e}{R_e^2\sqrt{1 - d_e^2}} \end{aligned}\right\} \tag{39}$$

where

$$\left.\begin{aligned} d_e &= -\left(\frac{aX + bY + cZ}{R_e}\right) \\ \text{and} \\ R_e &= \sqrt{X^2 + Y^2 + Z^2} \end{aligned}\right\} \tag{40}$$

Equations 39 and 40 also apply to the case of angle measurements from a star to the moon in a lunar coordinate system, except that the quantities subscripted by e in equations 39 and 40 are referred to the moon instead.

When a moon-star angle ζ_m is referenced to earth coordinates (or vice versa), let

$$-\underline{R}_{vm} = (X_m - X)\,\underline{i} + (Y_m - Y)\,\underline{j} + (Z_m - Z)\,\underline{k} \tag{41}$$

where X_m, Y_m, and Z_m are the coordinates of the moon in an earth-centered system. Then, proceeding as before, with the star direction defined by $S = a\underline{i} + b\underline{j} + c\underline{k}$,

$$\left.\begin{aligned}
\frac{\partial \rho_m}{\partial X} &= \frac{aR_{vm} + (X - X_m)\, d_{vm}}{R_{vm}^2 \sqrt{1 - d_{vm}^2}} \\
\frac{\partial \rho_m}{\partial Y} &= \frac{bR_{vm} + (Y - Y_m)\, d_{vm}}{R_{vm}^2 \sqrt{1 - d_{vm}^2}} \\
\frac{\partial \rho_m}{\partial Z} &= \frac{cR_{vm} + (Z - Z_m)\, d_{vm}}{R_{vm}^2 \sqrt{1 - d_{vm}^2}}
\end{aligned}\right\} \qquad (42)$$

where

$$\left.\begin{aligned}
d_{vm} &= -\left[\frac{a(X - X_m) + b(Y - Y_m) + c(Z - Z_m)}{R_{vm}}\right] \\
\text{and} \qquad & \qquad (43) \\
R_{vm} &= \sqrt{(X - X_m)^2 + (Y - Y_m)^2 + (Z - Z_m)^2}
\end{aligned}\right\}$$

The case of an earth observation referred to lunar coordinates is similar, of course, to equations 41 and 42.

3.2 Direct Range Measurements

For direct range measurements, the H matrix is given by:

$$H = \left[\frac{\partial R}{\partial X} \quad \frac{\partial R}{\partial Y} \quad \frac{\partial R}{\partial Z} \quad 0 \; 0 \; 0\right] \qquad (44)$$

For an earth range measurement in earth coordinates,

$$R = R_e = \sqrt{X^2 + Y^2 + Z^2} \qquad (45)$$

$$\left.\begin{aligned}
\partial R_e / \partial X &= X / R_e \\
\partial R_e / \partial Y &= Y / R_e \\
\partial R_e / \partial Z &= Z / R_e
\end{aligned}\right\} \qquad (46)$$

The results are identical in lunar coordinates.

3.3 Range Rate Measurements

For a system employing range rate as the observable, the H matrix is given by:

$$H = \left[\frac{\partial \dot{R}}{\partial X} \frac{\partial \dot{R}}{\partial Y} \frac{\partial \dot{R}}{\partial Z} \frac{\partial \dot{R}}{\partial \dot{X}} \frac{\partial \dot{R}}{\partial \dot{Y}} \frac{\partial \dot{R}}{\partial \dot{Z}} \right] \tag{47}$$

$$\text{Since } R = \sqrt{X^2 + Y^2 + Z^2} \tag{48}$$

$$\text{and } \dot{R} = \frac{X\dot{X} + Y\dot{Y} + Z\dot{Z}}{R}$$

$$\frac{\partial \dot{R}}{\partial X} = \frac{\dot{X}}{R} - \frac{X\dot{R}}{R^2}$$

$$\frac{\partial Y}{\partial R} - \frac{Y\dot{R}}{R^2}$$

$$\frac{\partial \dot{R}}{\partial Z} = \frac{\dot{Z}}{R} - \frac{Z\dot{R}}{R^2}$$

$$\partial \dot{R}/\partial \dot{X} = X/R \tag{49}$$

$$\partial \dot{R}/\partial \dot{Y} = Y/R$$

$$\partial \dot{R}/\partial \dot{Z} = Z/R$$

3.4 Optical Ranging by Measurement of Planet Disc

By measuring the apparent size of the planet from the spacecraft, range can be determined. In figure 2 the range is given in terms of θ, the half-subtense angle, by

$$R = \frac{r}{\sin \theta} \tag{50}$$

Then $H = \left[\frac{\partial R}{\partial X} \frac{\partial R}{\partial Y} \frac{\partial R}{\partial Z} 0 \; 0 \; 0 \right]$ and the partials are given by equation 46.

$$\partial R/\partial X = X/R \tag{51}$$

$$\partial R/\partial Y = Y/R$$

$$\partial R/\partial Z = Z/R$$

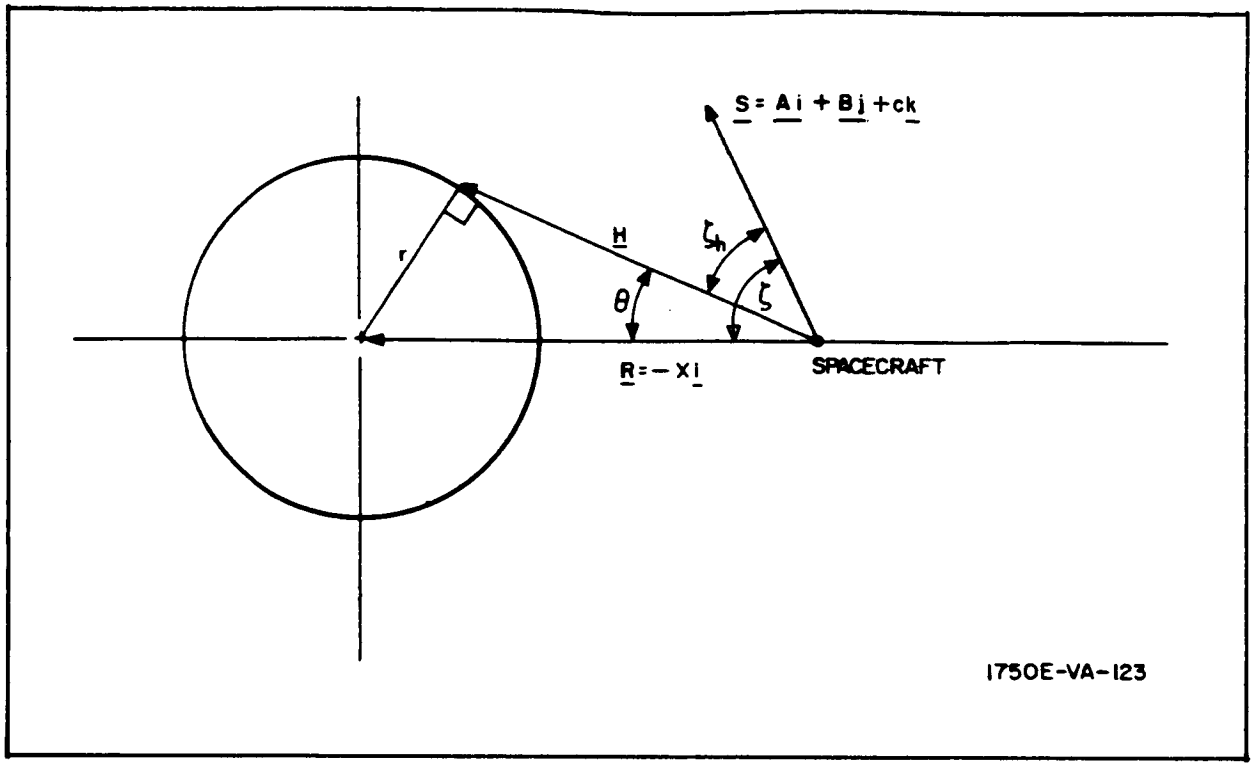

Figure 2. Planar Geometry of Star Horizon Angle Measurement

If the observed angle θ is used directly, then $H = \left[\partial\theta/\partial X \;\; \partial\theta/\partial Y \;\; \partial\theta/\partial Z \;\; 0 \;\; 0 \;\; 0 \right]$ and since $\theta = \sin^{-1}(r/R)$,

$$\left.\begin{aligned} \partial\theta/\partial X &= \frac{-X}{\sqrt{R\,(R^2 - r^2)}} \\ \partial\theta/\partial Y &= \frac{-Y}{\sqrt{R(R^2 - r^2)}} \\ \partial\theta/\partial Z &= \frac{-Z}{\sqrt{R(R^2 - r^2)}} \end{aligned}\right\} \qquad (52)$$

3.5 Star-Horizon Measurements

One way of measuring the angle between some star direction and a reference point on the earth or moon is to measure the elevation angle of a star above the horizon of the planet. This type of measurement is

illustrated by ζ_h in figure 35. The figure shows that the star horizon angle is equal to the difference between the angle ζ and the half-subtense angle θ; i. e.,

$$\zeta_h = \zeta - \theta \tag{53}$$

From equations 37 and 50

$$\zeta_h = \cos^{-1}\left(\frac{aX + bY + cZ}{R}\right) - \sin^{-1}\left(\frac{r}{R}\right) \tag{54}$$

Letting $H = \left[\partial\zeta_h/\partial X \quad \partial\zeta_h/\partial Y \quad \partial\zeta_h/\partial Z \quad 0 \quad 0 \quad 0\right]$, the components can be determined by differentiating equation 52:

$$\frac{\partial\zeta_h}{\partial X} = \frac{\partial\zeta}{\partial X} - \frac{\partial\theta}{\partial X}$$

From equations 39, 40, and 52, the partials are derived:

$$\frac{\partial\zeta_h}{\partial X} = \frac{aR + Xd}{R^2\sqrt{1-d^2}} + \frac{X}{\sqrt{R(R^2-r^2)}} \tag{55}$$

where

$$d = -\left(\frac{aX + bY + cZ}{R}\right) \tag{56}$$

If the angle from a star to the far horizon, rather than the near horizon as above, is used, then equation 54 becomes

$$\zeta_h = \zeta + \vartheta \tag{57}$$

and succeeding equations are modified accordingly.

4. EFFECT OF VELOCITY CORRECTIONS ON ESTIMATION AND DEVIATION STATISTICS

It was shown in paragraph 2.3.2 of Volume III that the covariance matrices, P, N, and V, representing the statistics of the errors in estimate, the deviations from the nominal trajectory, and the velocity correction commands respectively, are used to describe the average performance of the midcourse guidance system. Equations 2-45, 2-27 and 2-28 of Volume III show the computation of P and N when no corrections are made. In this

appendix the equations which statistically describe system performance when a correction is made are developed.

The changes in estimation errors are simplest to derive and will be treated first. The covariance matrix of estimation errors is defined:

$$P = E\left\{\tilde{\underline{x}}\,\tilde{\underline{x}}^T\right\} \tag{58}$$

where $\tilde{\underline{x}} = \underline{x} - \hat{\underline{x}}$, $\hat{\underline{x}}$ is the estimated state deviation vector, and $\underline{x}$ is the true state.

Letting P_c be the covariance matrix of estimation errors after a correction has been made, then

$$P_c = E\left\{(\tilde{\underline{x}} + \Delta\tilde{\underline{v}})\,(\tilde{\underline{x}} + \Delta\tilde{\underline{v}})^T\right\} \tag{59}$$

where $\Delta\tilde{\underline{v}}$ is a 6-vector whose three position components are zero, and whose velocity components are the errors in measuring the velocity correction. Then

$$P_c = E\left\{\tilde{\underline{x}}\,\tilde{\underline{x}}^T\right\} + E\left\{\Delta\tilde{\underline{v}}\,\tilde{\underline{x}}^T\right\} + E\left\{\tilde{\underline{x}}\,\Delta\tilde{\underline{v}}^T\right\} + E\left\{\Delta\tilde{\underline{v}}\,\Delta\tilde{\underline{v}}^T\right\} \tag{60}$$

Assuming that the errors in measuring the velocity corrections are uncorrelated with the trajectory estimation errors, then

$$E\left\{\Delta\tilde{\underline{v}}\,\tilde{\underline{x}}^T\right\} = E\left\{\tilde{\underline{x}}\Delta\tilde{\underline{v}}^T\right\} = O_{66} \tag{61}$$

and $$P_c = P + \begin{bmatrix} O_{33} & O_{33} \\ O_{33} & C \end{bmatrix}$$

where $C = E\left\{\Delta\dot{\tilde{\underline{v}}}\;\;\Delta\dot{\tilde{\underline{v}}}^T\right\}$ is the 3 x 3 covariance matrix of errors in measuring the velocity correction, where $\Delta\tilde{\underline{v}}$ is the 3-vector consisting of the velocity components of $\Delta\tilde{\underline{v}}$.

The covariance matrix of deviations from the nominal trajectory is defined as

$$N = E\left\{\underline{x}\,\underline{x}^T\right\} \tag{62}$$

After a velocity correction has been made, the vehicle's state is given by

$$\underline{x}_c = \underline{x} + G\hat{\underline{x}} + \underline{x}_Q \tag{63}$$

where $G\hat{\underline{x}}$ is the commanded velocity correction, based on the estimated state $\hat{\underline{x}}$, and $\underline{x}_Q$ is the error in implementing the correction. After a correction the covariance matrix of trajectory deviations is given by

$$N_c = E\left\{(\underline{x} + G\hat{\underline{x}} + \underline{x}_Q)\ (\underline{x} + G\hat{\underline{x}} + \underline{x}_Q)^T\right\} \tag{64}$$

$$N_c = E\left\{\underline{x}\underline{x}^T + \underline{x}\hat{\underline{x}}^T G^T + \underline{x}\underline{x}_Q^T + G\hat{\underline{x}}\underline{x}^T + G\hat{\underline{x}}\hat{\underline{x}}G^T + G\hat{\underline{x}}\underline{x}_Q^T + \underline{x}_Q\underline{x}^T \right. \tag{65}$$

$$\left. + \underline{x}_Q\hat{\underline{x}}^T G^T + \underline{x}_Q\underline{x}_Q^T \right\}$$

In this study it was assumed that the errors in making the velocity corrections were uncorrelated with the trajectory deviations so that the expected values of crossproduct terms in equation 65 involving $\underline{x}_Q$ are zero. This assumption, borrowed from Ref. 4, is not necessarily true, since the velocity correction errors should depend upon the velocity correction magnitude which in turn depends on the trajectory deviations. At any rate, the effect of eliminating these small crosscorrelations is small, and equation 65 is written

$$N_c = N + E\left\{\underline{x}\hat{\underline{x}}^T G^T + G\hat{\underline{x}}\underline{x}^T + G\hat{\underline{x}}\hat{\underline{x}}G^T\right\} + S \tag{66}$$

where

$$S = E\left\{\underline{x}_Q\underline{x}_Q^T\right\} = \begin{bmatrix} O_{33} & O_{33} \\ O_{33} & S' \end{bmatrix} \tag{67}$$

where S' is the 3 x 3 covariance matrix of errors in applying the velocity correction. (See equation 84, this section, for computation of S'.)

Ref. 4 McLean, J. D., S. F. Schmidt, and T. A. McGee, Optimal Filtering and Linear Prediction Applied to a Midcourse Navigation System for the Circumlunar Mission, NASA Ames, NASA TR D-1208, March 1962.

In order to reduce equation 66, the following derivation will show that

$$E\left\{\underline{\hat{x}}\underline{\hat{x}}^T\right\} = E\left\{\underline{\hat{x}}\underline{x}^T\right\} = E\left\{\underline{\hat{x}}\underline{\hat{x}}^T\right\} = \left[N\text{-}P\right]$$

In Ref. 2 it is shown that if $\underline{\hat{x}} = \underline{x} + \underline{\tilde{x}}$ (or $\underline{x} - \underline{\tilde{x}}$), then $E\left\{\underline{\hat{x}}\underline{\tilde{x}}^T\right\} = 0$. Then $E\left\{\underline{\tilde{x}}\underline{\hat{x}}^T\right\} = 0$. Now, for $\underline{\hat{x}} = \underline{x} - \underline{\tilde{x}}$,

$$E\left\{\underline{\hat{x}}\underline{x}^T\right\} = E\left\{\underline{\hat{x}}(\underline{\hat{x}} + \underline{\tilde{x}})^T\right\} = E\left\{\underline{\hat{x}}\underline{\hat{x}}^T + \underline{\hat{x}}\underline{\tilde{x}}^T\right\} = E\left\{\underline{\hat{x}}\underline{\hat{x}}^T\right\} \tag{68}$$

Also,

$$E\left\{\underline{x}\underline{\hat{x}}^T\right\} = E\left\{\underline{x}(\underline{x} - \underline{\tilde{x}})^T\right\} = E\left\{\underline{x}\underline{x}^T - \underline{x}\underline{\tilde{x}}^T\right\} \tag{69}$$

But

$$E\left\{\underline{x}\underline{\hat{x}}^T\right\} = E\left\{(\underline{\hat{x}} + \underline{\tilde{x}})\underline{\tilde{x}}^T\right\} = E\left\{\underline{\hat{x}}\underline{\tilde{x}}^T + \underline{\tilde{x}}\underline{\tilde{x}}^T\right\} \tag{70}$$

Since

$$E\left\{\underline{\hat{x}}\underline{\tilde{x}}^T\right\} = 0, \tag{71}$$

then

$$E\left\{\underline{x}\underline{\tilde{x}}^T\right\} = E\left\{\underline{\tilde{x}}\underline{\tilde{x}}^T\right\} \tag{72}$$

and

$$E\left\{\underline{x}\underline{\hat{x}}^T\right\} = E\left\{\underline{x}\underline{x}^T - \underline{\tilde{x}}\underline{\tilde{x}}^T\right\} = (N\text{-}P) \tag{73}$$

Similarly

$$E\left\{\underline{\hat{x}}\underline{x}^T\right\} = E\left\{(\underline{x} - \underline{\tilde{x}})\underline{x}^T\right\} = E\left\{\underline{x}\underline{x}^T - \underline{\tilde{x}}\underline{x}^T\right\} \tag{74}$$

$$E\left\{\underline{\tilde{x}}\underline{x}^T\right\} = E\left\{\underline{\tilde{x}}(\underline{\hat{x}} + \underline{\tilde{x}})^T\right\} = E\left\{\underline{\tilde{x}}\underline{\hat{x}}^T + \underline{\tilde{x}}\underline{\tilde{x}}^T\right\} \tag{75}$$

$$E\left\{\underline{\tilde{x}}\underline{\hat{x}}^T\right\} = E\left\{\underline{\hat{x}}\underline{\tilde{x}}^T\right\} = 0 \tag{76}$$

$$E\left\{\underline{\tilde{x}}\underline{x}^T\right\} = E\left\{\underline{\tilde{x}}\underline{\tilde{x}}^T\right\} \tag{77}$$

$$E\left\{\underline{\hat{x}}\underline{x}^T\right\} = E\left\{\underline{x}\underline{x}^T - \underline{\tilde{x}}\underline{\tilde{x}}^T\right\} = (N - P) \tag{78}$$

Substituting equations 68, 73, and 78 into equation 66

$$N_c = N + \left[(N - P)G^T + G(N - P) + G(N - P)G^T\right] + S \tag{79}$$

$$N_c = (I_{66} + G)\,(N - P)\,(I_{66} + G)^T + N + S \tag{80}$$

which is the form used in this study.

In order to complete the derivation of the change in the covariance matrix N due to velocity changes, S', the covariance matrix of errors in implementing the corrections must be developed. In Ref. 5, subsection 5.2, it is shown that the covariance matrix of errors in implementing the velocity correction is as follows:

$$S' = E\left\{\underline{\dot{x}}_Q \underline{\dot{x}}_Q^T\right\} = \sigma_k^2 V + \frac{\sigma_\gamma^2}{2}\left[u^2 I_{33} - V\right] \tag{81}$$

where σ_k^2 and σ_γ^2 are the variances of the magnitude and pointing error respectively, $V = E\left\{\underline{\Delta v}\ \underline{\Delta v}^T\right\}$ is the covariance matrix of velocity corrections, and u^2 is the trace of V.

Equation 81 lumps all sources of magnitude error together. If the velocity correction scheme involves thrusting with a fixed-thrust rocket engine for a certain period of time, however, then velocity correction magnitude errors will be due to two sources: an error in the applied thrust magnitude and an error in the time for which the thrust is applied. Mr. Gerald Smith of Ames Research Center suggested a method of revising equation 81 to account for the two possible sources of error in velocity correction magnitude.

Ref. 5

Battin, R. H., A Statistical Optimizing Navigation Procedure For Space Flight, ARSJ, Vol. 32, No. 11, Nov 1962, pp. 1681-1696

In equation 81, σ_k^2 is the variance of the error in velocity correction magnitude; i.e.,

$$\sigma_k^2 = E\left\{\left|\dot{\underline{x}}_Q\right|^2\right\} .$$

Letting

$$\left|\dot{\underline{x}}_Q\right| = \left|\dot{\underline{x}}_{QT}\right| + \frac{\epsilon}{u} \tag{82}$$

where ϵ is some error in timing the thrust and $\left|\dot{\underline{x}}_{QT}\right|$ is an error in thrust magnitude, then

$$\sigma_k^2 = E\left\{\left|\dot{\underline{x}}_Q\right|^2\right\} = E\left\{\left(\left|\dot{\underline{x}}_{QT}\right| + \frac{\epsilon}{u}\right)^2\right\} = \left(\sigma_K^2 + \frac{\sigma_\epsilon^2}{u^2}\right)$$

where σ_K^2 is the variance of the thrust magnitude errors while σ_ϵ^2 is the variance of the thrust timing errors, assuming ϵ and $\left|\dot{x}_{QT}\right|$ are uncorrelated. Substituting equation 82 into equation 81, we arrive at the velocity correction error formulation used in this study.

$$S' = \left(\sigma_K^2 + \frac{\sigma_\epsilon^2}{u^2}\right) V + \frac{\sigma_\gamma^2}{2} \left(u^2 I_{33} - V\right) \tag{83}$$

5. EQUATIONS USED IN COMPUTER PROGRAMS

All the equations used in the three midcourse guidance computer programs are listed here.

5.1 Nominal Trajectory Program

This program is used to generate the nominal trajectories by numerically integrating the following three equations:

$$\ddot{X} = -\frac{\mu_e X}{R_e^3} - \frac{\mu_m}{R_{vm}^3}(X - X_m) - \frac{\mu_m X_m}{R_m^3} \tag{84}$$

$$\ddot{Y} = -\frac{\mu_e Y}{R_e^3} - \frac{\mu_m (Y - Y_m)}{R_{vm}^3} - \frac{\mu_m Y_m}{R_m^3} \tag{85}$$

$$\ddot{Z} = -\frac{\mu_e Z}{R_e^3} - \frac{\mu_m}{R_{vm}^3}(Z - Z_m) - \frac{\mu_m Z_m}{R_m^3} \tag{86}$$

where μ_e and μ_m are the gravitational constants of the earth and moon and X, Y, Z and X_m, Y_m, Z_m are position coordinates of the space vehicle and moon in an earth-centered cartesian coordinate system. R_e, R_{vm} and R_m are distances defined by

$$R_e = \sqrt{X^2 + Y^2 + Z^2} \tag{87}$$

$$R_m = \sqrt{X_m^2 + Y_m^2 + Z_m^2} \tag{88}$$

$$R_{vm} = \sqrt{(X - X_m)^2 + (Y - Y_m)^2 + (Z - Z_m)^2} \tag{89}$$

The moon's revolution about the earth (assumed circular) is described by

$$X_m = R_m \cos\left[\frac{2\pi (t - t_o)}{T} + \psi_o\right] \tag{90}$$

$$Y_m = R_m \sin\left[\frac{2\pi (t - t_o)}{T} + \psi_o\right] \cos\phi \tag{91}$$

$$Z_m = R_m \sin\left[\frac{2\pi (t - t_o)}{T} + \psi_o\right] \sin\phi \tag{92}$$

where R_m is the earth-moon distance, ϕ is the inclination of lunar orbit to the earth's equatorial (XY) plane, T is the lunar orbital period, and ψ_o is the angle from the moon's ascending line of nodes to the earth-moon line at $t = t_o$ (time of injection into the lunar midcourse trajectory).

The initial conditions required for solution of equations 84 through 92 are X_o, Y_o, Z_o, $\dot{X}_o$, $\dot{Y}_o$, $\dot{Z}_o$, and ψ_o and the constants required are μ_e, μ_m, T, ϕ, and R_m. The quantities X, Y, Z, $\dot{X}$, $\dot{Y}$, $\dot{Z}$, X_m, Y_m, Z_m, $\dot{X}_m$, $\dot{Y}_m$, $\dot{Z}_m$, R_e, R_{vm}, and $V_e = \sqrt{\dot{X}^2 + \dot{Y}^2 + \dot{Z}^2}$ are printed out at 6-minute intervals. In addition, the position and velocity of the vehicle in moon-centered coordinates are printed out using the following equations:

$$\left.\begin{aligned} X_{vm} &= X - X_m \\ Y_{vm} &= Y - Y_m \\ &\vdots \qquad\quad \vdots \\ \dot{Z}_{vm} &= \dot{Z} - \dot{Z}_m \end{aligned}\right\} \tag{93}$$

$$\begin{aligned} R_{vm} &= \sqrt{X_{vm}^2 + Y_{vm}^2 + Z_{vm}^2} \\ V_{vm} &= \sqrt{\dot{X}_{vm}^2 + \dot{Y}_{vm}^2 + \dot{Z}_{vm}^2} \end{aligned} \tag{94}$$

5.2 Transition Matrix Program

The transition matrices $\Phi(t_k, t_{k-1})$ are the matrices which relate deviations from some reference trajectory at t_k to deviations at t_{k-1}. The transition matrix is the 6 x 6 matrix shown in equation 95.

$$\Phi = \begin{bmatrix} \phi_{11} & \phi_{12} & - & - & - & \phi_{16} \\ \phi_{21} & - & - & - & - & - \\ - & - & - & - & - & - \\ - & - & - & - & - & - \\ - & - & - & - & - & - \\ \phi_{61} & - & - & - & - & \phi_{66} \end{bmatrix} \tag{95}$$

where ϕ_{ij} is the change in the i^{th} deviation component at t_k caused by a unit deviation in the component at t_{k-1}. The elements of equation 95 are generated by simultaneous solution of the following set of linear differential equations:

$$\dot{X}_1 = X_4$$
$$X_2 = X_5$$
$$X_3 = X_6$$
$$\dot{X}_4 = (\partial f_1/\partial X) X_1 + (\partial f_1/\partial Y) X_2 + (\partial f_1/\partial Z) X_3$$
$$\dot{X}_5 = (\partial f_2/\partial X) X_1 + (\partial f_2/\partial Y) X_2 + (\partial f_2/\partial Z) X_3$$
$$\dot{X}_6 = (\partial f_3/\partial X) X_1 + (\partial f_3/\partial Y) X_2 + (\partial f_3/\partial Z) X_3 \qquad (96)$$

In equations 96 the partial derivatives are time-varying and are referred to the nominal trajectory described in subsection 5.1, so that the elements of the Φ matrix in equation 95 are generated by simultaneous solution of equations 96 and 84 through 86 over each 6-minute interval ($t_k - t_{k-1}$), using unit and zero initial conditions as described in Section 1.

5.3 Statistical Program

The computer programs just described are used to generate input information for the statistical program, which in turn is used to analyze various guidance systems. The inputs provided by these programs include the position and velocity of the vehicle in both earth and moon coordinates and the position and velocity of the moon in earth coordinates. Also, the Φ (transition) matrices just described are provided. Other inputs to the statistical program include (1) the guidance schedule, which is a list of times at which corrections and observations are made and the types of observations and (2) the rms errors in implementing the corrections and observations.

The three basic quantities used in the statistical program are: P, the covariance matrix of estimation uncertainties; N, the covariance matrix of deviations from the nominal trajectory; and V, the covariance matrix of

velocity corrections. Initially $P_o = N_o$ is an input to the computer program. Thereafter the change in P over a period when no velocity corrections are made is given by

$$P(t_{k+1}) = \Phi(t_{k+1}, t_k)\left[P(t_k) - K(t_k)H(t_k)P(t_k)\right]\Phi^T(t_{k+1}, t_k) \tag{97}$$

In equation 97, the operation $\Phi(t_{k+1}, t_k)[\quad]\Phi^T(t_{k+1}, t_k)$ indicates the change in P over a period when no observations have been made while the quantity in the brackets shows the reduction in P due to taking a measurement at t_k.

The equation for $K(t_k)$ is as follows:

$$K(t_k) = P_1(t_k)H_1^T(t_k)\left[H_1(t_k)P_1(t_k)H_1^T(t_k) + Q(t_k)\right]^{-1} \tag{98}$$

$Q(t_k)$ is the measurement variance, defined later, where $P_1(t_k)$ is the upper left-hand 3 x 3 position submatrix of $P(t_k)$ and $H_1(t_k)$ is the row vector,

$$H_1(t_k) = \left[\partial\zeta/\partial X \quad \partial\zeta/\partial Y \quad \partial\zeta/\partial Z\right] \tag{99}$$

for optical angle measurements.

For an earth-star angle measurement, the partials are:

$$\frac{\partial\zeta_e}{\partial X} = \frac{aR_e + Xd_e}{R_e^2\sqrt{1 - d_e^2}}$$

$$\frac{\partial\zeta_e}{\partial Y} = \frac{bR_e + Yd_e}{R_e^2\sqrt{1 - d_e^2}} \tag{100}$$

$$\frac{\partial\zeta_e}{\partial Z} = \frac{cR_e + Zd_e}{R_e^2\sqrt{1 - d_e^2}}$$

where

$$d_e = -\left(\frac{aX + bY + cZ}{R_e}\right) \tag{101}$$

and

$$R_e = \sqrt{X^2 + Y^2 + Z^2} \tag{102}$$

where a, b, and c are the star direction cosines (program inputs) and X, Y, and Z are the coordinates of the vehicle's position on the nominal trajectory at t_k.

For a moon-star angle measurement, the partials are:

$$\left.\begin{aligned}
\frac{\partial \zeta_m}{\partial X} &= \frac{aR_{vm} + (X - X_m)\, d_{vm}}{R_{vm}^2 \sqrt{1 - d_m^2}} \\
\frac{\partial \zeta_m}{\partial Y} &= \frac{bR_{vm} + (Y - Y_m)\, d_{vm}}{R_{vm}^2 \sqrt{1 - d_{vm}^2}} \\
\frac{\partial \zeta_m}{\partial Z} &= \frac{cR_{vm} + (Z - Z_m)\, d_{vm}}{R_{vm}^2 \sqrt{1 - d_{vm}^2}}
\end{aligned}\right\} \tag{103}$$

where

$$d_{vm} = -\left(\frac{a(X - X_m) + b(Y - Y_m) + c(Z - Z_m)}{R_{vm}}\right) \tag{104}$$

and

$$R_{vm} = \sqrt{(X - X_m)^2 + (Y - Y_m)^2 + (Z - Z_m)^2} \tag{105}$$

where the quantities X, Y, Z, X_m, Y_m, Z_m are again evaluated from the nominal trajectory at t_k.

The measurement variance on a star angle measurement is given by:

$$Q(t_k) = \sigma^2 + \left(\frac{k_i}{R_i(t_k)}\right)^2 \tag{106}$$

where σ^2 is the instrument accuracy, k_i is a constant, and $R_i(t_k)$ is the range to the planet from which the measurement is being taken at t_k. σ^2 and k_i are program inputs.

Equations 100 through 106 are for the optical angle measurements. For range measurements, the $H_1(t_k)$ vector is given by

$$H_1(t_k) = \left[\begin{array}{ccc} \frac{X}{R} & \frac{Y}{R} & \frac{Z}{R} \end{array}\right]_{t_k} \tag{107}$$

where R is the range from the planet to which the range is being taken. The variance of the range measurements is given by

$$Q(t_k) = \sigma_R^2 + (k_{iR} R)^2 \tag{108}$$

where σ_R and k_{iR} are program inputs and R is the range to the planet involved in the measurement.

The equations up through 108 complete the computations required to generate the matrix $P(t_k)$ over periods when no velocity corrections are made. The matrix N over this same period is simply calculated:

$$N(t_{k+1}) = \Phi(t_{k+1}, t_k)\, N(t_k)\, \Phi^T(t_{k+1}, t_k) \tag{109}$$

When a velocity correction is made at t_k, then V, the covariance matrix of velocity corrections, is given by

$$V(t_k) = G'(t_k)\, N(t_k)\, G'^T(t_k) \tag{110}$$

where

$$G'(t_k) = \left[A_2^{-1} A_1(t_a, t_k)\ I_{33}\right] \tag{111}$$

where $A_2(t_k)$ is the upper right-hand 3 x 3 submatrix of $\Phi(t_a, t_k)$ and $A_1(t_k)$ is the upper left-hand 3 x 3 submatrix. Also,

$$\Phi(t_a, t_k) = \Phi(t_a, t_{a-1})\,\Phi(t_{a-1}, t_{a-2}) \cdots \Phi(t_{k+1}, t_k) \tag{112}$$

The change in N when a correction is made is as follows:

$$N_c(t_k) = \left[I_{66} + G\right](N - P)\left[I_{66} + G\right]^T + P + S \tag{113}$$

where all quantities are evaluated at t_k before the correction is made, and S is the covariance matrix of errors made in applying the correction:

$$S(t_k) = \begin{bmatrix} 0_{33} & 0_{33} \\ 0_{33} & S'(t_k) \end{bmatrix} \tag{114}$$

$$S'(t_k) = \left(\sigma_k^2 + \frac{\sigma_\epsilon^2}{u^2}\right)V(t_k) + \frac{\sigma_\gamma^2}{2}\left(u^2 I_{33} - V(t_k)\right) \tag{115}$$

where u^2 is the trace of $V(t_k)$ and σ_k^2, σ_ϵ^2 and σ_γ^2 are program inputs.

In this computer program it was assumed that the velocity correction was not separately monitored, so that the uncertainties in applying the correction are equal to the uncertainties in estimating the correction. Thus when a velocity correction is made at t_k, the P matrix is incremented as follows:

$$P_c(t_k) = P(t_k) + S(t_k) \tag{116}$$

Equations 84 through 116 are used to determine the P, N, and V matrices throughout the trajectory. Operations which are performed on these matrices include the following:

$$
\left.
\begin{aligned}
r &= \sqrt{Tr(N_1)} \\
v &= \sqrt{Tr(N_4)} \\
\tilde{r} &= \sqrt{Tr(P_1)} \\
\tilde{v} &= \sqrt{Tr(P_4)} \\
u = \Delta v &= \sqrt{Tr(V)}
\end{aligned}
\right\} \qquad (117)
$$

where Tr indicates the trace of a matrix, and N_1 and P_1 are the upper left-hand 3 x 3 submatrices of N and P respectively, while N_4 and P_4 are the lower right-hand 3 x 3 submatrices. In equation 117, r and v are the rms deviations in position and velocity from the nominal trajectory, while $\tilde{r}$ and $\tilde{v}$ are the rms estimation errors, and Δv is the rms velocity magnitude at each correction. In addition to these five quantities, the predicted target error, T, is computed as follows:

$$T(t_k) = \Phi(t_a, t_k)\, P(t_k)\, \Phi^T(t_a, t_k) \qquad (118)$$

and

$$r_t = \sqrt{Tr(T_1)} \qquad (119)$$

$$v_t = \sqrt{Tr(t_4)}$$

The quantities P, $\tilde{r}$, $\tilde{v}$, T, r_t, v_t are computed before and after each observation and correction and at periselenum. In addition, R, r, and v are computed after each observation and correction and at periselenum. V and Δv are computed at each correction.

In addition to the operations mentioned, the following transformation on the periselenum error components is done:

$$P_G = MP(t_a)M^T \qquad (120)$$

$$N_G = MN(t_a)M^T$$

where $$M = \begin{bmatrix} M' & O_{33} \\ O_{33} & M' \end{bmatrix} \tag{121}$$

and $$M' = \begin{bmatrix} X/R & Y/R & Z/R \\ \dot{X}/R & \dot{Y}/R & \dot{Z}/R \\ \frac{Y\dot{Z}-Z\dot{Y}}{RV} & \frac{X\dot{Z}-Z\dot{X}}{RV} & \frac{X\dot{Y}-Y\dot{X}}{RV} \end{bmatrix}_{t_a} \tag{122}$$

where the components of M' are evaluated at t_a on the nominal trajectory in moon-centered coordinates. (See equations 93 and 94.)

6. EFFECT OF MEASUREMENT TIMING ERRORS

The effect of errors made in timing the optical observations was not included in the computer program used in this study. However, the following analysis will show the approximate upper bound on timing errors, which is insignificant compared to other guidance system errors.

In figure 3, the geometry of an error in timing a measurement to some landmark is illustrated. The maximum angular error caused by the timing error is given by

$$\Delta\zeta = \tan^{-1}\left(\frac{V_s \Delta t \sin\xi}{R_s - V\Delta t\cos\xi}\right) \simeq \frac{V_s \Delta t \sin\xi}{R_s} \tag{123}$$

where V_s is the spacecraft velocity, Δt is the error in timing the measurement, R_L is the range to the reference point, and ξ is illustrated in the figure.

Obviously the closer the range R_s, the greater effect timing errors have. Thus, two time-points are of particular interest: 69 hours, which is the last observation before the final correction on the standard schedule and 71.8 hours, which is the final observation before periselenum. Using values of R_s, V_s, and ξ from the standard 72.2-hour trajectory and solving equation 123 at 69 hours and 71.8 hours,

$$\left.\begin{aligned} \Delta\zeta\ (69.0) &= 3.04\ \frac{\text{sec of arc}}{\text{sec of time}} \\ \Delta\zeta\ (71.8) &= 312\ \frac{\text{sec of arc}}{\text{sec of time}} \end{aligned}\right\} \tag{124}$$

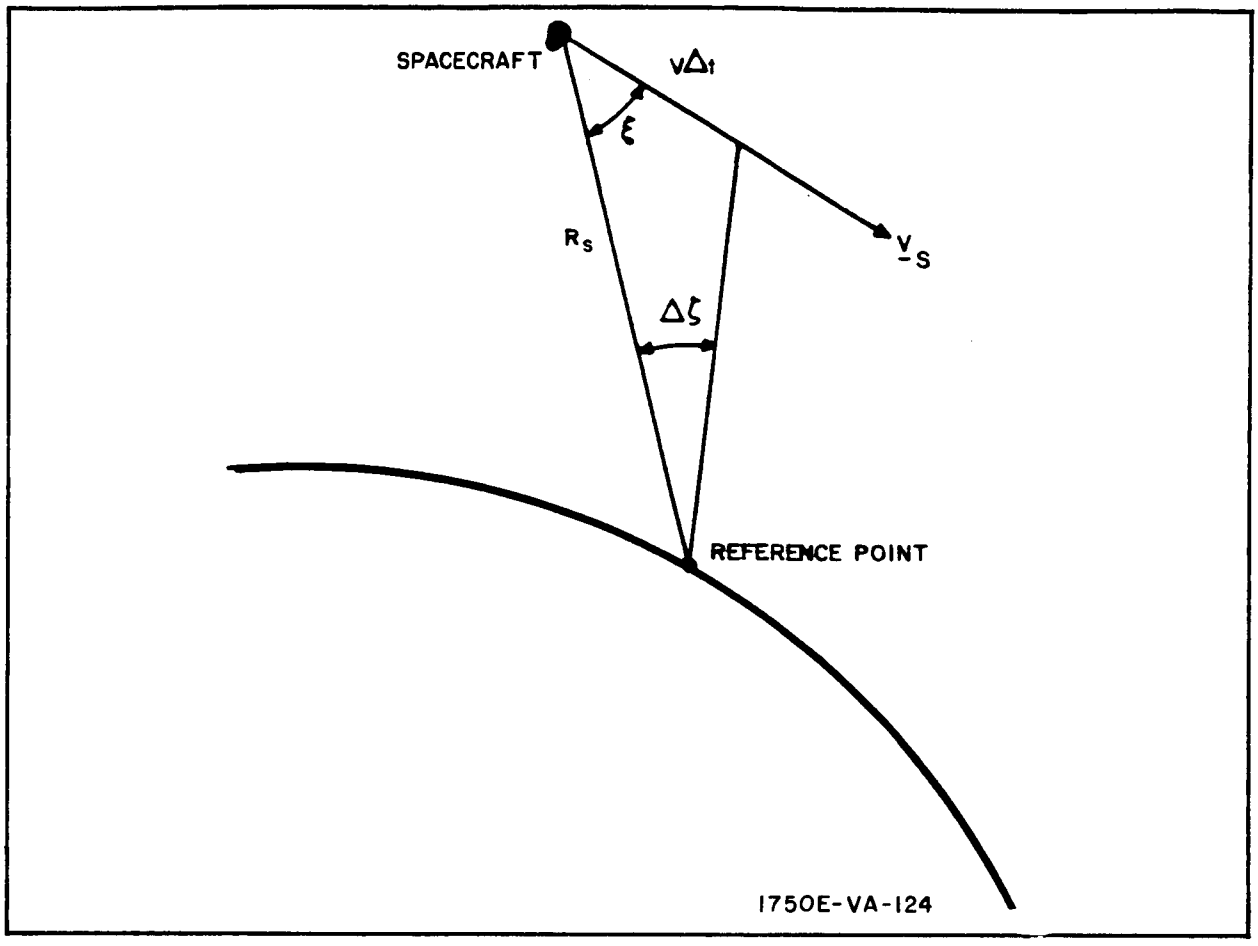

Figure 3. Geometry of Timing Errors

Since the errors caused by landmark, timing, and instrument uncertainties are independent, the rms measurement error, σ_ζ, is given by

$$\sigma_\zeta = \sqrt{\sigma_L^2 + \sigma_I^2 + \sigma_T^2}$$

At 69.0 hours, the rms angle measurement error caused by 0.8-kilometer landmark uncertainty is σ_L = 10 arc seconds. For a 1-second rms timing accuracy, σ_T = 3 arc seconds (from equation 124), and assuming a 10-arc second instrument error,

$$\sigma_\zeta = \sqrt{3^2 + 10^2 + 10^2} = 14.45 \text{ arc seconds}$$

Since the landmark and instrument errors alone yield a total error of 14.14 arc seconds, it can be seen that a timing error of 1 second will have a negligible effect on miss distance and fuel consumed, as these quantities are affected only by operations before the third correction at 70 hours and the case examined (t = 69 hours) is a worst case.

The observations after the third correction, which strongly influence the estimation errors $\tilde{Y}$ and $\tilde{V}$, are much more sensitive to timing errors. Calculations like those above, but at t = 71.8 hours instead of 69.0 hours, showed that 0.1 second accuracy is required to reduce timing errors to negligible importance.

7. BIAS AND ASTRODYNAMIC ERRORS

In formulating the computer program used in this study, it was assumed that exact astronomical constants were available, and that the measurement errors could be represented by Gaussian-distributed errors which are uncorrelated from one measurement to the next. This error model is not necessarily a good representation of an actual physical system, however, since it is expected that systematic errors such as those caused by astrodynamic uncertainties and instrument bias will be present.

It was indicated in paragraph 2.4.5 of Volume III that systematic as well as random errors could be accounted for in actual system by implementation of the minimum variance technique, using the so called augmented state vector which includes not only the six components of trajectory deviations but also components pertaining to each of the error sources. The process by which this is done is shown here.

Assume that in addition to uncorrelated random noise on each measurement, there is also some time-correlated noise. In addition, there is some uncertainty in the astrodynamic constants. Assuming some uncertainty in μ_e, μ_m, and R_{em} (earth gravitational constant, lunar gravitational constant, and earth-moon distance), the equations of motion can be written:

$$\left.\begin{aligned} \ddot{X} &= f_1 (X, Y, Z, \mu_e, \mu_m, R_{em}, t) \\ \ddot{Y} &= f_2 (X, Y, Z, \mu_e, \mu_m, R_{em}, t) \\ \ddot{Z} &= f_3 (X, Y, Z, \mu_e, \mu_m, R_{em}, t) \end{aligned}\right\} \qquad (125)$$

Taking a first-order Taylor series expansion about the reference trajectory and nominal values of μ_e, μ_m, and R_{em}, the perturbation equations are of the form

$$\begin{aligned} \Delta\ddot{X} = &\left(\frac{\partial f_1}{\partial X}\right) \Delta X + \left(\frac{\partial f_1}{\partial Y}\right) \Delta Y + \left(\frac{\partial f_1}{\partial Z}\right) \Delta Z \\ &+ \left(\frac{\partial f_1}{\partial \mu_e}\right) \Delta\mu_e + \left(\frac{\partial f_1}{\partial \mu_m}\right) \Delta\mu_m + \left(\frac{\partial f_1}{\partial R_{em}}\right) \Delta R_{em} \end{aligned} \qquad (126)$$

where $\Delta\ddot{Y}$ and $\Delta\ddot{Z}$ are similar in form, except that the partials relate to f_2 and f_3 respectively. Defining $\underline{x}(t)$ as the 6-vector whose components are Δx, Δy, Δz, $\Delta\dot{x}$, $\Delta\dot{y}$, $\Delta\dot{z}$ and $\underline{e}$ as the 3-vector whose components are $\Delta\mu_e$, $\Delta\mu_m$ and R_{em}, the perturbation equations can be written in matrix form:

$$\dot{\underline{x}}(t) = \begin{bmatrix} F(t) & E(t) \end{bmatrix} \begin{bmatrix} \underline{x} \\ \underline{e} \end{bmatrix} \tag{127}$$

where

$$F(t) = \begin{bmatrix} 0 & 0 & 0 & 1 & 0 & 0 \\ 0 & 0 & 0 & 0 & 1 & 0 \\ 0 & 0 & 0 & 0 & 0 & 1 \\ \frac{\partial f_1}{\partial X} & \frac{\partial f_1}{\partial Y} & \frac{\partial f_1}{\partial Z} & 0 & 0 & 0 \\ \frac{\partial f_2}{\partial X} & \frac{\partial f_2}{\partial Y} & \frac{\partial f_2}{\partial Z} & 0 & 0 & 0 \\ \frac{\partial f_3}{\partial X} & \frac{\partial f_3}{\partial Y} & \frac{\partial f_3}{\partial Z} & 0 & 0 & 0 \end{bmatrix} \tag{128}$$

$$E(t) = \begin{bmatrix} 0 & 0 & 0 \\ 0 & 0 & 0 \\ 0 & 0 & 0 \\ \frac{\partial f_1}{\partial \mu_e} & \frac{\partial f_1}{\partial \mu_m} & \frac{\partial f_1}{\partial R_{em}} \\ \frac{\partial f_2}{\partial \mu_e} & \frac{\partial f_2}{\partial \mu_m} & \frac{\partial f_2}{\partial R_{em}} \\ \frac{\partial f_3}{\partial \mu_e} & \frac{\partial f_3}{\partial \mu_m} & \frac{\partial f_3}{\partial R_{em}} \end{bmatrix} \tag{129}$$

where the partials in F(t) and E(t) are evaluated from the reference trajectory at time t.

Now considering the measurement error process, the measurements $\underline{y}$ can be represented by the following equation:

$$\underline{y}(t) = H(t)\,\underline{x}(t) + \underline{n}(t) \tag{130}$$

where $\underline{n}(t)$ is the noise on each measurement. Note that in equation 130 it is assumed that the measurements $\underline{y}(t)$ are uncoupled with the errors in the astrodynamic constants. This is not strictly true, since ΔR_{em} would have an effect on the measurements. However, this effect would be small in most cases and will be ignored here.

Assume that the measurement error process $\underline{n}(t)$ can be represented by the following equations:

$$\dot{\underline{w}}(t) = W(t)\underline{w}(t) + \underline{u}(t) \tag{131}$$

$$\underline{n}(t) = \Gamma(t)\underline{w}(t) \tag{132}$$

where $\underline{u}(t)$ is the white noise input to the linear dynamic process $\underline{w}(t)$. Equation 130 can thus be written

$$\underline{y}(t) = H(t)\underline{x}(t) + \Gamma(t)\underline{w}(t) \tag{133}$$

Now, adjoining equation 131 to equation 127,

$$\begin{bmatrix} \dot{\underline{x}} \\ \dot{\underline{e}} \\ \dot{\underline{w}} \end{bmatrix} = \begin{bmatrix} F & E & 0 \\ 0 & 0 & 0 \\ 0 & 0 & W \end{bmatrix} \begin{bmatrix} \underline{x} \\ \underline{e} \\ \underline{w} \end{bmatrix} + \begin{bmatrix} 0 \\ 0 \\ \underline{u} \end{bmatrix} \tag{134}$$

and equation 133 can be written

$$\underline{y} = \begin{bmatrix} H & 0 & \Gamma \end{bmatrix} \begin{bmatrix} \underline{x} \\ \underline{e} \\ \underline{w} \end{bmatrix} \tag{135}$$

Defining $\underline{x}^*(t)$ as the augmented state vector whose components are ΔX, ΔY, ΔZ, $\Delta \dot{X}$, $\Delta \dot{Y}$, $\Delta \dot{Z}$, $\Delta\mu_e$, $\Delta\mu_m$, ΔR_{em}, w_1, w_2 - - - w_p, where the w's are the various types of measurement errors, equation 134 can be written in the form

$$\dot{\underline{x}}^*(t) = F^*(t)\,\underline{x}^*(t) + U(t) \tag{136}$$

where the quantities $F^*(t)$ and $U(t)$ are defined by comparison with equation 134 . Also, the observations may be written in terms of the augmented state vector:

$$\underline{y}(t) = M(t)\,\underline{x}^*(t) \tag{137}$$

where $M = \left[H \quad 0 \quad \Gamma \right]$.

The general solution of equation 136 is given by

$$\underline{x}^*(t+1) = \Phi^*(t+1,\, t)\,\underline{x}(t) + \int_t^{t+1} \Phi^*(t+1,\, \tau)\ \ \underline{u}(\tau)\ \ d\tau \tag{138}$$

where $\Phi^*(t+1,\ t)$ is defined by $\Phi^*(t) = F^*(t)\,\Phi^*(t)$ and $\Phi^*(t,\ t) = I_{nn}$ where n is the order of the matrix.

Letting $\int_t^{t+1} \Phi^*(t+1, \tau)\,\underline{u}(\tau)\,d\tau = \underline{u}^*(t+1)$, then equations 138 and 137 can be written:

$$\left.\begin{aligned} \underline{x}^*(t+1) &= \Phi^*(t+1,\ t)\,\underline{x}(t) \ + \ \underline{u}^*(t+1) \\ \underline{y}(t) &= M(t)\,\underline{x}^*(t) \end{aligned}\right\} \tag{139}$$

In Ref. 2 the recursive equations for generating the optimal estimate $\hat{\underline{x}}^*(t)$ given the observations $\underline{y}(t)$ are derived. These equations, as modifed to suit the format of this study, are:

$$\begin{aligned} \hat{\underline{x}}^*(t_k) = \ & \Phi^*(t_k,\ t_{k-1})\,\hat{\underline{x}}^*(t_{k-1}) \\ & + K^*(t_k) \left[\underline{y}(t_k) - M(t_k)\ \Phi^*(t_k,\ t_{k-1})\,\hat{\underline{x}}^*(t_{k-1}) \right. \end{aligned} \tag{140}$$

$$K^*(t_k) = P^*(t_k)\,M^T(t_k) \left\{ M(t_k)\,P^*(t_k)\,M^T(t_k) \right\}^{-1} \tag{141}$$

$$P^*(t_{k+1}) = \Phi^*(t_{k+1}, t_k) \left[P^*(t_k) - K^*(t_k)\, M(t_k)\, P^*(t_k) \right] \Phi^{*T}(t_{k+1}, t_k) + Q^*(t_{k+1}, t_k) \tag{142}$$

$$Q^*(t_{k+1}, t_k) = E \left[\int_{t_k}^{t_{k+1}} \Phi^*(t_{k+1}, \tau)\, \underline{u}(\tau)\, \underline{u}^T(\tau)\, \Phi^*(t_{k+1}, \tau)\, d\tau \right] \tag{143}$$

Until this point the derivation given in paragraph 2.3.13 of Volume III is identical with that given here. However, the rest of that derivation is concerned with the special problem of no systematic errors on the measurements; i.e., only random noise which is uncorrelated from one measurement to the next. In this subsection, we will discuss the operations necessary to apply the estimation equations to the situation where the effects of both astrodynamic constant errors and bias errors are considered.

Implementation of the augmented state vector formulation requires computation of several quantities not needed in the case analyzed in Volume III. These quantities include Φ_e and Φ_w, the transition matrices of the astrodynamic errors and the noise process. Obviously, Φ_e is the unit matrix, since the errors in the astrodynamic constants will not change with time. Determination of Φ_w depends upon the mathematical model assumed for the noise process. As an example, consider the dynamic model shown in equation 131, which is rewritten here for convenience:

$$\dot{\underline{w}}(t) = W(t)\, \underline{w}(t) + \underline{u}(t) \tag{144}$$

Assume that $\underline{w}(t)$ is a 2-vector whose components w_1 and w_2 are uncoupled measurement noise components with different time constants.

Now for purposes of illustration, assume that $W(t) = \begin{bmatrix} -A_1 & 0 \\ 0 & -A_2 \end{bmatrix} = A$

where the A's are positive constants. Now applying equation 138, the general solution of equation 144 is:

$$\underline{w}(t) = \Phi_w(t, t_o)\, \underline{w}(t_o) + \int_{t_o}^{t} \Phi_w(t, \tau)\, \underline{u}(\tau)\, d\tau \tag{145}$$

where

$$\frac{d\Phi_w(t,\ t_o)}{dt} = A\Phi_w(t,\ t_o) \tag{146}$$

with the initial conditions $\Phi_w(t_o,\ t_o) = I_{22}$. Expanding equation 146,

$$\begin{bmatrix} \dot{\phi}_{11} & \dot{\phi}_{12} \\ \dot{\phi}_{21} & \dot{\phi}_{22} \end{bmatrix} = \begin{bmatrix} -A_1 & 0 \\ 0 & -A_2 \end{bmatrix} \begin{bmatrix} \phi_{11} & \phi_{12} \\ \phi_{21} & \phi_{22} \end{bmatrix} \tag{147}$$

where

$$\begin{aligned} &\phi_{11}(0) = \phi_{22}(0) = 1 \text{ and } \phi_{12}(0) = \phi_{21}(0) = 0 \\ &\dot{\phi}_{11}(t) = -A_1\phi_{11} \\ &\dot{\phi}_{12}(t) = -A_1\phi_{12} \\ &\dot{\phi}_{21}(t) = -A_2\phi_{21} \\ &\dot{\phi}_{22}(t) = -A_2\phi_{22} \end{aligned} \tag{148}$$

In equations 148 the equations for $\phi_{11}(t)$ and $\phi_{22}(t)$ have unit initial conditions, while the equations for $\phi_{12}(t)$ and $\phi_{21}(t)$ have zero initial conditions. Solving for ϕ_{11} first,

$$\frac{d\phi_{11}(t,\ t_o)}{dt} = -A_1\phi_{11}(t,\ t_o) \tag{149}$$

$$\int_{t_o}^{t} \frac{d\phi_{11}(t,\ t_o)}{\phi_{11}(t,\ t_o)} - \int_{t_o}^{t} A_1\, dt \tag{150}$$

$$\ln\left[\phi_{11}(t,\ t_o)\right] - \ln\left[\phi_{11}(t_o,\ t_o)\right] = -A_1(t - t_o) \tag{151}$$

Since

$$\left[\phi_{11}(t_o, t_o)\right] = 1, \ln\left[\phi_{11}(t_o, t_o)\right] = 0 \text{ and}$$

$$\phi_{11}(t, t_o) = e^{-A(t-t_o)} \tag{152}$$

solving for the other elements of the transition matrix:

$$\phi_{12}(t, t_o) = \phi_{21}(t, t_o) = 0$$

$$\phi_{22}(t, t_o) = e^{-A_2(t-t_o)} \tag{153}$$

Equation 145 can now be written in separated form:

$$\begin{bmatrix} w_1 \\ w_2 \end{bmatrix}_t = \begin{bmatrix} \phi_{11} & 0 \\ 0 & \phi_{22} \end{bmatrix} \begin{bmatrix} w_1 \\ w_2 \end{bmatrix}_{t_o} + \int_{t_o}^{t} \begin{bmatrix} \phi_{11} & 0 \\ 0 & \phi_{22} \end{bmatrix} \begin{bmatrix} u_1 \\ u_2 \end{bmatrix} d\tau \tag{154}$$

$$\left.\begin{aligned} w_1(t) &= \phi_{11} w_1(t_o) + \int_{t_o}^{t} \phi_{11}(\tau)\, u_1(\tau)\, d\tau \\ w_2(t) &= \phi_{22} w_2(t_o) + \int_{t_o}^{t} \phi_{22}(\tau)\, u_2(\tau)\, d\tau \end{aligned}\right\} \tag{155}$$

$$\left.\begin{aligned} w_1(t) &= e^{-A_1(t-t_o)} w_1(t_o) + \int_{t_o}^{t} e^{-A_1(t-\tau)} u_1(\tau)\, d\tau \\ w_2(t) &= e^{-A_2(t-t_o)} w_2(t_o) + \int_{t_o}^{t} e^{-A_2(t-\tau)} u_2(\tau)\, d\tau \end{aligned}\right\} \tag{156}$$

Note that equations 156 are in the form of the time domain representation of an RC filter excited by white noise $u_i(t)$. The function $W(t) = A(t)$ was chosen purposely to achieve this result for the purpose of illustration, as the form of equations 156 is a reasonable approximation to certain types of radar noise where the correlation time is determined by proper choice of A_i; i.e.,

$$E\left\{ w_1(t)\ w_1(t_o) \right\} < \epsilon$$

for all ϵ, given large enough A_i.

Implementation of the estimation equations 134 through 142 requires computation of the covariance matrix of the input as shown in equation 143:

$$Q^*(t,\ t_o) = E \int_{t_o}^{t} \Phi_w(t,\tau)\ \underline{u}(\tau)\ \underline{u}^T(\tau)\ \Phi_w^T(t,\tau)\ d\tau \tag{157}$$

where the transition submatrices $\Phi_w(t, \tau)$ are used instead of $\Phi^*(t, \tau)$, since the assumed measurement errors are uncoupled with the state deviations and astrodynamic errors. Since the Φ_w matrices are not random, then

$$Q^*(t,\ t_o) = \int_{t_o}^{t} \Phi_w(t,\tau)\ U_o(\tau)\ \Phi_w^T(t,\tau)\ d\tau \tag{158}$$

where $U_o(\tau)$ is the covariance matrix of the input noise; i.e., $U_o(\tau) = E\left\{ \underline{u}(\tau)\ \underline{u}^T(\tau) \right\}$. Solving for $Q^*(t,\ t_o)$ in terms of the individual components:

$$Q^*(t,\ t_o) = \begin{bmatrix} \int_{t_o}^{t} e^{-2A_1(t-\tau)}\ E\left\{ u_1^2 \right\}\ d\tau \\ \\ \int_{t_o}^{t} e^{-2A_2(t-\tau)}\ E\left\{ u_2^2 \right\}\ d\tau \end{bmatrix} \tag{159}$$

$$Q^*(t,\ t_o) = \begin{bmatrix} \dfrac{\sigma_1^2\left(1 - e^{-2A_1(t-t_o)}\right)}{2A_1} \\ \\ \dfrac{\sigma_2^2\left(1 - e^{-2A_2(t-t_o)}\right)}{2A_2} \end{bmatrix} \tag{160}$$

This completes the formulation of the "augmented state vector" estimation system for the case of a measurement noise consisting of two uncoupled error sources with different correlation times and variances. If required, other measurement error sources could be added simply by including more components in the $\underline{w}(t)$ vector.

A problem formulation such as that just described can be used for various types of error sources. For instance, for a bias error the time constant can be chosen very large (i.e., A_i very small). An important point, however, is that the dynamic model describing the random errors must be chosen on the basis of previous experience rather than on the data itself. Thus the "optimality" of the minimum variance procedure for reducing errors depends to some extent on the proper choice of a mathematical model to represent the dynamic process; i.e., for the type of estimation just described, the efficiency of the system depends upon proper choice of correlation times and input variance in equation 160. As Kalman remarked (Ref 2) in 1960, there is no known joint optimization of both the estimation procedure and the dynamic model.

It should also be pointed out that most of the above development is applicable to the use of radar tracking with its high data rate and attendant correlated noise characteristics. It is expected that for a low data-rate optical system with a measurement every half hour or hour, the errors can conveniently be described by one random, uncorrelated component and one bias component. However, even in these cases correct variances should be assigned to the measurement error components in order to achieve optimum performance. Recent results of other studies indicate that overall system performance is not badly affected by ignorance of some error sources (Ref. 6).

8. CHANGE OF COORDINATE SYSTEM

After transferring the space vehicle from the vicinity of the earth to that of the moon, it will be advantageous to convert the guidance and control calculations from an earth-centered to a moon-centered coordinate system. This procedure is indicated primarily because by so doing, the errors caused by uncertainties of the moon's position and velocity with respect to the earth are reduced in importance. Thus these small errors are not carried along throughout the lunar phase of the mission as was done in the analysis of astrodynamic constants in Ref. 6. In that analysis, the constant R_{em}, the earth-moon distance, was shown to have a significant effect on measurements in the vicinity of the moon although ΔR_{em} was assumed to be only 2 kilometers. This could have been avoided by a coordinate change as will be seen below.

Ref. 6 Smith, G. L., Secondary Errors and Off-Design Conditions in Optional Estimation of Space Vehicle Trajectories, NASA Ames, NASA 7N D-2129, January 1964.

Assume that at t_c, the vehicle's state has been determined in earth coordinates to be $\underline{x} = (X_e, Y_e, Z_e, \dot{X}_e, \dot{Y}_e, \dot{Z}_e)$. There is some error in the state estimate, and there is also an error, $\Delta\underline{x}_m$, in the estimate of the moon's position and velocity. Then the error $\tilde{\underline{x}}_m$ after coordinate transformation is given by:

$$\tilde{\underline{x}}_m = \tilde{\underline{x}} + \Delta\tilde{\underline{x}}_m \tag{161}$$

The covariance matrix of the estimation errors after coordinate transformation is then given by:

$$\begin{aligned} P_m &= E\left\{(\tilde{\underline{x}} + \Delta\tilde{\underline{x}}_m)(\tilde{\underline{x}} + \Delta\tilde{\underline{x}}_m)^T\right\} \\ &= E\left\{\tilde{\underline{x}}\tilde{\underline{x}}^T + \tilde{\underline{x}}\,\Delta\tilde{\underline{x}}_m^T + \Delta\tilde{\underline{x}}_m\tilde{\underline{x}}^T + \Delta\tilde{\underline{x}}_m\Delta\tilde{\underline{x}}_m^T\right\} \end{aligned} \tag{162}$$

Thus the covariance matrix is the sum of the covariance matrices of the trajectory estimation errors and the lunar estimation errors plus the covariance matrices of crossproducts. These crossproducts are not necessarily negligible, but in any case the maximum by which the uncertainties in each component can increase after coordinate transformation is $E(\Delta\tilde{\underline{x}}_m\Delta\tilde{\underline{x}}_m^T)$. The covariance matrices $E(\tilde{\underline{x}}\,\Delta\tilde{\underline{x}}_m^T)$ and $E(\Delta\tilde{\underline{x}}_m\tilde{\underline{x}}^T)$ are negative along the major diagonals, because when each angular measurement is made to the moon, a positive error in the moon's position in earth coordinates results in a negative error in the estimation of the position of the vehicle in earth coordinates.

Since the P matrix is incremented by $E(\Delta\tilde{\underline{x}}_m\Delta\tilde{\underline{x}}_m^T)$ at worst, it can be seen that the degradation of the estimate by adding in the small uncertainties in lunar position and velocity will be slight, so long as the coordinate conversion has been made early enough. Using the standard guidance schedule described in Volume III, paragraph 2.4.2, table 2-8, it is seen that t = 63.5 hours is a reasonable time for coordinate conversion on the 72.2-hour trajectory; i.e., just after the last sequence of earth-angle measurements has been made. It was shown in computer runs that increase in the P matrix by a small amount at this point had little effect on the final results. What can happen if the coordinate conversion is not made, however, can be illustrated simply as in figure 4.

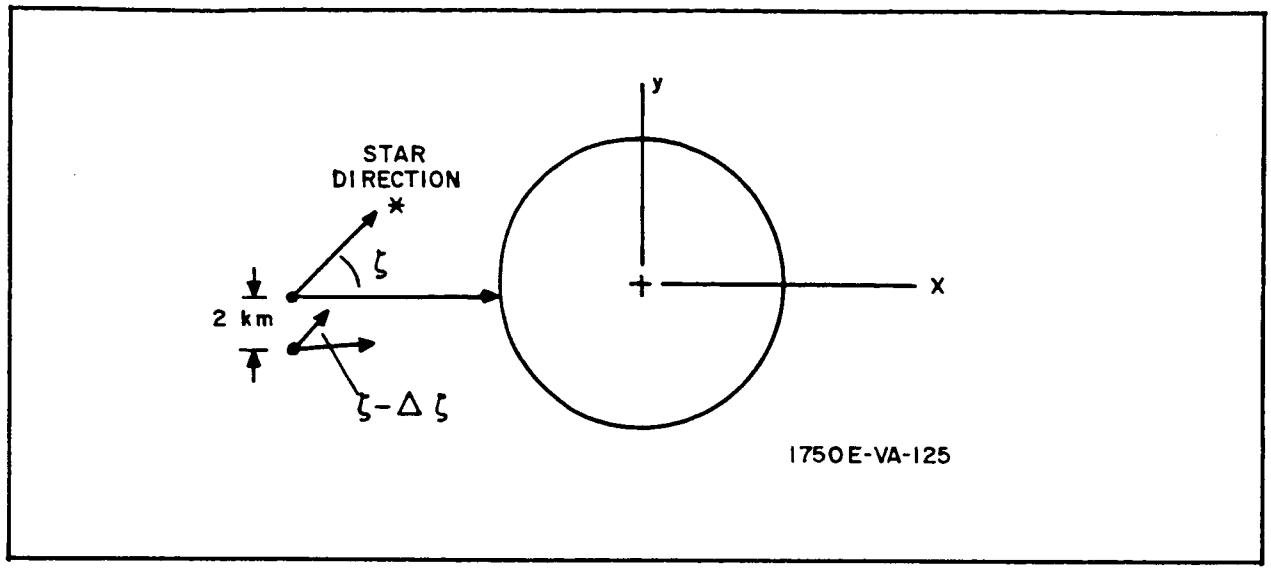

Figure 4. Illustration of Effect of Uncertainty in Moon's Position

In the planar diagram of figure 4, an error in the moon's position of 2 km along the y-axis results in an angle measurement error of:

$$\Delta\zeta \tilde{=} \frac{\Delta Y_m}{R} \tilde{=} \frac{2}{2000} = 1 \text{ milliradian} \qquad (163)$$

Thus it can be seen that errors of this type will be similar to the landmark errors described in paragraph 2.4.3.4 of Volume III.

9. POWER AND ANTENNA SIZE REQUIREMENTS FOR TWO-WAY MICROWAVE RANGING OFF LUNAR SURFACE

In this subsection rough requirements are developed for a two-way microwave system for determining the range of a spacecraft from the moon. Lasers are not considered since their only apparent advantage would be the generation of a narrow beam without a large antenna.

In paragraph 2.4.6.2 of Volume III it was shown that ranging information some 17,000 kilometers from the moon's center with an accuracy of about 10 kilometers would be useful in reducing trajectory uncertainties. It is apparent that the requirements of a two-way microwave system for this kind of performance are severe. Before going into these problems, however, some of the factors which may contribute to ranging errors are considered. The following analysis will assume that the ranging measurements are to be made at 69.1 hours on the standard 72.2-hour trajectory. At this time the spacecraft is 16,403 kilometers from the center of the moon and is travelling at a velocity of 1325 meters per second with respect to the moon.

First, consider the maximum range error due to space vehicle movement during the two-way transit time of the ranging signal. At a distance of $d = 16,403 - 1738 = 14,665$ kilometers, the transit time is [2/]

$$\Delta t = \frac{2d}{c} = \frac{2\,(1.4665)\,(10^4)}{3\,(10^5)} = 0.098 \text{ second} \tag{164}$$

At a velocity of 1325 meters per second, the maximum error which could be caused is

$$\Delta d = (1325)\,(0.098) = 132 \text{ meters} \tag{165}$$

which is negligible compared to the assumed allowable random errors of 10 kilometers.

Also, uncertainty in the velocity of propagation will cause negligible errors. If c is known to within 400 meters per second, the error in a 0.1-second round-trip time is only 40 meters.

Pointing error will cause a problem only if this error is greater than half the beamwidth. It will be shown below that a half beamwidth on the order of 0.5 degree may be required.

[2/] The notation used in this section is not necessarily consistent with the notation used in other sections of the appendix and should be considered independently.

A possible error source in microwave ranging at the distances considered will come from the fact that the moon's surface is curved and much of the reflected power will be returned from distances greater than desired. Obviously this could be time-gated out, but then some of the transmitted power, which is at a premium at the ranges considered, would be wasted. Therefore the allowable beamwidth is defined by the ranging error which can be tolerated.

The situation is illustrated in figure 5.

The range spreading error, is defined as:

$$\Delta R = \ell - (R - r_m) \tag{166}$$

$$\Delta R = R \cos \psi - \sqrt{r_m^2 - R^2 \sin^2 \psi} - R + r_m \tag{167}$$

For

$$\left(\frac{R \sin \psi}{r_m}\right)^2 \ll 1,$$

$$\Delta R \tilde{=} \frac{R^2 \sin^2 \psi}{2 r_m} \tag{168}$$

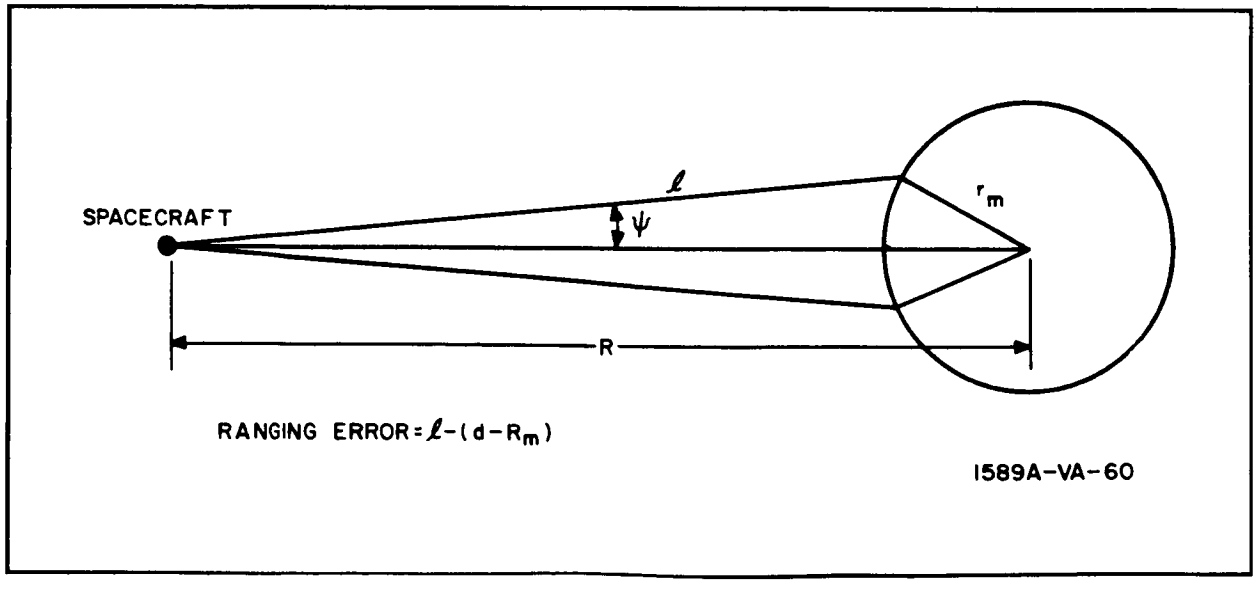

Figure 5. Ranging Error Due to Curvature

Equation 168 has been plotted for half-beamwidths of 0.5 and 1 degree as a function of range on figure 6. It is apparent that at ranges on the order of 10,000 to 20,000 kilometers, a half-beamwidth of 0.5 degree is required to keep the range spreading from exceeding 10 kilometers.

Wider beamwidths could be used, but then the power requirements would be increased due to the range spreading.

Another source of error would be variation of the lunar surface altitude. This would be averaged out over a wide region, however, when ranging is done at long distances.

In order to calculate power and antenna size requirements for a microwave system, the following two-way radar equations from Skolnik (Ref. 7) for a parabolic antenna system are employed:

Received power:

$$P_r = \frac{P_t G^2 \lambda^2 \sigma}{(4\pi)^3 R^4} \tag{169}$$

Antenna gain:

$$G = \frac{4\pi A\rho}{\lambda^2} \tag{170}$$

Antenna beamwidth:

$$\theta = \frac{65\lambda}{\ell} \text{ degrees} \tag{171}$$

where

P_r = received power

P_t = transmitted power

λ = wavelength

σ = reflective area

R = one-way range

Ref. 7 Skolnik, M.I., Introduction to Radar Systems, New York; McGraw-Hill, 1962

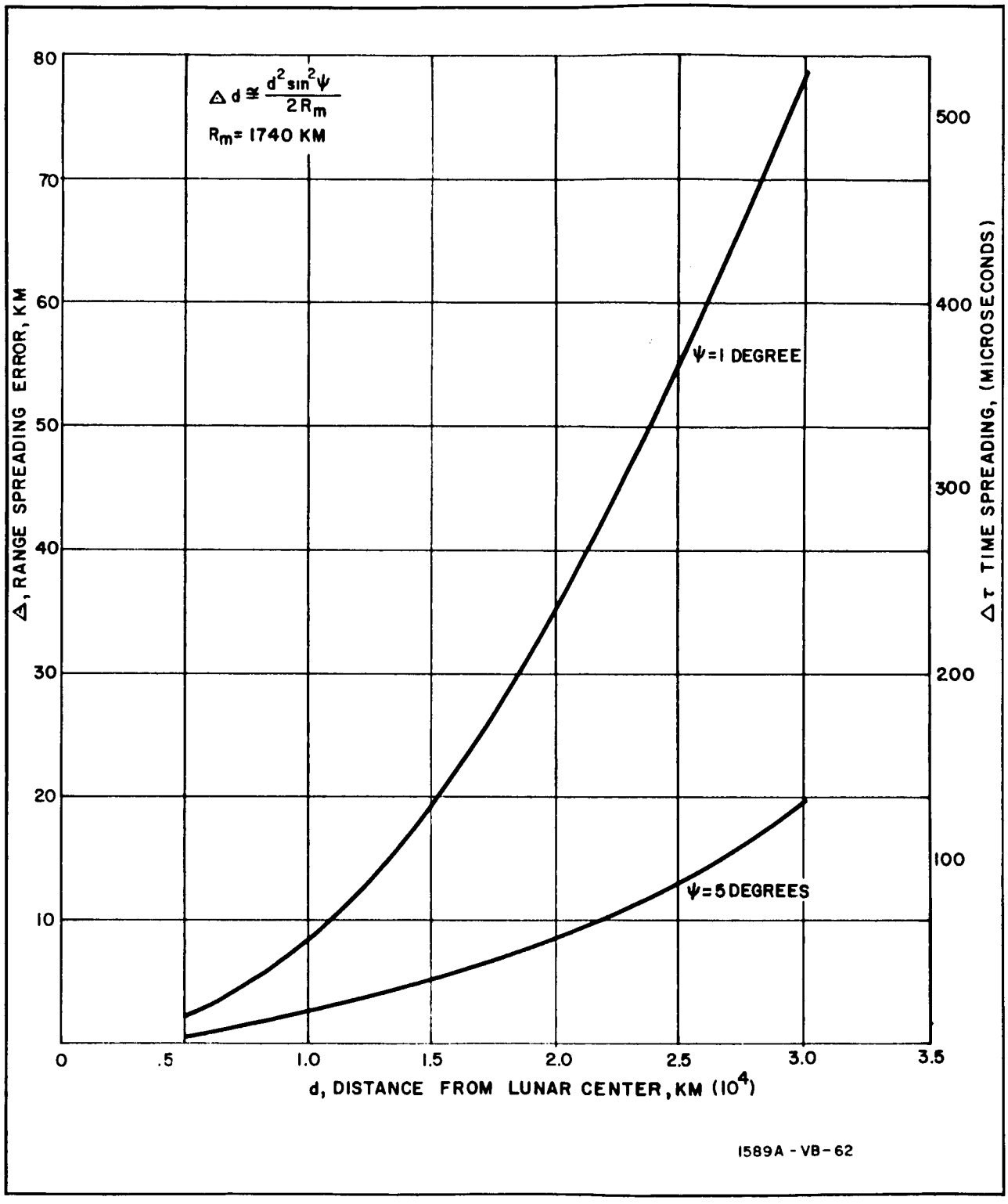

Figure 6. Range Spreading Error as a Function of Range From Moon for 0.5 and 1 Degree Beams

A = antenna capture area

ρ = antenna efficiency

θ = beamwidth

ℓ = antenna diameter

G = antenna gain

Since all the transmitted power hits the target (the lunar surface) the target cross section, σ, is given by

$$\sigma \tilde{=} k\pi\left(\frac{R\theta}{2}\right)^2 \tag{172}$$

where k is the reflection coefficient and θ is in radians. Substituting equation 172 into equation 169, combining equations 169, 170, and 171, and solving for the transmitted power,

$$P_t = 20.2\left[\frac{R}{\rho\ell}\right]^2 \frac{P_r}{k} \tag{173}$$

which gives transmit power as a function of received power, range, antenna size, and the two constants. Assuming antenna efficiency $\rho = 0.55$ and the reflection coefficient [3/] $k = -12$ db (or 0.063),

$$P_t = 1060\left[\frac{R}{\ell}\right]^2 P_r \tag{174}$$

To calculate the receiver minimum detectable signal level, the receiver bandwidth must be defined. Assuming a pulsed system with a required range resolution of 10 kilometers the pulse length (assuming no pulse compression) is approximately

$$\tau \tilde{=} \frac{2\Delta d}{c} = \frac{2\,(10)}{(3)\,(10^5)} = 66.7 \text{ microseconds} \tag{175}$$

[3/] This value is quite uncertain. The nature of electromagnetic reflections from the lunar surface is the subject of considerable investigation at the present time by Evans and Pettengill at Lincoln Laboratory.

and the system bandwidth is $B = \frac{1}{\tau} = 1/66.7 = 15$ kc. For a receiver noise figure, $\overline{F}$, of 10 db, the minimum detectable signal (MDS) (noise level) is

$$MDS = kT\Delta f\overline{F} = -152 \text{ dbm} \tag{176}$$

Substituting this value into equation 173, the power required for a 0-db S/N ratio per pulse with no losses can be determined. Assuming a signal-to-noise ratio requirement of 10 db, system losses of 5 db, and incoherent pulse integration gain (200 pulses) of 12 db, the required peak transmit power can be written

$$P_t \text{ (dbm)} = 20 \log_{10} \left(\frac{R}{\ell}\right) - 118.75 \tag{177}$$

For a 6-inch antenna at 10,000 kilometers, $P_t = 5750$ watts peak. Obviously, a larger antenna is required. With a 4-foot antenna, 90 watts peak is required, which is a little more reasonable. A curve showing peak power requirements versus range for several antenna sizes is given in figure 16 of Volume III.

The assumption of 200 pulses integration is based on the number of pulses which can reasonably be transmitted before receipt of the return pulses. As shown previously, the round-trip time is about 0.1 second. Then the duty cycle for 66.7-microsecond pulses will be

$$\frac{66.7}{10^5} = 0.133$$

which is the ratio of average power to peak power.

It is to be emphasized that the analysis presented in this section is not necessarily applicable to any particular radar system, and it is not known whether or not the system described could be mechanized. The objective in this appendix is to use fundamental relationships to determine the approximate power and antenna requirements for microwave ranging off the moon.

10. COORDINATE ROTATION

Throughout most of the analysis, a cartesian earth-or moon-centered (XYZ) coordinate system is used. In analyzing guidance system performance at periselenum, however, it is often more convenient to rotate the error matrices from cartesian coordinates to an altitude-downrange-crossrange (adc) coordinate system. The situation is illustrated in figure 7, where it is desired to rotate an error vector from the planet-centered XYZ system to an adc system.

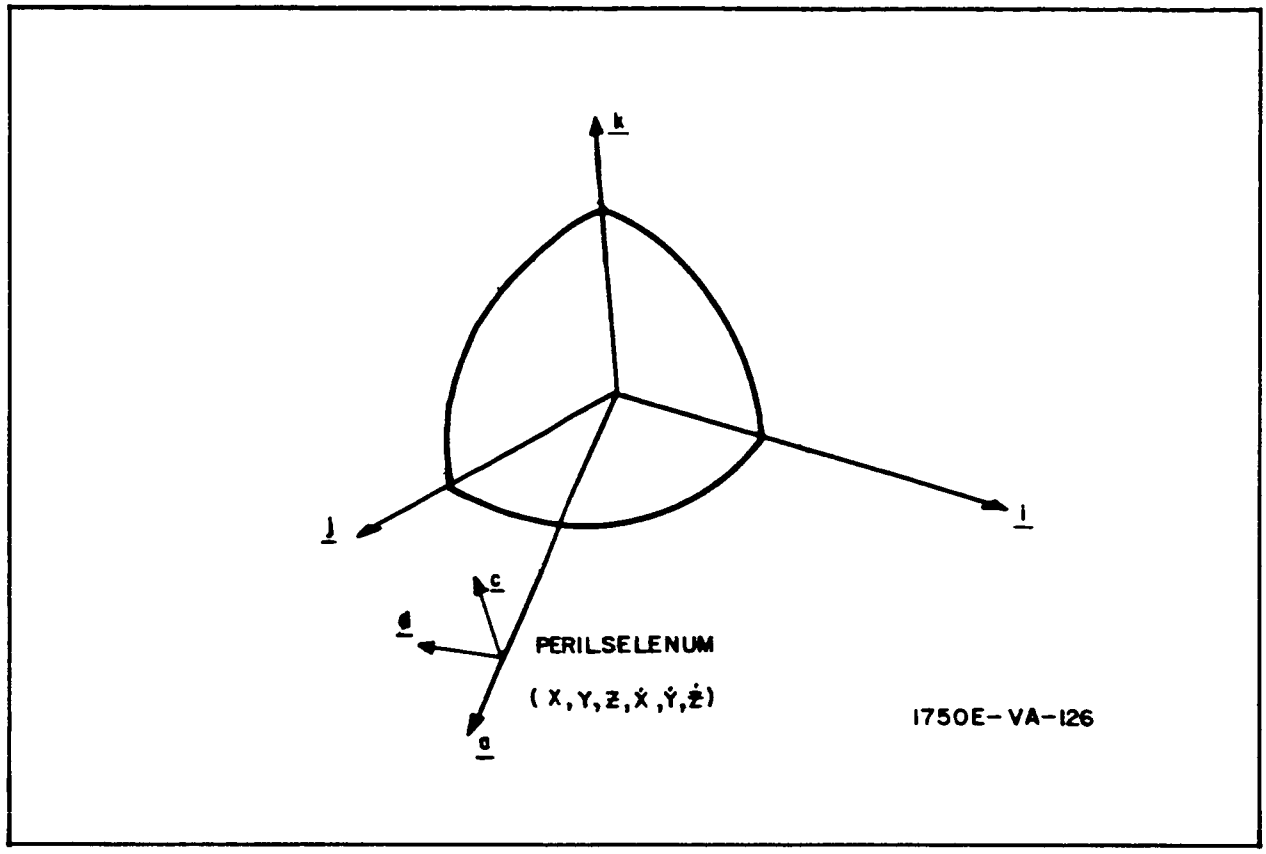

Figure 7. Geometry of Coordinate Conversion from XYZ System to Altitude-Downrange-Crossrange System

Assume that the desired periselenum conditions are described by (X, Y, Z, $\dot{X}$, $\dot{Y}$, $\dot{Z}$). Then unit vectors in the altitude and downrange directions can be written:

$$\underline{a} = \frac{X\underline{i} + Y\underline{j} + Z\underline{k}}{R} \tag{178}$$

$$\underline{d} = \frac{\dot{X}\underline{i} + \dot{Y}\underline{j} + \dot{Z}\underline{k}}{V} \tag{179}$$

where $R = \sqrt{X^2 + Y^2 + Z^2}$ is the desired periselenum radius and $V = \sqrt{\dot{X}^2 + \dot{Y}^2 + \dot{Z}^2}$ is the desired velocity. In order to generate an orthogonal coordinate system, $\underline{c}$, the cross-range unit vector is given by the product of $\underline{a}$ and $\underline{d}$.

$$\underline{c} = \underline{d} \times \underline{a} = \frac{(Y\dot{Z} - Z\dot{Y})\underline{i} + (X\dot{Z} - Z\dot{X})\underline{j} + (X\dot{Y} - Y\dot{X})\underline{k}}{RV} \tag{180}$$

Assume a position error vector at periselenum of $\underline{r}_e = e_x\underline{i} + e_y\underline{j} + e_z\underline{k}$. The component of $\underline{r}_e$ in the direction of a unit vector $\underline{a}$ is given by $\underline{r}_e \cdot \underline{a}$, so that

$$\text{Comp}_{\underline{a}}(\underline{r}_e) = \underline{r}_e \cdot \underline{a} = \frac{e_x X + e_y Y + e_z Z}{R} \tag{181}$$

$$\text{Comp}_{\underline{d}}(\underline{r}_e) = \underline{r}_e \cdot \underline{d} = \frac{e_x \dot{X} + e_y \dot{Y} + e_z \dot{Z}}{V} \tag{182}$$

$$\text{Comp}_{\underline{c}}(\underline{r}_e) = \underline{r}_e \cdot \underline{c} = \frac{e_x (Y\dot{Z} - Z\dot{Y}) + e_y (X\dot{Z} - Z\dot{X}) + e_z (X\dot{Y} - Y\dot{X})}{RV} \tag{183}$$

Defining the components of $\underline{r}_e$ in the altitude, downrange, and crossrange directions as e_a, e_d, e_c, equations 181 through 183 can be adjoined and written in matrix form:

$$\begin{bmatrix} e_a \\ e_d \\ e_c \end{bmatrix} = \begin{bmatrix} X/R & Y/R & Z/R \\ \dot{X}/V & \dot{Y}/V & \dot{Z}/V \\ \dfrac{Y\dot{Z} - Z\dot{Y}}{RV} & \dfrac{X\dot{Z} - Z\dot{X}}{RV} & \dfrac{X\dot{Y} - Y\dot{X}}{RV} \end{bmatrix} \begin{bmatrix} e_x \\ e_y \\ e_z \end{bmatrix} \tag{184}$$

$$\underline{r}_a = M'\underline{r}_e \tag{185}$$

Rotation of the velocity errors can be accomplished in a similar manner, so that

$$\underline{v}_a = M'\underline{v}_e \tag{186}$$

Defining the 6-dimensional error vector as $\underline{\varepsilon}_a$ (after rotation) and $\underline{\varepsilon}_e$ before

$$\underline{\varepsilon}_a = \begin{bmatrix} \underline{r}_a \\ \underline{v}_a \end{bmatrix} \begin{bmatrix} M' & O_{33} \\ O_{33} & M' \end{bmatrix} \begin{bmatrix} \underline{r}_e \\ \underline{v}_e \end{bmatrix} = M\underline{\varepsilon}_e \tag{187}$$

Now the covariance matrix of errors in the terminal position is given in terms of the rotated coordinates by

$$\text{Cov}(E_a) = E\left\{\underline{\varepsilon}_a \underline{\varepsilon}_a^T\right\} = E\left\{M\underline{\varepsilon}_e \underline{\varepsilon}_e^T M^T\right\} = ME\left\{\underline{\varepsilon}_e \underline{\varepsilon}_e^T\right\} M^T \quad (188)$$

But $E\left\{\underline{\varepsilon}_e \underline{\varepsilon}_e^T\right\}$ is just the covariance matrix of deviations from the nominal trajectory, or the N matrix, as previously defined. Then calling the N matrix after rotation into the altitude downrange and crossrange system, N_a,

$$N_a = MNM^T \quad (189)$$

where M is defined in equation 187. Either the position or velocity 3 x 3 covariance submatrices can be rotated separately by using M'; e.g.,

$$(N_1)_a = M'N_1 M'^T \quad (190)$$

A development identical with that employed above can also be used to rotate the P matrices; i.e.,

$$P_a = MPM^T \quad (191)$$

It may have occurred to the reader that all that is done in this appendix is to rotate the error matrix from one Cartesian coordinate system into another, when what should be done is to convert the errors into a spherical coordinate system, since this would be a more meaningful way of describing errors relative to the moon. However, it should be mentioned here that the error analysis done in this report is concerned only with second-order statistical averages - i.e., covariance matrices - which are completely described by an ellipsoid. This means that there is some discrepancy between the real distribution of errors around the moon, and that which can be described by an ellipsoid. This is illustrated in figure 8, where the error distributions are shown as different volumes in order to illustrate the difference in shapes. Note that the shaded error distribution cannot be described in terms of second order averages since terms of the form $E(X^2Y)$ and $E(Y^2X)$ are required. There are two reasons why this is not done: (1) comparison of second-order statistical averages with actual distributions indicates that the approximation is good and (2) use of third-order averages is too difficult mathematically (if it can be done at all).

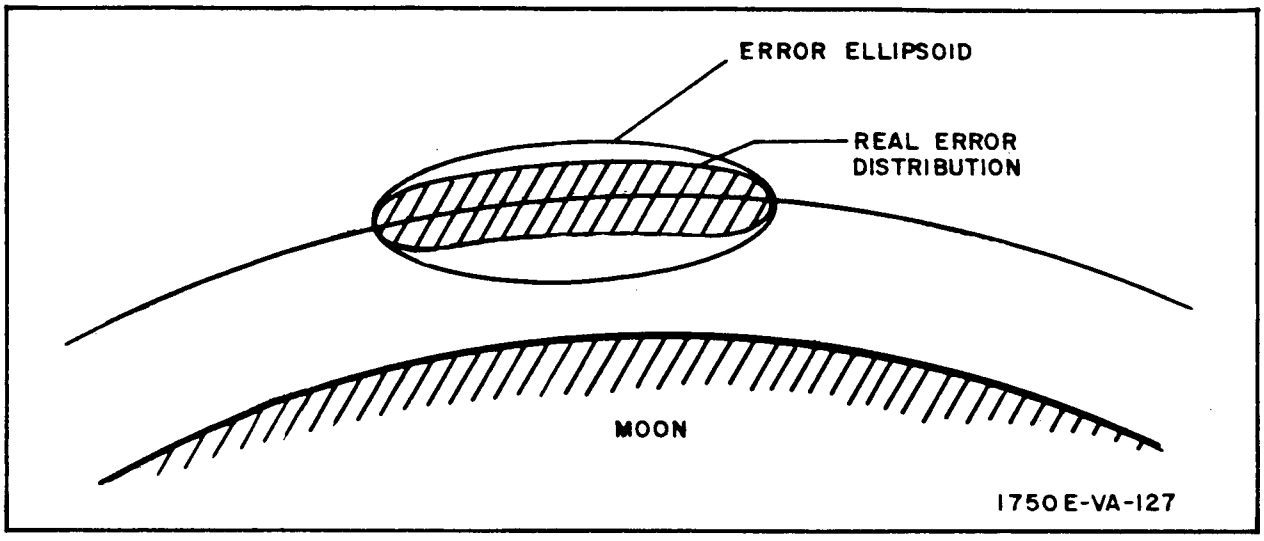

Figure 8. Difference Between Real Error Distribution and Covariance Ellipsoid

APPENDIX C

LUNAR PARKING AND DESCENT ORBITS

Much of the analytical background for this phase of the mission is an integral part of either the simulation description (Volume III) or Appendix A (Volume V). In fact, all that remains is a detailed derivation of the various trajectory parameters and a determination of input error magnitudes to be considered.

The cartesian vector solutions to the Keplerian orbit (Ref. 1) are repeated here, since they dominate much of the nominal orbit derivation.

Given the state vector ($\underline{X}_k$) at time (t_k), the position vector components at time (t_m) are:

$$X_{mj} = \left[1 - \frac{a}{r_k}(1-\cos\nu)\right] X_{kj} + \left[t_m - t_k - \frac{a^{\frac{3}{2}}}{\sqrt{\mu}}(\nu - \sin\nu)\right] X_{k,j+3} \qquad (1)$$

$$j = 1, 2, 3$$

and the velocity vector components are:

$$X_{mj} = \left[-\frac{\sqrt{\mu a}}{r_m r_k}\sin\nu\right] X_{k,\ j-3} + \left[1 - \frac{a}{r_m}(1-\cos\nu)\right] X_{kj} \qquad (2)$$

$$j = 4, 5, 6$$

where μ is the lunar gravitational constant, a is the semimajor axis of the ellipse, and ν is the incremental eccentric anomaly, which conforms to the equation

$$\frac{\sqrt{\mu}}{a^{3/2}}(t_m - t_k) = \nu - \sin\nu + \frac{r_k}{a}\sin\nu + \frac{d_k}{\sqrt{\mu a}}(1 - \cos\nu) \qquad (3)$$

Ref. 1 Pines, S., H. Wolf, D. Woolston, and R. Squires, Goddard Minimum Variance Orbit Determination Program, Goddard Space Flight Center Report.

The saclars r_i and d_i represent the radius vector magnitude $\left|\underline{R}_i\right|$ and the dot product of the radius and velocity vectors $\underline{R}_i \cdot \underline{V}_i$ respectively.

Major notation used in the analysis is listed below.

LIST OF NOTATION

English Alphabet

B Astronomical length vector

E Eccentric anomaly beyond periselenum

F Velocity increment vector

G Guidance law matrix

H Row vector of partial derivatives of observables

I Identity matrix

K Six-dimensional weighting vector

M Total number of observations on parking orbit

N Covariance matrix of deviations from nominal state

P Covariance matrix of errors in estimated state

Q Variance of measurement errors

R Selenocentric instantaneous vehicle position vector

S Selenocentric unit vector in the direction of a known star

T Period of parking orbit

U Unit eigenvector corresponding to maximum position uncertainty

V Selenocentric instantaneous velocity vector

W Direction cosine matrix for final tangential, vertical, and transverse error

X Six-dimensional state vector

Y Magnitude of an observable

a Parking orbit radius, semimajor axis (general)

a_d Descent orbit semimajor axis

b Length or component of $\underline{B}$ vector

c Random error

d Dot product of $\underline{R}$ and $\underline{V}$

e_d Descent orbit eccentricity

f Deviation from nominal velocity increment vector

i Inclination angle between the earth's equator and the earth-moon plane

q Mean lunar radius

r Magnitude of $\underline{R}$

s Component of S vector

t Time

u Component of U vector

v Magnitude of $\underline{V}$

x Deviation from nominal state vector

y Deviation of observable from reference value

Greek Alphabet

$\underline{\beta}$ Unit vector normal to $\underline{R}$ in star-vertical measurement plane[1/]

Γ Covariance matrix of input errors

δ Variation

θ True anomaly

θ_M Displacement of moon beyond vernal equinox

θ_S Displacement of sun beyond vernal equinox

Λ Eigenvalue of position uncertainty covariance matrix

λ Selenocentric latitude

μ Lunar gravitational constant

μ_e Gravitational constant of earth

μ_s Gravitational constant of sun

γ Incremental eccentric anomaly

σ Standard deviation

τ Time interval between observations on parking orbit

Φ State transition matrix

ψ Selenocentric longitude

[1/] Except in Section 3.

Superscripts

$[\ ]^T$ Matrix transpose

$[\ ]^{-1}$ Matrix inverse

Subscripts

A	Pertaining to termination of midcourse
E	Pertaining to termination of parking orbit
F	Pertaining to beginning of descent orbit
i,j	Vector or matrix components [2]
L	Pertaining to termination of descent orbit
m	Pertaining to the m^{th} observation
M	Pertaining to the last observation
n	Star index number
O	Pertaining to the beginning of parking orbit
P	Pertaining to the first pass over desired periselenum
1,2,3	X, Y, and Z cartesian position components respectively
4,5,6	X, Y, and Z cartesian velocity components respectively

Symbols Above Letters

$\bar{(\ )}$ Predicted value

$(\ )'$ Actual value

$\tilde{(\ )}$ Uncertainty, error in estimated value

$\hat{(\ )}$ Indicated or observed value

Symbols Below Letters

$\underline{(\ )}$ Vector

1. DETERMINATION OF NOMINAL FLIGHTPATH

With the nominal parking orbit defined by two noncolinear vectors,

[2] For time-varying vectors and matrices, the first subscript denotes the time.

$$\underline{R}_O = \begin{vmatrix} r_O \cos \lambda_O \cos \psi_O \\ r_O \cos \lambda_O \sin \psi_O \\ r_O \sin \lambda_O \end{vmatrix} \tag{4}$$

$$\underline{R}_P = \begin{vmatrix} r_P \cos \lambda_P \cos \psi_P \\ r_P \cos \lambda_P \sin \psi_P \\ r_P \sin \lambda_P \end{vmatrix} \tag{5}$$

of equal magnitude,

$$r_O = r_P = a \tag{6}$$

The period of the circular orbit is

$$T = \frac{2\pi a^{3/2}}{\sqrt{\mu}} \tag{7}$$

With the vector ($\underline{R}_P$) as the orbital plane reference,

$$E_P = 0 \tag{8}$$

and the eccentric anomaly at time (t_O) is

$$E_O = \theta_O = \left\{ \text{sgn} \left(\theta_O \right) \right\} \arccos \left\{ \frac{1}{a^2} \left(\underline{R}_O \cdot \underline{R}_P \right) \right\} \tag{9}$$

This defines the quadrant of the angle, when the inverse cosine function is defined as the principal value, less than π radians in absolute value.

With the injection point as the reference in the orbital plane,

$$\nu_O = 0 \tag{10}$$

the incremental eccentric anomaly separating (t_O) and (t_P) is

$$\nu_P = 2\pi - E_O \tag{11}$$

for a retrograde orbit.

The fraction of a period separating the two vectors is merely $(\nu_P/2\pi)$. Finally, the radius vector is always normal to the velocity vector in a circular orbit, so that

$$d_O = 0 \tag{12}$$

All of the necessary quantities are now available for computation of the initial velocity vector $\underline{V}_O$. This completes the geometric definition of the parking orbit.

In order to provide an automatic rendezvous capability in the event that no landing is made after descent, the descent orbit period is chosen equal to the period of the circular orbit. It follows that

$$a_d = a \tag{13}$$

The eccentricity of the descent orbit is

$$e_d = 1 - \frac{r_L}{a_d} \tag{14}$$

The eccentric anomaly of the descent arc (E_F) must be 90 degrees for equation 13 to hold. From the well known relation

$$\sin \theta_F = \frac{\sqrt{1 - e_d^2}\, \sin E_F}{1 - e_d \cos E_F} \tag{15}$$

plus the fact that the true anomaly separating t_F and t_L is the same for the circular and elliptical orbits,

$$\sin \theta_E = \sqrt{1 - e_d^2} \tag{16}$$

Since the true anomaly is never smaller than the corresponding eccentric anomaly, and t_E lags t_L, the principal value of θ_E is negative and greater than $\pi/2$ radians in absolute value. The eccentric anomaly of the descent arc, as measured on the circular orbit, is

$$E_E = \theta_E \tag{17}$$

Since descent is initiated on the second revolution, the incremental eccentric anomaly at descent time is

$$\nu_E = 2\pi + \left\{ \text{principal value of } (E_E - E_O) \right\} \tag{18}$$

In this case E_E is negative and E_O is positive; the value of (ν_E) is

$$\nu_E = 4\pi - \left| E_E \right| - E_O \tag{19}$$

Since this is measured along the circular orbit, the time interval separating t_O and t_E is

$$t_E - t_O = \frac{\nu_E}{2\pi} (T) \tag{20}$$

By substituting E for m and O for k in equation 1, the position vector $\underline{R}_E = \underline{R}_F$ at descent initiation can now be computed.

Now with t_F as the reference initial point of the descent orbit,

$$\nu_F = 0 \tag{21}$$

so that the incremental eccentric anomaly at time t_L is

$$\nu_L = - E_F \tag{22}$$

The descent time can be computed from Kepler's second law:

$$t_L - t_F = \frac{a_d^{3/2}}{\sqrt{\mu}} \left\{ \left| E_F \right| - e_d \sin \left| E_F \right| \right\} \tag{23}$$

Finally, with

$$r_F = a = a_d \tag{24}$$

the velocity vector at time t_F can be computed from equation 2:

$$X_{F,\ j+3} = \frac{X_{Lj} - (\cos \nu_L)\, X_{Fj}}{(t_L - t_F) - \frac{(a_d)^{3/2}}{\mu} (\nu_L - \sin \nu_L)} \tag{25}$$

in which the position vector ($\underline{R}_L$) is the nominal periselenum radius vector,

$$\begin{vmatrix} X_{L1} \\ X_{L2} \\ X_{L3} \end{vmatrix} = \begin{vmatrix} r_L \cos \lambda_P \cos \psi_P \\ r_L \cos \lambda_P \sin \psi_P \\ r_L \sin \lambda_P \end{vmatrix} \tag{26}$$

Magnitudes of radius vectors, velocity vectors, and their dot products are always computed from the same simple expressions:

$$r_K = \sqrt{(X_{K1})^2 + (X_{K2})^2 + (X_{K3})^2} \tag{27}$$

$$v_K = \sqrt{(X_{K4})^2 + (X_{K5})^2 + (X_{K6})^2} \tag{28}$$

$$d_K = \underline{R}_K \cdot \underline{V}_K \tag{29}$$

The nominal perigee velocity vector is readily computed from equation 2 with the subscripts m and k replaced by L and F respectively and (a) replaced by (a_d).

The nominal velocity impulses are merely the vector differences between velocities before and after thrust application. Since injection into the parking orbit is assumed impulsive and tangential,

$$X_{Aj} = X_{Oj}, \qquad 1 \le j \le 3 \tag{30}$$

$$X_{Aj} = (v_A/v_O)\ X_{Oj}, \qquad 4 \le j \le 6 \tag{31}$$

where v_A is the assumed speed at midcourse termination.

A typical speed of 2400 meters/per second is assumed for (v_A), and

$$F_{Aj} = X_{O,\ j+3} - X_{A,\ j+3},\quad 1 \leq j \leq 3 \tag{32}$$

Similarly,

$$F_{Ej} = X_{F,\ j+3} - X_{E,\ j+3},\quad 1 \leq j \leq 3 \tag{33}$$

in which the velocity vector at t_F is computed from equation 25 and the velocity vector at t_E follows from equation 2 with the subscript m replaced by E and k replaced by O.

2. TYPICAL INPUT ERROR MAGNITUDES

2.1 Thrust Tolerances

With three independent and orthogonal thrust error components of zero mean and equal variance, the total rms thrust error is

$$\sqrt{3}\quad \sigma_T \tag{34}$$

where σ_T is the rms thrust error in each axis. This applies to both thrust application and thrust measurement.

Although the velocity increments are assumed impulsive for the analysis, typical error figures should be derived on the basis of finite pulse width. At injection the total impulse is

$$v_A - \sqrt{\frac{\mu}{a}} = 2400 - 1589 = 811 \text{ meters/sec} \tag{35}$$

This is equivalent to a time-acceleration product of 82,8 earth g's, corresponding to 13.8 g's for 6 seconds in the allowable acceleration limit (Ref. 2). At half thrust for twice as long an interval, the acceleration is essentially

---

Ref. 2

Bryson, A. E., K. Mikami, and C. T. Battle, Optimum Lateral Turns for a Reentry Glider, Aerospace Engineering, Vol. 21, No. 3, March 1963, p. 21.

7 g's for 12 seconds. The linearity error in an accelerometer is the predominant factor at this g-level; a reasonable estimate of total thrust measurement error at injection is:

$$\frac{10^{-5}\ \text{g's}}{\text{g}} \times 7\text{g} \times 12\ \text{sec} = 0.00825\ \text{meter/sec} \tag{36}$$

or an rms error in each axis of

$$\frac{0.00825}{\sqrt{3}} \doteq 0.005\ \text{meter/sec.} \tag{37}$$

Actually, this uncertainty in the applied impulse is outweighed by orbital velocity uncertainties typically encountered. To avoid possible implication of stringent impulse measurement specifications, a lenient tolerance of 0.05 meters per second rms error in each axis is assumed here, [3/] and therefore the thrust measurement error plays a very minor role in this study.

Descent thrust pulse width is not as readily fixed by obvious considerations, and no detailed attention has been devoted to descent mechanization. As an expedient, the rms impulse measurement errors have been assumed equal for descent and injection into the parking orbit.

For control of applied thrust, the errors are not expected to be so small. One percent of the applied impulse is a reasonable estimate of rms application error. For injection, then, the rms error in each axis is typically

$$\frac{(0.01)(2400-1589)}{3} \doteq 5\ \text{meters/sec} \tag{38}$$

For descent, the total nominal impulse is 150 meters per second; rms error for each axis in applying the descent impulse is typically

$$\frac{(0.01)\ (150)}{3} \doteq 1\ \text{meter/sec} \tag{39}$$

Unfortunately, however, this is an excessive amount of error for the FTOA guidance system assumed here. As a rough indication of the resulting rms tangential periselenum miss distance, consider the extra arc length traveled over a quarter of an orbit (90-degree descent) due to an excess

[3/] See Table 3-2 of Volume III.

velocity of 1 meter per second: Equation 7 gives about 2 hours as the period of a low altitude orbit, and

$$1 \frac{\text{meter}}{\text{sec}} \times (1/4 \times 7200) \text{ seconds} \doteq 1800 \text{ meters} \qquad (40)$$

The 3-σ tangential error would then exceed the allowable specification of 5 kilometers, even without any navigation errors.

To prevent the guidance errors from dominating the results, it is necessary to assume an applied descent thrust error of 0.1 meters per second rms in each axis and to determine the navigation requirements with the understanding that the FTOA guidance scheme is inadequate and a superior technique must be used in the actual system mechanization.

2.2 Initial Conditions

In previous studies (Ref. 3 and Ref. 4) it is assumed that the initial state vector estimate coincides with the nominal trajectory. At the beginning of the lunar parking orbit, however, a more accurate state vector estimate will be available from midcourse navigation information. A distinction is therefore made between the deviations from the nominal initial state and the uncertainty in the actual state. For a simulation in which the sensitivity coefficients used in data processing are computed from the estimated trajectory, the initial deviations from nominal state obviously play a minor role. Initial rms values of 10 kilometers and 10 meters per second were chosen as the standard position and velocity deviations in each axis respectively.

The standard initial uncertainties in each axis were assumed to be 1 kilometer and 1 meter per second for position and velocity respectively. These values were selected in order that the total rms initial uncertainties would lie roughly in the vicinity of the terminal midcourse navigation errors as given in Section 2 of Volume III.

Ref. 3

Smith, G. L., S. F. Schmidt, and L. A. McGee, Application of Statistical Filter Theory to the Optimal Estimation of Position and Velocity on Board a Circumlunar Vehicle, NASA TND-1208, 1961.

Ref. 4

McLean, J. D., S. F. Schmidt, and L. A. McGee, Application of Statistical Filter Theory to the Optimal Estimation of Position and Velocity on Board a Circumlunar Vehicle, NASA TND-1208, 1961.

2.3 Measurement Errors

As explained in subsection 3.2 of Volume III, the errors in the measured angles are dominated by local vertical pointing error. Due to the absence of a lunar atmosphere, errors on the order of a tenth of one degree are considered within the anticipated state of the art. Because of the tradeoff between measurement uncertainty and frequency of observation, the choice of an assumed standard measurement error for this analysis is not especially critical. A value of 1 milliradian rms was chosen for the first series of runs, and larger values were investigated for the complete guidance simulation.

Wherever applicable, the rms uncertainty in the observed altitude was assumed to be 1 kilometer, including terrain irregularities.

3. TRIAXIAL LUNAR OBLATENESS (Ref. 5)

The i^{th} component of perturbing acceleration due to the nonspherical shape of the moon can be approximated as

$$\ddot{\Delta X}_i = -\frac{\mu X_i}{r^3}\left\{k_o \frac{q^2}{r^2}\right\}\left[\gamma\left(k_1 - \frac{5X_2^2}{r^2}\right) + \beta\left(k_2 - \frac{5X_3^2}{r^2}\right)\right] \quad i = 1, 2, 3 \qquad (41)$$

where

$$\gamma \doteq (1 - 0.61)\beta \qquad (42)$$

$$\beta \doteq 0.0006294 \qquad (43)$$

and

$$k_o = \left(\frac{3}{2}\right)(0.397) = 0.5955 \qquad (44)$$

Ref. 5

Brouwer, D. and G. M. Clemence, "Moments of Inertia of the Moon," A Review of Space Research, National Academy of Sciences, National Research Council Publication 1079, Iowa State University, June - August 1962, pp. 3-9, 3-10.

In these equations, k_1 and k_2 take the values

$$\left.\begin{aligned} k_1 &= 1, \quad i = 1, 3 \\ k_1 &= 3, \quad i = 2 \\ k_2 &= 1, \quad i = 1, 2 \\ k_2 &= 3, \quad i = 3 \end{aligned}\right\} \tag{45}$$

4. STATE TRANSITION MATRIX

The transition matrix elements follow directly from equations 1 and 2. For $1 \leq i \leq 3$,

$$\begin{aligned} \phi_{mij} = & \left[1 - \frac{a_{m-1}}{\hat{r}_{m-1}} \left(1 - \cos \nu_m \right) \right] \delta(i, j) \\ & - X_{m-1, i} \left[\frac{a_{m-1}}{\hat{r}_{m-1}} \sin \nu_m \nabla_j \left(\nu_m \right) \right. \\ & \left. - \left(1 - \cos \nu_m \right) \left(\frac{a_{m-1}}{\hat{r}_{m-1}} \right)^2 \nabla_j \left(\frac{\hat{r}_{m-1}}{a_{m-1}} \right) \right] \\ & + \left[\left(t_m - t_{m-1} \right) - \frac{a_{m-1}^{3/2}}{\sqrt{\mu}} \left(\nu_m - \sin \nu_m \right) \right] \delta (j, i + 3) \\ & - \frac{\hat{X}_{m-1, i+3}}{\sqrt{\mu}} \left[a_{m-1}^{3/2} \left(1 - \cos \nu_m \right) \nabla_j \left(\nu_m \right) \right. \\ & \left. + \frac{3}{2} \sqrt{a_{m-1}} \left(\nu_m - \sin \nu_m \right) \nabla_j \left(a_{m-1} \right) \right] \end{aligned} \tag{46}$$

and for $4 \le i \le 6$,

$$\phi_{mij} = \left[-\frac{\sqrt{\mu a_{m-1}}}{\bar{r}_m \hat{r}_{m-1}} \sin \nu_m \right] \delta(i-3, j)$$

$$- \sqrt{\mu}\, \hat{X}_{m-1,\, i-3} \left\{ \frac{1}{\bar{r}_m \hat{r}_{m-1}} \left[\sqrt{a_{m-1}} \cos \nu_m \nabla_j(\nu_m) \right. \right.$$

$$\left. + \frac{\sin \nu_m}{2\sqrt{a_{m-1}}} \nabla_j(a_{m-1}) \right]$$

$$\left. - \frac{\sqrt{a_{m-1}} \sin \nu_m}{\bar{r}_m^2 \hat{r}_m^2} \left[\bar{r}_m \nabla_j(\hat{r}_{m-1}) + \hat{r}_{m-1} \nabla_j(\bar{r}_m) \right] \right\} \tag{47}$$

$$+ \left[1 - \frac{a_{m-1}}{\bar{r}_m}(1 - \cos \nu_m) \right] \delta(i, j)$$

$$- \hat{X}_{m-1,\, i} \left\{ \frac{1}{\bar{r}_m} \left[a_{m-1} \sin \nu_m \nabla_j(\nu_m) \right. \right.$$

$$\left. \left. + (1 - \cos \nu_m) \nabla_j(a_{m-1}) \right] - \frac{a_{m-1}(1 - \cos \nu_m)}{\bar{r}_m^2} \nabla_j(\bar{r}_m) \right\}$$

where

$$\delta(m, n) = \begin{cases} 1, & m = n \\ 0, & m \neq n \end{cases} \tag{48}$$

and

$$\nabla_j(\quad) \triangleq \frac{\partial(\quad)}{\partial X_{m-1,\, j}} \tag{49}$$

can be found by differentiation of the various Keplerian relationships; e.g., from the definition of the semimajor axis,

$$\nabla_j\left(a_{m-1}\right) = -\,a_{m-1}^2\,\nabla_j\left(\frac{1}{a_{m-1}}\right)$$

$$= 2a_{m-1}^2\,\hat{X}_{m-1,j}\left\{\left(\hat{r}_{m-1}\right)^{-3}\left[\delta\left(1,j\right)+\delta\left(2,j\right)+\delta\left(3,j\right)\right]\right.$$

$$\left.+\frac{1}{\mu}\left[\delta\left(4,j\right)+\delta\left(5,j\right)+\delta\left(6,j\right)\right]\right\}$$

APPENDIX D

LUNAR LANDING ANALYSES

In this appendix equations for the lunar landing analyses are derived and choices of landing parameters are explained. Mathematical notation used is listed below.

LIST OF NOTATION

English Alphabet

F	General control quantity
f	Deviation of F from the reference value
g_o	Acceleration of gravity at the earth's surface, 9.80665 m/sec^2
h	Altitude above the lunar surface
I_{sp}	Fuel specific impulse
R	Line-of-sight range from the spacecraft to the desired landing site
r_c	Mean lunar radius, 1738 kilometers
T	Magnitude of the vehicle thrust vector
t	Time, referenced to the time of landing maneuver initiation
V	Magnitude of the spacecraft velocity vector
X	General state variable
x	Deviation of X from the reference value
Y	The general observable quantity
y	Deviation of Y from the reference value

Greek Alphabet

α	Orientation of the spacecraft thrust vector relative to the velocity vector
γ	Spacecraft flight path angle relative to spacecraft local horizontal
θ	Angular displacement of the spacecraft from the desired landing site in lunar central coordinates
μ	Lunar gravitational constant; 4.89820×10^{12} m^3/sec^2
σ	Root mean squared value
ϕ	Line-of-sight angle from the spacecraft to the desired landing site referenced to spacecraft local vertical
Ω	Line-of-sight angle from the desired landing site to the spacecraft referenced to landing site local vertical

Superscripts

$[\ ]^T$	Matrix transpose
$[\ ]^{-1}$	Matrix inverse

Subscripts

B	Denotes quantities pertaining to a system using beacon tracker observables
D	Denotes quantities pertaining to a system using doppler navigation observables
f	Denotes final value
i, j	Matrix or vector element indices
m	Time index
M	The maximum value of m
n	Indicates a random error quantity
o	Denotes initial value
p, q	Matrix or vector indices
r	Denotes reference value (value on the nominal trajectory)
X	Denotes a quantity pertaining to the state variable, X
Y	Denotes a quantity pertaining to the observable, Y

Operators

$\dot{(\ )}$ Derivative with respect to time $\frac{d(\ )}{dt}$

$\overset{\circ}{(\ )}$ Derivative with respect to τ, $\frac{d(\ )}{d\tau}$

$\langle(\ )\rangle_{av}$ Ensemble average overall possible missions

Symbols above and below quantities

$\hat{(\ )}$ Estimated value or value computed on the basis of observed information

$\tilde{(\ )}$ Estimation error, difference between the actual value and the estimated value

$\underline{(\ )}$ A vector (column matrix)

1. OPTIMUM TRAJECTORY PROGRAM

1.1 Equations of Motion

This is a steepest ascent program designed primarily for determining optimum lunar landing trajectories for constant-thrust vehicles.[1] The program uses the method of steepest ascents to determine the coefficients of a second order polynomial (in time) vehicle pitch program which will enable the vehicle to land in minimum time.

The equations of motion are: (See figure 1)

$$\dot{s} = \frac{u}{r_c + h} - \frac{\mu}{(r_c + h)^2} + \frac{T \sin\eta}{m}$$

$$\dot{u} = \frac{us}{r_c + h} + \frac{T \cos\eta}{m} \qquad (1)$$

$$\dot{h} = s$$

$$\dot{\theta} = \frac{180}{\pi} \frac{u}{r_c + h} \qquad \text{(deg/sec.)}$$

[1] A more thorough explanation of this method of obtaining optimum trajectories can be found in A. E. Bryson and W. F. Deuham, "A Steepest Ascent Method for Solving Optimum Program Problems, Journal of Applied Mechanics, June 1962, pp. 247-257.

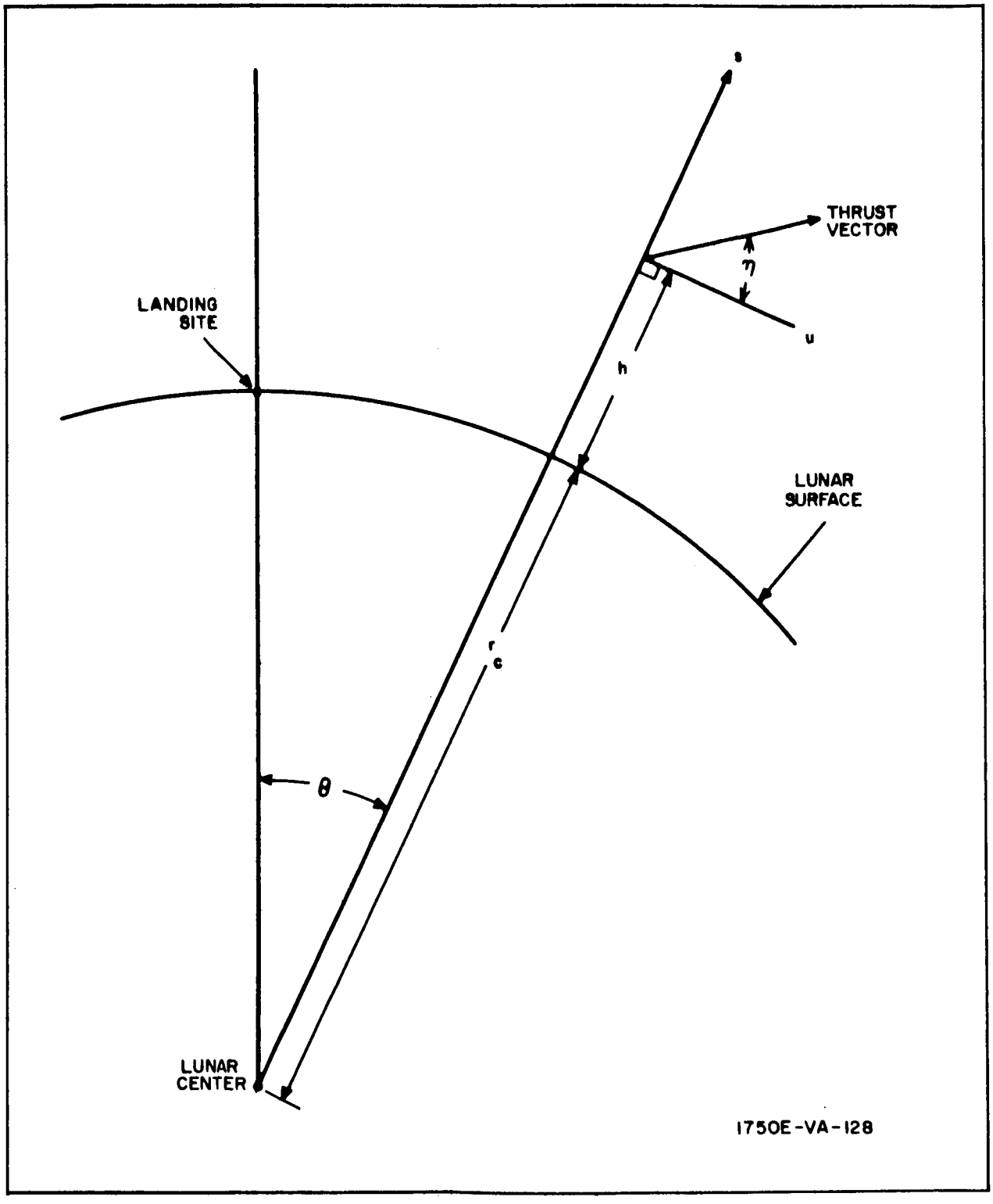

Figure 1. Lunar Landing Geometry

where

$m = m_o + \dot{m}t$ ($\dot{m}$ = constant)

$\eta = \eta_1 + \eta_2 t + \eta_3 t^2$: pitch program

s = vertical velocity

u = horizontal velocity

m_o = initial vehicle mass

$\dot{m}$ = mass rate of flow

h = altitude of the vehicle

θ = the central angle covered

η_1, η_2, and η_3 are the coefficients determined by the steepest ascent procedure.

Using numerical integration, the program computes the trajectory determined by the vector equation

$$\dot{\underline{b}} = \underline{f}(\underline{b}, t, \underline{\eta}^\circ) \tag{2}$$

where

$\dot{\underline{b}}$ = a column vector whose components are $\dot{u}$, $\dot{s}$, $\dot{h}$, $\dot{\theta}$

$\underline{b}$ = a column vector whose components are u, s, h, θ

t = time

$\underline{\eta}^\circ$ = a column whose components are η_1, η_2, η_3

Simultaneously with this computation, three additional trajectories are generated by using:

$$\dot{\underline{B}}^i = \underline{f}\left[\underline{B}^{(i)}, t, \underline{\eta}^\circ + \delta\underline{\eta}^{(i)}\right] ; \left\{i = 1, 2, 3\right\} \tag{3}$$

where

$\delta\underline{\eta}^{(i)}$ = the i^{th} column of the 3 x 3 matrix $[\delta\eta]$ of perturbations in $\underline{\eta}$ defined as:

$$[\delta\eta] = \begin{bmatrix} \delta\eta_1 & 0 & 0 \\ 0 & \delta\eta_2 & 0 \\ 0 & 0 & \delta\eta_3 \end{bmatrix} \tag{4}$$

$\dot{\underline{B}}^{(i)}$ = the i^{th} column of the matrix $[\dot{B}]$ with elements $\dot{u}_i$, $\dot{s}_i$, $\dot{h}_i$, and $\dot{\theta}_i$.

$\underline{B}^{(i)}$ = the i^{th} column of the matrix $[B]$ with elements u_i, s_i, h_i, and θ_i.

Integration of equation 2 stops when $s = s_f$ (the desired final value of s). The time is denoted by t_n. Integration of equation 3 stops when $s_i = s_f$. The time is denoted by t_i.

1.2 Optimization of Pitch Program

When the integrations indicated above have been completed, the program automatically computes new values of η_1, η_2, and η_3 to be used in the next iteration of the optimizing process. The computations performed are indicated below and are written in the nomenclature used by Bryson and Deuham.

$$\underline{\psi} = \begin{bmatrix} (u_f - u(t_n)) \\ (h_f - h(t_n)) \end{bmatrix} \tag{5}$$

$$\underline{\delta\psi}_i = \begin{bmatrix} (u_i(t_i) - u(t_n)) \\ (h_i(t_i) - h(t_n)) \end{bmatrix} = \begin{bmatrix} \delta\psi_i^{(1)} \\ \delta\psi_i^{(2)} \end{bmatrix} \qquad i = \{1, 2, 3\} \tag{6}$$

$$\phi = t_n$$

$$\delta\phi_i = (t_i - t_n) \quad \{i = 1, 2, 3\} \tag{7}$$

(8)

$$\left[\lambda_\psi\right]=\begin{bmatrix} \frac{\delta\psi_1^{(1)}}{\delta\eta_1} & \frac{\delta\psi_1^{(2)}}{\delta\eta_1} \\ \frac{\delta\psi_2^{(1)}}{\delta\eta_2} & \frac{\delta\psi_2^{(2)}}{\delta\eta_2} \\ \frac{\delta\psi_3^{(1)}}{\delta\eta_3} & \frac{\delta\psi_3^{(2)}}{\delta\eta_3} \end{bmatrix} \qquad (9)\underline{2/}$$

$$\underline{\lambda}_\phi=\begin{bmatrix} \frac{\delta\phi_1}{\delta\eta_1} \\ \frac{\delta\phi_2}{\delta\eta_2} \\ \frac{\delta\phi_3}{\delta\eta_3} \end{bmatrix} \qquad (10)\underline{3/}$$

In addition, the following definitions are made:

$$\left[I_{\psi\psi}\right]=\left[\lambda_\psi\right]^T\left[\Lambda\right]^{-1}\left[\lambda_\psi\right] \qquad (11)$$

$$\underline{I}_{\psi\phi}=\left[\lambda_\psi\right]^T\left[\Lambda\right]^{-1}\underline{\lambda}_\phi \qquad (12)$$

$$I_{\phi\phi}=\underline{\lambda}_\phi^{\,T}\left[\Lambda\right]^{-1}\underline{\lambda}_\phi \qquad (13)$$

The matrix $\left[\Lambda\right]$ is a 3 x 3 diagonal weighting matrix used in determining the relation between the changes in η_1, η_2, and η_3 to be made from iteration

---

$\underline{2/}$ The transpose of the quantity defined as $\left[\lambda_\psi\right]$ here is the same as the product $\left[\lambda_\psi\right]^T\left[G\right]$ in Bryson and Denham.

$\underline{3/}$ The transpose of $\underline{\lambda}_\phi$ is equal to the quantity $\underline{\lambda}_\phi^{\,T}\left[G\right]$ in Bryson and Denham.

to iteration. (The values of the elements of $[\Lambda]$ used in this analysis are not included in the report provided by Raytheon.)

Next the vector $\underline{d\beta}$ is defined; $\underline{d\beta}$ can take on two possible values, depending on the sign of the quantity $(dP)^2 - \underline{\psi}^T \left[I_{\psi\psi}\right]^{-1} \underline{\psi}$; where (dP) is a predetermined constant dependant on the maximum step size of the changes in quantities η_1, n_2, and η_3 to be allowed from iteration to iteration. (The value of (dP) used by Raytheon is not reported.)

If

$$(dP)^2 - \underline{\psi}^T \left[I_{\psi\psi}\right]^{-1} \underline{\psi} \geq o \tag{14}$$

Then

$$\underline{d\beta} = \underline{\psi}$$

Should the indicated difference be less than zero,

$$\underline{d\beta} = \left[\frac{(dP)}{\underline{\psi}^T \left[I_{\psi\psi}\right]^{-1} \underline{\psi}}\right] \underline{\psi} \tag{15}$$

The change in $\underline{\eta}$ to be made for the next trial run is determined from the following expression:

$$\underline{d\eta} = \begin{bmatrix} d\eta_1 \\ d\eta_2 \\ d\eta_3 \end{bmatrix} = -\left[\Lambda\right]^{-1} \left\{ \underline{\lambda}_\phi - \left[\lambda_\psi\right] \left[I_{\psi\psi}\right]^{-1} \underline{I}_{\psi\phi} \right\} \left\{ \frac{(dP)^2 - \underline{d\beta}^T \left[I_{\psi\psi}\right]^{-1} \underline{d\beta}}{I_{\phi\phi} - \underline{I}_{\psi\phi}^T \left[I_{\psi\psi}\right]^{-1} \underline{I}_{\psi\phi}} \right\}$$

$$+\left[\Lambda\right]^{-1} \left[\lambda_\psi\right] \left[I_{\psi\psi}\right]^{-1} \underline{d\beta} \tag{16}$$

Then

$$\underline{\eta}_{new} = \underline{\eta}_{old} + \underline{d\eta} \tag{17}$$

The process outlined above is repeated using the new values of η_1, η_2, and η_3 until u, s, and h converge to the desired final values u_f, s_f, and h_f while t_n is minimized, thus producing an optimum trajectory.

1.3 Typical Optimum Trajectory Characteristics

Figures 2 through 6 illustrate some characteristics of the class of trajectories obtained by the preceding optimization technique.

Figure 2 illustrates two optimum pitch programs developed for two sets of inputs. The input quantities and the resulting pitch program equations are included in the figure.

Figures 3 and 4 show typical X-Y profiles of the trajectories generated. Input conditions are summarized in the figures.

Figure 5 illustrates the line-of-sight angular rate ($\dot{\Omega}$) as a function of time for trajectories corresponding to three sets of input conditions.

Figure 6 shows the characteristic velocity, ΔV, required for an optimum descent from periselenum of a synchronous approach orbit. Other pertinent parameters are summarized in the figure.

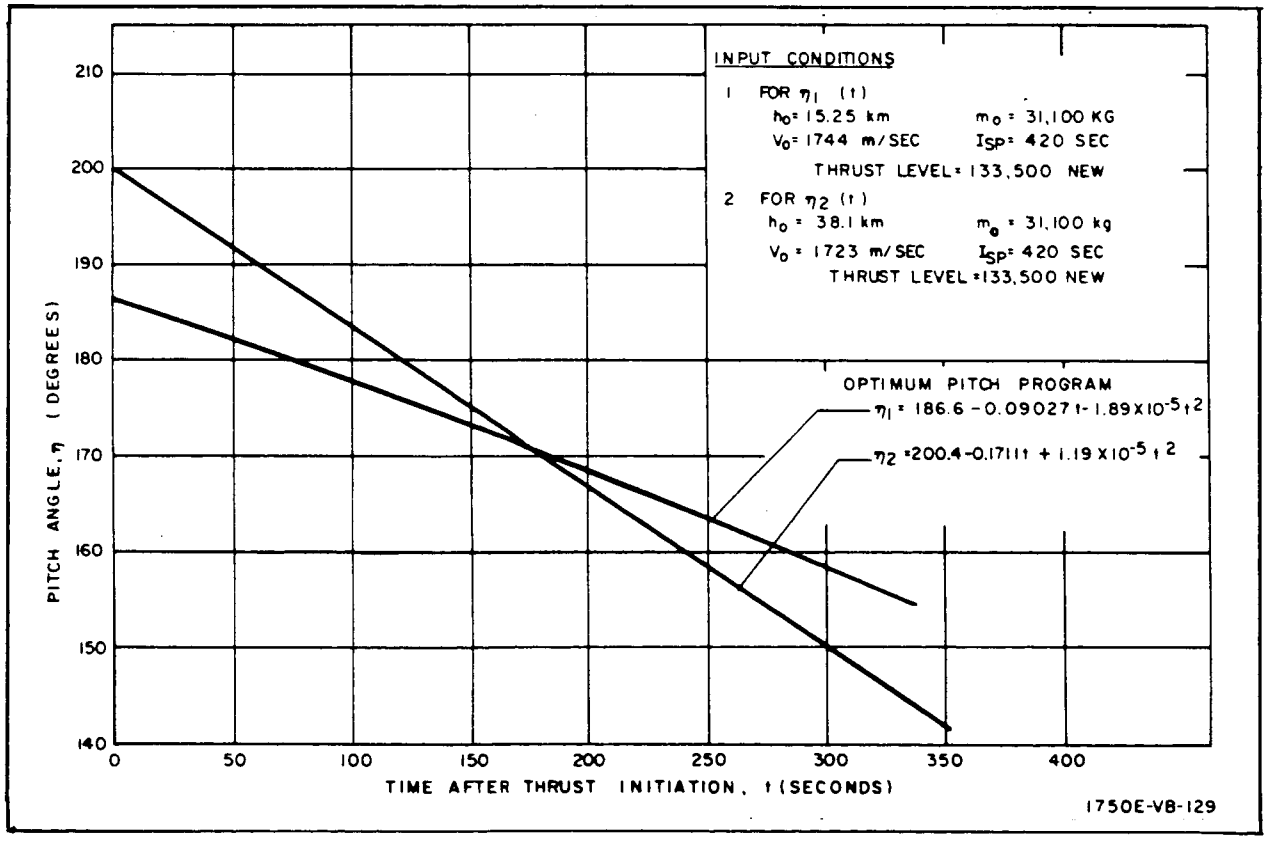

Figure 2. Typical Optimum Pitch Programs

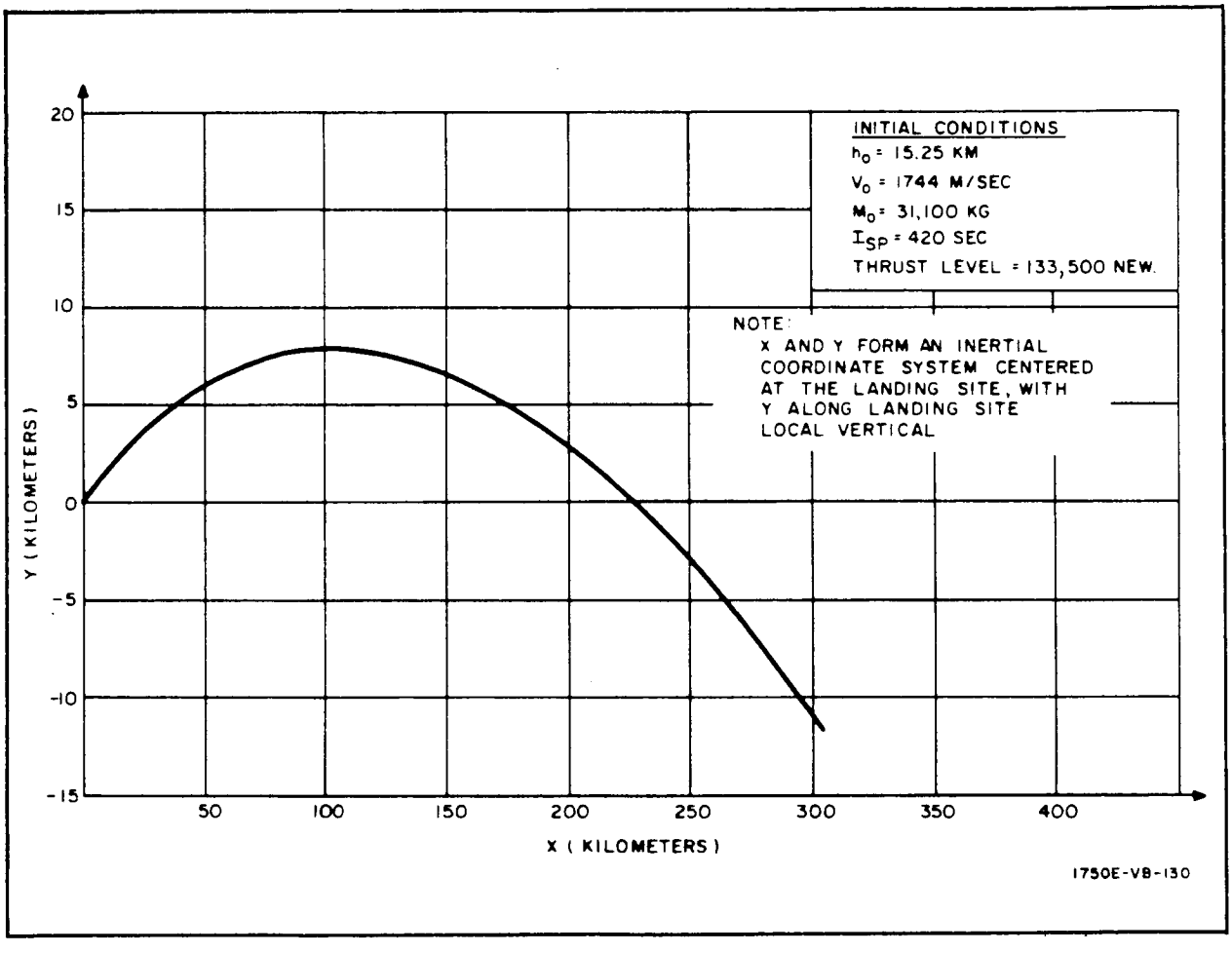

Figure 3. Typical Landing Trajectory Profile

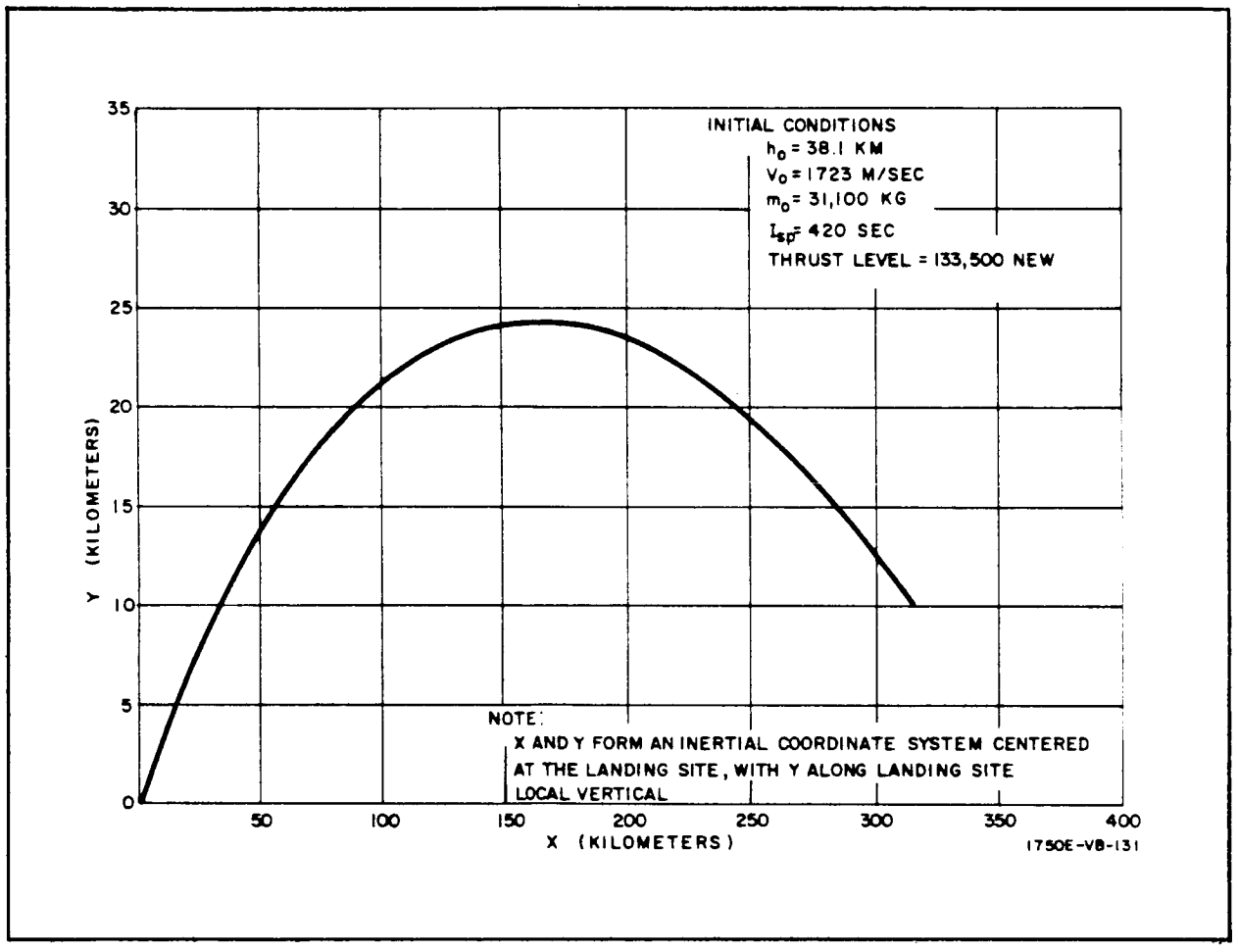

Figure 4. Typical Landing Trajectory Profile

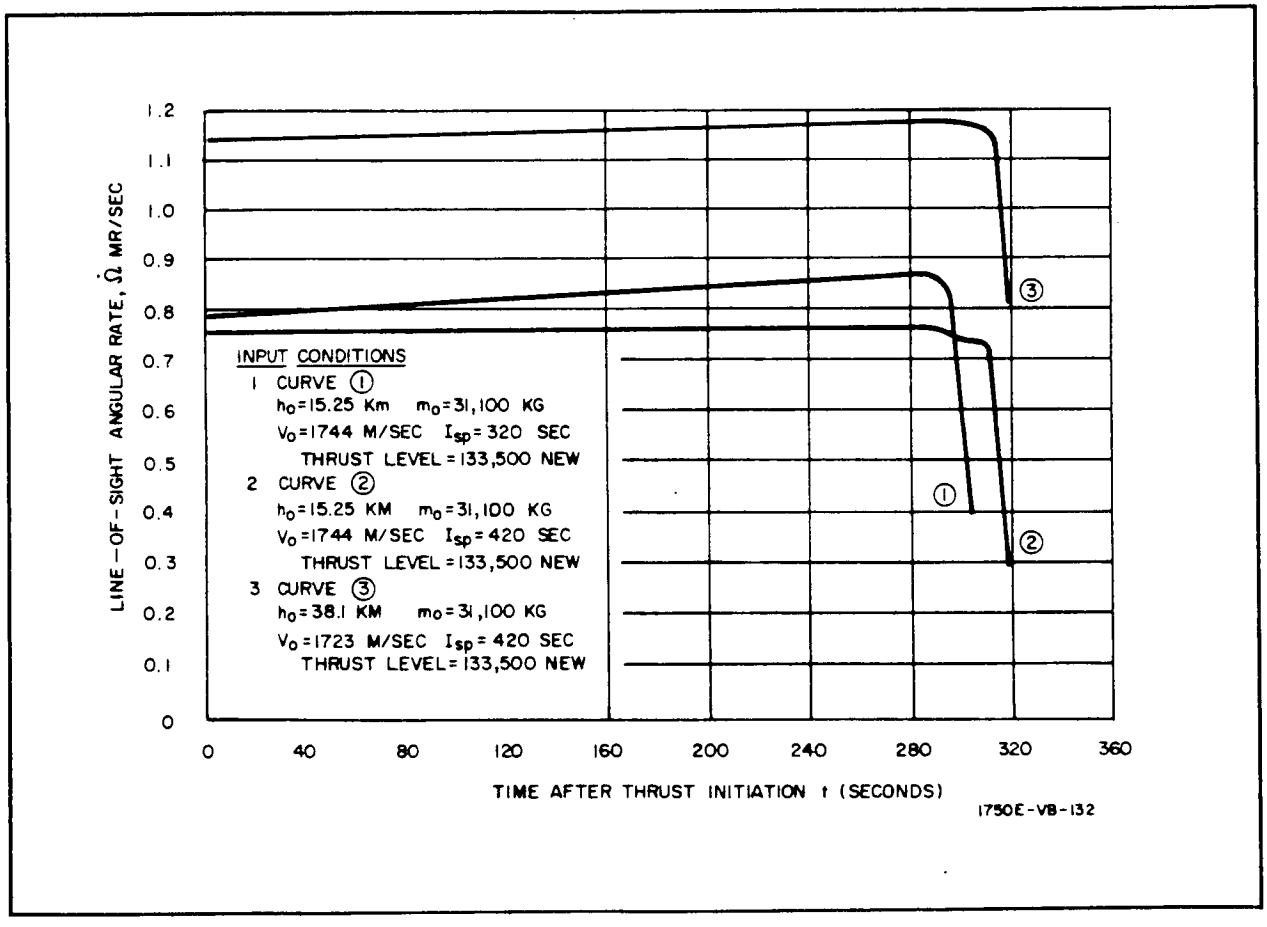

Figure 5. Typical Plots of Line-of-Sight Angular Rate, $\dot{\Omega}$, vs Time

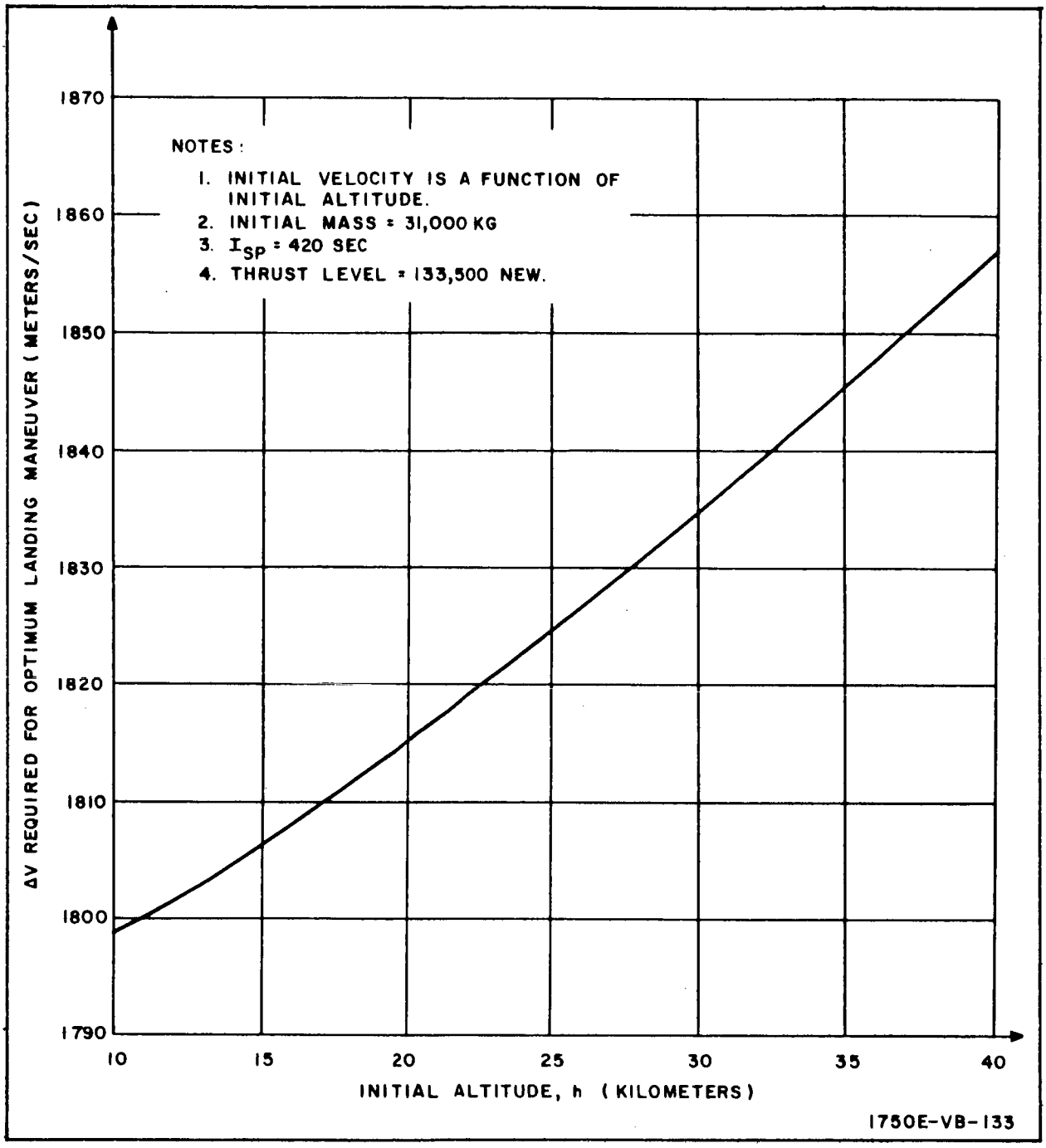

Figure 6. Characteristic Velocity (ΔV) Required for Optimum Descent

2. LINE OR PREDICTIVE GUIDANCE

2.1 Navigation Equations

This subsection derives expressions for the state variables h, θ, γ, and V in terms of the quantities observed by the two navigation concepts, beacon tracking and doppler navigation. The beacon tracking observables are line-of-sight range, angle, and their time derivatives (R, $\dot{R}$, ϕ, $\dot{\phi}$) measured to a beacon located at the nominal landing site. The second navigation concept observes altitude (h), line-of-sight angle to the landing site (ϕ), and range rate in three known directions ($\dot{R}_1$, $\dot{R}_2$, and $\dot{R}_3$). Since a two-dimensional problem is assumed, the range rate observations are assumed to be made in such directions that $\dot{R}_2$ and $\dot{R}_3$ are always equal. Thus the doppler navigation observables are h, ϕ, $\dot{R}_1$ and $\dot{R}_2$.

2.1.1 Beacon Tracking Navigation Equations

Figure 7 illustrates the geometrical situation existing for the descent phase. The symbols that will be used are defined as follows:

γ = the angle between the velocity vector and the local horizontal plane measured in the plane of motion (flightpath angle)

h = altitude of vehicle above a reference lunar sphere of radius r_c

θ = the angular displacement of the vehicle from the landing site in moon-centered coordinates (measured in the plane of motion)

V = magnitude of space vehicle velocity vectory

R = line-of-sight range from vehicle to landing site

$\dot{R}$ = time derivative of R

ϕ = angle between local vertical and the line of sight to the landing site

$\dot{\phi}$ = time derivative of ϕ

r_c = radius of moon at landing site

The landing site is allowed to be in the plane formed by the velocity vector and local vertical.

To derive expressions relating the state variables h, θ, γ, and V to the radar observables R, $\dot{R}$, ϕ, and $\dot{\phi}$, proceed as follows. The known quantities are R, $\dot{R}$, ϕ, $\dot{\phi}$, and r_c. The angle θ can be computed by applying the law of sines to triangle AOB.

$$\frac{\sin\theta}{R} = \frac{\sin\phi}{r_c}$$

$$\therefore \quad \theta = \sin^{-1} \frac{R \sin \phi}{r_c} \tag{18}$$

Then the quantity h is available from the law of sines.

$$\frac{r_c + h}{\sin\left[\pi - (\phi + \theta)\right]} = \frac{r_c}{\sin \phi}$$

$$r_c + h = \frac{r_c \sin (\phi + \theta)}{\sin \phi}$$

$$\therefore \quad h = \frac{r_c \left[\sin \phi \cos \theta + \cos \phi \sin \theta\right]}{\sin \phi} - r_c$$

$$h = R \cos \phi + \left[r_c^2 - R^2 \sin^2 \phi\right]^{1/2} - r_c \tag{19}$$

Functions relating γ and V to the observables are most conveniently derived through vector analysis. In the following analysis an underlined quantity refers to a vector, and the quantity is the vector magnitude. For example, $\underline{V}$ is the velocity vector and $V = \left|\underline{V}\right|$.

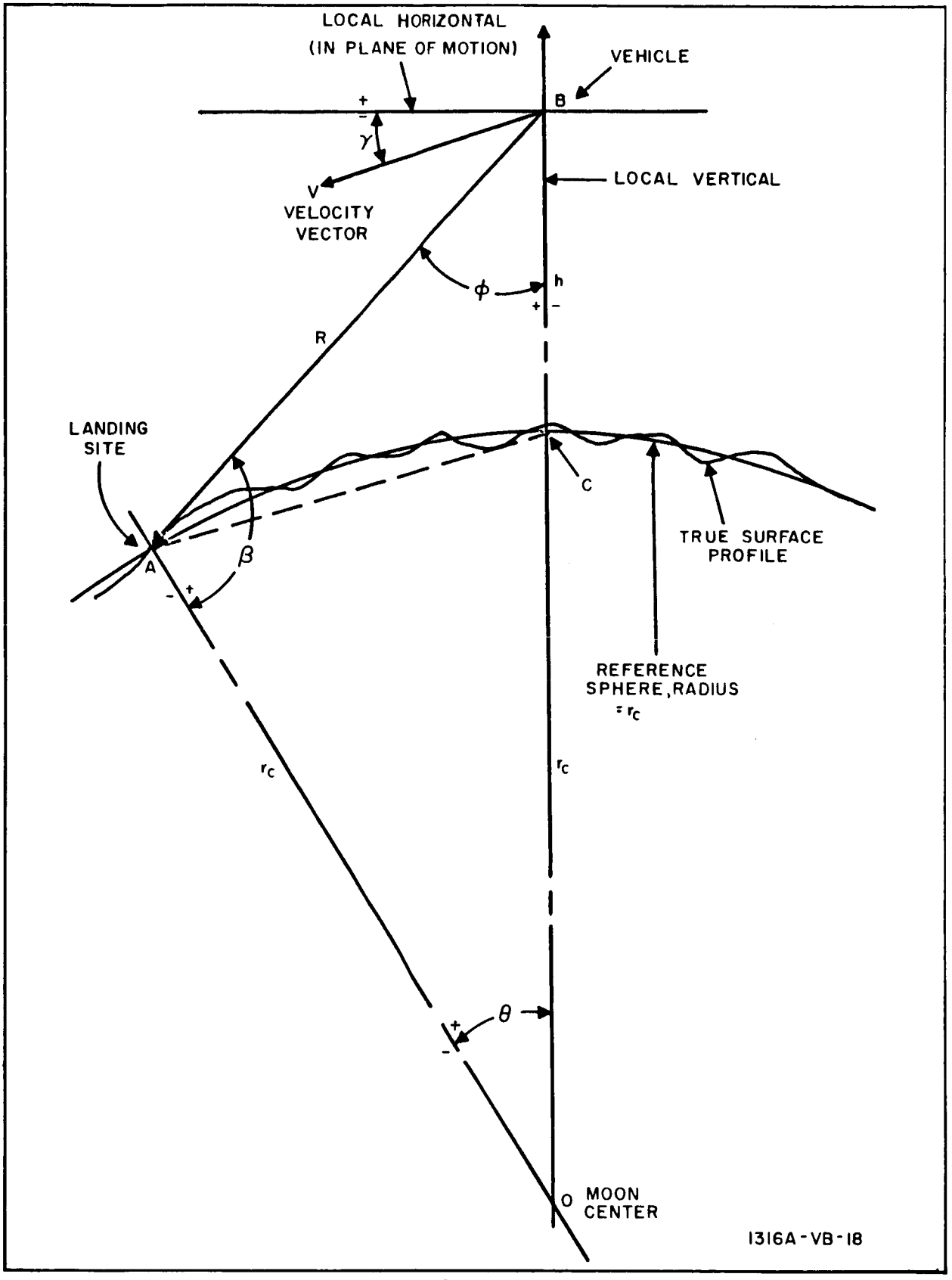

Figure 7. Landing Phase Geometry

The following definitions refer to figure 8:

$\underline{A}$ = A vector from point O to A

$\underline{B}$ = A vector from point O to B

$\underline{R}$ = A vector from point B to point A

$\underline{V}$ = the velocity of point B

In vector notation,

$$\underline{R} = \underline{A} - \underline{B} \tag{20}$$

and

$$\dot{\underline{R}} = \dot{\underline{A}} - \dot{\underline{B}} \tag{21}$$

Since $\underline{A}$ is a constant vector, $\dot{\underline{A}}$ is zero, and

$$\dot{\underline{R}} = -\dot{\underline{B}} = -\dot{\underline{V}} \tag{22}$$

Vector differentiation results in the expression:

$$\dot{\underline{R}} = \frac{dR}{dt}\frac{\underline{R}}{R} + \underline{\omega} \times \underline{R} \tag{23}$$

$\underline{R}/R$ is a unit vector in the direction of $\underline{R}$.

The vector $\underline{\omega}$ is perpendicular to the plane formed by $\underline{A}$ and $\underline{R}$ and equal in magnitude to $\dot{\beta}$. For the geometry of figure 8, $\underline{\omega}$ is positive toward the reader. The quantity $\underline{\omega} \times \underline{R}$ is perpendicular to $\underline{R}$ and in the plane formed by $\underline{A}$ and $\underline{R}$. The positive senses of all vector quantities are illustrated in figure 8. The following statements can be made.

$dR/dt = \dot{R}$ = an observable

$$\beta = \pi - (\phi + \theta)$$

$$\omega = \dot{\beta} = -\dot{\phi} - \dot{\theta}$$

where $\dot{\phi}$ is an observable, and $\dot{\theta}$ as a function of observables can be obtained by differentiation of the expression obtained earlier for θ.

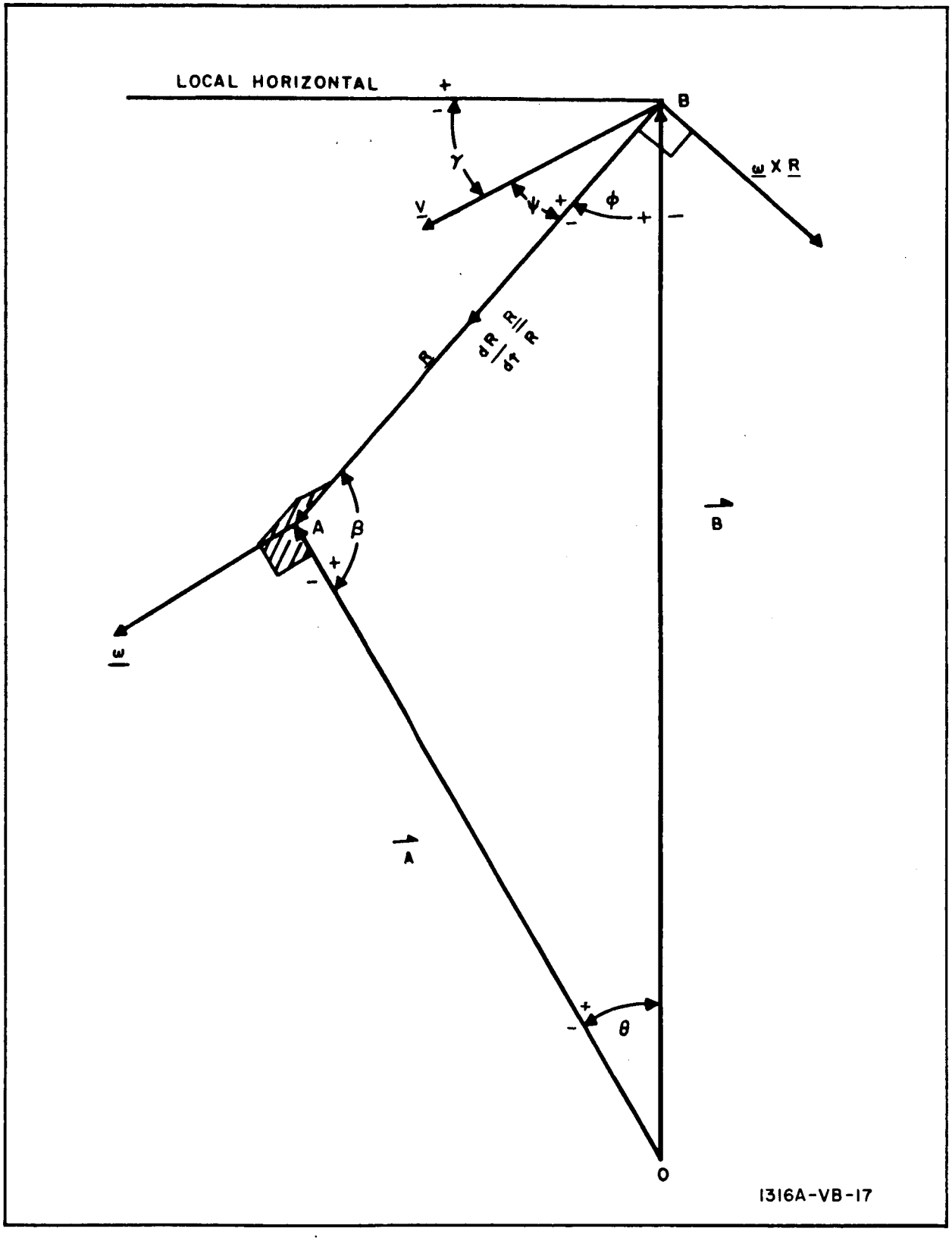

Figure 8. Vector Diagram of Landing Maneuver

$$\theta = \sin^{-1}\left[\frac{R}{r_c}\sin\phi\right]$$

$$\dot{\theta} = \frac{d\theta}{dt} = \frac{R\dot{\phi}\cos\phi \quad \dot{R}\sin\phi}{\left[r_c^2 - R^2\sin^2\phi\right]^{1/2}} \tag{24}$$

Therefore, if

$$\dot{\underline{R}} = \dot{R}\frac{\underline{R}}{R} + \underline{\omega} \times \underline{R}$$

then

$$V^2 = (\dot{R})^2 + R^2(\dot{\phi} + \dot{\theta})^2$$

$$V = \left[(\dot{R})^2 + R^2(\dot{\phi} + \dot{\theta})^2\right]^{1/2} \tag{25}$$

and

$$\tan\psi = \tan\left[-\tan^{-1}\left(\frac{\omega R}{\dot{R}}\right)\right] = -\frac{\omega R}{\dot{R}}$$

$$\tan\psi = \frac{R(\dot{\phi} + \dot{\theta})}{\dot{R}}$$

From figure 8 it can be shown that:

$$\phi + \psi - \gamma = \pi/2$$

$$\gamma = \phi + \psi - \pi/2$$

$$\therefore \gamma = \phi - \frac{\pi}{2} + \tan^{-1}\left[\frac{R(\dot{\phi} + \dot{\theta})}{\dot{R}}\right] \tag{26}$$

The four resulting transformation equations are:

$$\theta = \sin^{-1}\left[\frac{R}{r_c}\sin\phi\right]$$

$$h = R\cos\phi + \left[r_c^2 - R^2\sin^2\phi\right]^{1/2} - r_c \tag{27}$$

$$\gamma = \phi - \frac{\pi}{2} + \tan^{-1}\left[\frac{R(\dot{\phi}+\dot{\theta})}{\dot{R}}\right]$$

$$V = \left[(\dot{R}) + R^2(\dot{\phi}+\dot{\theta})^2\right]^{1/2} \qquad (27)$$

where

$$\dot{\theta} = \frac{R\dot{\phi}\cos\phi + \dot{R}\sin\phi}{\left[r_c^2 - R^2\sin^2\phi\right]^{1/2}}$$

The term $\dot{\theta}$ appearing in the expressions for γ and V appreciably complicates the partial derivative equations required for the linearized error analysis. However, over the range of parameter values covered by the landing maneuver, $\dot{\theta}$ is very much smaller than $\dot{\phi}$ so that the approximation $\dot{\phi} + \dot{\theta} \doteq \dot{\phi}$ is very accurate. The equations from which the partial derivatives were derived are then:

$$\theta = \sin^{-1}\left[\frac{R}{r_c}\sin\phi\right]$$

$$h = R\cos\phi + \left[r_c^2 - R^2\sin^2\phi\right]^{1/2} - r_c$$

$$\gamma \doteq \phi - \frac{\pi}{2} + \tan^{-1}\left[\frac{R\dot{\phi}}{\dot{R}}\right]$$

$$V \doteq \left[(\dot{R})^2 + (R\dot{\phi})^2\right]^{1/2} \qquad (28)$$

The resulting partial derivative expressions which are used in the analysis are:

$$\frac{\partial h}{\partial R} = \cos\phi - \frac{R\sin^2\phi}{\left[r_c^2 - R^2\sin^2\phi\right]^{1/2}}$$

$$\frac{\partial \theta}{\partial R} = \frac{\sin\phi}{\left[r_c^2 - R^2\sin^2\phi\right]^{1/2}}$$

$$\frac{\partial \gamma}{\partial R} \doteq \frac{\dot{R}\,\dot{\phi}}{\left[(\dot{R})^2 + (R\dot{\phi})^2\right]}$$

$$\frac{\partial V}{\partial R} \doteq \frac{R\dot{\phi}^2}{\left[(\dot{R})^2 + (R\dot{\phi})^2\right]^{1/2}}$$

$$\frac{\partial h}{\partial \dot{R}} = 0$$

$$\frac{\partial \theta}{\partial \dot{R}} = 0$$

$$\frac{\partial \gamma}{\partial \dot{R}} \doteq - \frac{R\dot{\phi}}{(\dot{R})^2 + (R\dot{\phi})^2}$$

$$\frac{\partial V}{\partial \dot{R}} \doteq \frac{\dot{R}}{\left[(\dot{R})^2 + (R\dot{\phi})^2\right]^{1/2}}$$

$$\frac{\partial h}{\partial \phi} = - R \sin\phi \left\{ 1 + \frac{R \cos\phi}{\left[r_c^2 - R^2 \sin^2\phi\right]^{1/2}} \right\}$$

$$\frac{\partial \theta}{\partial \phi} = \frac{R \cos\phi}{\left[r_c^2 - R^2 \sin^2\phi\right]^{1/2}}$$

$$\frac{\partial \gamma}{\partial \phi} \doteq 1$$

$$\frac{\partial V}{\partial \phi} \doteq 0$$

$$\frac{\partial h}{\partial \dot{\phi}} = 0$$

$$\frac{\partial \theta}{\partial \dot{\phi}} = 0$$

$$\frac{\partial \gamma}{\partial \dot{\phi}} \doteq \frac{R\dot{R}}{\left[(\dot{R})^2 + (R\dot{\phi})^2\right]^{1/2}}$$

$$\frac{\partial V}{\partial \dot{\phi}} \doteq \frac{R^2 \dot{\phi}}{\left[(\dot{R})^2 + (R\dot{\phi})^2\right]^{1/2}}$$

2.1.2 Doppler Navigation Equations

a. Description of the Observation Scheme. - The doppler navigation combination of observables consists of altitude, line-of-sight angle to the landing site, and range rate to the surface in each of three directions. For ease of visualization, the devices producing this information can be thought of as an altimeter, some sort of optical device, and a three-beam doppler radar system. (Knowledge of local vertical is assumed.) The altimeter determines altitude, and the three-beam doppler radar provides sufficient information to allow calculation of V and γ. All parameters pertinent to discussion of the three-beam doppler radar are illustrated and defined in figure 9. The antenna system for this analysis is assumed to be gimbaled and controlled so that the beam pattern remains fixed with respect to the coordinate system, X, Y, Z. This is done by controlling the direction vector OP so that it is always along local vertical. (Errors is establishing local vertical can be lumped with range rate measurement errors.) The vehicle pitch axis (X') and the X axis are allowed to be coincident. Since the two-dimensional trajectory is assumed, they will remain coincident throughout the landing maneuver.

Several parameters of the system are known prior to landing:

- The angles Λ_1, Λ_2, and ζ which define the geometrical properties of the beam pattern
- The vector OP is along local vertical.
- The vector OA is in the Y' - Z' plane. (For a two dimensional analysis, OA is also in the Y - Z plane.)

The three observable quantities are:

$\dot{R}_1$ = Vehicle range rate to the surface along vector OA

$\dot{R}_2$ = Vehicle range rate to the surface along vector OB

$\dot{R}_3$ = Vehicle range rate to the surface along vector OC

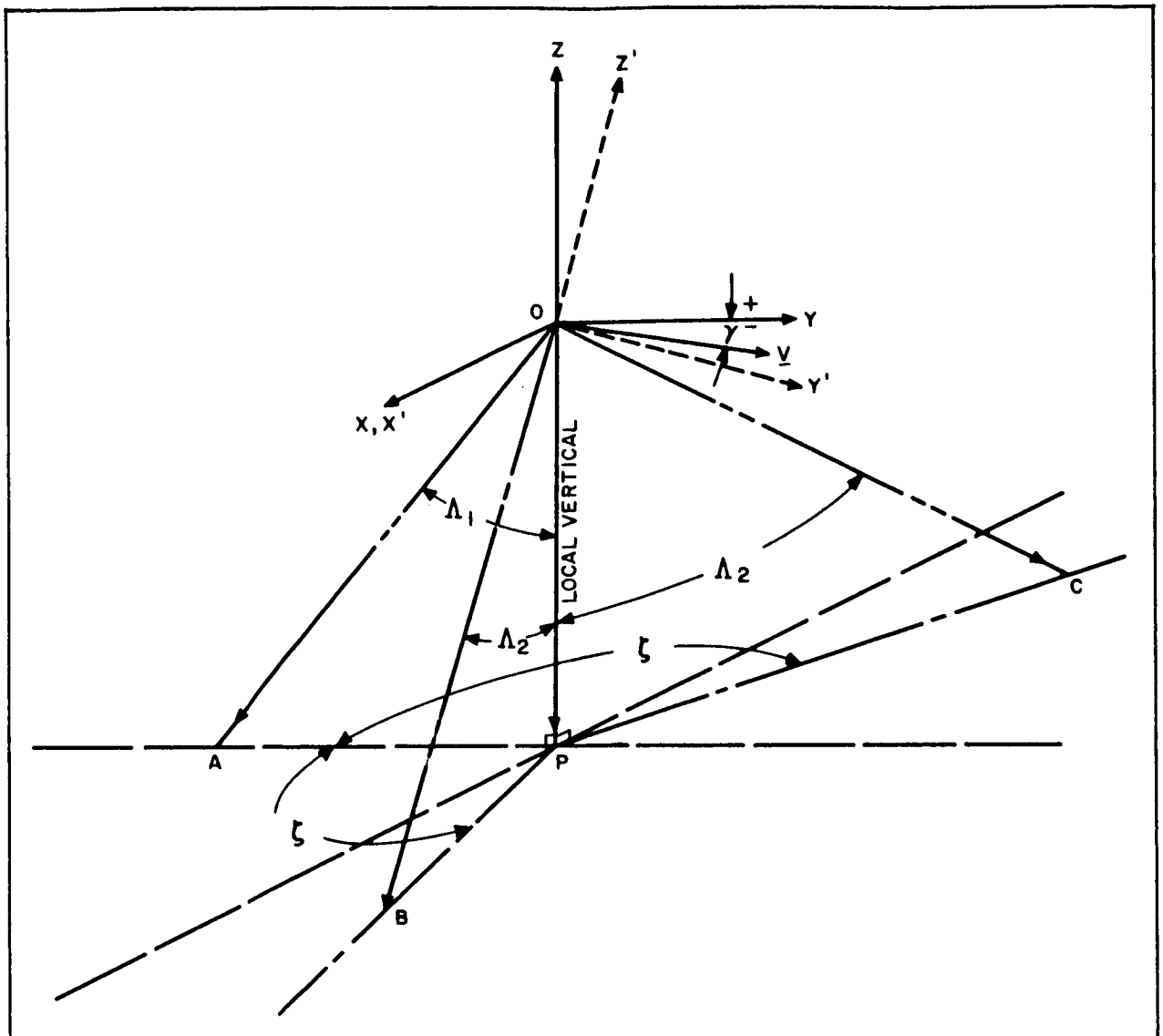

Figure 9. Geometry of a Three-Beam Doppler System for Velocity Determination

By allowing the Y-Z and Y' - Z' planes to be coincident, the vector $\underline{OA}$ is in the plane of motion with the result that the observables $\dot{R}_2$ and $\dot{R}_3$ are always equal. Therefore only one of these quantities must actually be observed. Thus the set of observables when the trajectory is restricted to two dimensions is: $h, \phi, \dot{R}_1$, and $\dot{R}_2$.

b. Doppler Navigation Equations. - Three sets of relationships are required by the digital error analysis program. First, the observables themselves must be defined in terms of the state variables; second, the state variables must be defined in terms of the observables. Finally a matrix of partial derivatives, $[G]$, where g_{ij} is the partial derivative of the i^{th} state variable with respect to the j^{th} observable quantity, must be formed.

The following statements and constraints facilitate definition of these quantities (see figure 9 for definition of terms).

- The angles Λ_1, Λ_2, and ζ are known.
- Vector $\underline{OA}$ is in the Y' - Z' plane.
- Vector $\underline{OP}$ is in the direction of local vertical.
- The landing trajectory is two-dimensional, all motion being in the Y-Z plane.
- The X and X' axes are coincident.

With these restrictions, the expressions for state variables in terms of observables are:

$$h = h$$

$$\theta = \frac{\pi}{2} - \phi - \cos^{-1}\left[\frac{r_c + h}{r_c} \sin \phi\right]$$

$$\gamma = \tan^{-1}\left[\frac{\dot{R}_2 \sin \Lambda_2 - \dot{R}_1 \cos \zeta \sin \Lambda_1}{\dot{R}_1 \cos \Lambda_1 - \dot{R}_2 \cos \Lambda_2}\right]$$

$$V = \frac{\dot{R}_1 \left[(\dot{R}_1 \cos \Lambda_1 - \dot{R}_2 \cos \Lambda_2)^2 + (\dot{R}_2 \sin \Lambda_2 - \dot{R}_1 \cos \zeta \sin \Lambda_1)^2 \right]^{1/2}}{\cos \Lambda_2 \left[\dot{R}_2 \sin \Lambda_2 - \dot{R}_1 \cos \zeta \sin \Lambda_1 \right] + \sin \Lambda_2 \left[\dot{R}_1 \cos \Lambda_1 - \dot{R}_2 \cos \Lambda_2 \right]} \quad (29)$$

Conversely, the expressions which define observables in terms of state variables are:

$$h = h$$

$$\phi = \sin^{-1} \left\{ \frac{r_c \sin \theta}{\left[r_c^2 + (r_c + h)^2 - 2 r_c (r_c + h) \cos \theta \right]^{1/2}} \right\} \quad (30)$$

$$\dot{R}_1 = V \left[\sin \gamma \cos \Lambda_2 + \cos \gamma \sin \Lambda_2 \right]$$

$$\dot{R}_2 = V \left[\cos \gamma \cos \zeta \sin \Lambda_1 + \sin \gamma \cos \Lambda_1 \right]$$

The expressions for the matrix, $[G]$, of partial derivatives are derived from equations 29. The subscript i refers to state variables as follows:

$i = 1 \rightarrow h$

$i = 2 \rightarrow \theta$

$i = 3 \rightarrow \gamma$

$i = 4 \rightarrow V$

Similarly, observables quantities are denoted by the subscript j:

$j = 1 \rightarrow h$

$j = 2 \rightarrow \dot{R}_1$

$j = 3 \rightarrow \phi$

$j = 4 \rightarrow \dot{R}_2$

Equations defining the elements of $[G]$ in terms of the observables are:

$$g_{11} \equiv \frac{\partial h}{\partial h} = 1$$

$$g_{12} \equiv \frac{\partial h}{\partial \dot{R}_1} = 0$$

$$g_{13} \equiv \frac{\partial h}{\partial \phi} = 0$$

$$g_{14} \equiv \frac{\partial h}{\partial \dot{R}_2} = 0$$

$$g_{21} \equiv \frac{\partial \theta}{\partial h} = \frac{\cos\phi}{\left[r_c^2 - (r_c + h)^2 \sin^2 \phi\right]^{1/2}}$$

$$g_{22} \equiv \frac{\partial \theta}{\partial \dot{R}_1} = 0$$

$$g_{23} \equiv \frac{\partial \theta}{\partial \phi} = -1 + \frac{(r_c + h)\cos\phi}{\left[r_c^2 - (r_c + h)^2 \sin^2 \phi\right]^{1/2}}$$

$$g_{24} \equiv \frac{\partial \theta}{\partial \dot{R}_2} = 0$$

$$g_{31} \equiv \frac{\partial \gamma}{\partial h} = 0$$

$$g_{32} \equiv \frac{\partial \gamma}{\partial \dot{R}_1} = \frac{-\dot{R}_2\left[\cos\Lambda_1 \sin\Lambda_2 - \cos\zeta \sin\Lambda_1 \cos\Lambda_2\right]}{\left[\dot{R}_1 \cos\Lambda_1 - \dot{R}_2 \cos\Lambda_2\right]^2 + \left[\dot{R}_2 \sin\Lambda_2 - \dot{R}_1 \cos\zeta \sin\Lambda_1\right]^2}$$

$$g_{33} \equiv \frac{\partial \gamma}{\partial \phi} = 0$$

$$g_{34} \equiv \frac{\partial \gamma}{\partial \dot{R}_2} = \frac{\dot{R}_1\left[\cos\Lambda_1 \sin\Lambda_2 - \cos\zeta \sin\Lambda_1 \cos\Lambda_2\right]}{\left[\dot{R}_1 \cos\Lambda_1 - \dot{R}_2 \cos\Lambda_2\right]^2 + \left[\dot{R}_2 \sin\Lambda_2 - \dot{R}_1 \cos\zeta \sin\Lambda_1\right]^2}$$

$$g_{41} \equiv \frac{\partial V}{\partial h} = 0$$

$$g_{42} \equiv \frac{\partial V}{\partial \dot{R}_1} = \frac{\dot{R}_1\left[\cos^2\Lambda_1 + \cos^2\zeta \sin^2\Lambda_1\right] \quad -\dot{R}_2\left[\cos\Lambda_1 \cos\Lambda_2 - \cos\zeta \sin\Lambda_1 \sin\Lambda_2\right]}{\left[\cos\Lambda_1 \sin\Lambda_2 - \cos\zeta \sin\Lambda_2 \cos\Lambda_2\right]\left[\left(\dot{R}_1 \cos\Lambda_1 - \dot{R}_2 \cos\Lambda_2\right)^2 + \left(\dot{R}_2 \sin\Lambda_2 - \dot{R}_1 \cos\zeta \sin\Lambda_1\right)^2\right]^{1/2}}$$

$$g_{43} \equiv \frac{\partial V}{\partial \phi} = 0$$

$$g_{44} \equiv \frac{\partial V}{\partial \dot{R}_2} = \frac{\dot{R}_2 - \dot{R}_1 \left[\cos \Lambda_1 \cos \Lambda_2 + \cos \zeta \sin \Lambda_1 \sin \Lambda_2\right]}{\left[\cos \Lambda_1 \sin \Lambda_2 - \cos \zeta \sin \Lambda_2 \cos \Lambda_2\right] \left[(R_1 \cos \Lambda_1 - \cdots \right.}$$
$$\left. \cdots - \dot{R}_2 \cos \Lambda_2)^2 + (\dot{R}_2 \sin \Lambda_2 - \dot{R}_1 \cos \zeta \sin \Lambda_1)^2\right]^{1/2}$$

2.2 Gravity Turn Nominal Trajectory

2.2.1 Trajectory Determination Program

Knowledge of reference trajectory parameters is required to perform the error analysis of the linear predictive guidance concept. Therefore a computer program was developed to yield the necessary information. The basic method is to provide the computer with sufficient information to specify one and only one constant-thrust gravity turn trajectory and then let the computer determine exactly with trajectory it is.

The input information consists of specification of the nominal initial altitude h_o, initial velocity V_o, initial flightpath angle γ_o, initial mass m_o, fuel specific impulse I_{sp}, nominal terminal altitude h_f, and nominal terminal velocity V_f. In addition, the fact that a gravity turn trajectory is to be flown is programmed. The initial value of θ is set equal to zero. Thus a complete set of initial state variables is specified, and two desired terminal conditions are known. In addition the applicable equations of motion are known:

$$\dot{h} = V \sin \gamma$$

$$\dot{\theta} = -\frac{V}{r_c + h} \cos \gamma$$

$$\dot{\gamma} = \frac{V \cos \gamma}{r_c + h} - \frac{T \sin \alpha}{mV} - \frac{\mu \cos \gamma}{V (r_c + h)^2} \qquad (31)$$

$$\dot{V} = \frac{T \cos \alpha}{m} - \frac{\mu \sin \gamma}{(r_c + h)^2}$$

where

$$m = m_o + \int_o^t \dot{m}\, dt$$

The constant-thrust gravity turn trajectory specification means that the angle α is zero, that the magnitude of the thrust vector (T) is constant at its initial value (T_o), and that $\dot{m}$ is a constant. If these facts are substituted into equations 31, the modified equations of motion given below result.

$$\dot{h} = V \sin \gamma$$

$$\dot{\theta} = -\frac{V}{r_c + h} \cos \gamma$$

$$\dot{\gamma} = \frac{V \cos \gamma}{r_c + h} - \frac{\mu \cos \gamma}{V(r_c + h)^2}$$

$$\dot{V} = \frac{T_o}{m_o + \dot{m}t} - \frac{\mu \sin \gamma}{(r_c + h)^2} \qquad (32)$$

Given the initial condition data above and an assumed value for T_o, the equations of motion are numerically integrated until the velocity is equal to the nominal terminal value. At this time the existing value of h is compared to the desired value h_f. If h is greater than h_f, the value of T_o is reduced by a small amount for the next trial and vice versa. When the terminal values of V and h are within prescribed error limits of the desired values V_f and h_f, the nominal trajectory has been determined. (The error limits used are 0.1 meters per second in velocity and 1 meter in altitude.) The following quantities which completely described the nominal trajectory are then available:

- Initial values of all state variables, control quantities, and the initial mass
- State variables as functions of time along the trajectory
- Complete set of terminal conditions including the nominal flight time, t_f

One notes that the initial value of θ is arbitrarily set equal to zero above. This is not consistent with definition of θ given in paragraph 4.3.1.1.a of Volume III, where θ equal to zero is seen to correspond to the landing site and not to the point of trajectory initiation. This switch in the reference point for θ is permissible because the quantity θ does not appear in the equations of motion. To obtain the value of θ_o in the coordinate system

referenced to the landing site, the quantity ($\theta_f - \theta_o$) computed by the trajectory determination program is subtracted from zero (the arbitrarily assumed initial value of θ). For example, if the computed value of θ_f is -0.1 radian, the nominal initial value of θ in the coordinate system indicated in paragraph 4.3.1.1a of Volume III is +0.1 radian and the nominal terminal value is zero. All values of θ presented in the following subsection of this appendix are referenced to the landing site.

Nominal trajectories are determined for 8 sets of input information as summarized in table 1.

Values of constants used in the program are:

r_c = mean lunar radius = 1738 km

μ = lunar gravitational constant = 4.89820×10^{12} m^3/sec^2

g_o = earth's gravitational attraction (at earth's surface) = 9.80665 m/sec^2

2.2.2 Nominal Trajectory Characteristics

The material presented herein summarizes the geometrical and fuel consumption characteristics of the constant-thrust gravity-turn family of trajectories determined by the previously discussed computer program. Geometrical data is given in table 2 and in figures 10 through 18, the contents of which are summarized below.

Table 2: Nominal values of initial thrust level, T_o; initial thrust-to-mass ratio, T_o/m_o; initial angular displacement from the landing site, θ_o; initial velocity, V_o; nominal flight time, t_f, corresponding to the selected values of initial altitude, h_o

Figure 10: Plots of initial thrust level, T_o, and initial thrust-to-mass ratio, T_o/m_o, versus initial altitude, h_o

Figure 11: Plot of initial angular displacement from the landing site, θ_o, versus initial altitude, h_o

Figure 12: Plot of total flight time, t_f, versus initial altitude, h_o

Figure 13: Plots of altitude, h, versus time after thrust initiation, t, for the selected values of initial altitude, h_o

TABLE 1

TRAJECTORY DETERMINATION INPUT CONDITIONS

Program Input Quantity	TRAJECTORY NUMBER							
	1	2	3	4	5	6	7	8
Initial altitude (meters)	10,000	15,000	20,000	25,000	30,000	40,000	50,000	60,000
Initial velocity (meters/sec)	1753.6	1749.0	1744.5	1739.9	1735.4	1726.4	1717.5	1708.6
Initial flight path angle (rad)	0.0	0.0	0.0	0.0	0.0	0.0	0.0	0.0
Initial central angle[a] (rad)	0.0	0.0	0.0	0.0	0.0	0.0	0.0	0.0
Initial time (sec)	0.0	0.0	0.0	0.0	0.0	0.0	0.0	0.0
Initial mass (kilograms)	11,340	11,340	11,340	11,340	11,340	11,340	11,340	11,340
Desired terminal altitude (meters)	500	500	500	500	500	500	500	500
Desired terminal velocity (meters/sec)	0.0	0.0	0.0	0.0	0.0	0.0	0.0	0.0
Fuel specific impulse (sec)	400	400	400	400	400	400	400	400

[a]See accompanying discussion.

Figure 14: Plots of angular displacement from the landing site, θ, versus time after thrust initiation, t, for the selected values of initial altitude, h_o

Figure 15: Plots of flightpath angle, γ, versus time after thrust initiation, t, for the selected values of initial altitude, h_o

Figure 16: Plots of velocity, V, versus time after thrust initiation, t, for the selected values of initial altitude, h_o

Figure 17: Plots altitude rate, $\dot{h}$, versus altitude, h, for the selected values of initial altitude, h_o

Figure 18: Plots of altitude, h, versus angular displacement from the landing site, θ, for the selected values of initial altitude, h_o

TABLE 2

VALUES OF COMPUTED NOMINAL TRAJECTORY PARAMETERS

h_o (km)	T_o (newtons)	T_o/m_o (m/sec^2)	θ_o (rad)	V_o (m/sec)	t_f (sec)
10	68406	6.032	0.1269	1753.6	238.9
15	55644	4.907	0.1553	1749.0	296.0
20	48212	4.251	0.1783	1744.5	344.3
25	43216	3.811	0.1979	1739.9	387.0
30	39564	3.489	0.2151	1735.4	426.0
40	34494	3.042	0.2442	1726.4	495.8
50	31074	2.740	0.2683	1717.5	558.4
60	28570	2.519	0.2888	1708.6	615.9

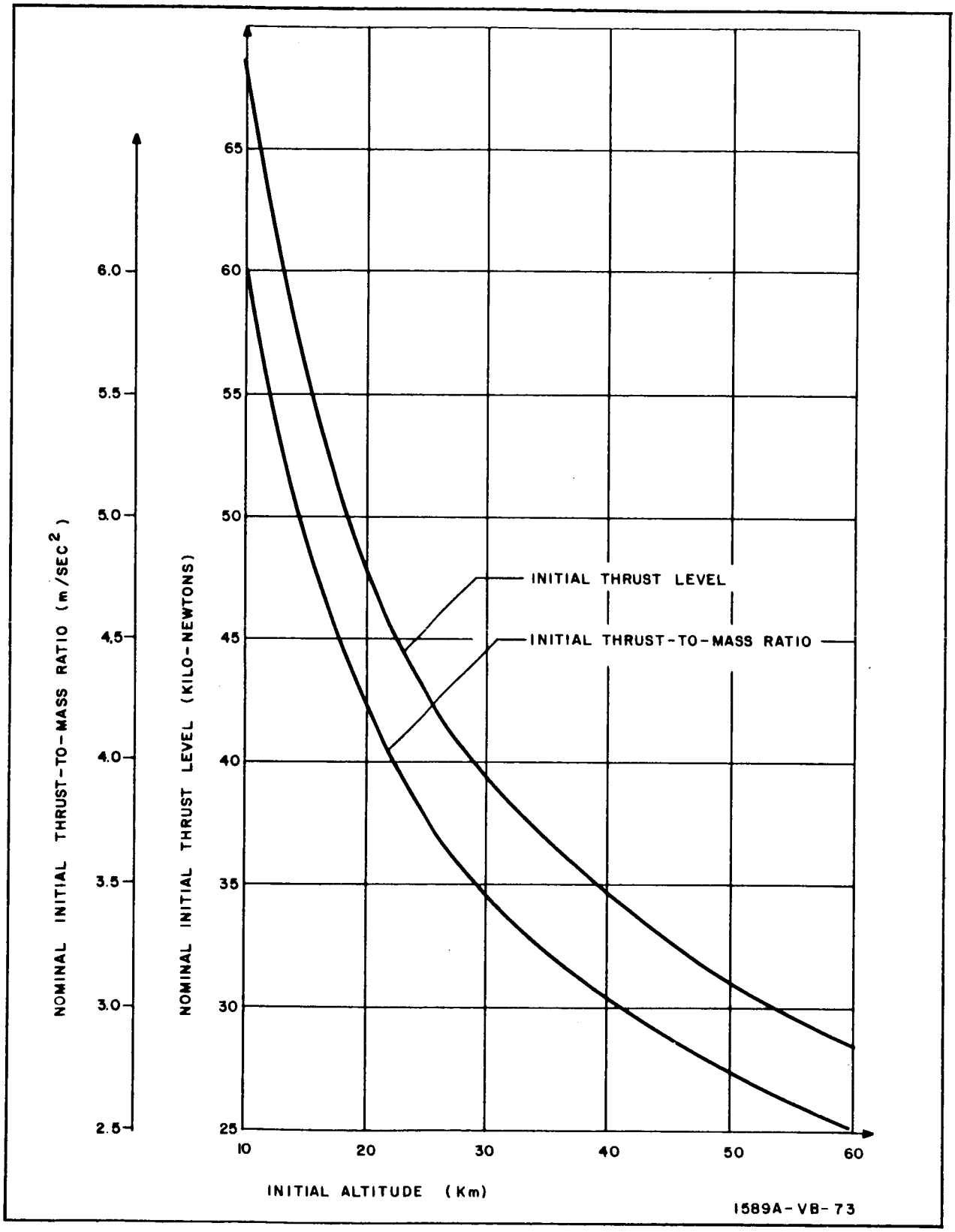

Figure 10. Nominal Trajectory Characteristics, T_o and T_o/m_o vs h_o

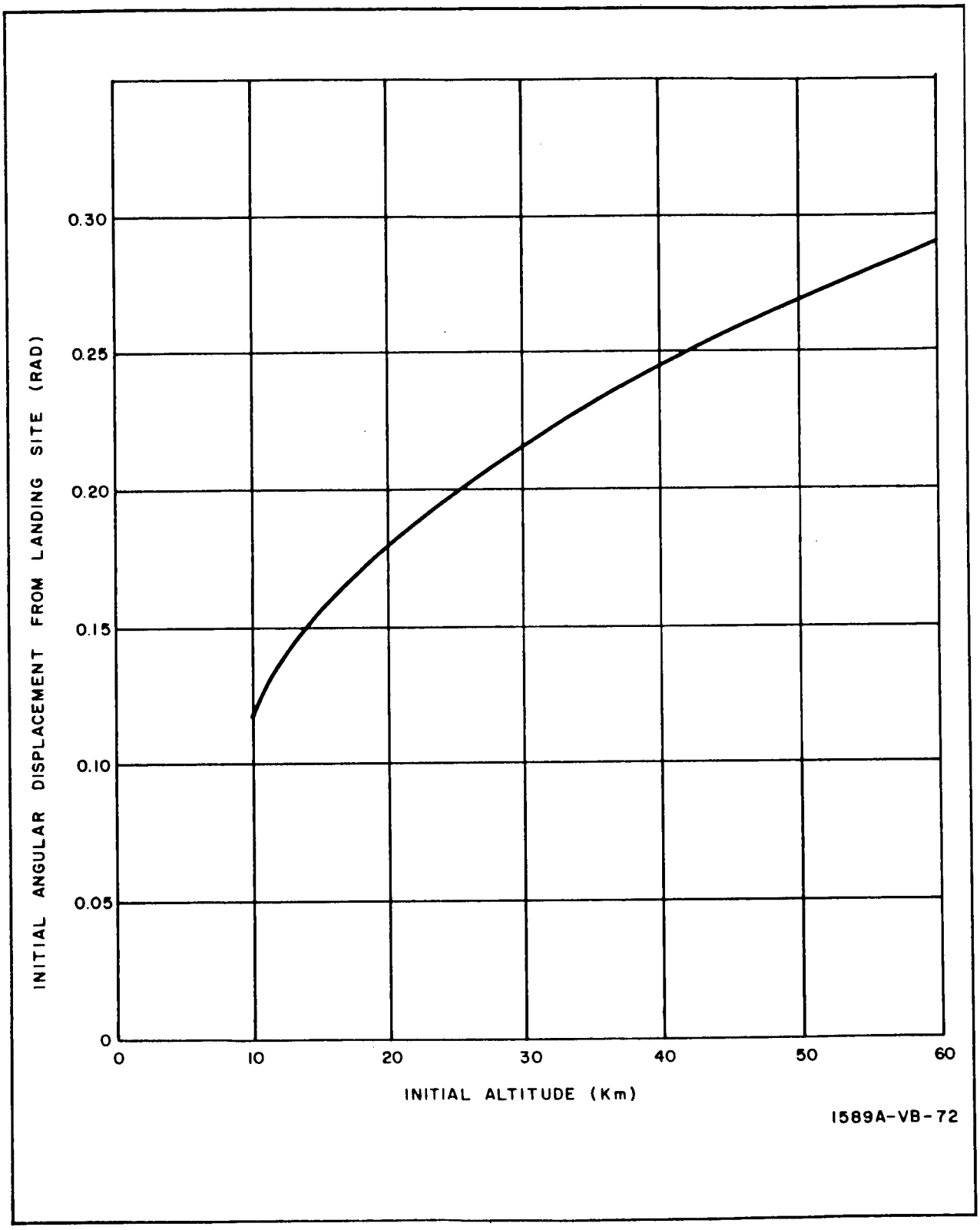

Figure 11. Nominal Trajectory Characteristics, θ_o vs h_o

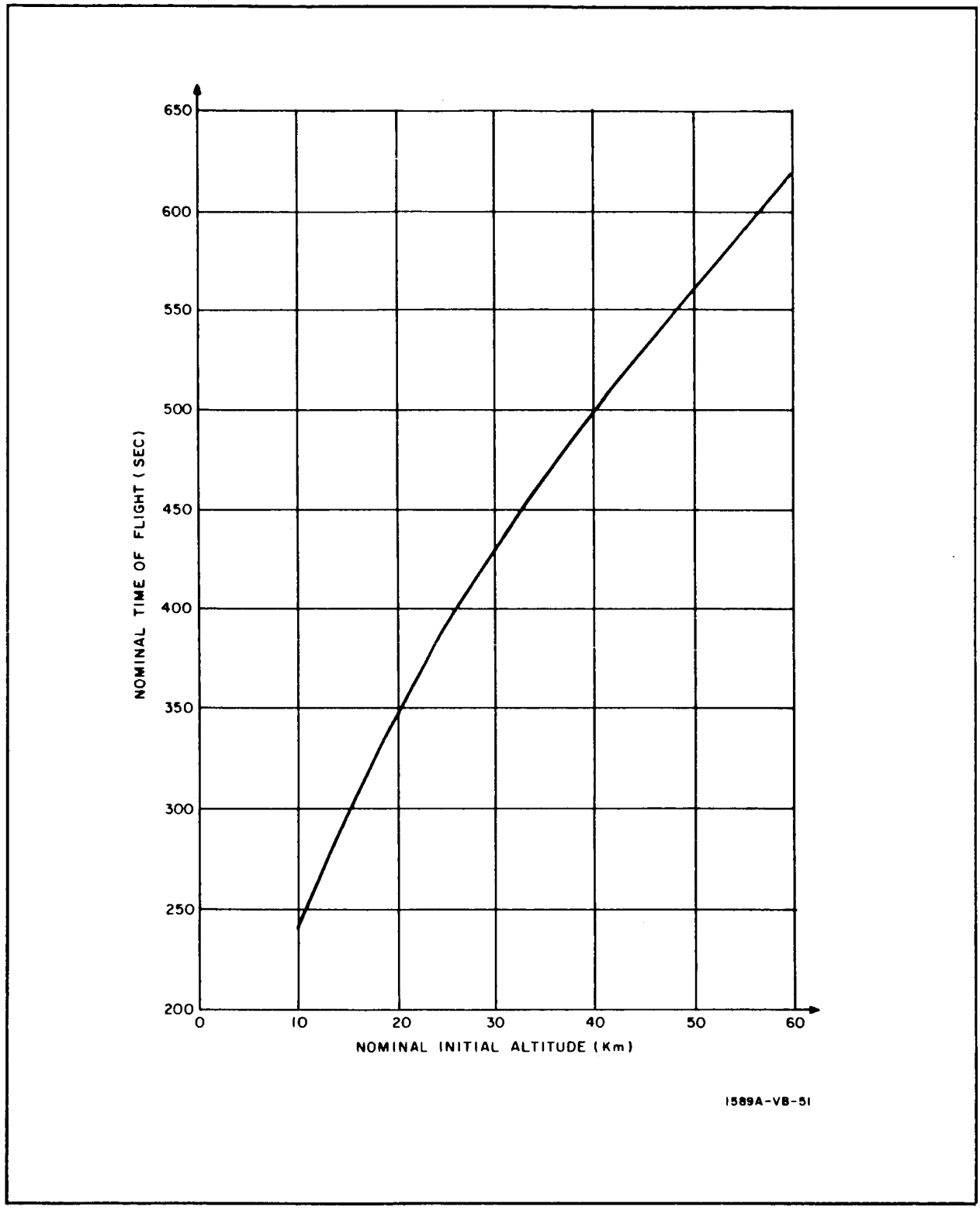

Figure 12. Nominal Trajectory Characteristics, t_f vs h_o

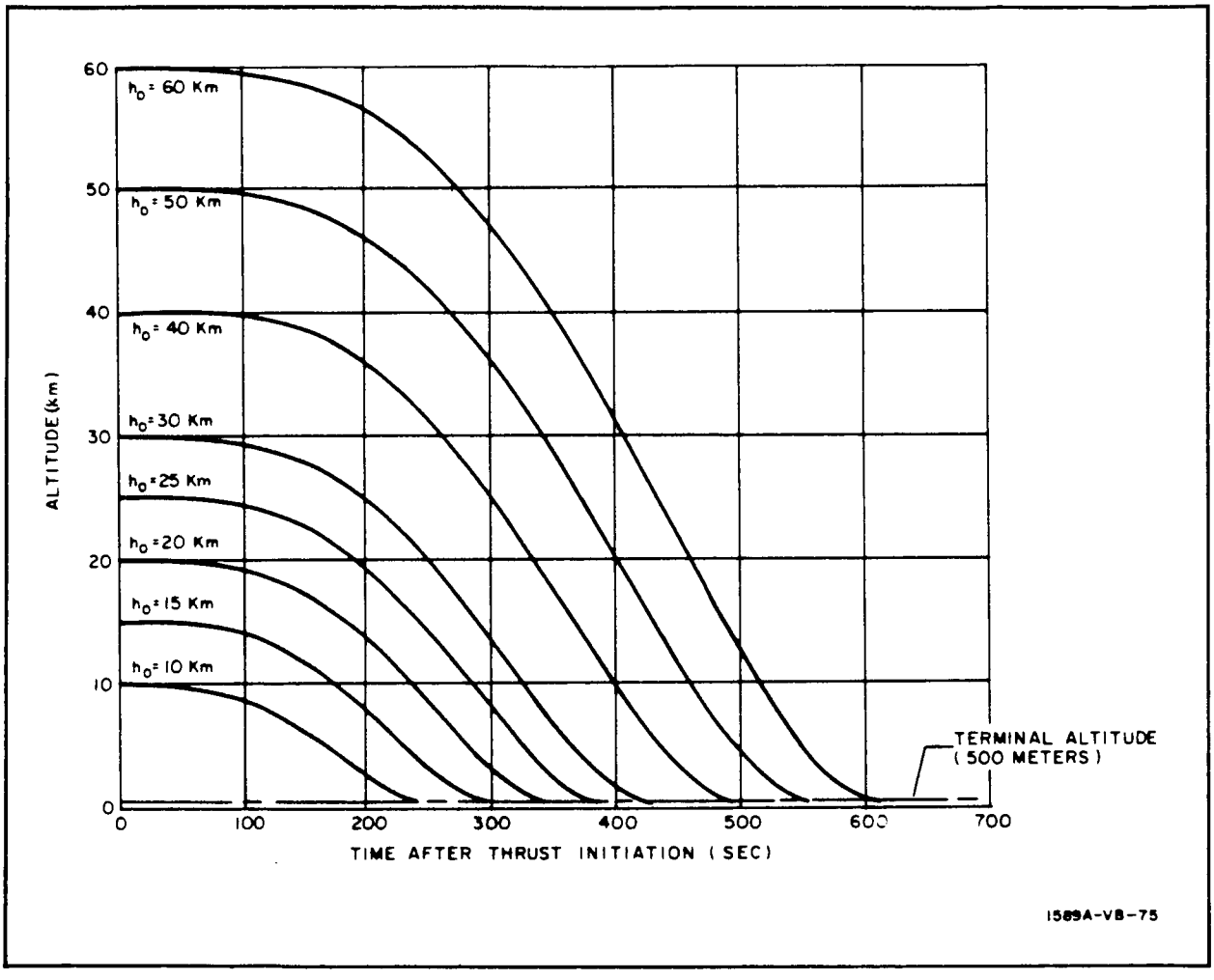

Figure 13. Nominal Trajectory Characteristics, h vs t

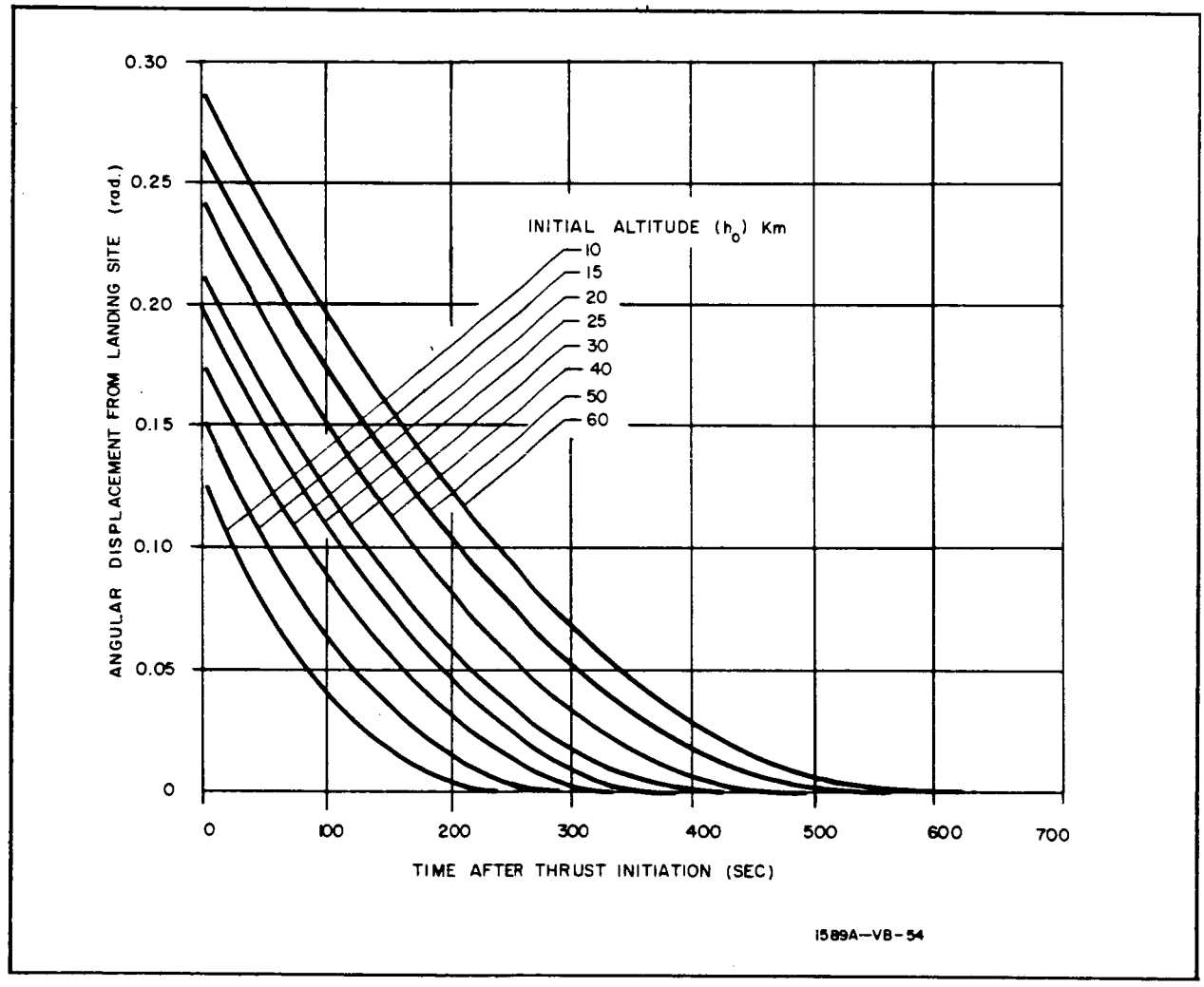

Figure 14. Nominal Trajectory Characteristics, θ vs t

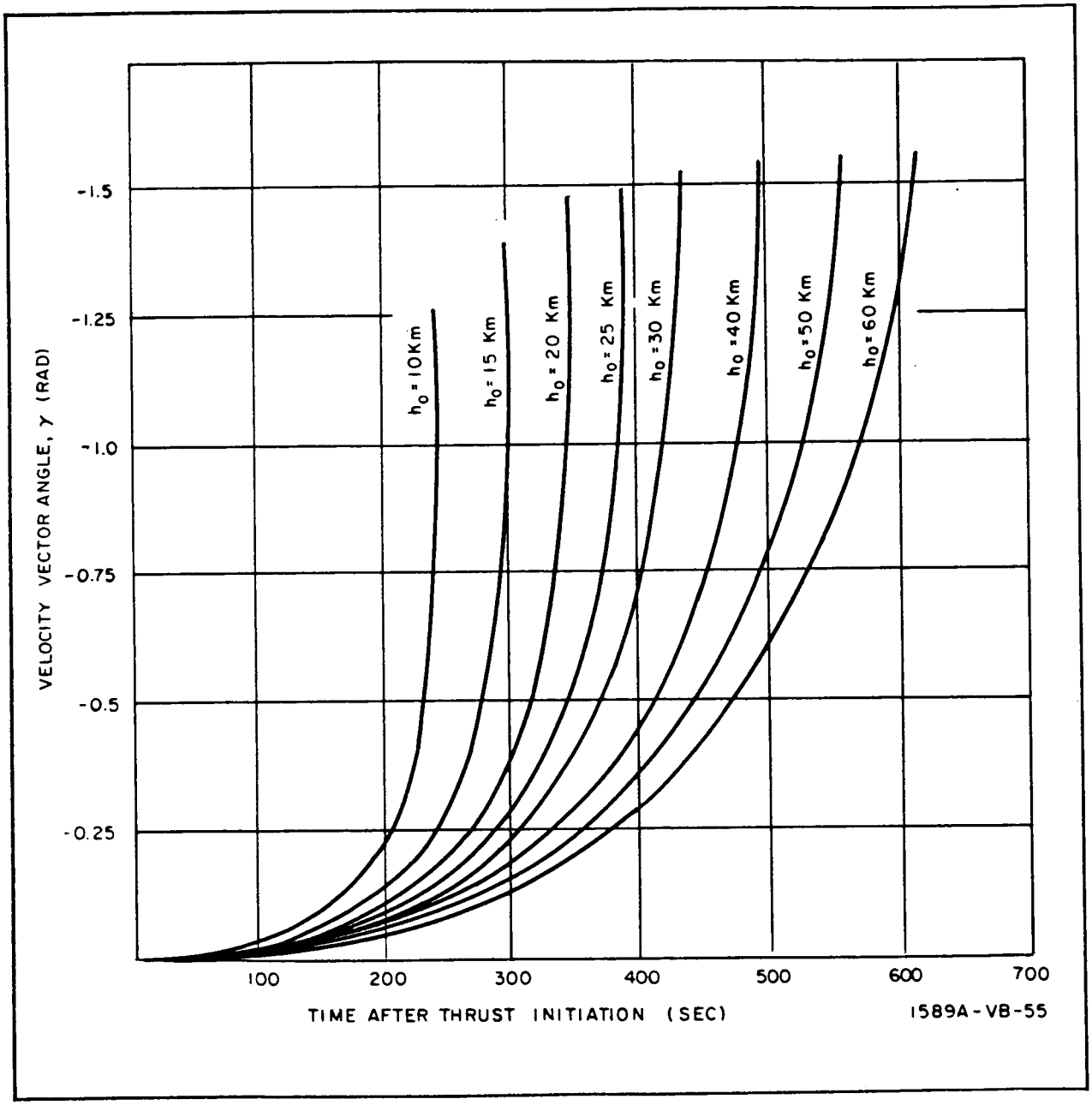

Figure 15. Nominal Trajectory Characteristics, γ vs t

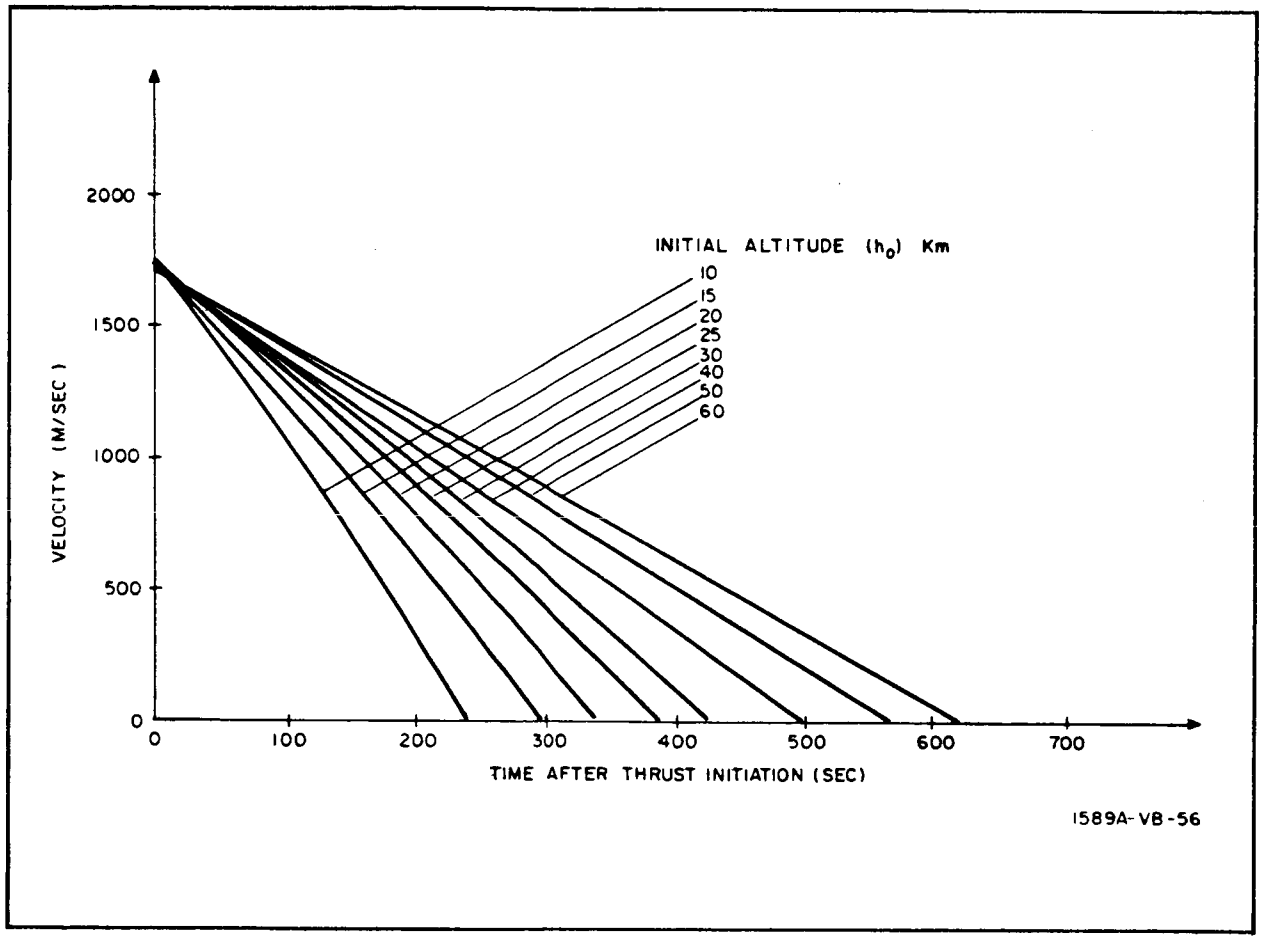

Figure 16. Nominal Trajectory Characteristics, V vs t

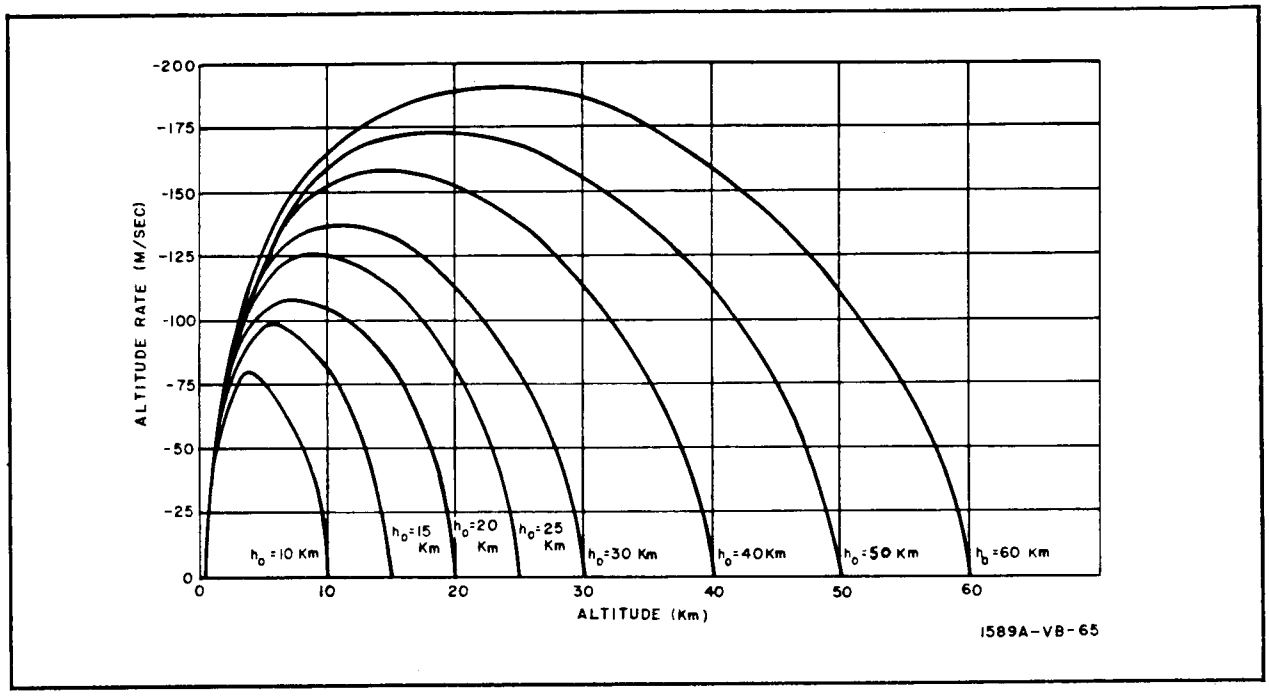

Figure 17. Nominal Trajectory Characteristics, $\dot{h}$ vs h

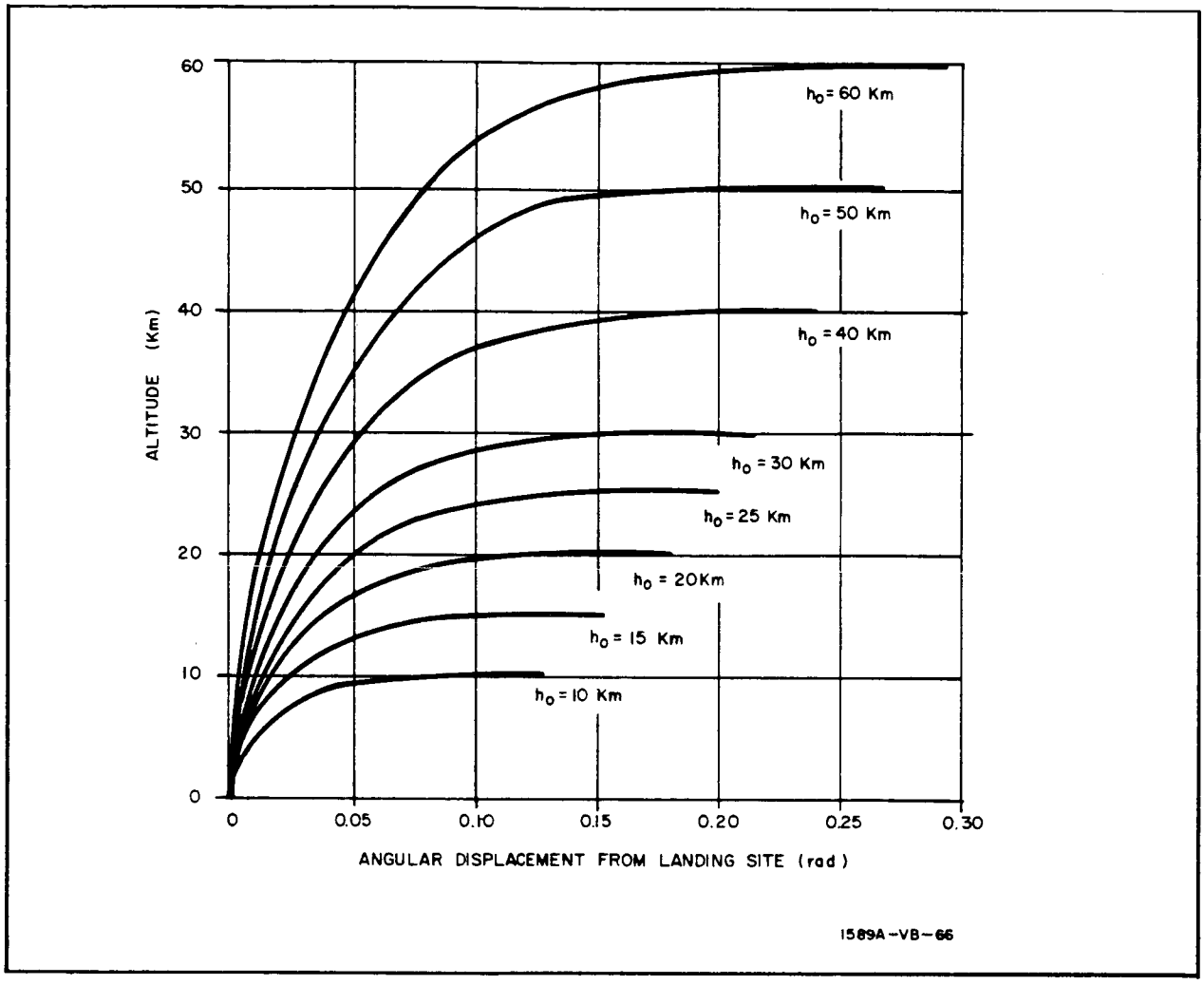

Figure 18. Nominal Trajectory Characteristics, h vs θ

The nominal trajectory is restricted to a constant thrust level. This assumption makes determination of nominal fuel consumption parameters an easy task. Two quantities related to fuel consumption can be computed. These are ΔV, which is defined in equation 33, and m_p, defined in equation 34. Quantity m_p is the mass of propellent consumed during the landing maneuver. Thus, m_p is a truer measure of fuel consumption than is ΔV.

The definitions of ΔV and m_p are

$$\Delta V = \int_0^{t_f} \frac{T(t)}{m(t)}\, dt \tag{33}$$

$$m_p = -\int_0^{t_f} \frac{dm}{dt}\, dt \text{ (m = total vehicle mass)} \tag{34}$$

Since the mass rate of flow is constant (constant thrust), the expressions for ΔV and m_p are integrable in closed form.

$$\frac{dm}{dt} = k = \frac{-T_o}{I_{sp}\, g_o} \tag{35}$$

I_{sp} = fuel specific impulse = 400 sec

g_o = gravitational acceleration at earth's surface = 9.80665 m/sec^2

$$\Delta V = \int_0^{t_f} \frac{T_o}{m_o + kt}\, dt \tag{36}$$

$$= -I_{sp}\, g_o \ln\left[\frac{m_o + kt_f}{m_o}\right] \tag{37}$$

$$\therefore \Delta V = -I_{sp}\, g_o \ln\left[\frac{m_o - \frac{T_o\, t_f}{I_{sp} g_o}}{m_o}\right] \tag{38}$$

$$m_p = -\int_0^{t_f} k\, dt = -kt_f$$

$$\therefore m_p = \frac{T_o t_f}{I_{sp} g_o} \tag{39}$$

The quantity m_p/m_o is the nominal fraction of initial landing vehicle mass that is consumed during the landing maneuver. Figure 19 illustrates the variation of nominal ΔV requirements with the initial altitude of the trajectory. Figure 20 contains plots of m_p and m_p/m_o versus h_o. All the quantities required to produce these curves are contained in table 2 with the exception of m_o, which is constant at 11340 kilograms.

As expected, fuel consumption parameters increase as h_o increases. Perhaps the most important piece of information contained in these plots is the relative sensitivity of ΔV and m_p to changes in h_o. If h_o is increased, the fractional increase in m_p is less than the fractional increase in ΔV. Thus, if ΔV is used as a measure of fuel consumption, pessimistic results will be obtained. Whenever a significant fraction of the total vehicle mass is consumed during a thrusting maneuver, the quantity ΔV is no longer an accurate measure of fuel consumption, and the parameter m_p should be used.

3. MODIFIED PROPORTIONAL NAVIGATION GUIDANCE LAW

3.1 Modified Proportional Navigation Guidance Digital Simulation

This program is written to simulate the trajectory and the guidance system of a vehicle attempting to make a soft lunar landing using a modified form of proportional navigation.

The vehicle is assumed to be moving in a central force field influenced only by lunar gravity and vehicle thrust. The most general form of the guidance law employed causes the vehicle to fly initially toward a fictitious target Y_H meters directly above the desired landing site, as shown in figure 21. When the relative range to the fictitious target, R_1, is less than R_t, an arbitrary constant, guidance system parameters change, and the vehicle is made to proceed toward the desired landing site. This general form is seen to be the MPN/VT-B guidance concept described in paragraph 4.3.2.1b of Volume III.

3.1.1 Coordinate Systems and Equations of Motion

The equations of motion are written in a target-centered inertial cartesian coordinate system. The Y-axis is positive upward along the landing site vertical, the X-axis is along the horizontal and is positive toward the landing vehicle, and the Z-axis completes the right-handed system. The equations of motion are:

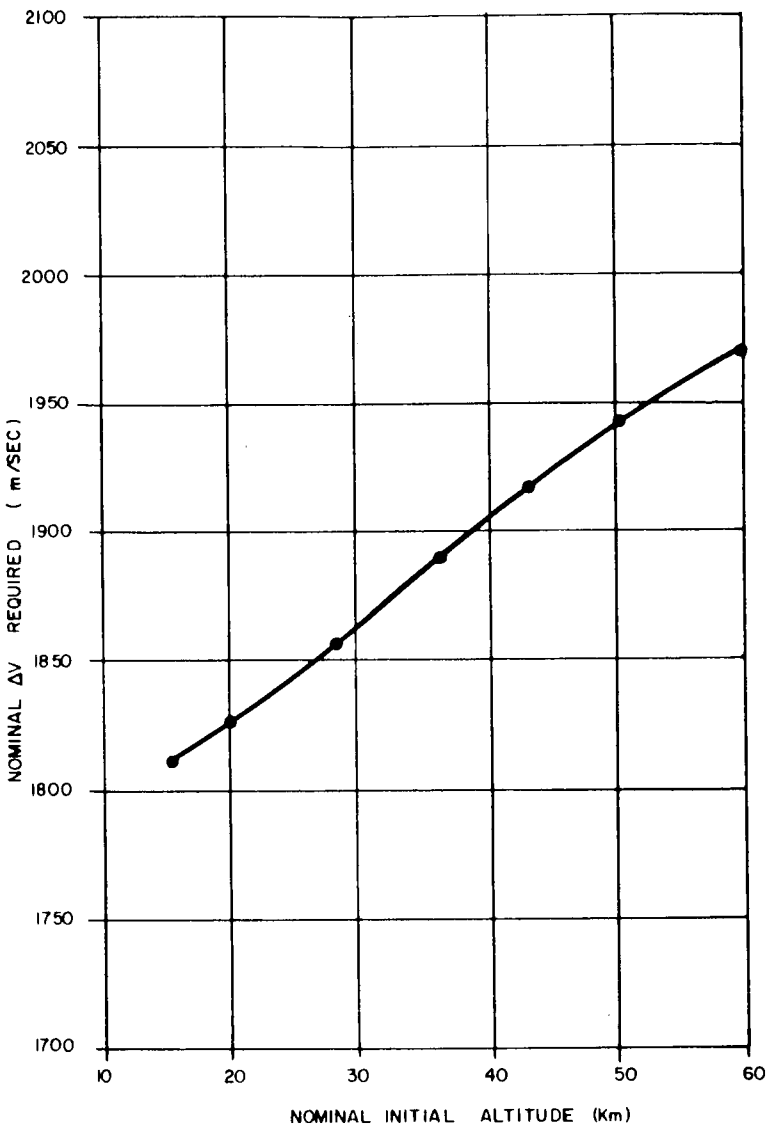

Figure 19. Nominal Trajectory ΔV Requirements

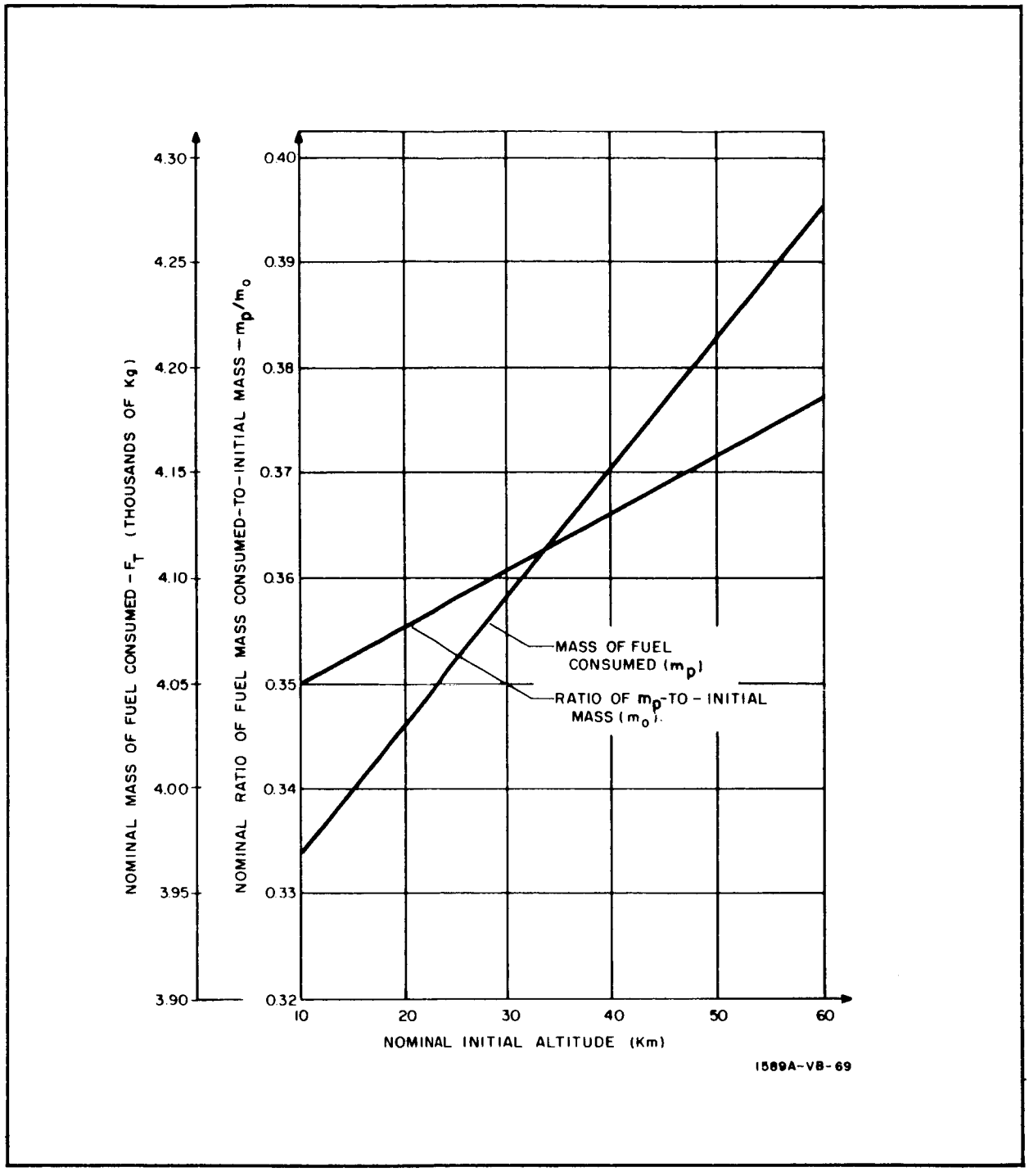

Figure 20. Nominal Trajectory Fuel Consumption

$$\ddot{X} = -\frac{\mu}{r^3} X + a_x$$

$$\ddot{Y} = -\frac{\mu}{r^3} (Y + r_c) + a_y \qquad (40)$$

$$\ddot{Z} = -\frac{\mu}{r^3} Z + a_z$$

where

X, Y, Z = coordinates of the vehicle's position

$\ddot{X}, \ddot{Y}, \ddot{Z}$ = vehicle accelerations in the X, Y, Z directions

μ = lunar gravitational constant

r = distance from the center of the moon to the vehicle

r_c = radius of the moon at the desired landing site (taken to be the mean lunar radius)

a_x, a_y, a_z = vehicle thrust accelerations in the X, Y, Z directions

The set of equations 40 are integrated numerically to obtain the vehicle's motion.

Let X_B, Y_B, Z_B represent a second cartesian coordinate system corresponding to the roll, yaw, and pitch axes of the landing vehicle respectively. An attitude control system, identical to that described in Appendix B of Volume IV, roll-rate stabilizes the vehicle while maintaining the X_B axis along the line of sight to the target. In a two-dimensional situation, the Y_B axis is maintained in the plane of line-of-sight rotation. The guidance equations determine the command accelerations in the X_B, Y_B, and Z_B directions. These accelerations are then resolved into the X, Y, and Z directions by means of an Euler transformation.

3.1.2 Guidance Equations

When the range to the fictitious target is estimated to be greater than R_t, the command accelerations are given by

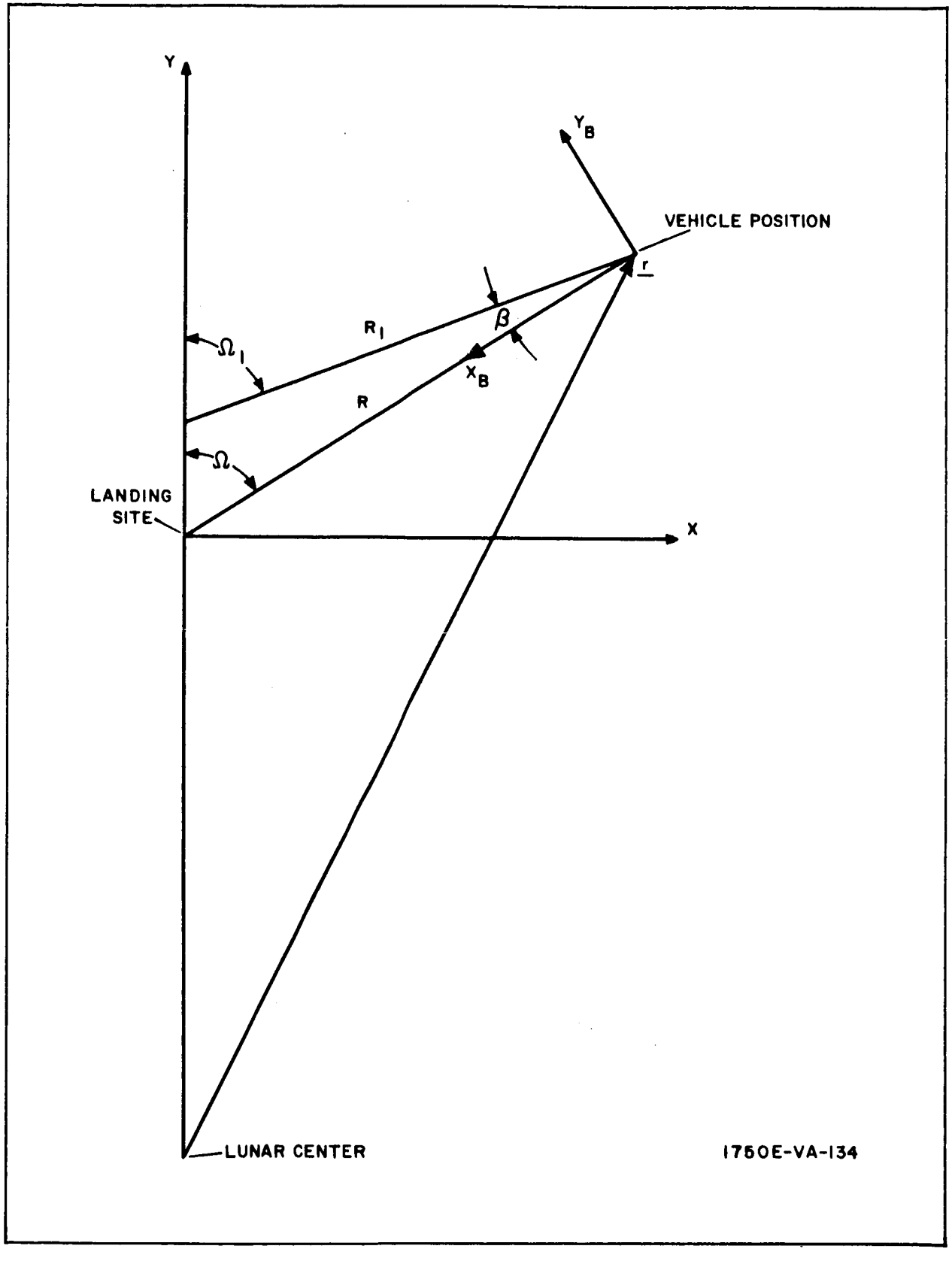

Figure 21. Lunar Landing Geometry

$$\hat{a}_{x_B} = -\left[\frac{K-1}{K}\,\frac{(\hat{\dot{R}}_1)^2}{\hat{R}_1} + g_m \cos\left(\hat{\Omega}+\hat{\beta}\right)\right]\cos\hat{\beta}$$

$$-\left[-\left(S+\frac{K-1}{K}\right)\hat{\dot{R}}_1\,\hat{\Omega} + g_m \sin\left(\hat{\Omega}+\hat{\beta}\right)\right]\sin\hat{\beta} \qquad (41)$$

$$\hat{a}_{y_B} = -\left[\frac{(K-1)}{K}\,\frac{(\hat{\dot{R}}_1)^2}{\hat{R}_1} + g_m \cos\left(\hat{\Omega}+\hat{\beta}\right)\right]\sin\hat{\beta}$$

$$+\left[-\left(S+\frac{K-1}{K}\right)\hat{\dot{R}}_1\,\hat{\Omega}_1 + g_m \sin\left(\hat{\Omega}+\hat{\beta}\right)\right]\cos\hat{\beta}$$

$$\hat{a}_{z_B} = 0 \text{ (for two-dimensional motion)}$$

where the symbol $\hat{}$ denotes an observed quantity or a quantity computed from observed data, and

$\hat{a}_{x_B}, \hat{a}_{y_B}, \hat{a}_{z_B}$ = command accelerations in body axis coordinates

K, S = guidance parameters

g_m = lunar surface acceleration of gravity

$\hat{\beta}$ = estimated value of β (see figure 21) which is

$$\hat{\beta} = \sin^{-1}\left[\frac{Y_H \sin\hat{\Omega}}{\hat{R}_1}\right]$$

$\hat{\Omega}$ = observed value of Ω and is given by the following expression in the digital simulation:

$$\hat{\Omega} = \int_0^t \frac{\Omega - \hat{\Omega} + \Omega_b + (\Omega p_b)\left(\frac{\Omega}{100}\right)}{\tau_\Omega}\,dt$$

Ω_b = a bias error in the observation of Ω.

Ω = actual angle between the Y axis and the line of sight

Ω^{p_b} = a scale factor error in the observation of Ω

τ_Ω = a time lag in the observation of Ω

R_1 = estimated value of R_1, given by

$$\hat{R}_1 = \left[Y_H^2 + \hat{R}^2 - 2 Y_H \hat{R} \cos \hat{\Omega} \right]^{1/2}$$

Y_H = altitude of the fictitious target above the desired landing point

$\hat{R}$ = observed value of R represented by

$$\hat{R} = \int_0^t \frac{R - \hat{R} + R_b + ({}_R p_b)\left(\frac{R}{100}\right)}{\tau_R} \, dt$$

R = the actual range to the desired landing point:

$$R = \left[X^2 + Y^2 + Z^2 \right]^{1/2}$$

R_b = a bias error in the observation of R

R^{p_b} = a scale factor error in the observation of R

τ_R = a time lag in the observation of R

$\hat{\dot{R}}_1$ = estimated value of $\dot{R}_1$ given by

$$\hat{\dot{R}}_1 = \hat{\dot{R}} \cos \hat{\beta} + \hat{R}\, \hat{\dot{\Omega}} \sin \hat{\beta}$$

$\hat{\dot{R}}$ = observed value of $\dot{R}$ represented by

$$\hat{\dot{R}} = \int_0^t \frac{\dot{R} - \hat{\dot{R}} + \dot{R}_b + ({}_{\dot{R}} p_b)\left(\frac{\dot{R}}{100}\right)}{\tau_{\dot{R}}} \, dt$$

$\dot{R}$ = actual value of the range rate to the desired landing site

$\dot{R}_b$ = a bias error in the observation of $\dot{R}$

$\dot{R}^{p_b}$ = a scale factor error in the observation of $\dot{R}$

$\tau_{\dot{R}}$ = a time lag in the observation of $\dot{R}$

$\hat{\dot{\Omega}}$ = observed value of $\dot{\Omega}$, represented by

$$\hat{\Omega} = \int_0^t \frac{\dot{\Omega} - \hat{\dot{\Omega}} + \dot{\Omega}_b + (\dot{\Omega}^{p_b})\left(\frac{\dot{\Omega}}{100}\right)}{\tau_{\dot{\Omega}}} dt$$

$\dot{\Omega}$ = actual value of the line-of-sight rotation rate

$\dot{\Omega}_b$ = a bias error in the observation of $\dot{\Omega}$

$\dot{\Omega}^{p_b}$ = a scale factor error in the observation of $\dot{\Omega}$

$\tau_{\dot{\Omega}}$ = a time lag in the measurement of $\dot{\Omega}$

$\hat{\dot{\Omega}}_1$ = estimated value of $\dot{\Omega}_1$ (see figure 21) given by

$$\hat{\dot{\Omega}}_1 = \frac{1}{\hat{R}_1}\left(- \hat{\dot{R}} \sin\hat{\beta} + \hat{R}\,\hat{\dot{\Omega}} \cos\hat{\beta}\right)$$

When the range to the fictitious target is less than R_t, the guidance equations become

$$\hat{a}_{x_B} = -\left[\frac{(K_1 - 1)}{K_1}\frac{(\hat{R})^2}{\hat{R}}\right]$$

$$\hat{a}_{y_B} = -\left[S_1 \hat{\dot{R}}\,\hat{\dot{\Omega}} - S_2 \frac{(\hat{\dot{R}})^2}{\hat{R}}\,\hat{\Omega}\right] \qquad (42)$$

$$\hat{a}_{z_B} = 0 \text{ (for two-dimensional motion)}$$

where K_1, S_1, and S_2 are guidance parameters and the remaining quantities are previously defined.

The thrust required to provide the command accelerations is

$$T_R = \left[m_o + \int_0^t \dot{m} dt \right] \left[(\hat{a}_{x_B})^2 + (\hat{a}_{y_B})^2 + (\hat{a}_{z_B})^2 \right]^{1/2} \quad (43)$$

where

T_R = required thrust vector magnitude

m_o = initial mass of the vehicle

$\dot{m}$ = rate of mass flow = $\dfrac{-T}{g_o I_{sp}}$

T = actual vehicle thrust vector magnitude

g_o = gravitational acceleration at the earth's surface

I_{sp} = fuel specific impulse

If $T_{min} < T_R < T_{max}$, the vehicle thrust is set equal to T_R and the vehicle body accelerations. a_{x_B}, a_{y_B}, and a_{z_B} are set equal to the command accelerations. If the required thrust is less than T_{min}, the problem stops. When T_R exceeds T_{max}, the thrust vector magnitude is set equal to T_{max}, and the actual accelerations are then

$$\begin{aligned} a_{x_B} &= A_{max} \sin \delta_2 \cos \delta_1 \\ a_{y_B} &= A_{max} \cos \delta_2 \\ a_{z_B} &= A_{max} \sin \delta_2 \sin \delta_1 \end{aligned} \quad (44)$$

where

$$A_{max} \equiv \frac{T_{max}}{m_o + \int_0^t \dot{m}\, dt}$$

$$\delta_1 \equiv \cos^{-1} \frac{\hat{a}_{x_B}}{\left[(\hat{a}_{x_B})^2 + (\hat{a}_{z_B})^2\right]^{1/2}}$$

$$\delta_2 = \cos^{-1}\left\{\frac{\hat{a}_{y_B}}{\left[(\hat{a}_{x_B})^2 + (\hat{a}_{y_B})^2 + (\hat{a}_{z_B})^2\right]^{1/2}}\right\}$$

By proper selection of parameters Y_H, R_t, S, K, S_1, S_2, and K_1 a large number of different combinations of landing points and guidance laws can be obtained. For example, setting

Y_H = 0.0

R_t = 0.0

S = any desired value

K = any desired value

S_1, S_2, K_1 = 0.0 (they have no effect)

causes the vehicle to proceed directly to the landing site using modified proportional navigation guidance (MPN). Changing Y_H to some positive value causes the vehicle to proceed to a hover point directly over the desired landing site. By setting $S_1 = S + \frac{K-1}{K}$, $S_2 = 0.0$, R_t equal to some positive value, and Y_H to some positive value MPN is flown throughout descent, the vehicle flying first toward the hover point and then, when $R_1 < R_t$, toward the desired landing point. As another alternative, the vehicle can be made to fly the MPN/VT guidance law all the way by setting R_t to be greater than the initial range.

3.2 A Modified Proportional Navigation Guidance System with a Vertical Landing Velocity Constraint

A modified form of proportional navigation (MPN) for use with a terminal lunar landing guidance system has been proposed by Kriegsman and Reiss.[2/] This guidance system yields a rather shallow approach to

[2/] B. A. Kriegsman and M. H. Reiss, "Terminal Guidance and Control Techniques for Soft Lunar Landing," ARS Journal, Volume 32 (March 1962), pp. 401 - 413.

the desired landing area and a nonvertical touchdown. The guidance technique described herein, which is a modified version of MPN, constrains the vehicle to land from a vertical direction. It has been named "Modified Proportional Navigation/Vertical Touchdown" (MPN/VT).

3.2.1 Derivation of Guidance Equations

Let X and Y represent the axes of a coordinate system centered at the desired landing point on a flat moon. Let R and Ω be the polar coordinates of a vehicle attempting to soft-land at the origin from a vertical direction. From figure 22,

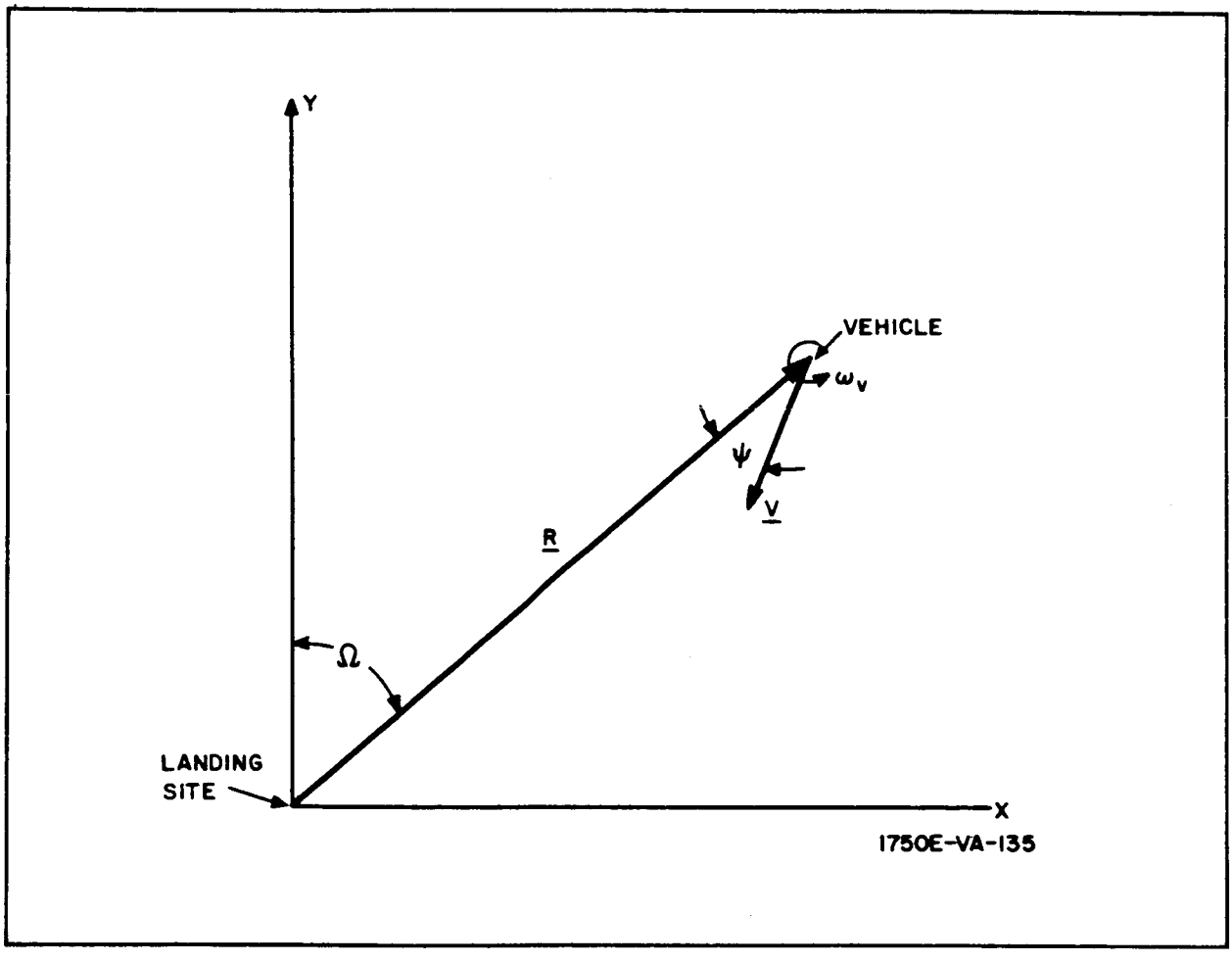

Figure 22. Reference Coordinate System

$$\dot{R} = - V \cos \psi \tag{45}$$

$$R \dot{\Omega} = V \sin \psi \tag{46}$$

$$\dot{\psi} - \dot{\Omega} = \omega_v \tag{47}$$

where

V = magnitude of the velocity vector

ψ = angle between the velocity and range vectors

ω_v = angular rotation rate of the velocity vector

From equations 45 and 46,

$$\tan \psi = -\frac{R\dot{\Omega}}{\dot{R}} \tag{48}$$

Differentiation yields

$$\dot{\psi} \sec^2 \psi = -\frac{\dot{R}\,(R\ddot{\Omega} + \dot{R}\dot{\Omega}) - R\dot{\Omega}\dot{R}}{\dot{R}^2} \tag{49}$$

$$\dot{\psi} = -\cos^2 \psi \left[\frac{R\,\ddot{\Omega}}{\dot{R}} + \dot{\Omega}\left(1 - \frac{R\ddot{R}}{(\dot{R})^2}\right)\right] \tag{50}$$

An equidimensional differential equation results if the following assumptions are made:

$$\omega_v = -S_1\,\dot{\Omega} + S_2\,\frac{\dot{R}}{R}\,\Omega \tag{51}$$

$$a_\Omega = S_1\,\dot{R}\,\dot{\Omega} - S_2\,\frac{(\dot{R})^2}{R}\,\Omega \tag{52}$$

$$a_R = \ddot{R} = \frac{K_1 - 1}{K_1}\,\frac{(\dot{R})^2}{R} \tag{53}$$

$$\frac{R}{R_o} = \tau^{K_1};\ \frac{\dot{R}}{\dot{R}_o} = \tau^{K_1 - 1};\ \tau = 1 - \frac{t}{t_f};\ t_f = \frac{KR_o}{\dot{R}_o} \tag{54}$$[3/]

3/ The expressions of equation 54 are taken from the approximate closed-form solutions to the nonlinear differential equations of motion developed in Appendix C of Volume IV.

where

S_1, S_2, and K_1 = guidance parameters

a_Ω = command acceleration normal to the line-of-sight range vector

a_R = command acceleration along the line-of-sight range vector

τ = normalized time to go

t_f = the nominal time of flight

R_o and $\dot{R}_o$ = the initial values of R and $\dot{R}$

Substituting equations 53 and 54 into 50 yields

$$\dot{\psi} = -\cos^2\psi\left[\frac{R_o}{\dot{R}_o}\,\tau\,\ddot{\Omega} + \frac{\dot{\Omega}}{K_1}\right] \tag{55}$$

From equations 47, 51, and 55 the following expression is obtained:

$$(\cos^2\psi)\,\frac{R_o}{\dot{R}_o}\,\tau^2\,\ddot{\Omega} + \left[(1 - S_1) + \frac{\cos^2\psi}{K_1}\right]\tau\,\dot{\Omega} + S_2\,\frac{\dot{R}_o}{R_o}\,\Omega = 0 \tag{56}$$

Making use of equation 54,

$$-(\cos^2\psi)\,\frac{t_f}{K_1}\,\tau^2\,\ddot{\Omega} + \left[(1 - S_1) + \frac{\cos^2\psi}{K_1}\right]\tau\,\dot{\Omega} - \frac{S_2 K_1}{t_f}\,\Omega = 0 \tag{57}$$

and $\dot{\Omega}$ can be written as:

$$\dot{\Omega} = \frac{d\Omega}{dt} = \frac{d\Omega}{d\tau}\,\frac{d\tau}{dt} = -\frac{1}{t_f}\,\frac{d\Omega}{d\tau} = \frac{-\overset{\circ}{\Omega}}{t_f}$$

where $\overset{\circ}{\Omega}$ is defined to be $\frac{d\Omega}{d\tau}$:

Similarly $\ddot{\Omega}$ can be shown to be:

$$\ddot{\Omega} = \frac{\overset{\circ\circ}{\Omega}}{t_f^2}$$

where

$$\overset{\circ\circ}{\Omega} = \frac{d^2 \Omega}{d\tau^2}$$

Substituting these two expressions into equation 57 and simultaneously multiplying both sides by the expression $-\frac{K_1 t_f}{\cos^2 \psi}$ yields the following equidimensional equation:

$$\tau^2 \overset{\circ\circ}{\Omega} + K_1 \left[\frac{1-S_1}{\cos^2 \psi} + \frac{1}{K_1} \right] \tau \dot{\Omega} + \frac{S_2 K_1^2}{\cos^2 \psi} \Omega = 0 \qquad (58)$$

If the angle ψ is small, as it is during the final portion of the landing maneuver where MPN/VT guidance is to be used, the quantity $\cos^2 \psi$ is approximately equal to unity and equation 58 is approximately

$$\tau^2 \overset{\circ\circ}{\Omega} + \left[1 + K_1 (1 - S_1) \right] \tau \overset{\circ}{\Omega} + S_2 K_1^2 \Omega = 0 \qquad (59)$$

This equation is recognized to be in the form of Euler's differential equation[4/] for which the solution is known. This solution has the form

$$\Omega(\tau) = C_1 \tau^{a_1} + C_2 \tau^{a_2} \qquad (60)$$

where C_1 and C_2 are constants of integration and a_1 and a_2 are given by

$$a_1, a_2 = \frac{K_1 (S_1 - 1)}{2} \left[1 \pm \left(1 - \frac{4 S_2}{(S_1 - 1)^2} \right)^{1/2} \right] \qquad (61)$$

If $a_1 = a_2$, the solution to equation 59 has a different form:

$$\Omega(\tau) = \tau^{a_1} (C_1 + C_2 \ln \tau) \qquad (62)$$

[4/] C.R. Wylie, Advanced Engineering Mathamatics, New York:McGraw-Hill Book Company, Inc., 1956, p. 282.

This form is an outgrowth of the requirement to maintain two independent constants of integration when the roots of the characteristic equation of a second order linear homogeneous differential equation with constant coefficients are equal.[5]

If a_1 and a_2 are to be real and distinct, then:

$$\frac{4S_2}{(S_1 - 1)^2} < 1; \text{ or } S_2 < \frac{(S_1 - 1)^2}{4} \tag{63}$$

If in addition it is desired to have zero range rate at zero range in a free space environment, the value of K_1 must be greater than 2. A lower bound on the permissible value of S_2 can be obtained by requiring the normal acceleration given by expressions 64 to be finite at τ equal zero.

$$a_\Omega(\tau) = \frac{R}{t_f^2}\ddot{\Omega} - 2\frac{\dot{R}}{t_f}\dot{\Omega}$$

$$= \frac{R_o}{t_f^2}\tau^{K_1}\left[C_1 a_1 (a_1 - 1)\tau^{(a_1 - 2)} + C_2 a_2 (a_2 - 1)\tau^{(a_2 - 2)}\right] \tag{64}$$

$$- \frac{2\dot{R}_o \tau^{(K_1 - 1)}}{t_f}\left[C_1 a_1 \tau^{(a_1 - 1)} + C_2 a_2 \tau^{(a_2 - 1)}\right]$$

This condition is satisfied if

$$K_1 + a_1 - 2 > 0$$

and

$$K_1 + a_2 - 2 > 0 \tag{65}$$

---

[5] J.H. Lanning and R.H. Battin, Random Processes in Automatic Control, New York: McGraw-Hill Book Company, 1956.

or since K_1 is already selected to be greater than 2, $a_1 > 0$, $a_2 > 0$. In addition it is desired that Ω and $\dot{\Omega}$ be finite at τ equals zero. Examination of expression 60 shows that this requirement further restricts the permissible values of a_1 and a_2. Specifically, $a_1 > 1$ and $a_2 > 1$. These restrictions on a_1 and a_2 determine a lower bound on the permissible value of S_2 in the form

$$S_2 > \frac{K_1 (S_1 - 1) - 1}{K_1^2} \tag{66}$$

The lower bound of S_2 is plotted versus S_1 in figure 23 with K_1 as a parameter.

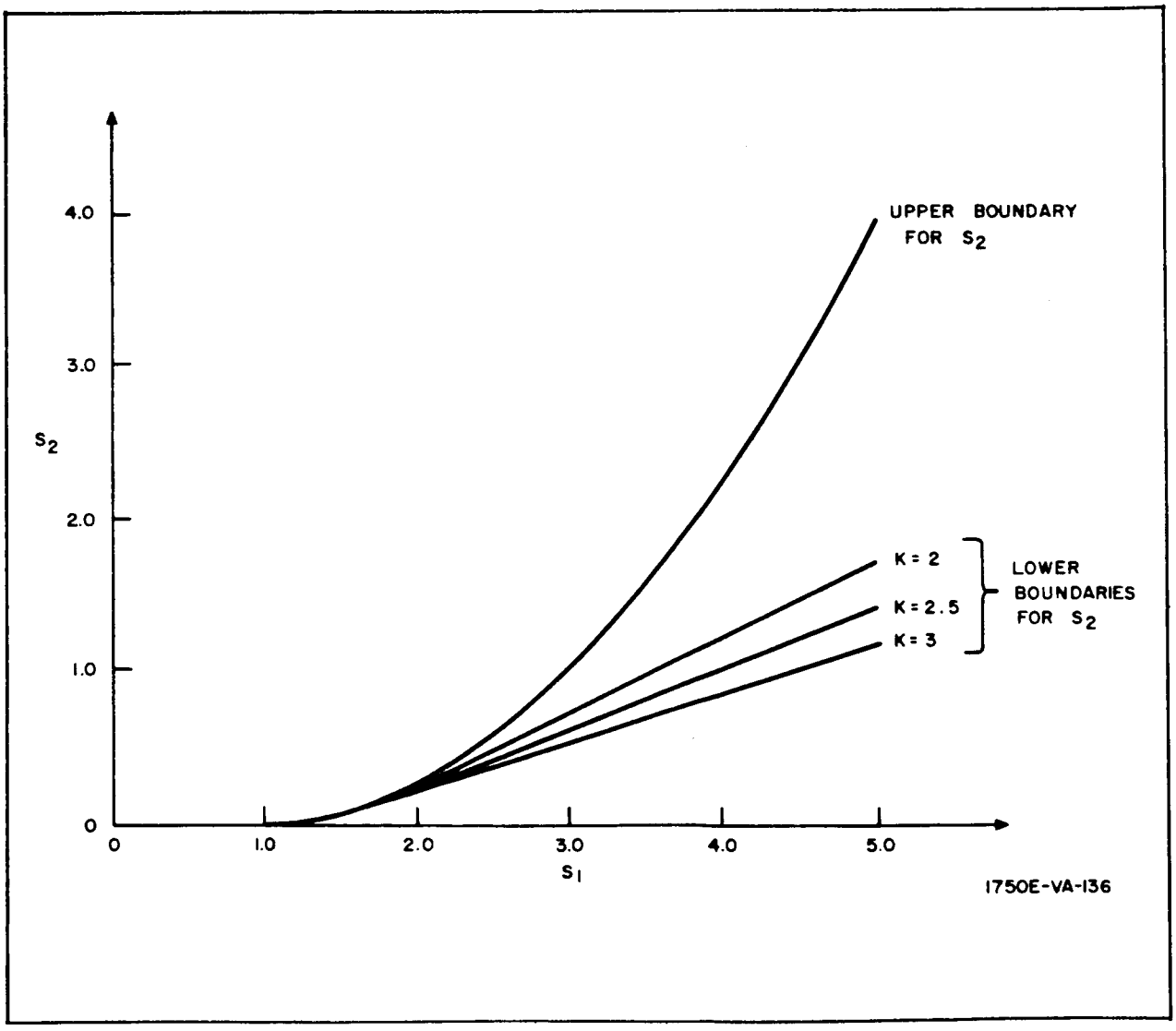

Figure 23. Admissible Values for Guidance Parameters

Equations 54 and 60 describe the motion of the spacecraft as a function of normalized time-to-go when the vehicle's engines provide the accelerations given by equations 52 and 53; the guidance parameters S_1, S_2, and K_1 are within the bounds defined by expressions 63 and 66; and K_1 is restricted to values greater than 2.

The assumptions made in arriving at the guidance law and its analytical solution require that the relative range to the desired touchdown point, and the range rate be small. Therefore the results are useful only for the final flareout and letdown maneuver of the lunar landing.

3.2.2 Evaluation of Guidance Technique

The MPN/VT guidance law defined by the acceleration commands of equations 52 and 53 is evaluated by means of the digital simulation program discussed in subsection 3.1. The equations of motion of a body moving in a central force field are written in the cartesian X, Y, Z coordinate system centered at the desired landing point on a spherical, nonrotating homogeneous moon. The Y axis is vertical and the X axis horizontal in the vehicle plane of motion (two-dimensional analysis) and positive toward the vehicle.

A comparison between the analytic solution represented by equations 54, 60, and 62 and the more exact digital computer solution is presented in figures 24 through 27. The variables R_1, $\dot{R}_1$, Ω, and $\frac{d\Omega}{d\tau}$ are plotted as functions of normalized time-to-go, τ. In each case the maximum error occurs in midflight and is as much as 15 percent for R_1, $\dot{R}_1$, and Ω, while the maximum error is about 30 percent for $\frac{d\Omega}{d\tau}$. Guidance parameter values used for this comparison are

$$K_1 = 2$$

$$S_1 = 2$$

$$S_2 = 0.25$$

The discrepancies noted above are attributed to the effects of gravity and to errors introduced by linearizing the control law to obtain an analytical solution.

3.3 Lunar Landing Tradeoffs and System Design

This subsection illustrates the methods used and the tradeoffs performed in determining parameters such as spacecraft thrust-to-mass ratio,

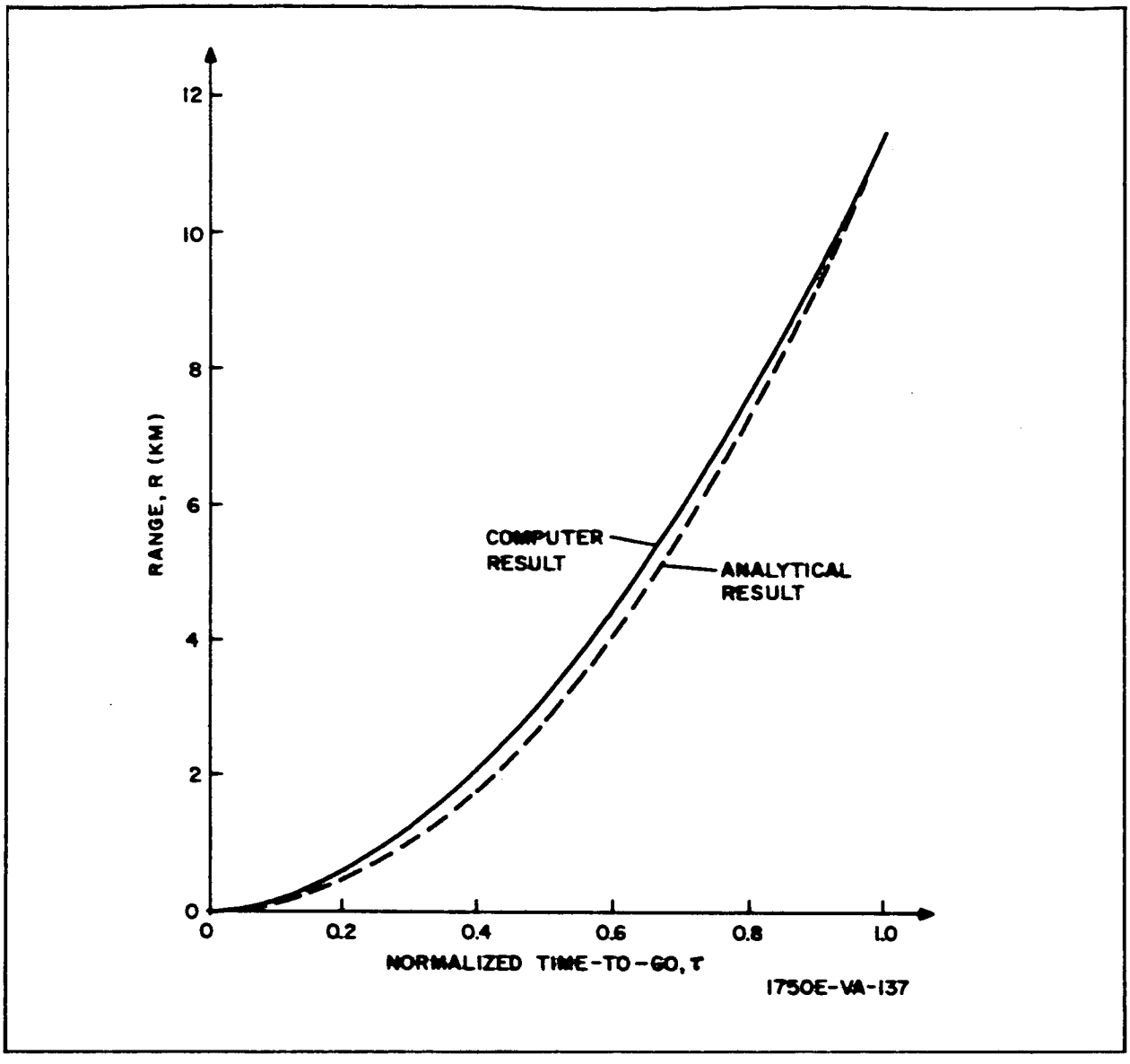

Figure 24. Comparison of Analytical and Computer Results

periselenum altitude, guidance techniques, simplicity, and acceptable sensor random and bias errors. Subsection 4.2 in Volume III, indicates the mission constraints and assumptions used and subsection 3.1 of this appendix explains the analysis techniques used in obtaining most of the data presented in this section.

The performance of the lunar landing guidance system will be measured in terms of payload mass and the ability of the guidance system to deliver the payload to a preselected point on the lunar surface without damage. As the guidance system and sensor requirements are evolved, numerous trade-offs must be performed and constraints imposed. This subsection will

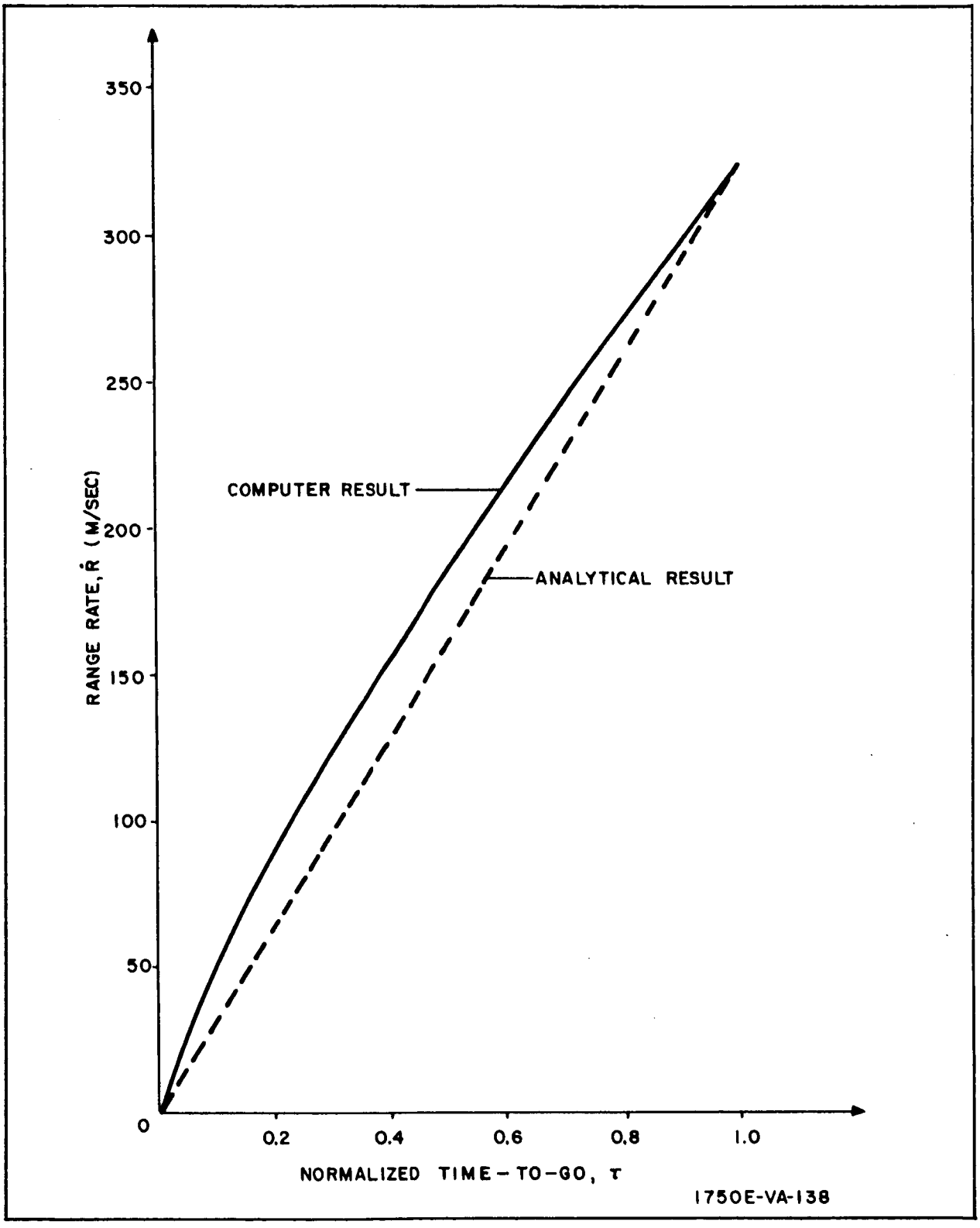

Figure 25. Comparison of Analytical and Computer Results

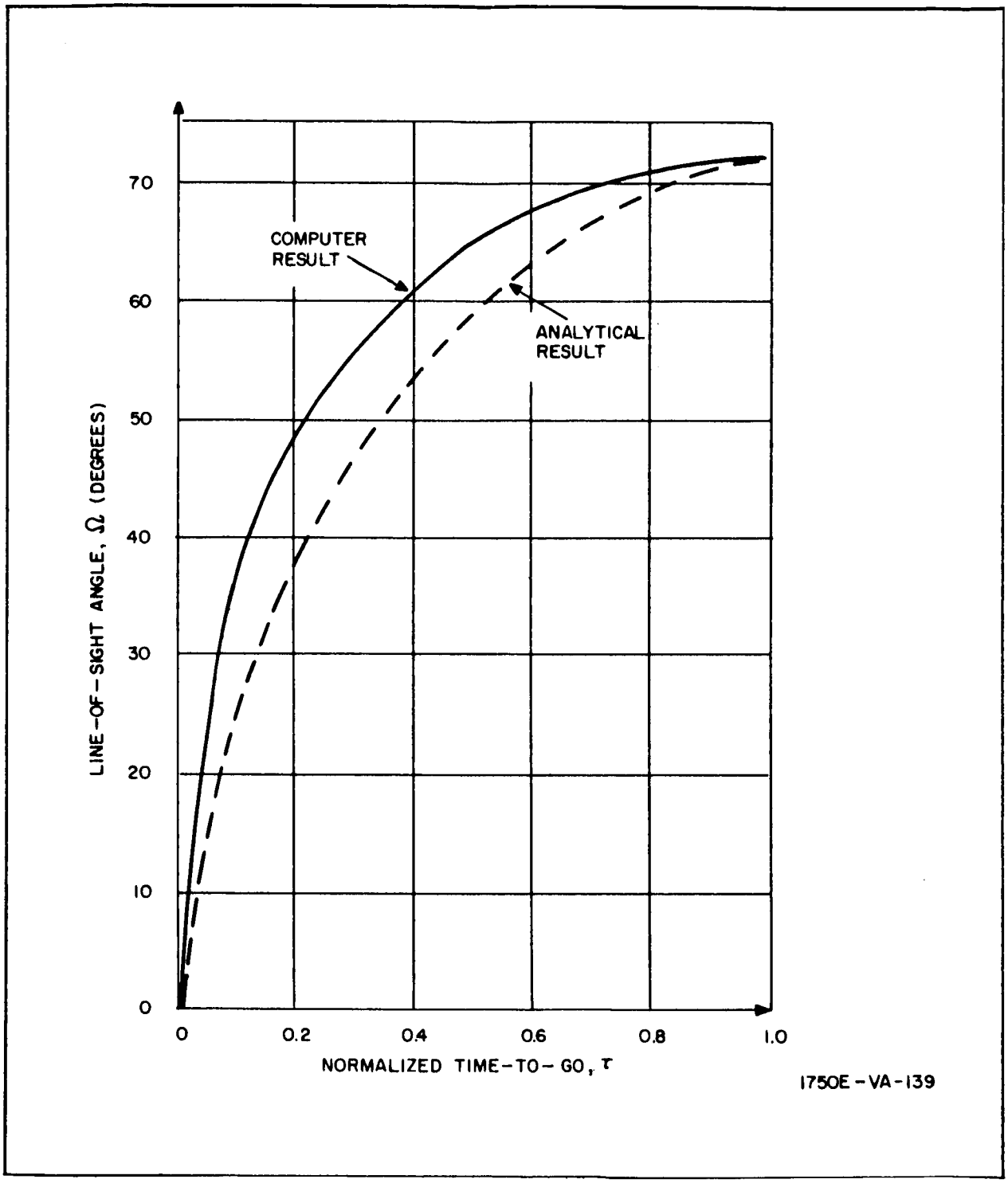

Figure 26. Comparison of Analytical and Computer Results

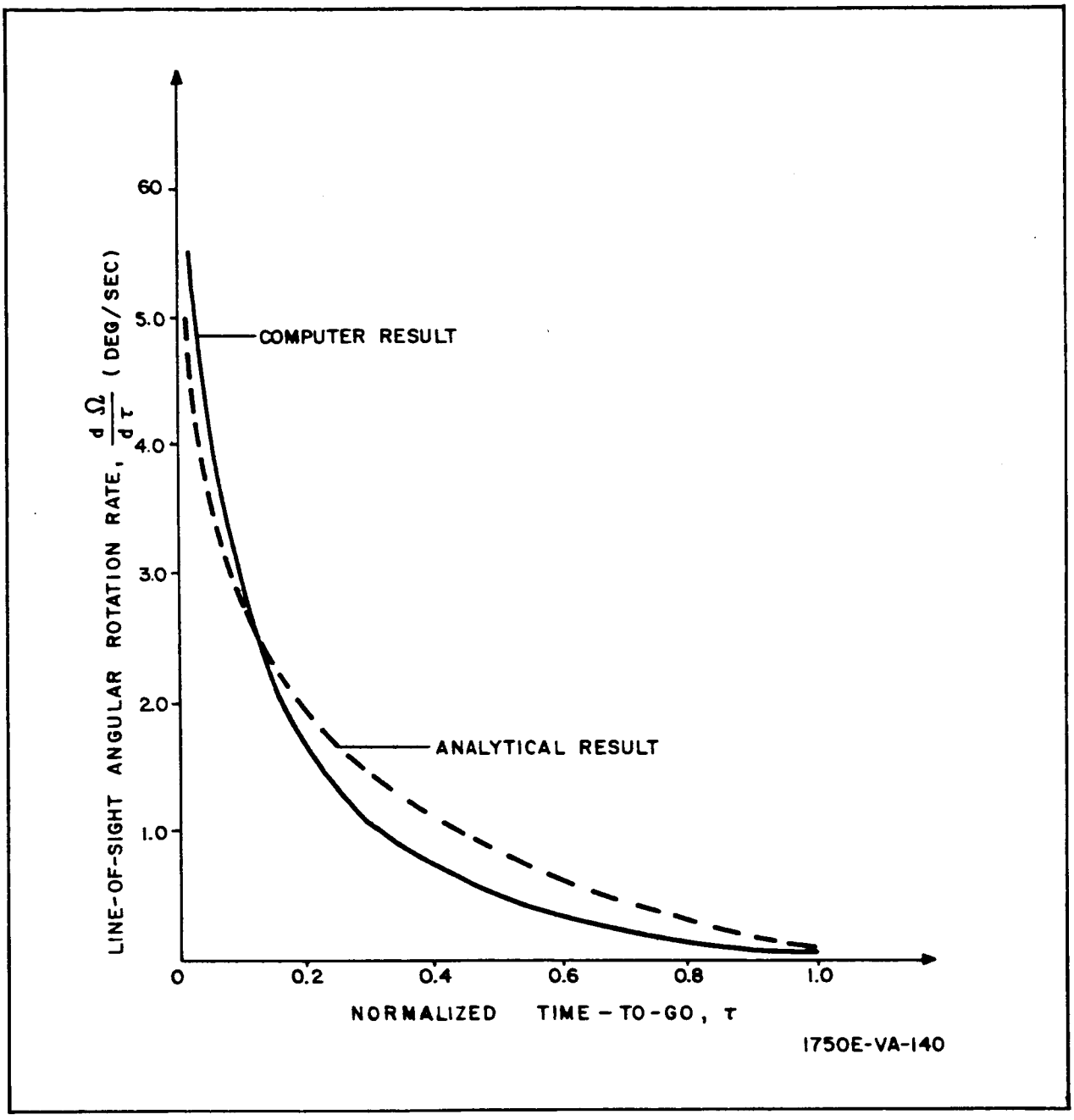

Figure 27. Comparison of Analytical and Computer Results

explore the tradeoffs which exist while imposing typical mission profiles and state of the art constraints.

As discussed in subsection 4.2 of volume III, a synchronous transfer ellipse is presently planned for the Apollo mission as the intermediate transfer orbit from the deorbit point to periselenum. Although the use of a synchronous transfer ellipse will result in an overall mission fuel penalty of

approximately 120 meters per second [6/] in comparison with a Hohmann transfer ellipse, as shown in figure 28, the synchronous transfer ellipse has been chosen for the purpose of this study. This choice will incur a net payload penalty of approximately 590 kilograms but will not create any significant difference in the terminal landing trajectory. Consequently the landing guidance methods developed in paragraph 3.3.1 will be suitable for either a synchronous transfer orbit or a Hohmann transfer orbit.

As previously discussed, the deboost maneuver is assumed to commence when the transfer orbit reaches periselenum. The term initial thrust-to-mass ratio, $(T/m)_o$, is used to indicate the ratio of spacecraft

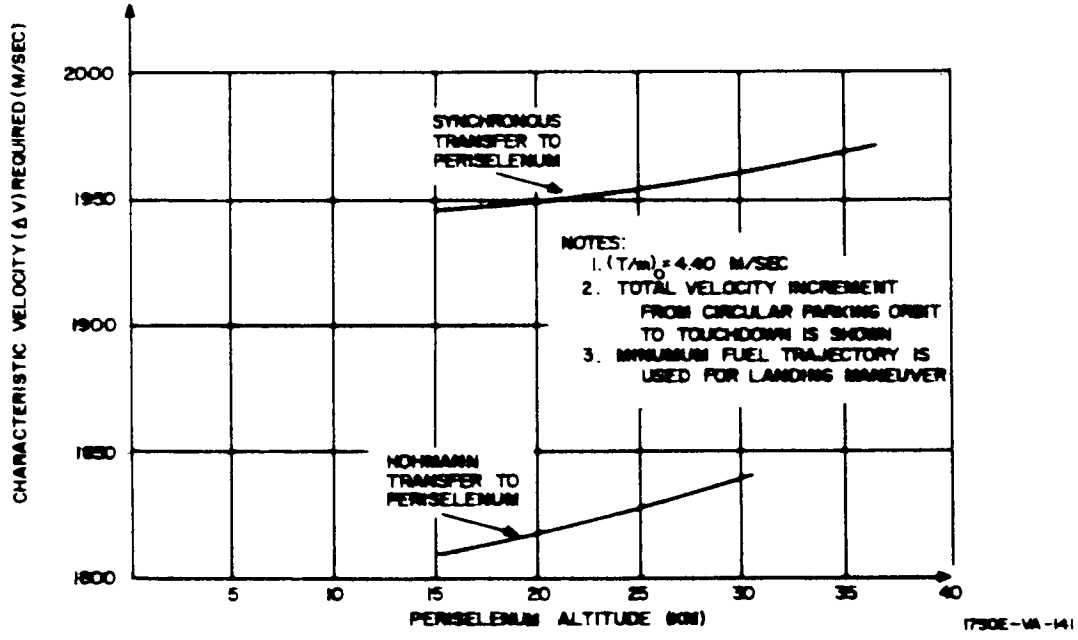

Figure 28. Characteristic Velocity Required for Landing vs Periselenum Altitude

[6/] Fuel penalties are often discussed in terms of incremental velocity penalties (ΔV).

thrust level to spacecraft mass at the commencement of the deboost maneuver.

3.3.1 Assumptions

The requirement that the landing site be visible at the start of the landing maneuver (periselenum) is imposed. For the purpose of this phase of the study, the characteristics of the RL-10 engine are selected to represent the class of engine which is to be available in the 1967 time period. Typical engine characteristics are given below:

Thrust level	66,765 newtons (15,000 lb)
Weight	136.5 kg (300 lb)
Throttling range	10:1

According to paragraph 4.3.2.1d of Volume III, the spacecraft mass at periselenum will be 31,100 kilograms. For reference purposes initial thrust-to-mass ratios for spacecraft configuration employing one, two, and three RL-10's are given in table 3.

TABLE 3

THRUST TO MASS RATIO

Number of RL-10 Engines	Initial Thrust-to-Mass Ratio $(T/m)_o$ (m/sec^2)
1	2.15
2	4.30
3	6.45

The spacecraft will be required to perform a soft pinpoint landing at a preassigned point.

3.3.2 Determination of I_{sp}

The effect of fuel specific impulse, I_{sp}, upon touchdown mass (gross spacecraft mass at the landing point) is shown in figure 29. Since a state of

the art constraint limits the maximum value of I_{sp} which can be chosen, an I_{sp} of 420 seconds has been selected for the purposes of this study. This choice appears to be commensurate with the most efficient fuels which will be available in the 1967 time period. Substantially larger values of I_{sp} are generally associated with very low-thrust engines and, in addition, are assumed to be unavailable in the 1967 time period. The data shown in figure 29 was obtained by generating minimum fuel landing trajectories for various values of I_{sp} where the initial altitude is 15.25 kilometers and initial thrust-to-mass ratio is 4.30 meters per second per second (133,500 newtons thrust with an initial spacecraft mass of 31,100 kilograms).

3.3.3 Determination of Periselenum Altitude and Thrust Level

Fuel penalty, in terms of incremental velocity, incurred by increasing periselenum altitude is illustrated in figure 28 for the synchronous transfer. Similar data for the Hohmann transfer is included for reference. These curves indicate the combined deorbit and periselenum-to-touchdown velocity increments required to perform the landing. A minimum fuel trajectory for

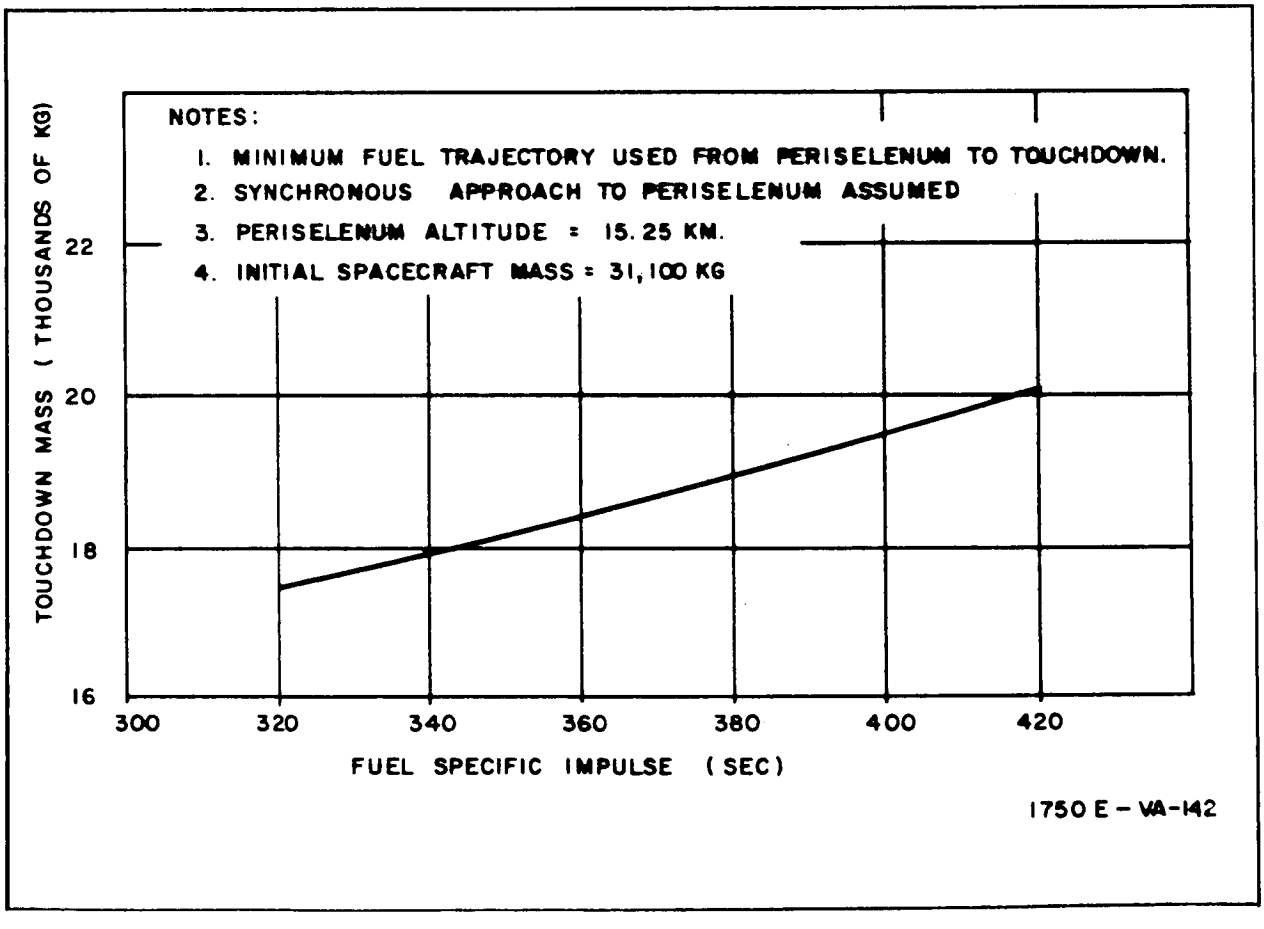

Figure 29. Touchdown Mass vs Fuel Specific Impulse

an initial thrust-to-mass ratio of 4.30 meters per second per second is used to obtain the velocity increment from periselenum to touchdown. The synchronous transfer curve indicates a fuel (ΔV) penalty of approximately 1.2 meters per second per 1000 meters increase in periselenum altitude.

Figure 30 illustrates the downrange distance (subtended central angle) to the horizon as a function of altitude and shows the total downrange distance traveled by the spacecraft as a function of periselenum altitude for two synchronous transfer cases and one Hohmann transfer case. The altitude versus downrange distance histories for the spacecraft are obtained from minimum fuel trajectory results (Section 1) from periselenum to touchdown. Two synchronous transfer cases are shown, one for $(T/m)_o$ = 4.30 meters per second per second and the other for $(T/m)_o$ = 6.45 meters per second per second. The Hohmann transfer is given for $(T/m)_o$ = 4.30 meters per second per second. Note that in all cases spacecraft downrange travel is relatively insensitive to periselenum altitude. The intersection of the horizon curve and synchronous transfer curve for $(T/m)_o$ = 4.30 meters per second per second and occurs at an altitude of 28.0 kilometers while the horizon curve intersection of the synchronous transfer curve for $(T/m)_o$ - 6.45 meters per second per second occurs at an altitude of approximately 12.8 kilometers. These intersections indicate minimum periselenum altitudes where the landing site is just visible at periselenum.

Figure 31 presents data similar to that of figure 30 except that the curve shows the altitude at which the landing site is located on the horizon at periselenum as a function of $(T/m)_o$. Since attention here has been focused on discrete values of $(T/m)_o$ in increments of 2.15 meters per second per second, this particular curve provides no additional tradeoff data but has been included for reference purposes in the event that $(T/m)_o$ different from those assumed here are of interest.

For a minimum fuel trajectory with a periselenum altitude of 15.25 kilometers, the tradeoff between $(T/m)_o$ and ΔV (fuel) requirements from periselenum to touchdown is displayed in figure 32. This curve indicates that a decrease in engine thrust level $(T/m)_o$ will increase fuel requirements. Note, however, that only small decreases in fuel expenditure can be expected as $(T/m)_o$ is increased beyond 4.9 meters per second per second.

Figure 33 shows the tradeoff between $(T/m)_o$ and total landed mass. Again, this curve is obtained from minimum fuel trajectory results with a periselenum altitude of 15.25 kilometers. Here is an indication of the sensitivity of

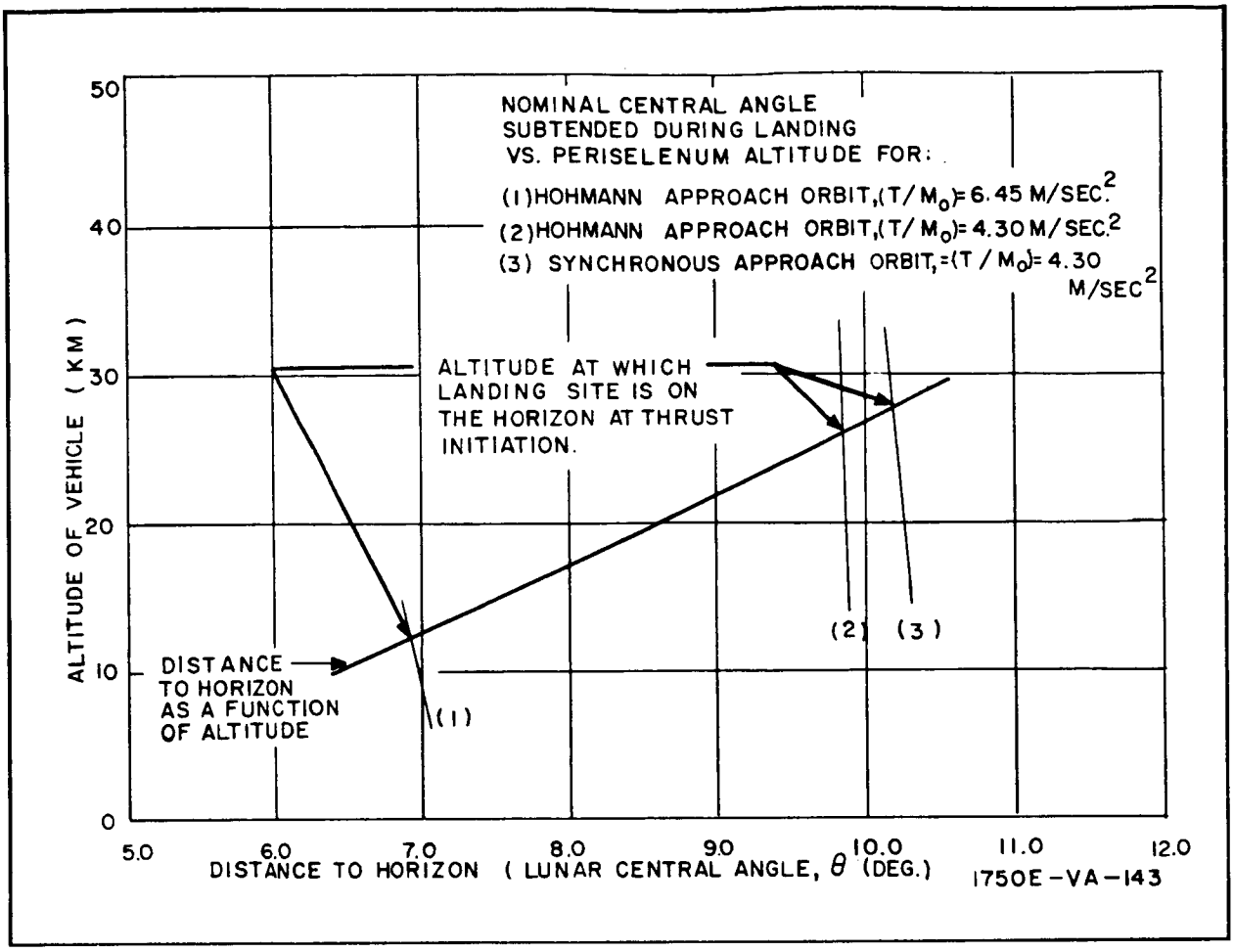

Figure 30. Spacecraft Altitude vs Distance to Horizon

spacecraft total touchdown mass as $(T/m)_o$ is increased. Although the curve indicates that an increase in $(T/m)_o$ is accompanied by an increase in total landing mass, the increase indicated for a $(T/m)_o$ exceeding 4.9 meters per second per second is very small. For example, a net increase in landed mass of 45.5 kilograms is obtained when $(T/m)_o$ is increased from 4.30 meters per second per second (2 RL-10's) to 6.45 meters per second per second (3 RL-10's). (Figures 32 and 33 complement one another and are in effect different forms of the same basic data.)

Figure 32 indicates that the minimum ΔV requirement to perform the landing maneuver is somewhat greater than the synchronous transfer periselenum velocity of 1744 meters per second (at 15.25 kilometers). This result is physically reasonable since the periselenum point of the transfer trajectory is not tangent to the lunar surface. Hence the minimum ΔV

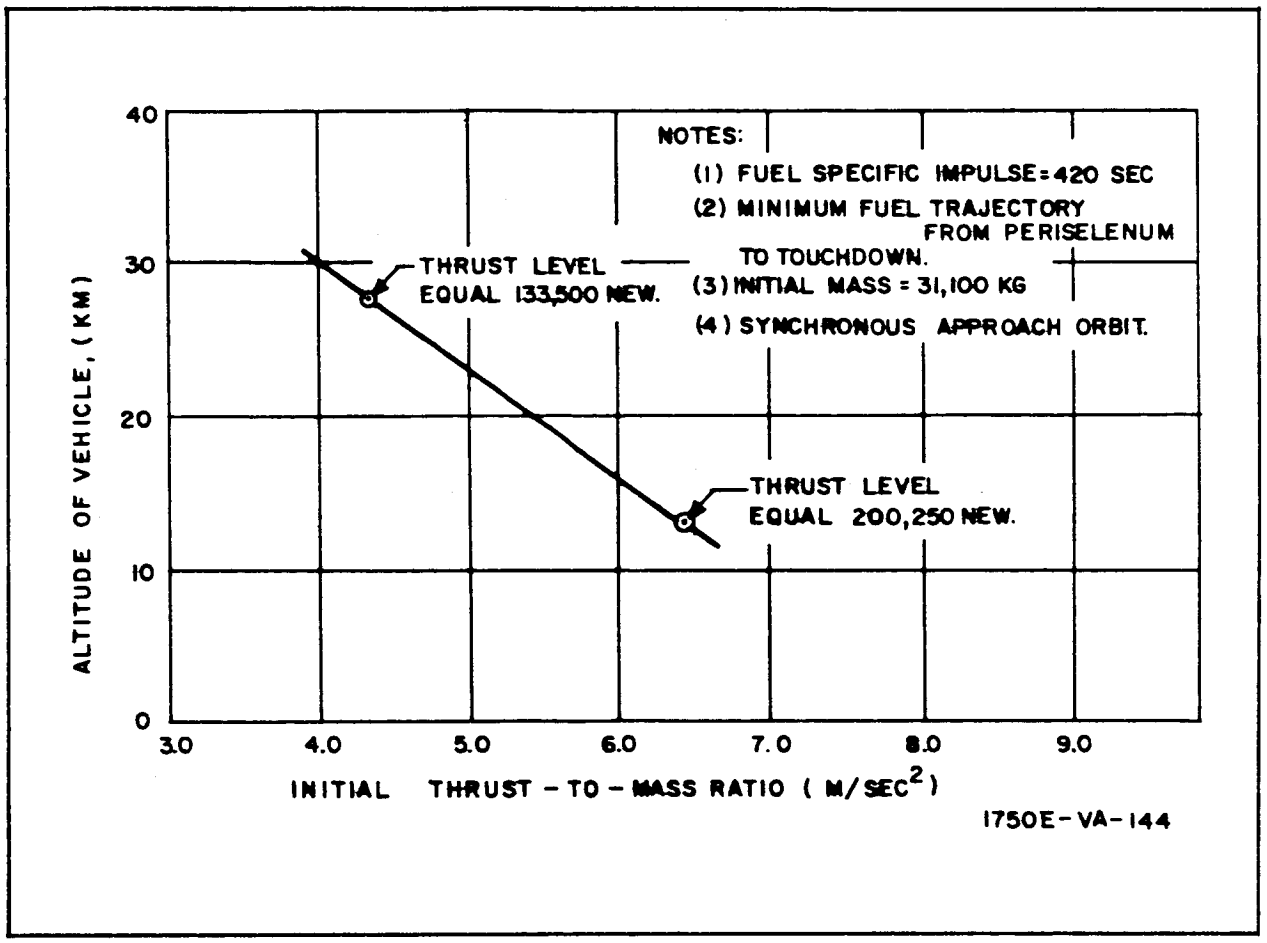

Figure 31. Altitude at which Landing Site is Located on the Horizon at Thrust Initiation vs Initial Thrust-to-Mass Ratio

required to achieve a soft touchdown will be somewhat greater than the spacecraft's velocity at periselenum because the spacecraft is required to translate from the periselenum altitude to the lunar surface.

Landed mass as a function of $(T/m)_o$ is shown in figure 34 where the periselenum altitude is not fixed at 15.25 kilometers, as in figure 33. The periselenum altitude corresponding to any given $(T/m)_o$ on the curve will place the landing site on the horizon when periselenum occurs. Consequently, this curve indicates the combined landed mass penalty as a function of $(T/m)_o$ caused by two sources, the penalty incurred as $(T/m)_o$ is decreased when periselenum altitude is held fixed and the penalty incurred by increasing the periselenum altitude requirement as $(T/m)_o$ is decreased to maintain the landing site on the horizon at periselenum.

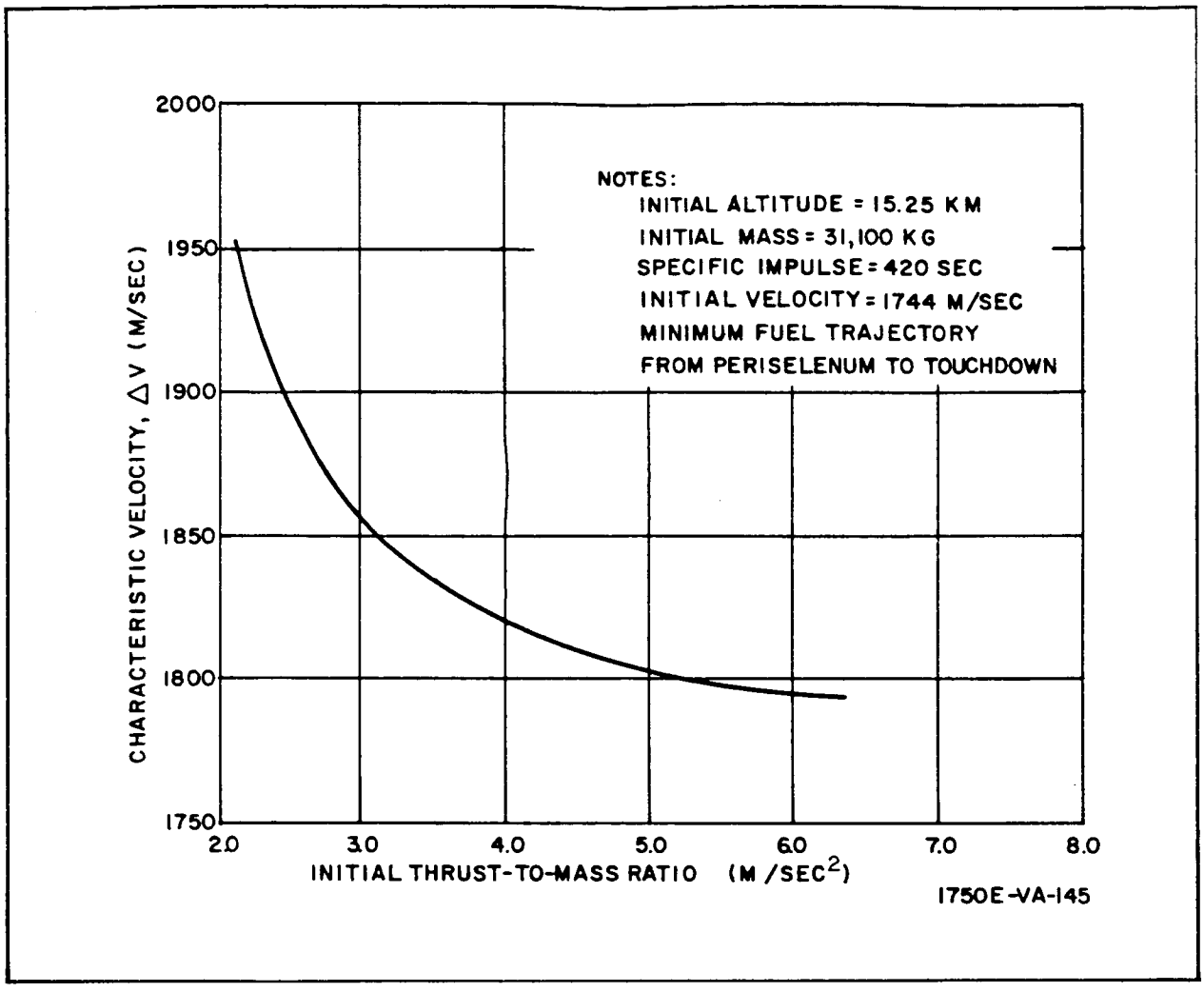

Figure 32. Characteristic Velocity vs Initial Thrust-to-Mass Ratio

Since the predominant tradeoffs and fuel management influences have been identified and studied, the selection of periselenum altitude and thrust level can proceed in an orderly and objective manner. A three-way trade involving payload (net landed) mass, thrust level, and periselenum altitude is required. However, a constraint on minimum periselenum altitude must be considered. Because of irregular lunar terrain, likely altitude errors at periselenum (even if partially compensated during the coasting phase between deorbit and periselenum arrival), and departures of the lunar body from a spherical shape, periselenum altitude must exceed 15.25 km. Consequently, the total net increase in landed mass arising from $(T/m)_o$ = 6.45 meters per second per second indicated in figure 34 cannot be completely realized in terms of additional payload mass. Reference to exact data for a minimum fuel trajectory for $(T/m)_o$ = 6.45 meters per second per second at 15.25 kilometers indicates that the net landing weight advantage of the 3 RL-10 engine

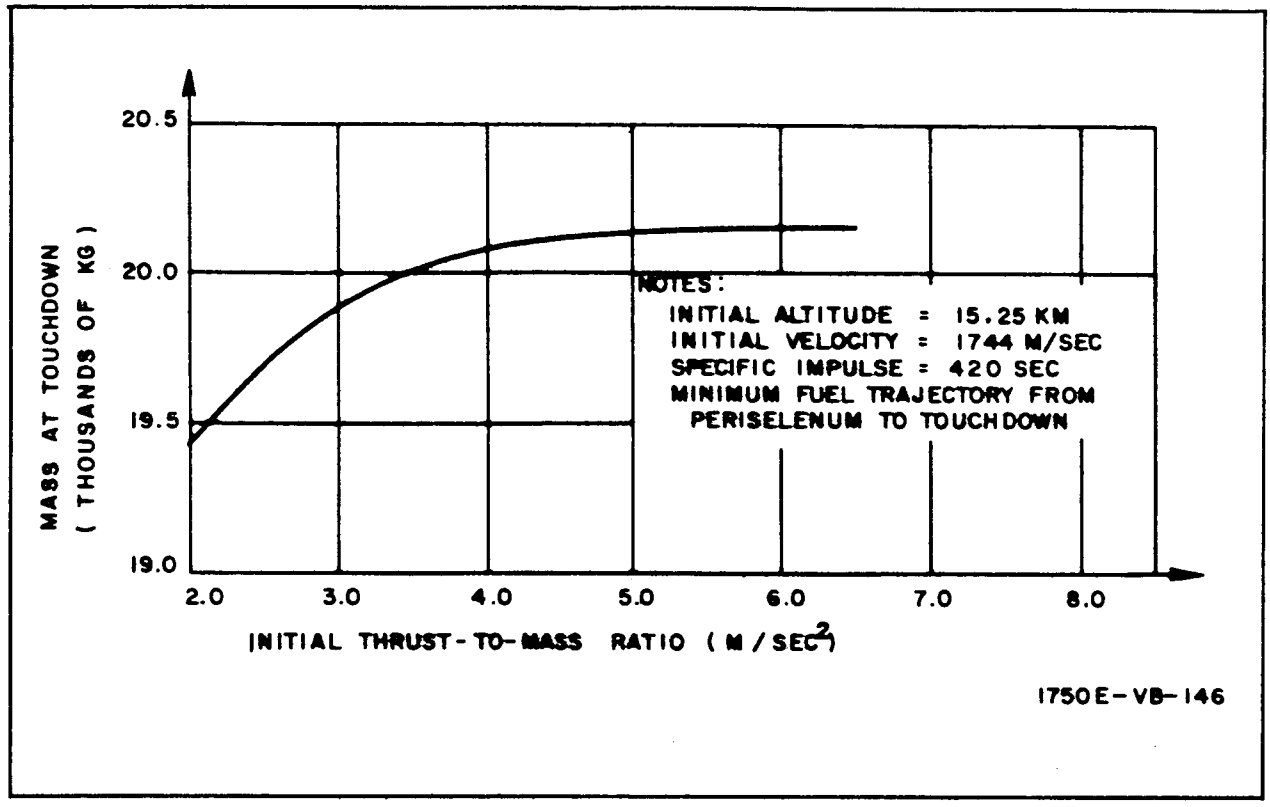

Figure 33. Touchdown Mass vs Initial Thrust-to-Mass Ratio

configuration over the 2 RL-10 engine configuration $(T/m)_o$ = 4.30 meters per second per second at periselenum of 28.0 kilometers) is 162 kg. This landed weight advantage is achieved by employing an additional RL-10 engine which has the following weight breakdown:

		Kilograms	Pounds
Engine weight	=	136.5	300
Mounting Structure	=	13.6	30
Fuel Lines, etc.	=	4.6	10
Total		154.7	340

This tradeoff indicates that three RL-10 engines, $(T/m)_o$ = 6.45 meters per second per second should be used in preference to two. The minute (7-kilogram) payload weight increase obtained with the use of 3 RL-10

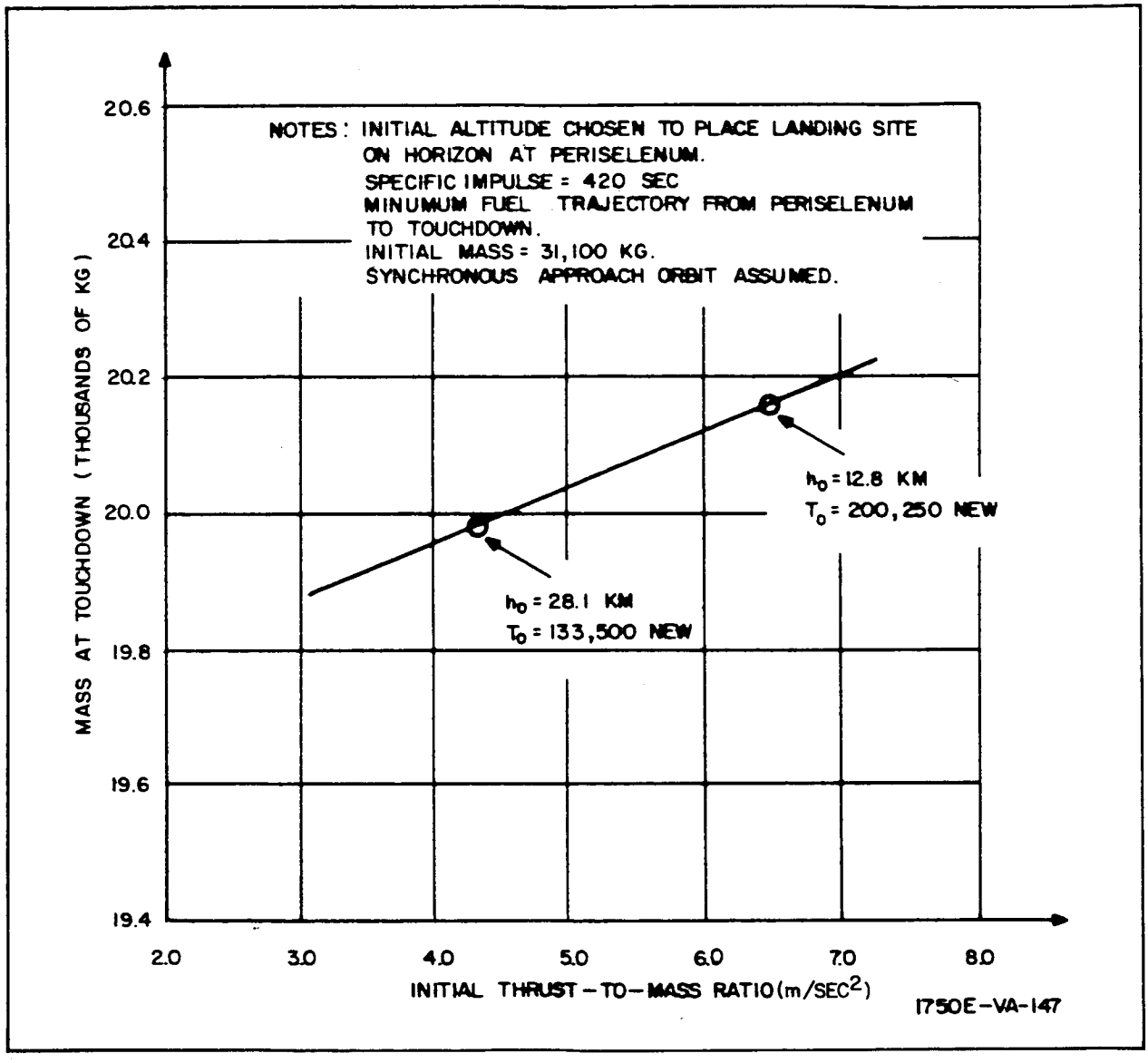

Figure 34. Touchdown Mass vs Initial Thrust-to-Mass Ratio

engines also suggests that a payload weight penalty will occur if a three-engine and a four-engine configuration are compared.[7/] Consequently, the selection of a three-engine configuration cannot be made solely upon net payload performance, particularly here where the net additional payload is for all practical purposes negligible.

A much stronger consideration, which does not involve the tradeoff relationships developed in figures 28 through 34, is the relative reliability of the use of two or three engines. Since the mission profile requires the vehicle to perform a soft pinpoint landing at a preselected site, the failure of one engine to operate properly is likely to result in mission failure since all engines must be capable of developing maximum thrust to achieve the touchdown requirements. Since the reliability factor, (reliability of one engine)^N where N = number of engines, decreases as the number of individual components increases, the two-engine configuration is selected, providing a $(T/m)_o$ = 4.30 meters per second per second.

This choice of $(T/m)_o$ automatically determines the lower bound on periselenum altitude. To provide a safety margin for altitude errors at periselenum and to provide flexibility in landing in an 18-to-27-kilometer radius around a beacon located on the horizon at periselenum, minimum periselenum altitude is to be 33.6 kilometers. This additional altitude will result in a net payload mass penalty of approximately 36 kilograms.

In the event that "engine out" capability is desired, the most feasible method for providing it seems to be to provide a third engine on the spacecraft and maintain the thrust level required to achieve the soft touchdown pinpoint landing at 133,500 newtons ($(T/m)_o$ = 4.30 meters per second per second) as previously chosen.

3.3.4 Selection of Guidance Technique

The determination of fuel specific impulse (I_{sp}) thrust level and periselenum altitude has been based upon minimum fuel landing trajectories. The pitch angle program guidance technique required to obtain the minimum fuel

---

[7/] This conclusion is supported by the very flat shape of figure 33 at $(T/m)_o$ is increased (e.g., no increase in landed mass as $(T/m)_o$ is increased and periselenum altitude is held constant) and by the fact that the minimum periselenum altitude constraint will not allow any increase in landed mass by the four-engine configuration, which ideally can be obtained with a decrease in periselenum altitude.

trajectory is basically open loop in nature and does not lend itself easily to mechanization as a closed loop type of system capable of achieving a soft pinpoint landing at a preselected landing site. This section is directed toward the selection of a closed loop guidance technique which efficiently performs the landing maneuver in terms of fuel management and also yields a soft pinpoint landing at a preselected landing site.

Table 4 presents a fuel management comparison of two basic guidance techniques that are available; namely the modified proportional navigation system (MPN) and the programmed pitch angle system (OPT) which yields the optimum fuel trajectory (as derived in Section 1). The optimum fuel trajectory results (OPT) provide a basis to evaluate the performance of the MPN as well as to establish whether or not a requirement might exist, in view of fuel management considerations, to mechanize the programmed pitch angle system. The periselenum conditions arise from the use of a synchronous transfer ellipse. Two periselenum altitudes, 15.25 and 38.1 kilometers are used to provide comprehensive comparison of the relative performance of the guidance techniques. In all cases I_{sp}=420 seconds and a periselenum mass of 31,100 kilograms are used.

The performance results of the programmed pitch angle optimum fuel trajectory, MPN with 133,500-newton (30,000-lb) thrust limit, and MPN without thrust limiting for a periselenum altitude of 38.1 kilometers indicate that the MPN system with a 133,500 thrust limit out-performs MPN without thrust limiting by ΔV = 8 meters per second. It is important to note that imposing a thrust level constraint on the MPN system improves fuel performance. This result is particularly noteworthy in view of the fact that a 133,500-newton thrust limit will physically exist with the mission profile and system configuration chosen in previous sections.

The MPN minimum fuel trajectory with a 133,500-newton thrust limit and MPN without thrust limiting are compared in table 4 for a periselenum altitude of 15.25 kilometers. The MPN systems are also compared to the programmed pitch angle optimum fuel trajectory which corresponds to a thrust level of 133,500 newtons. The MPN system with the 133,500-newton thrust limit requires ΔV = 3 meters per second more fuel than the optimum fuel trajectory.

The values of guidance parameters S and K used in table 4 are determined by the procedure described in the following paragraphs.

TABLE 4

COMPARISON OF GUIDANCE SYSTEM PERFORMANCE

I_{SP} = 420 sec, periselenum mass = 31,100 (kg)					
Periselenum Altitude (km)	Periselenum Velocity (m.sec)	Downrange Distance to Landing Point (km)[a]	Max Thrust Available (newtons)	Guidance Law	Fuel Usage, ΔV m/sec
15.25	1744	311.5	133,500	Programmed Pitch Angle (OPT)[b]	1806
			13,500	Modified proportional navigation (MPN), S=1.5, K=2	1809
			No limit		1818
38.1	1723	308.8	133,500	Programmed Pitch Angle (OPT)[b]	1851
			133,500	Modified proportional navigation (MPN), S=1.5, K=2	1860
		312.7	No limit		1868
			133,500	Modified proportional navigation, (MPN), S=3.0, K=2	1884
			No limit		1925

[a] Downrange distance from periselenum (where thrust is initiated) to the landing point

[b] Optimum trajectory described in Section 1

Reference to figure 5 in subsection 1.3 shows that line-of-sight angular rotation rate is nearly constant for this class of optimized trajectories. This suggests that the MPN guidance parameters should be selected to yield a guidance law which causes the spacecraft to fly an essentially constant line-of-sight rate trajectory. Investigation reveals that MPN is well suited to this approach. First change equation 4-5 of Volume III to read

$$\hat{a}_{\Omega} = (S + \frac{K-1}{K}) \hat{R} (\hat{\Omega} - \dot{\Omega}_b) + \frac{\mu}{r_c^2} \sin \hat{\Omega}$$

where $\dot{\Omega}_b$ is a bias value of LOS rotation rate. This guidance law tends to hold $\dot{\Omega}$ equal to $\dot{\Omega}_b$.

Kriegsman and Reiss show that the time history of $\dot{\Omega}$ in a free space or perfect gravity compensation environment can be expressed by

$$\dot{\Omega} = V_o \sin (\psi_o / R_o) (1 - t/t_f)^{\left[K (S-1) - 1\right]}$$

where V_o = initial velocity magnitude

ψ_o = initial angle between the LOS and the velocity vector

R_o = initial range to the landing site

t = time after landing initiation

t_f = nominal flight time = $K (R_o \psi_o)/(V_o \sin \psi_o)$

S and K = guidance parameters

One can see that setting $K (S-1) - 1 = 0$
produces a constant $\dot{\Omega}$ trajectory. In addition, a particular value of K corresponds to constant acceleration along the line-of-sight, which corresponds roughly to the maximum thrust requirement for the minimum fuel trajectory. Selecting this value of K, which is 2, requires that S be 1.5 to satisfy the above equation.

It is found by digital simulation that the above values of S and K produce a trajectory very similar to the optimum trajectory derived in Section 1.

Spacecraft landing trajectories from a 38.1-km periselenum altitude to touchdown are shown in figure 35 for each of the guidance systems.

Notice that the optimum fuel trajectory and the trajectory corresponding to MPN with thrust limiting are practically identical, indicating the basic reason why the fuel expenditures for these two trajectories are substantially identical. From a fuel standpoint MPN with thrust limiting outperforms MPN without thrust limiting because with thrust limiting deceleration during the initial portion of the trajectory is somewhat less than the commanded deceleration, thereby reducing the total time to reach the landing site with an attendant reduction of the total time during which the effect of lunar gravity must be counteracted.

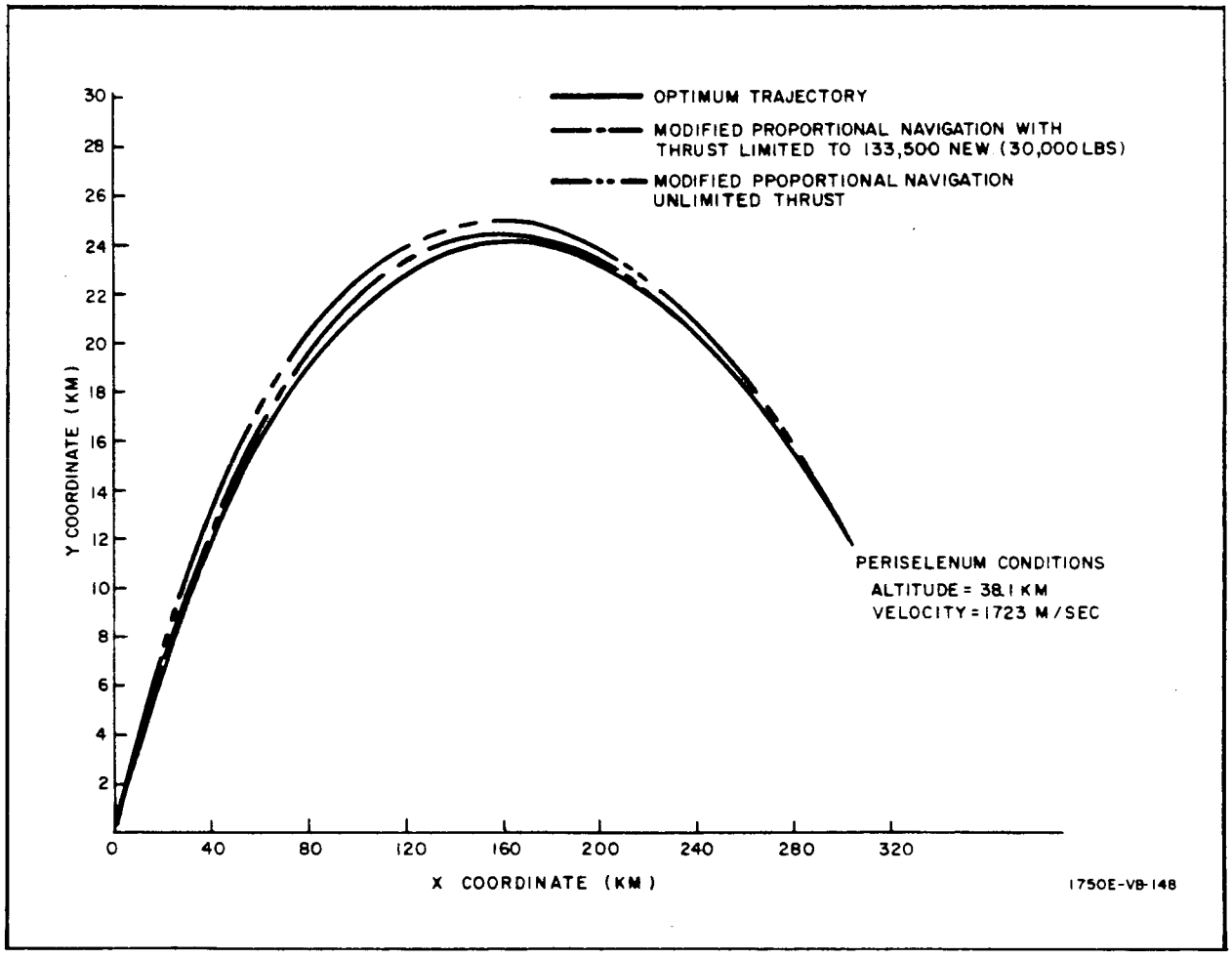

Figure 35. Comparison of Modified Proportional Navigation Trajectories with a Minimum Fuel Trajectory

Figure 36 provides further substantiation of the remarkable similarity of the optimum fuel trajectory and the trajectory corresponding to the MPN guidance law with thrust limiting. Comparisons of range and range rate to the landing site as functions of time are shown for both trajectories.

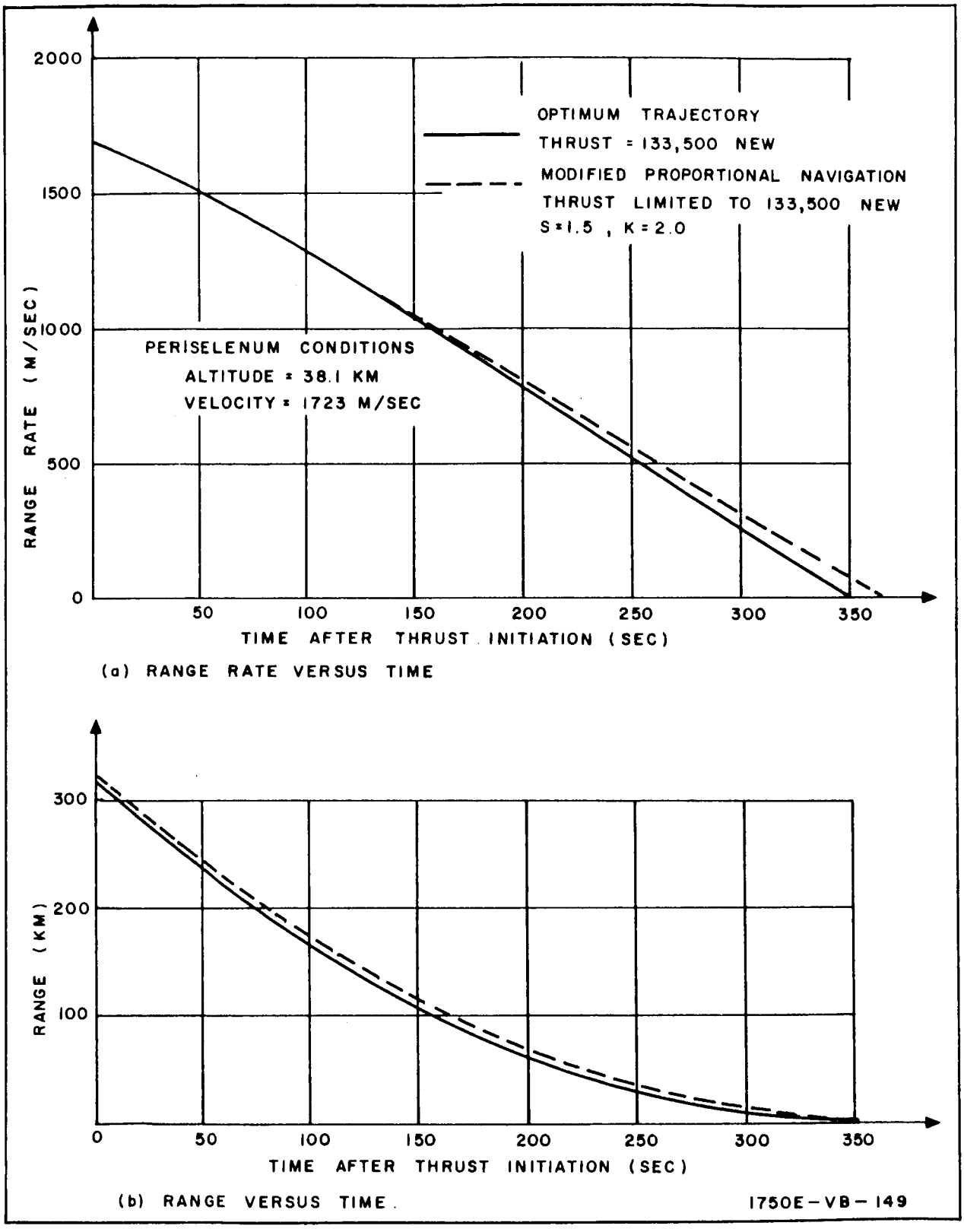

Figure 36. Comparison of Thrust-Limited Modified Proportional Navigation Trajectory with an Optimum Trajectory

The effects of MPN/VT guidance system gain constants upon touchdown velocity, and attendant fuel penalty as well as the effect of MPN/VT switch-over point along the nominal MPN trajectory upon touchdown velocity and attendant fuel penalty are summarized in table 5. The fuel penalty term used here refers to the increase in fuel usage, in terms of ΔV, incurred by the use of MPN/VT to obtain the vertical touchdown with respect to the fuel usage of the MPN system with thrust limiting. Total fuel expenditure for performing the landing maneuver can be computed by summing the total fuel required to perform the landing via MPN with thrust limiting and the fuel penalty associated with the use of the MPN/VT system.

The basic guidance method utilizing the combined MPN and MPN/VT control scheme is described in detail in paragraph 4.3.2.1.C of Volume III. Two techniques are considered, MPN/VT-A and MPN/VT-B. MPN/VT-A involves switching from MPN to MPN/VT when the spacecraft range rate to the landing site is reduced to 305 meters per second while MPN/VT-B involves switching from MPN to MPN/VT when the spacecraft range to a fictitious hover point is reduced to 305 meters. Fuel penalties and touchdown conditions for both these methods are given in table 5. The MPN/VT-B technique uses less fuel and is capable of achieving nearly zero touchdown velocities for suitable choices of the gain constants S_1, S_2, and K_1. Another important aspect of the MPN/VT-B trajectory is that the spacecraft velocity vector is essentially vertical at touchdown.

A comparison of trajectories during the final phase of landing is illustrated in figure 37. The optimum fuel trajectory and trajectories for MPN/VT-B and MPN with thrust limiting are shown. Note that both the optimum fuel trajectory and the MPN trajectory arrive at the landing point with the spacecraft velocity vector approximately 25 degrees to the horizontal while the MPN/VT-B trajectory arrives nearly vertically.

While the significant performance index during the landing phase will be fuel management, system performance will be judged on both fuel performance and touchdown conditions during the final phase. Because of structural and landing gear considerations, the spacecraft's velocity vector is required to be vertical, thereby implying a nearly vertical spacecraft attitude at the touchdown point. This requirement will limit the choice of guidance techniques to MPN/VT-A and MPN/VT-B.

Table 4 and figures 35 and 36 indicate that the MPN with thrust-limiting guidance technique is the logical choice for performing the landing maneuver

TABLE 5

COMPARISON OF TERMINAL PHASE
(maximum thrust available = 133,500 newtons)

Control Law	Guidance Concept	K_1	S_1[a]	S_2	Fuel Penalty[b] $[\Delta V]$ (m/sec)	Interface Range (km)	Interface Range Rate (m/sec)	Terminal Conditions			
								X (m)	$\dot{X}$ (m/sec)	Y (m)	$\dot{Y}$ (m/sec)
MPN/VT	MPN/VT-A[c]	2	3.1	0.8	Crashes	10.15	-312	-207	-36.6	-38.7	-102
MPN/VT	MPN/VT-A	2	3.1	0.8	Crashes	10.15	-312	-55.7	-17.7	+64.3	-82.9
MPN/VT	MPN/VT-A	2.5	3.1	0.8	52	10.15	-312	0	0	0	0
MPN	-	6.0	2.0	0.0	0	10.15	-312	0	0	0	0
MPN/VT	MPN/VT-B[e]	2.0	3.1	0.8	Crashes	0.496	-43.5	0	-0.27	1.11	-8.05
MPN/VT	MPN/VT-B	2.5	3.1	0.8	8.2	0.496	-43.5	0	0	0	0.38
MPN/VT[d]	MPN/VT-B	2.5	3.1	0.8	20.1	0.496	-43.5	0	0	0	0
MPN/VT	MPN/VT-B	3.0	3.1	0.8	9.1	0.496	-43.5	0	0	0	0
MPN	-	2.0	2.0	0.0	0	0.496	-43.5	0	0	0	0

[a] $S_1 = 2.0$, $S_2 = 0$ Corresponds to S = 1.5 for MPN guidance.

[b] Fuel Penalty with respect to the MPN trajectory; S = 1.5, K = 2, with thrust limiting

[c] Guidance concept MPN/VT-A indicates MPN/VT guidance initiated at the indicated interface range and range rate. No fictitious landing point is used.

[d] Gravity Compensation included; all other cases except the two using MPN control law are without gravity compensation.

[e] Guidance method MPN/VT-B indicates MPN/VT guidance initiated at the indicated interface range and range rate. This occurs when the range to the fictitious landing point is 305 meters (1000 ft).

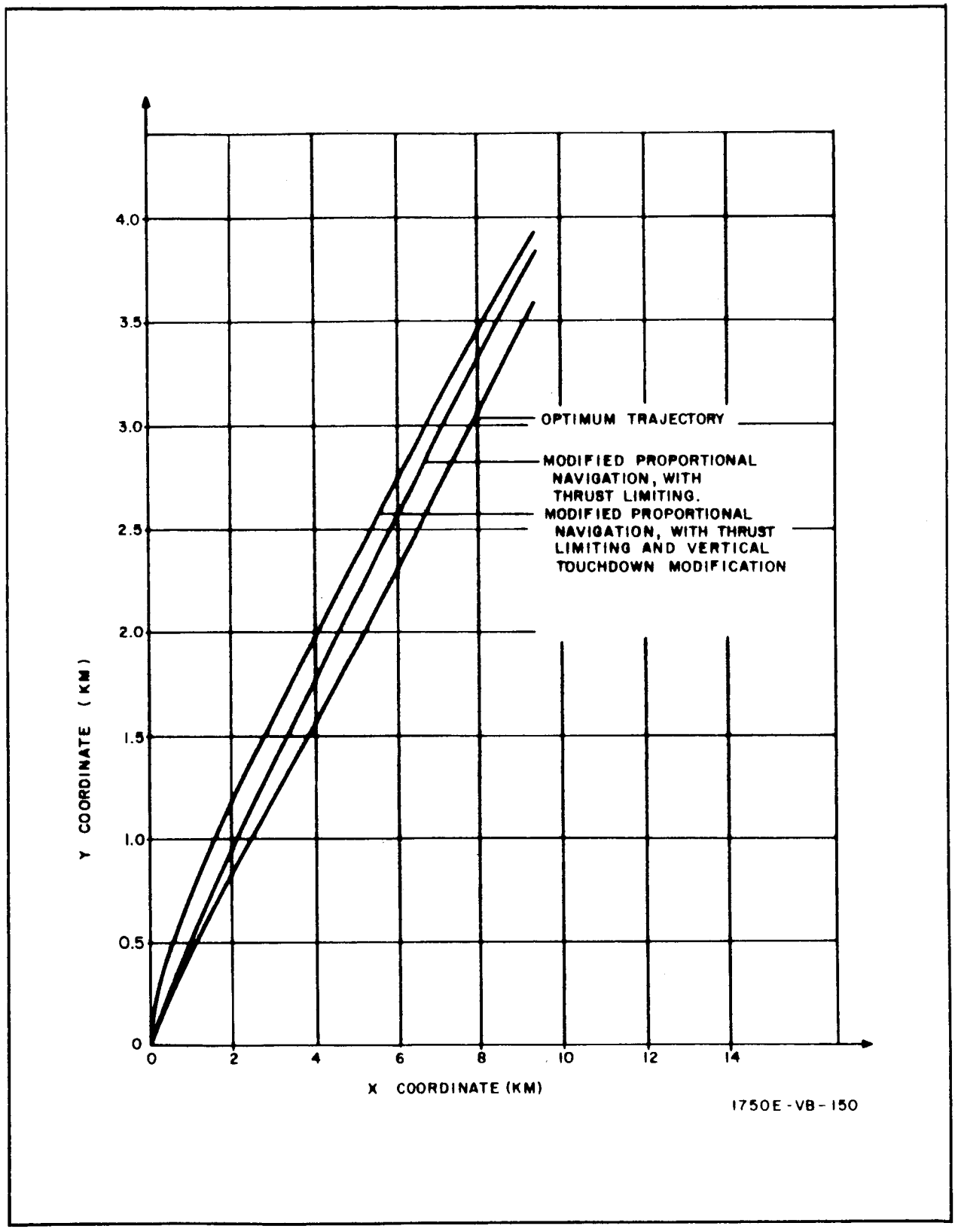

Figure 37. Comparison of Trajectories During Final Portion of the Landing Maneuver

from a periselenum of 38.1 kilometers. This guidance technique incurs a small fuel penalty of approximately 9 meters per second compared to an optimum fuel trajectory but exhibits the following significant advantages over the optimum fuel trajectory:

a. MPN is a closed-loop guidance scheme.

b. MPN is simple to mechanize.

c. A vertical touchdown can be achieved by using MPN during the major portion of the landing maneuver and switching to MPN/VT for the final phase.

Since acceptable touchdown conditions can be achieved with both MPN/VT-A and MPN/VT-B, the latter is selected because of the overall fuel advantage indicated in table 5. Table 5 also indicates that the selection of $S_1 = 3.1$, $S_2 = 0.8$, $K_1 = 3.0$ and no gravity compensation leads to excellent touchdown conditions and a relatively small fuel penalty. A smaller fuel penalty can be obtained by accepting a larger terminal condition departure from zero horizontal and vertical velocity, but the attendant value of $K_1 = 2$ will increase system sensitivity to bias and random errors. This final selection of guidance technique indicates a total fuel penalty of 18.1 mps in comparison with the optimum fuel trajectory.

3.4 Lunar Landing Sensor Error Digital Program

This subsection develops the adjoint system for lunar landing which employs the modified proportional navigation/vertical touchdown guidance law. The nonlinear equations of motion and control expressed in a polar coordinate frame are linearized and restricted here to two dimensions. The resultant adjoint equations are solved by the lunar landing sensor error program (LLSE) to obtain the influence coefficients which relate sensor bias and random (fluctuation) errors to touchdown condition errors. These influence coefficients correspond to partial derivatives of the terminal conditions with respect to sensor bias and random error inputs along the landing trajectory wherein the partials are evaluated at the nominal terminal time.

This subsection is divided into four paragraphs: the linearization of the kinematic and control equations, the development of the adjoint model, the definition of the nominal trajectory, and a brief discussion of the application of the LLSE program.

3.4.1 Linearization of Kinematics and Control Equations

To apply the method of adjoint systems, the equations of motion and control must be linearized. The moon is assumed to be a homogeneous, spherical, nonrotating body, and the spacecraft is assumed to be operating in an ideal central force field. All equations are expressed in terms of polar coordinates centered at the landing site and in the plane of motion as shown in figure 21.

$$\ddot{\underline{r}}\Big|_I = \ddot{\underline{R}}\Big|_I = \frac{\underline{F}(t)}{m} + \underline{F}_g \tag{67}$$

where

$\underline{F}(t)$ = force applied to the spacecraft

$\left|\underline{F}_g\right|$ = gravitational force = $\frac{\mu}{r^2}$

$\underline{R}$ = vector range from landing point to spacecraft

$\underline{r}$ = radius vector from the center of the moon to the spacecraft

m = instantaneous mass of spacecraft

$(\dot{})_I$ = derivative of ( ) taken with respect to an inertial coordinate frame

μ = lunar gravitational constant

In terms of the polar coordinate frame,

$$\ddot{\underline{R}}\Big|_I = \underline{i}_R (\ddot{R} - R\dot{\Omega}^2) + \underline{i}_\Omega (R\ddot{\Omega} + 2\dot{R}\dot{\Omega}) \tag{68}$$

where $\ddot{\underline{R}}\Big|_I$ is $\frac{d^2(\underline{R})}{dt^2}$ with respect to inertial coordinates. Also,

$$\frac{\underline{F}(t)}{m} = a_R \underline{i}_R + a_\Omega \underline{i}_\Omega \tag{69}$$

where

a_R = spacecraft acceleration along $\underline{R}$

a_Ω = spacecraft acceleration normal to $\underline{R}$

$\underline{i}_R$ = unit vector along $\underline{R}$

$\underline{i}_\Omega$ = unit vector normal to $\underline{R}$

The gravity force vector $\underline{F}_g$ can be expressed as

$$\underline{F}_g = \underline{i}_R \left| \underline{F}_g \right| \cos(\Omega - \theta) + \underline{i}_\Omega \left| \underline{F}_g \right| \sin(\Omega - \theta) \tag{70}$$

Hence, the equations of motion can be written in scalar form:

$$a_R - F_g \cos(\Omega - \theta) = \ddot{R} - R\dot{\Omega}^2 \tag{71}$$

$$a_\Omega + F_g \sin(\Omega - \theta) = R\ddot{\Omega} \quad 2\dot{R}\dot{\Omega}$$

where

$$F_g = \left| \underline{F}_g \right|$$

Linearization of equation 71 yields

$$\begin{aligned} \delta \ddot{R} &= \delta a_R + F_g \left[-\sin(\Omega - \theta)\delta\theta + \sin(\Omega - \theta)\,\delta\Omega \right] \\ &\quad + \dot{\Omega}^2 \delta R + 2R\,\dot{\Omega}\,\delta\dot{\Omega} \end{aligned} \tag{72}$$

$$\begin{aligned} \delta\ddot{\Omega} &= \frac{1}{R}\left\{ \delta a_R + F_g \left[-\cos(\Omega - \theta)\delta\theta + \cos(\Omega - \theta)\,\delta\Omega \right] \right. \\ &\quad \left. -\ddot{\Omega}\delta R - 2\dot{\Omega}\delta\dot{R} - 2\dot{R}\delta\dot{\Omega} \right\} \end{aligned}$$

where the operator $\delta(\ )$ denotes a deviation of the bracketed/quantity from the nominal value. Equation 72 is a linear, variable-coefficient differential equation. The variable coefficients of the deviations are evaluated using the nominal solution to the original nonlinear differential equation. Approximate closed-form solutions to the nonlinear differential equations, obtained in subsection 3.3 of this appendix and in Appendix D of Volume IV, are listed in paragraph 3.4.3 for reference.

Neglecting the term $\delta\theta$, the linearized equations of motion become

$$\begin{aligned} \delta \ddot{R} &= \delta a_R + F_g \sin(\Omega - \theta)\,\delta\Omega + \dot{\Omega}^2 \delta R + 2R\dot{\Omega}\,\delta\dot{\Omega} \\ \delta\ddot{\Omega} &= \frac{1}{R}\left\{ \delta a_\Omega + F_g \cos(\Omega - \theta)\,\delta\Omega - \ddot{\Omega}\delta R - 2\dot{\Omega}\,\delta\dot{R} - 2\dot{R}\,\delta\dot{\Omega} \right\} \end{aligned} \tag{73}$$

Next, the control equations are linearized to obtain linear expressions for δa_R and δa_Ω. The nonlinear equation used to control range rate as a function of range is

$$a_R = \frac{K_1 - 1}{K_1} \left[\frac{\dot{R}^2 - \dot{R}_b^2}{R - R_b} \right] \tag{74}$$

Linearization of this expression yields

$$\delta a_R = \frac{\partial a_R}{\partial R} \delta R + \frac{\partial a_R}{\partial \dot{R}} \delta \dot{R} \tag{75}$$

where

$$\frac{\partial a_R}{\partial R} = - \frac{K_1 - 1}{K_1} \left[\frac{\dot{R}^2 - \dot{R}_b^2}{(R - R_b)^2} \right]$$

$$\frac{\partial a_R}{\partial \dot{R}} = \frac{2(K_1 - 1)}{K_1} \frac{\dot{R}}{(R - R_b)}$$

The nonlinear expression used to control normal acceleration in the MPN/VT guidance mode is

$$a_\Omega = S_1 \dot{R} \dot{\Omega} - S_2 \frac{\dot{R}^2}{R} \Omega \tag{76}$$

Linearization of equation 76 yields

$$\delta a_\Omega = \frac{\partial a_\Omega}{\partial R} \delta R + \frac{\partial a_\Omega}{\partial \dot{R}} \delta \dot{R} + \frac{\partial a_\Omega}{\partial \Omega} \delta \Omega + \frac{\partial a_\Omega}{\partial \dot{\Omega}} \delta \dot{\Omega} \tag{77}$$

where

$$\frac{\partial a_\Omega}{\partial R} = S_2 \left(\frac{\dot{R}^2}{R^2} \right) \Omega$$

$$\frac{\partial a_\Omega}{\partial \dot{R}} = S_1 \dot{\Omega} - 2 S_2 \frac{\dot{R}}{R} \Omega$$

$$\frac{\partial a_\Omega}{\partial \Omega} = - S_2 \frac{\dot{R}^2}{R}$$

$$\frac{\partial a_\Omega}{\partial \dot{\Omega}} = S_1 \dot{R}$$

The partial derivatives indicated in equations 75 and 77 are evaluated on the nominal solution of the nonlinear equations of motion.

3.4.2 Adjoint Model

The method of adjoint error analysis used is described in detail in subsection 6.2 of Appendix A of this volume. In essence the adjoint set of equations provides the capability to estimate the effects of bias and random errors occurring throughout the lunar landing trajectory on terminal conditions without resorting to Monte Carlo techniques. Prior experience indicates that the terminal error is seriously affected only by sensor errors occurring in the final portion of the landing maneuver. Therefore the adjoint error analysis is applied only to that portion of the landing using the MPN/VT guidance law.

Mathematically a linear first-order matrix differential equation

$$\dot{\underline{x}}(t) = \left[A(t)\right] \underline{x}(t) \; ; \; \underline{x}(o) = \underline{x}_o \tag{78}$$

has a corresponding linear first-order matrix differential equation which is adjoint to the original set, given by

$$\left[\dot{\Lambda}(t)\right] = - \left[A(t)\right]^T \left[\Lambda(t)\right] \; ; \left[\Lambda(t_f)\right] = \left[\Lambda_f\right] \tag{79}$$

where both $\left[\Lambda(t)\right]$ and $\left[A(t)\right]$ are matrices. By using normalized final conditions for the adjoint equations, $\left[\Lambda_f\right] = \left[I\right]$, the solution of equation 79 yields information that can be used to calculate sensitivity coefficients which relate sensor errors to the resulting terminal deviations.

Figure 38 illustrates the adjoint equations in block diagram form. (The relationship between the adjoint system block diagram and the block diagram of the linearized actual system is given by Laning and Battin. [8] In addition to the linearized kinematics and control equations, second order filters are

[8] J.H. Laning and R.H. Battin, Random Processes in Automatic Control, New York, McGraw-Hill Book Company, 1956.

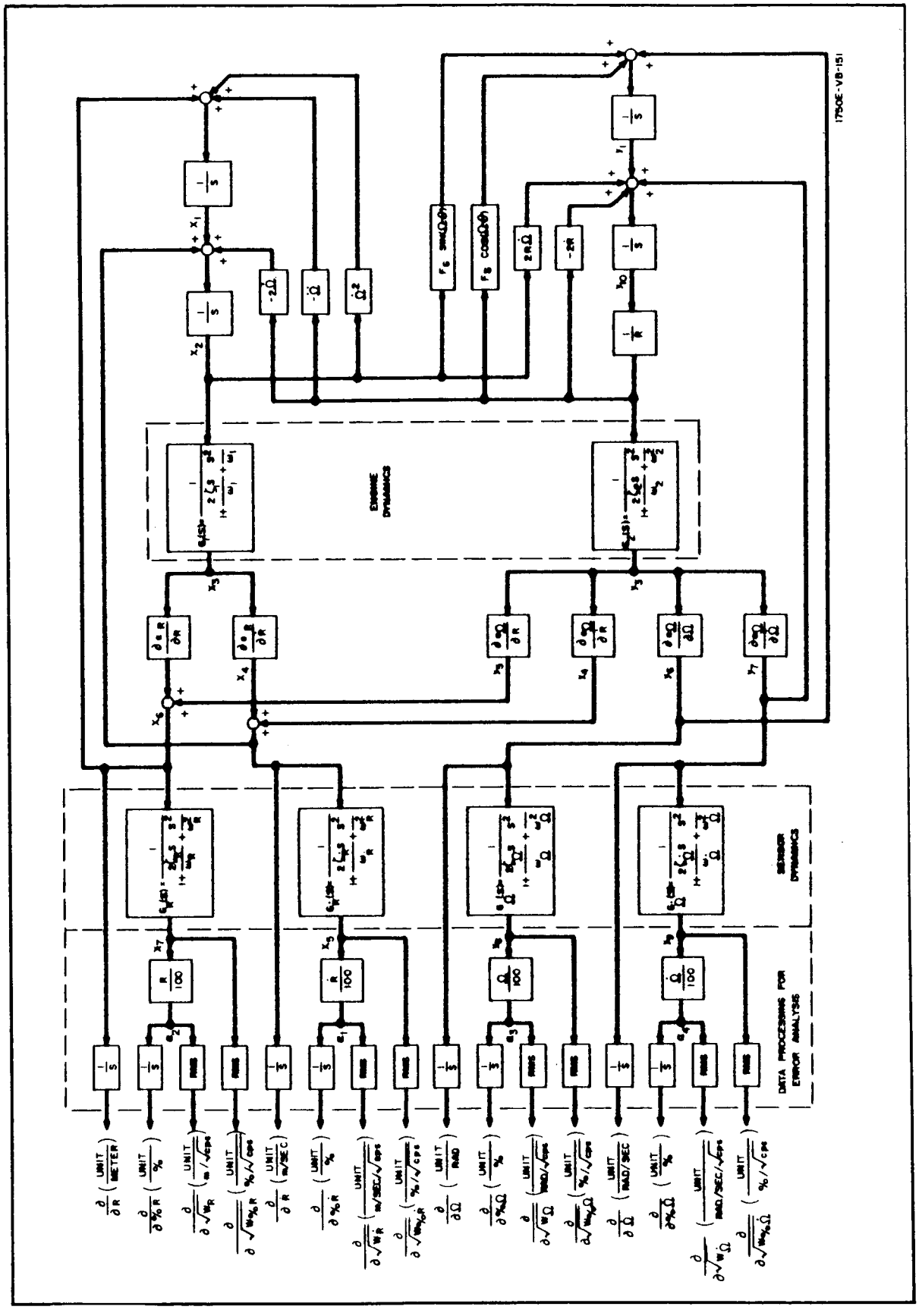

Figure 38. Adjoint System Block Diagram

included to represent lateral and longitudinal engine responses as well as sensor dynamics. The figure also includes data processing blocks added to the adjoint system for the purpose of determining error sensitivity coefficients.

Note that the adjoint method of error analysis is subject to the principle of linearization. Consequently, the results of the analysis are applicable only when small departures from the nominal solution to the nonlinear equations are considered.

3.4.3 Nominal Solution

Nominal solutions to the nonlinear differential equations are developed in closed form in subsection 3.3 of this appendix and in Appendix D of Volume IV. These closed form solutions, used to evaluate the time-varying coefficients of the linearized equations, are given below for reference.

$$R = \begin{cases} R_b - \dot{R}_b \tau \; ; \; o \le \tau \le \tau_1 \\ \\ R_b + (R_o - R_b) \left[1 + \dfrac{\dot{R}_o (t_f - \tau)}{K (R_o - R_b)} \right]^K \; ; \; \tau_1 \le \tau \le t_f \end{cases} \tag{80}$$

$$\tau = t_f - t \tag{81}$$

$$\dot{R} = -\left\{ \dot{R}_b^{\,2} + (\dot{R}_o^{\,2} - \dot{R}_b^{\,2}) \left[\frac{R - R_b}{R_o - R_b} \right]^{\frac{2(K-1)}{K}} \right\}^{1/2} \tag{82}$$

$$t_f = \frac{K (R_o - R_b)}{-\dot{R}_o} \left\{ 1 - \left[\frac{\dot{R}_b^{\,2}}{R_o^{\,2} - \dot{R}_b^{\,2}} \right]^{\frac{1}{2(K-1)}} \right\} + \tau_1 \tag{83}$$

$$\tau_1 = - \frac{R_o - R_b}{\dot{R}_b} \left[\frac{\dot{R}_b^{\,2}}{\dot{R}_o - \dot{R}_b^{\,2}} \right]^{\frac{K}{2(K-1)}} \tag{84}$$

$$\Omega = \frac{C_1 \tau^{a_1}}{t_f^{a_1}} + \frac{C_2 \tau^{a_2}}{t_f^{a_2}} \tag{85}$$

$$\dot{\Omega} = \frac{d\ \Omega}{dt} \tag{86}$$

$$\ddot{\Omega} = \frac{d\ (\dot{\Omega})}{dt} \tag{87}$$

$$a_1 = \frac{K\ (S_1 - 1)}{2} \left\{ 1 + \left[1 - \frac{4S_2}{(S_1 - 1)^2} \right]^{1/2} \right\} \tag{88}$$

$$a_2 = \frac{K\ (S_1 - 1)}{2} \left\{ 1 - \left[1 - \frac{4S_2}{(S_1 - 1)^2} \right]^{1/2} \right\} \tag{89}$$

$$C_1 = \frac{t_f}{a_2 - a_1} \left[\dot{\Omega}_o + \frac{a_2 \Omega_o}{t_f} \right] \tag{90}$$

$$C_2 = \frac{t_f}{a_1 - a_2} \left[\dot{\Omega}_o + \frac{a_1 \Omega_o}{t_f} \right] \tag{91}$$

3.4.4 Method of Application

To recapitulate, the adjoint method of analysis, and specifically the LLSE program, yields the influence coefficients which relate touchdown error to sensor bias and random (fluctuation) errors which occur throughout the entire nominal trajectory. These influence coefficients represent partial derivatives of the various touchdown quantities, namely R, $\dot{R}$, Ω, and $\dot{\Omega}$, with respect to the numerous sensor measurement error quantities, and scale factor, or percentage errors in these quantities. These partials are in effect evaluated at the nominal touchdown time and therefore represent the value of the partials evaluated at a fixed time. This accounts for the appearance of influence coefficients for all touchdown quantities.

The validity of the results is subject to the accuracy with which the non-linear differential equations can be represented by variable coefficient linear

differential equations linearized for small departures about a nominal solution (trajectory).

Although the adjoint program has been written specifically for MPN/VT, the program can be used to obtain results for the MPN system by properly adjusting the nominal solution.

Previous sections of this appendix have developed the adjoint system and given the nominal trajectory solutions about which the adjoint equations are linearized. Next, the initial conditions placed upon the adjoint system and outputs of the adjoint system are discussed.

Initial conditions for the adjoint equations are determined by the output errors of interest. In the lunar landing problem we are interested in the position and velocity errors at the terminal point. In the polar coordinate system used, the errors are specified by departures from the nominal touchdown conditions in position R, Ω, and velocity, $\dot{R}$, $\dot{\Omega}$. Hence the initial conditions applied to the adjoint equations are unit initial conditions on the variables x_1, x_2, y_1, and y_{10} shown in figure 38. The unit initial conditions are applied individually (one at a time); the initial condition on x_1 generating R (range) error sensitivity coefficients, $x_2(0) = 1$ giving $\dot{R}$ error coefficients, $y_1(0) = 1$ giving Ω angular error coefficients, and $y_{10}(0) = 1$ giving $\dot{\Omega}$ error sensitivity coefficients.

The various output quantities shown in figure 38 are the result of postulating certain types of sensor output errors. The 16 sensor errors postulated are listed below.

a. Bias errors

(1) Constant range bias	m_R
(2) Range scale factor error	SF_R
(3) Constant range rate bias	$m_{\dot{R}}$
(4) Range rate scale factor error	$SF_{\dot{R}}$
(5) Constant angle bias	m_Ω
(6) Angle scale factor error	SF_Ω
(7) Constant angle rate bias	$m_{\dot{\Omega}}$
(8) Angle rate scale factor error	$SF_{\dot{\Omega}}$

b. Random (fluctuation) errors

(1) Fixed level range error $\sqrt{W_R}$

(2) A percentage of range error $\sqrt{W_{PR}}$

(3) Fixed level range rate error $\sqrt{W_{\dot{R}}}$

(4) A percentage of range rate error $\sqrt{W_{P\dot{R}}}$

(5) Fixed level angle error $\sqrt{W_{\Omega}}$

(6) A percentage of angle error $\sqrt{W_{P\Omega}}$

(7) Fixed angle rate error $\sqrt{W_{\dot{\Omega}}}$

(8) A percentage of angle rate error $\sqrt{W_{P\dot{\Omega}}}$

W refers to the spectral density of the noise in the sensor indicated by the accompanying subscript.

Thus the adjoint system provides 64 influence coefficients (4 output errors for 16 types of input errors) which are used in determining the allowable magnitude of sensor errors to meet a certain tolerable set of output errors. The influence coefficients are printed out in two 4 x 8 matrices, one matrix for bias errors, one matrix for random errors.

APPENDIX E

LUNAR ASCENT

1. ERROR EQUATIONS FOR GUIDANCE SYSTEM

The error equations are mathematical formulations which represent the accelerometer, gyro, and platform errors as functions of the thrust accelerations and error coefficients. The basic method with slight modifications is taken directly from Pitman (Ref. 1).

The error equation for the accelerometer is:

$$\Delta A_i = a_{0i} + a_{1i}A_i + a_{2i}A_i^2 + a_{3i}A_i^3 + a_{4i}A_j + a_{5i}A_jA_i + a_{6i}A_k + a_{7i}A_kA_i \quad (1)$$

where

ΔA = the component of acceleration error,

a_{0i} = a bias term,

a_{1i} = a linear scale factor error,

a_{2i}, a_{3i} = a nonlinear coefficient,

a_{4i}, a_{5i} = cross-axis bias,

a_{6i}, a_{7i} = cross-axis scale factor,

i = input axis,

A_i, A_j, A_k = components of thrust acceleration,

i, j, k, take on cyclical permutations of x, y, z.

Ref. 1: Pitman, G. R. (Editor), Inertial Guidance, John Wiley and Sons, Inc., 1962.

The components of velocity and position are

$$\Delta V_i = \int_0^t \Delta A_i \, dt, \tag{2}$$

and

$$\Delta S_i = \int_0^t \Delta V_i \, dt: \tag{3}$$

Along the x-axis, the values of ΔV_x are:

$$\Delta V_x = a_{0x} t + a_{1x} \int_0^t A_x dt + a_{2x} \int_0^t A_x^2 \, dt + a_{3x} \int_0^t A_x^3 \, dt + a_{4x} \int_0^t A_y \, dt$$
$$+ a_{5x} \int_0^t A_y A_x \, dt + a_{6x} \int_0^t A_z \, dt + a_{7x} \int_0^t A_z A_x \, dt. \tag{4}$$

In a similar manner, ΔV_y and ΔV_z are obtained. The values of ΔS_x, ΔS_y, and ΔS_z are obtained by a second integration. All the integral coefficients of a_{ox}, a_{1x}, - - -, are tabulated in tables 1 and 2 for the direct and parking ascents respectively. All integral coefficients containing A_y and V_y are zero since the ascent trajectory is in the x-y plane.

The error equation for the gyro is

$$\dot{\phi}_i = b_{0i} + b_{1i} A_i + b_{2i} A_s + b_{3i} A_i A_s \tag{5}$$

where

$\dot{\phi}_i$ = the drift rate about the input axis,

b_{0i} = the fixed drift rate about the input axis,

b_{1i}, b_{2i} = mass unbalance along the input and spin axes respectively,

b_{3i} = the anisoelastic effects,

A_i, A_s = components of thrust acceleration along the input and spin axes.

TABLE 1.

VELOCITY AND POSITION INTEGRALS FOR DIRECT ASCENT

Velocity Coefficient Integrals					Position Coefficient Integrals				
		Value					Value		
Symbol	Integral	Short Boost	Long Boost	Units	Symbol	Integral	Short Boost	Long Boost	Units
I_1	$\int_0^t A_x dt$	146.2	156.8	g-sec	${}_1I_1$	$\int_0^t I_1 dt$	1.5×10^4	2.64×10^4	$g\text{-sec}^2$
I_2	$\int_0^t A_x^2 dt$	100.5	66.2	g^2-sec	${}_2I_2$	$\int_0^t I_2 dt$	9.3×10^3	8.74×10^3	$g^2\text{-sec}^2$
I_3	$\int_0^t A_x^3 dt$	71.0	31.0	g^3-sec	${}_3I_3$	$\int_0^t I_3 dt$	5.46×10^3	3.26×10^3	$g^3\text{-sec}^2$
I_4	$\int_0^t A_z dt$	26.7	183.1	g-sec	${}_4I_4$	$\int_0^t I_4 dt$	4.75×10^3	3.17×10^4	$g\text{-sec}^2$
I_5	$\int_0^t A_z^2 dt$	5.71	32.9	g^2-sec	${}_5I_5$	$\int_0^t I_5 dt$	5.40×10^3	1.10×10^4	$g^2\text{-sec}^2$
I_6	$\int_0^t A_z^3 dt$	1.18	10.6	g^3-sec	${}_6I_6$	$\int_0^t I_6 dt$	1.20×10^3	1.90×10^3	$g^3\text{-sec}^2$
I_7	$\int_0^t A_x A_z dt$	16.53	24.9	g^2-sec	${}_7I_7$	$\int_0^t I_7 dt$	1.42×10^3	6.59×10^3	$g^2\text{-sec}^2$
I_8	$\int_0^t A_x t dt$	1.93×10^4	4.16×10^4	$g\text{-sec}^2$	${}_8I_8$	$\int_0^t I_8 dt$	1.31×10^6	4.8×10^6	$g\text{-sec}^3$
I_9	$\int_0^t A_z t dt$	1.58×10^3	1.03×10^4	$g\text{-sec}^2$	${}_9I_9$	$\int_0^t I_9 dt$	2.40×10^5	3.56×10^6	$g\text{-sec}^2$
I_{10}	$\int_0^t v_x A_x dt$	1.10×10^4	1.23×10^4	$g^2\text{-sec}^2$	${}_{10}I_{10}$	$\int_0^t I_{10} dt$	6.99×10^5	1.80×10^6	$g^2\text{-sec}^3$
I_{11}	$\int_0^t v_x A_z dt$	8.7×10^2	1.53×10^3	$g^2\text{-sec}^2$	${}_{11}I_{11}$	$\int_0^t I_{11} dt$	2.20×10^5	6.41×10^5	$g^2\text{-sec}^3$
I_{12}	$\int_0^t v_z A_x dt$	3.26×10^3	1.18×10^4	$g^2\text{-sec}^2$	${}_{12}I_{12}$	$\int_0^t I_{12} dt$	3.62×10^5	1.75×10^6	$g^2\text{-sec}^3$
I_{13}	$\int_0^t v_z A_z dt$	3.5×10^2	4.02×10^3	$g^2\text{-sec}^2$	${}_{13}I_{13}$	$\int_0^t I_{13} dt$	1.55×10^5	1.31×10^6	$g^2\text{-sec}^3$

NOTE: All integrals containing A_y or v_y are zero and are not listed above.

TABLE 2

VELOCITY AND POSITION INTEGRALS FOR PARKING ASCENT

VELOCITY COEFF. INTEGRALS *					POSITION COEFF. INTEGRALS *				
SYMBOL	INTEGRAL	VALUE		UNITS	SYMBOL	INTEGRAL	VALUE		UNITS
		SHORT BOOST	LONG BOOST				SHORT BOOST	LONG BOOST	
I_1	$\int_0^t Axdt = Vx$	124.1	152.6	g-SEC	${}_1I_1$	$\int_0^t I_1\,dt$	12.5×10^3	23.5×10^3	g-SEC^2
I_2	$\int_0^t Aydt = Vy$	0	0	g-SEC	${}_2I_2$	$\int_0^t I_2 dt$	0	0	g-SEC^2
I_3	$\int_0^t Azdt = Vz$	38.5	61.9	g-SEC	${}_3I_3$	$\int_0^t I_3 dt$	4.39×10^3	26.57×10^3	g-SEC^2
I_4	$\int_0^t Axtdt$	21.9×10^3	47.0×10^3	g-SEC^2	${}_4I_4$	$\int_0^t I_4 dt$	14.2×10^5	54.3×10^5	g-SEC^3
I_5	$\int_0^t Aytdt$	0	0	g-SEC^2	${}_5I_5$	$\int_0^t I_5 dt$	0	0	g-SEC^3
I_6	$\int_0^t Aztdt$	2.44×10^3	2.05×10^3	g-SEC^2	${}_6I_6$	$\int_0^t I_6\,dt$	3.50×10^5	32.77×10^5	g-SEC^3
I_7	$\int_0^t VxAzdt$	2.71×10^3	-1.67×10^3	g^2-SEC^2	${}_7I_7$	$\int_0^t I_7 dt$	3.55×10^5	3.54×10^5	g^2-SEC^3
I_8	$\int_0^t VzAxdt$	4.08×10^3	11.13×10^3	g^2-SEC^2	${}_8I_8$	$\int_0^t I_8 dt$	3.37×10^5	14.76×10^5	g^2-SEC^3
I_9	$\int_0^t VzAzdt$	12.9×10^3	45.5×10^3	g^2-SEC^2	${}_9I_9$	$\int_0^t I_9\,dt$	8.56×10^5	9.55×10^5	g^2-SEC^3
I_{10}	$\int_0^t AxAydt$	0	0	g^2-SEC	${}_{10}I_{10}$	$\int_0^t I_{10} dt$	0	0	g^2-SEC^2
I_{11}	$\int_0^t AxAzdt$	24.58	2.94	g^2-SEC	${}_{11}I_{11}$	$\int_0^t I_{11} dt$	1.99×10^3	4.69×10^3	g^2-SEC^2
I_{12}	$\int_0^t AyAzdt$	0	0	g^2-SEC	${}_{12}I_{12}$	$\int_0^t I_{12} dt$	0	0	g^2-SEC^2

* EVALUATED BETWEEN LAUNCH AND THRUST CUTOFF.

TABLE 23.4-2: MISS COEFFICIENT INTEGRAL SET FOR SENSOR AND PLATFORM ERROR-FORCING FUNCTIONS

1316A-VB-30

The error equations for the gyro become:

$$\text{x-axis; } \phi_{yz} = \int_0^t \left[b_{0x} + b_{1x}A_x + b_{2x}A_y + b_{3x}A_xA_y \right] dt, \tag{6}$$

$$\text{y-axis; } \phi_{zx} = \int_0^t \left[b_{0y} + b_{1y}A_y + b_{2y}A_z + b_{3y}A_yA_z \right] dt, \tag{7}$$

$$\text{z-axis; } \phi_{xy} = \int_0^t \left[b_{0z} + b_{1z}A_z + b_{2z}A_y + b_{3z}A_zA_y \right] dt, \tag{8}$$

where

ϕ_{yz} = angular displacement in the y-z plane about the x-axis,

ϕ_{zx} = angular displacement in the z-x plane about the y-axis,

ϕ_{xy} = angular displacement in the x-y plane about the z-axis.

This is shown in figure 1.

Note that the acceleration term A_y in the last element of equation 8 does not follow a cyclical order. This is from the orientation of the z-gyro as shown in figure 2. By orienting the z-gryo in this manner rather than a cyclical order, a substantial simplification of the formulas results since $A_y = 0$ and $V_y = 0$.

Misalignment of the accelerometer input axis causes measurement of the normal acceleration components given by

$$A_I = A_i \cos \phi_{ij} \cos \phi_{ik} + A_j \sin \phi_{ij} - A_k \sin \phi_{ik} \tag{9}$$

where

A_I = the resultant acceleration input to the I accelerometer

I and i, j, k, take on cyclical permutations of x, y, z.

On the assumption of small angles, the velocity errors become

$$\Delta V_I \cong \int_0^t \left[A_j \phi_{ij} - A_k \phi_{ik} \right] dt. \tag{10}$$

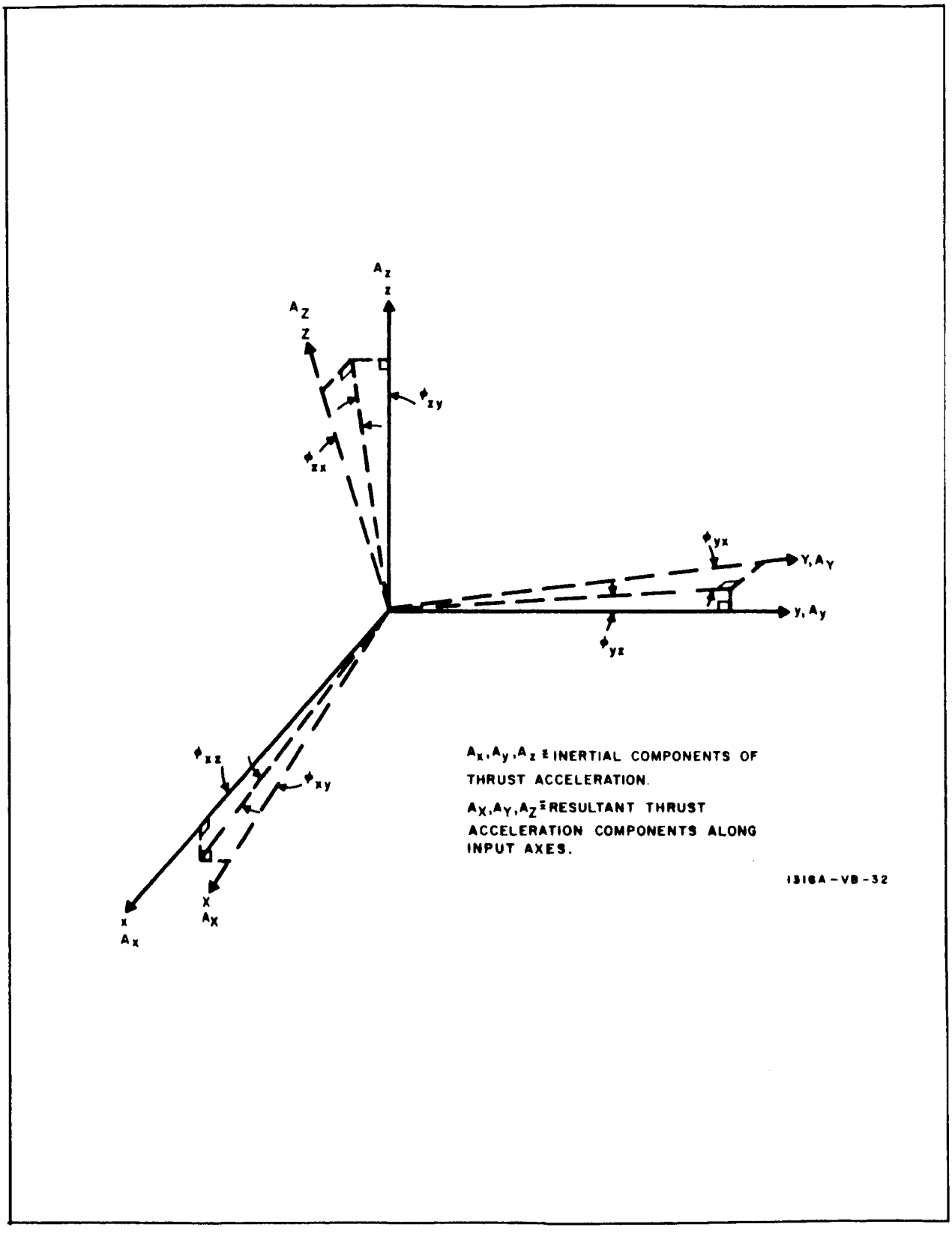

Figure 1. Misalignment Angles of Accelerometer Input Axes

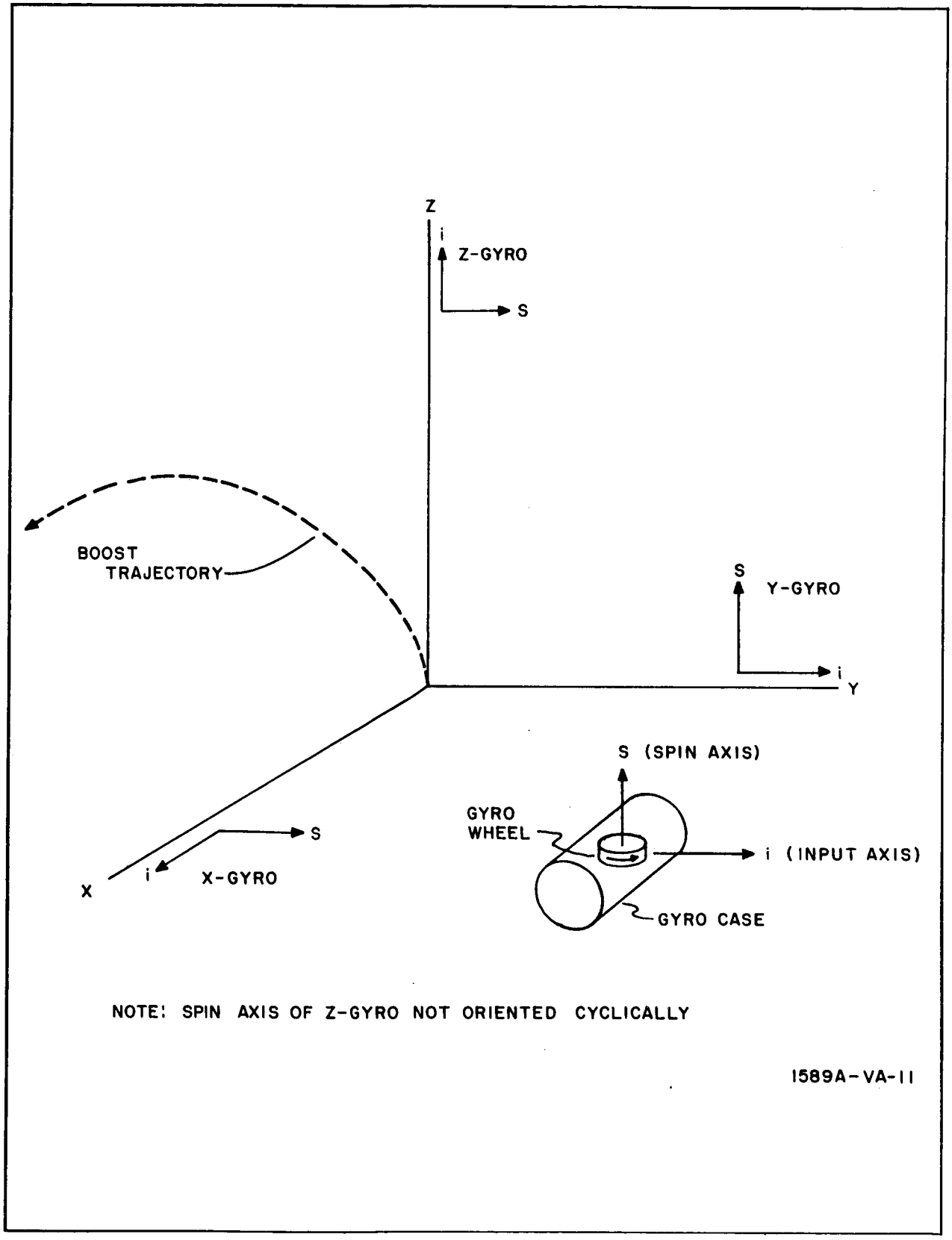

Figure 2. Gyroscope Orientation

A second integration gives position errors. Equations 10 and 11

$$\Delta S_I = \int_0^t \Delta V_i \, dt \tag{11}$$

relate velocity and position errors to the gyro coefficients. The values of ΔV and ΔS are calculated for the direct and parking ascents.

The platform error model equation is:

$$\phi_{ij} = \phi_{ij}(0) + e_k + p_{ij} A_i + q_{ij} A_j \tag{12}$$

where

ϕ_{ij} = angular displacement in the i, j plane about the i-axis

$\phi_{ij}(0)$ = initial angular displacement in the i, j plane about the i-axis

e_k = stabilization servo error about the k-axis in the i-j plane

p_{ij}, q_{ij} = platform deformations along the i-axis caused by A_i and A_j acceleration components

These equations have the same form as the gyro error equations. By substituting equation 12 into equations 10 and 11 the velocity and position errors related to the table errors are obtained.

2. TRANSFER MATRIX

The lunar ascent study is primarily concerned with determining the sensor specifications for the boost phase. It is of interest to compare the effect of the position and velocity errors at thrust termination on the final position and velocity states at terminal rendezvous. This section is concerned with the variation in the initial and final states of a transfer ellipse which is considered as a thrust free coast phase.

Since the position and velocity errors at thrust termination are given in moon centered navigational axes, the errors must be transformed

through the central angle traversed during the thrust phase. The transformation matrix is:

$$\begin{bmatrix} \Delta s_o \\ \Delta y_o \\ \Delta r_o \end{bmatrix} = \begin{bmatrix} \cos \phi_f & 0 & -\sin \phi_f \\ 0 & 1 & 0 \\ \sin \phi_f & 0 & \cos \phi_f \end{bmatrix} \begin{bmatrix} \Delta x \\ \Delta y \\ \Delta z \end{bmatrix}$$

where

ϕ_f = the central angle traversed during boost,

$\Delta x, \Delta y, \Delta z$ = position errors at thrust termination in navigational coordinates,

Δs_o = the tangentent error component along the trajectory,

Δy_o = the normal error component to the orbital plane,

Δr_o = the radial component.

The velocity conditions may be obtained by substituting the velocity components. The resulting position and velocity errors are now properly oriented to be transformed for the coast phase.

The transfer matrix in the most general form for any centrally traversed angle is:

$$\begin{bmatrix} \Delta r/r \\ \Delta s/r \\ \Delta y/r \\ \Delta v_{r/v} \\ \Delta v_{t/v} \\ \Delta v_{n/v} \end{bmatrix} = \begin{bmatrix} d_{11} & 0 & 0 & d_{14} & d_{15} & 0 \\ d_{21} & 1 & 0 & d_{24} & d_{25} & 0 \\ 0 & 0 & \cos \phi_f & 0 & 0 & d_{36} \\ d_{41} & 0 & 0 & d_{44} & d_{45} & 0 \\ d_{51} & 0 & 0 & d_{54} & d_{55} & 0 \\ 0 & 0 & d_{63} & 0 & 0 & d_{66} \end{bmatrix} \begin{bmatrix} \Delta r_{o/r_o} \\ \Delta s_{o/r_o} \\ \Delta y_{o/r_o} \\ \Delta v_{r_o/v_o} \\ \Delta v_{t_o/v_o} \\ \Delta v_{n_o/v_o} \end{bmatrix}$$

The zero subscript denotes the initial errors at the injection point of the transfer ellipse.

$$d_{11} = 2 - \frac{A \cos^2\theta_1}{(1+ e \cos\phi)} \left\{ \frac{A-1}{e} \left(- \frac{\sin\phi_f}{\sin\phi_1} \right) + \cos\phi_f \, (1 + \cot\phi_1 \, \tan\phi_f) \right\}$$

$$d_{14} = -2 \left\{ \tan\theta_1 - \frac{A \sin 2\theta_1}{2(1-e\cos\phi)} \left[\left(\frac{A-2}{2e} \right) \left(\frac{- \sin\phi_f}{\sin\phi_1} \right) + \cos\phi_f \, (1 + \cot\phi_1 \, \tan\phi_f) \right] \right\}$$

$$d_{15} = 2 \left\{ 1 - \frac{A \cos^2\theta_1}{1 + e\cos\phi} \left[\left(\frac{A-1}{e} \right) \left(\frac{-\sin\phi_f}{\sin\phi_1} \right) + \cos\phi_f \, (1 + \cot\phi_1 \, \tan\phi_f) \right] \right\}$$

$$d_{21} = -\left\{ \frac{A \sin 2\theta_1}{2\, e^2} + \frac{2(A-1)\sin\phi}{e\,(2-A)} \left(\frac{2 + e\cos\phi}{2} \right) + \left(\frac{(1+ e\cos\phi)^2}{(1 - e^2)^2 \, (1 + e\cos\phi_1)^2} \right) \left(\frac{(A-1)\sin\phi_1}{e(2-A)} \right) x \, (2 + e\cos\phi_1) + \frac{3\,\phi_f (1 + e\cos\phi)^2}{(A-2)\,(1-e^2)^{5/2}} \right\}$$

$$d_{24} = -\left\{ 1 + \frac{A\,(A-2)\sin\phi\,\sin 2\theta\,(2 + e\cos\phi_1)}{2e} - \frac{(1 + e\cos\phi)^2}{(1 - e^2)^2\,(1 + e\cos\phi_1)^2} \; x \left[\frac{A(1 - e^2)}{(A - 1)} - \frac{A\,(A-2)\sin\phi\,\sin 2\theta\,(2 + e\cos\phi_1)}{2e} \right] + \frac{3\,\phi_f \tan\theta_1\,(1 + e\cos\phi)^2}{(1 - e^2)^{5/2}} \right\}$$

$$d_{25} = \frac{A \sin 2\theta_1}{e^2} + \frac{2 \sin\phi (A-1)(2 + e\cos\phi)}{e(2-A)}$$

$$+ \frac{(1 + e\cos\phi)^2}{(1-e^2)(1 + e\cos\phi_1)^2} \cdot \frac{2(A-1)\sin\phi_1 (2 + e\cos\phi_1)}{e(2-A)}$$

$$+ \frac{3\phi_f A (1 + e\cos\phi)^2}{(A-2)(1-e^2)^{5/2}}$$

$$d_{36} = \frac{\sin\phi_f}{\cos\theta_1}$$

$$d_{41} = \frac{A\cos^4\theta_1}{(1 + e\sin\phi)} \left[\frac{(A-1)\cos\phi_f}{e\sin\phi_1} + \sin\phi_f (1 - \cot\phi_1 \cot\phi_f) \right]$$

$$d_{44} = \frac{-A\cos^2\theta_1 \sin 2\theta_1}{(1 + e\sin\phi)^2} \left[\frac{(A-2)\cos\phi_f}{2e\sin\phi_1} + \sin\phi_f (1 - \cot\phi_1 \cot\phi_f) \right]$$

$$d_{45} = \frac{2A\cos^4\theta_1}{(1 + e\sin\phi)^2} \left[\frac{(A-1)\cos\phi_f}{e\sin\phi_1} + \sin\phi_f (1 - \cot\phi_f \cot\phi_1) \right]$$

$$d_{51} = \frac{(A-1)}{e(2-A)} \left\{ \cos\phi (2 - e\cos\phi) - e\sin^2\phi \right\}$$

$$- \frac{2e\sin\phi(1 + e\cos\phi)}{(1-e^2)(1 + e\cos\phi_1)^2} \cdot \frac{\sin\phi_1 (A-1)(2 + e\cos\phi_1)}{e(2-A)}$$

$$d_{54} = \frac{A\,(A-2)\,\sin 2\theta_1\,\cos\phi\,(2 + e\cos\phi_1)}{2e}$$

$$+ \frac{2\,e\,\sin\phi\,(2 + e\cos\phi)}{(1-e^2)^2\,(1 + e\cos\phi_1)^2}\left\{\frac{A\,(1-e^2)}{A-1} - \frac{A\,(A-2)\,\sin 2\theta_1\,\sin\phi}{2\,e\,(2 + e\cos\phi_1)^{-1}}\right\}$$

$$+ \frac{(1 + e\cos\phi)^2\,A(A-2)\,(2 + e\cos\phi_1)\cos\phi\,\sin 2\theta_1}{e\,(1-e^2)^2\,(1 + e\cos\phi_1)^2}$$

$$+ \frac{3\tan\phi_1\,(1 + e\cos\phi)}{(1 - e^2)^{5/2}} + \left((1 + e\cos\phi) - 2\,\phi_f\,e\sin\phi\right)$$

$$d_{55} = \frac{2\,(A - 1)}{e\,(2 - A)}\left\{(2 + e\cos\phi)\cos\phi - e\sin^2\phi\right\}$$

$$- \frac{2\,(1 + e\cos\phi)\,e\sin\phi}{(1 - e^2)\,(1 + e\cos\phi_1)^2}\left\{\frac{2\,(A - 1)\,\sin\phi_1\,(2 + e\cos\phi_1)}{e\,(2 - A)}\right\}$$

$$+ \frac{3A\,(1 + e\cos\phi)}{(A-2)\,(1-e^2)^{5/2}}\left\{(1 + e\cos\phi) - 2\,\phi_f\,e\sin\phi\right\}$$

$$d_{63} = -\sin\phi_f\,\frac{(1 + e\cos\phi) + \cos\phi_f\,e\sin\phi}{(1 + 2\,e\cos\phi + e^2)^{1/2}}$$

$$d_{66} = \frac{\cos\phi_f\,(1 + e\cos\phi) + \sin\phi_f\,e\sin\phi}{\cos\theta_1\,(1 + 2\,e\cos\phi + e^2)^{1/2}}$$

where

r = the selenocentric radius,

v = the velocity,

θ_1 = the angle between velocity and tangent plane,

ϕ = the selenocentric angle measured from perigee,

e = the orbit eccentricity,

$A = rv^2/\mu$

μ = the gravitational constant,

f = the final value (subscript),

$\phi_f = \phi_1 + \phi$

For the 180 degree Hohmann transfer $\phi_1 = 0$ degree and $\phi = 180$ degrees.

This subject is treated in greater detail in Ref. 2.

3. PARKING ORBIT INITIAL ERROR PROPAGATION

The transfer matrix of Section 2 can be reduced to the following form for the parking orbit.

$$\begin{bmatrix} \Delta r/r \\ \Delta s/r \\ \Delta y/r \\ \Delta v_r/v \\ \Delta v_t/v \\ \Delta v_n/v \end{bmatrix} = \begin{bmatrix} 2-\cos\phi & 0 & 0 & \sin\phi & 2(1-\cos\phi) & 0 \\ 2\sin\phi - 3\phi & 1 & 0 & -2(1-\cos\phi) & -3(\phi - 4\sin\phi) & 0 \\ 0 & 0 & \cos\phi & 0 & 0 & \sin\phi \\ \sin\phi & 0 & 0 & \cos\phi & 2\sin\phi & 0 \\ 2\cos\phi - 3 & 0 & 0 & -2\sin\phi & -3 + 4\sin\phi & 0 \\ 0 & 0 & -\sin\phi & 0 & 0 & 0 \end{bmatrix} \begin{bmatrix} \Delta r_o/r_o \\ \Delta s_o/r_o \\ \Delta y_o/r_o \\ \Delta v_{r_o}/v_o \\ \Delta v_{t_o}/v_o \\ \Delta v_{n_o}/v_o \end{bmatrix}$$

Ref. 2: Gretz, R. W., Error Sensitivities in Satellite Ascent and Orbital Transfer, ARS Journal, Vol. 32, No. 12, Dec. 1962.

Similar forms for the transfer matrix are given in Ref. 3 and 4. The elements of the transfer matrices in both Sections 2 and 3 are approximations; however, for the purposes of this study, the variations are of second order magnitudes. The results are graphed in figures 3 and 4 in normalized form.

4. VELOCITY REQUIREMENTS BETWEEN TWO CIRCULAR CO-PLANAR ORBITS

Problem definition consists of determining the minimum total velocity impulse for a theoretical 2-impulse transfer between co-planar circular orbits with arbitrary terminals. Only two geometrical restrictions are implied, tangential (or apogee) capture at the target orbit and intersection with the inner orbit.

In addition to the exact solution, an approximate solution is given for obtaining quick and accurate estimates for cases where the radii ratio is near unity and the central transfer angle is above 40 degrees. For transfers below 40 degrees, severe fuel requirements are imposed on the interceptor for circle-to-circle transfer.

Nomenclature (see figure 5).

v_t = circular target velocity

v_p = circular parking velocity

v_2 = elliptical velocity at apogee (point 2)

v_1 = elliptical velocity at injection (point 1)

$\Delta v_2 = v_t - v_2$ = velocity increment required at point 2.

$\Delta v_1 = \left| \underset{\sim}{v}_1 - \underset{\sim}{v}_p \right|$ = velocity increment required at point 1.

$\Delta v_1 = \Delta v_1 + \Delta v_2$ = total velocity increment.

r_2 = target orbit radius

Ref. 3: Duke, W.M., E.A. Goldberg, and I. Pfeffer, Error Analysis Considerations for a Satellite Rendezvous, ARS Journal, Vol. 31, No. 4, April 1961, p. 505-513.

Ref. 4: Jensen, J., J. Lock, D. Kraft, and G. Townsend, Design Guide to Orbital Flight 1, McGraw Hill, 1962

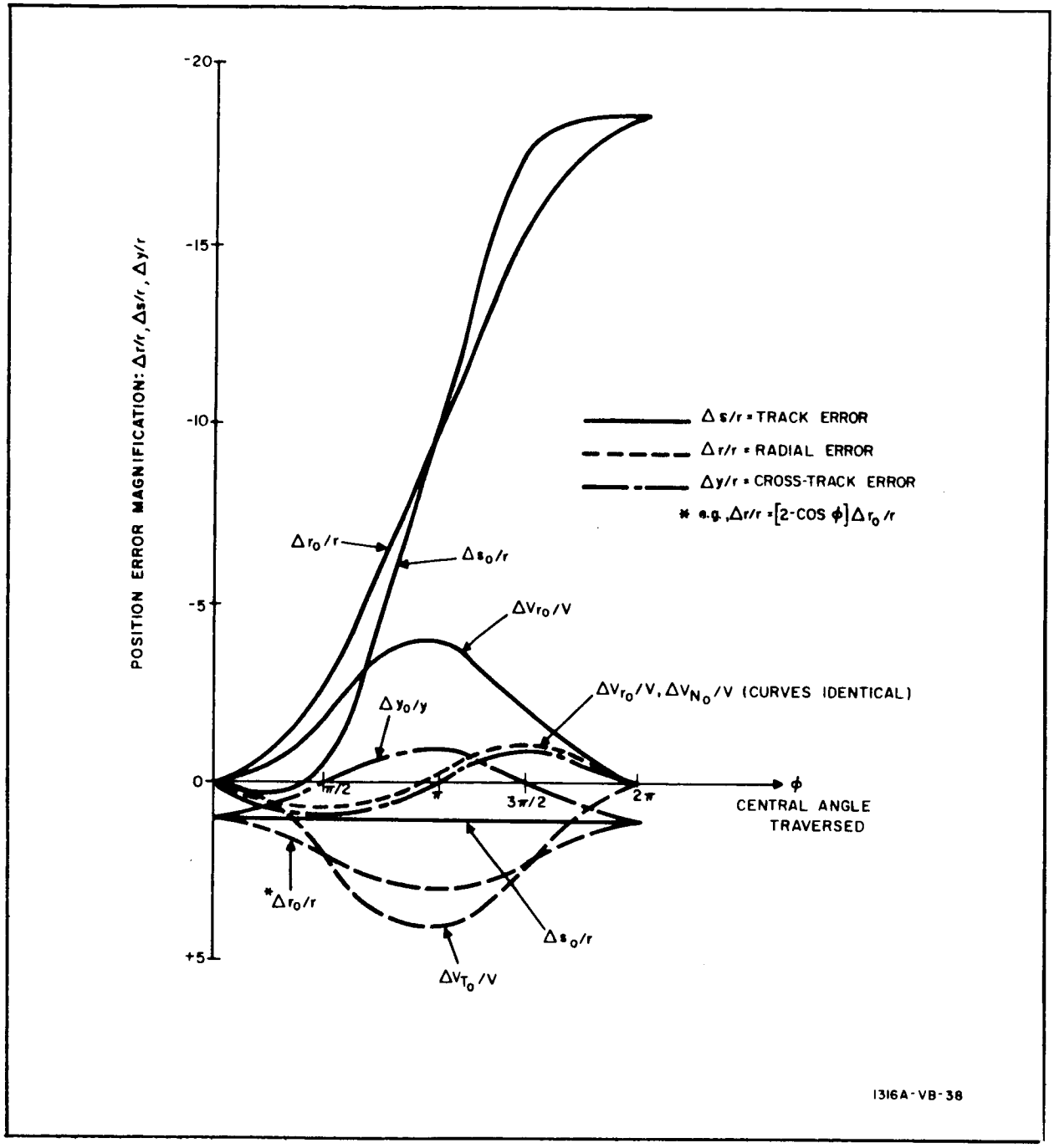

Figure 3. Effect of Initial State Errors on Final State Position Errors for Near Circular Orbits

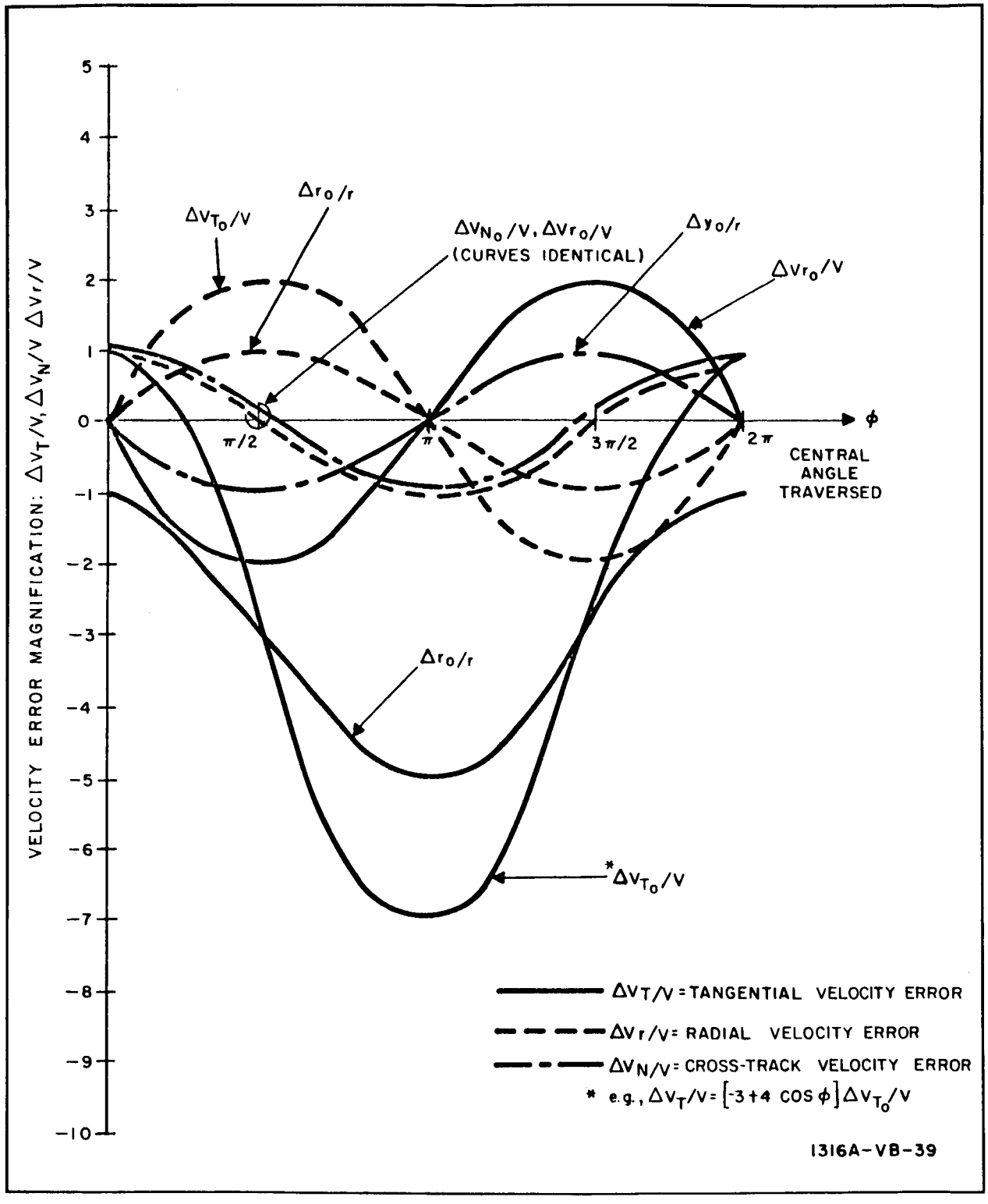

Figure 4. Effect of Initial State Errors on Final State Velocity Errors for Near-Circular Orbits

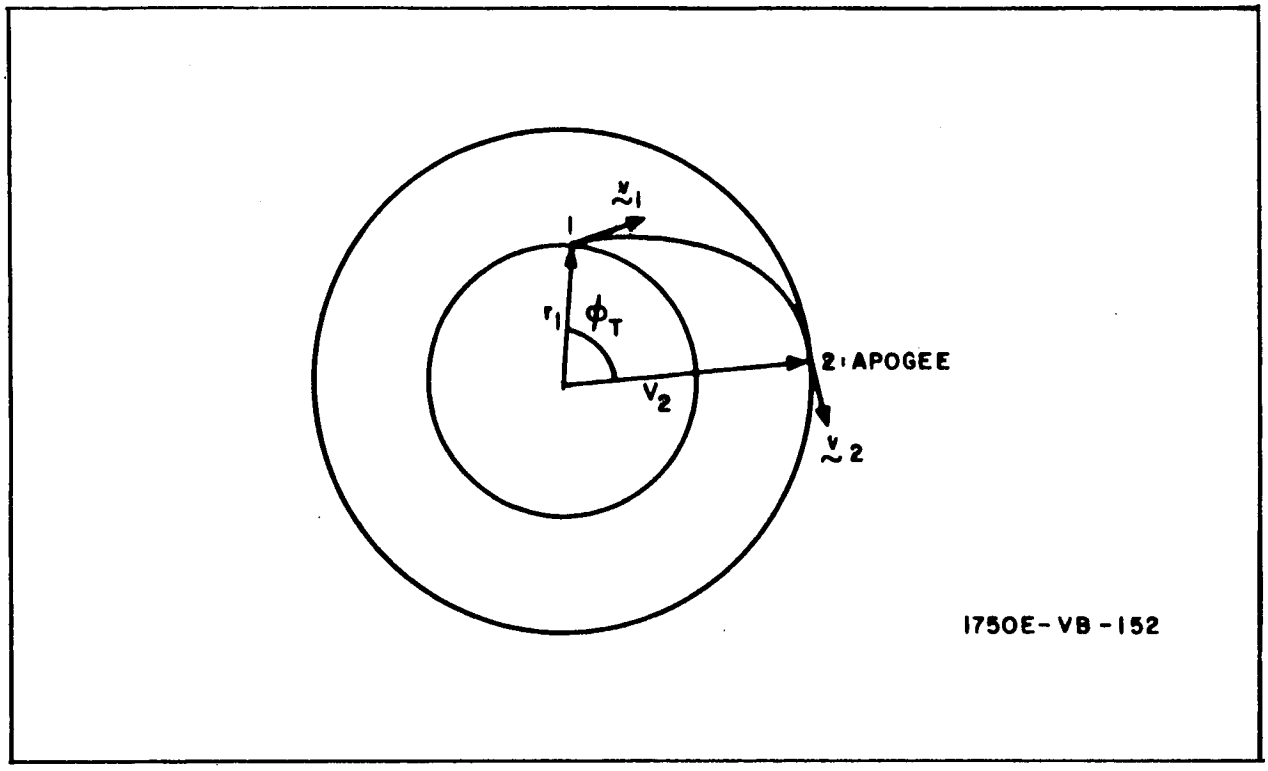

Figure 5. Tangential Capture for Transfer Between Circular Orbits

r_1 = parking orbit radius

ϕ_t = true anomaly between injection and target contact

μ = gravitational constant

a = semi-major axis of transfer ellipse

γ = flight path angle

$\rho = r_2 - r_1$

To obtain the total velocity increment, consider the following relationships available from orbital mechanics,

$$v = \sqrt{\mu \left(\frac{2}{r} - \frac{1}{a}\right)} = \frac{\sqrt{\mu\, a\, (1 - e^2)}}{r \cos \gamma} \qquad (13)$$

Substituting into the velocity increment required at point 2 and normalizing with respect to the target:

$$\frac{\Delta v_2}{v_t} = 1 - \frac{v_2}{v_t} = 1 - \sqrt{2 - \frac{r_2}{a}} \qquad (14)$$

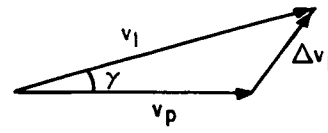

The cosine law yields $\frac{\Delta v_1}{v_t}$:

$$\frac{\Delta v_1}{v_t} = \sqrt{\left(\frac{v_1}{v_t}\right)^2 + \left(\frac{v_p}{v_t}\right)^2 - \cos\gamma \frac{v_1 v_p}{v_t^2}} \qquad (15)$$

Substituting 13 in 15

$$\frac{\Delta v_1}{v_t} = \sqrt{3\frac{r_2}{r_1} - \frac{r_2}{a} - 2\frac{r_2}{r_1}\sqrt{\frac{a}{r_1}(1 - e^2)}} \qquad (16)$$

To eliminate a and e and obtain ϕ_t as an independent variable, two additional equations for the ellipse are required. Imposing the minimum fuel constraint; i.e., target radius equalling transfer apogee:

$$r_2 = a(1 + e)$$

and at injection,

$$r = r_1 = \frac{r_2(1 - e)}{1 - e\cos\phi_t}$$

Substituting these two equations into 14 and 16, and summing to obtain the total required velocity increment:

$$\frac{\Delta v}{v_t} = 1 - x + \sqrt{3K - 2 + x^2 - 2K^{3/2}x} \qquad (17)$$

where

$$x = \frac{1 - \cos \phi_t}{K - \cos \phi_t}$$

$$K = \frac{r_2}{r_1}$$

The above differences under the radical are very small when the radii ratio is nearly unity and hence double precision on a digital computer was required to obtain the graphical results appearing in figure 6. Comparison between Δv and the required total Hohmann increment $\Delta v_{HOH.}$ was obtained by simply normalizing the computer program yielding $\Delta v/\Delta v_{HOH.}$.

The following analysis provides a workable analytical approximation of $\Delta v/\Delta v_{HOH.}$, not requiring a digital computer program. The results are justified graphically by comparison with the above exact derivation.

The authors in Ref. 3 have provided a first-order linear approximation to the relationships between the initial and final state variations for low-eccentricity orbits. Only the relevant equations in Ref. 3 will be used in this derivation. These are given as follows:

$$\Delta r = (2 - \cos M)\, \Delta r_o + 2r\,(1 - \cos M) \frac{\Delta v_x}{v} + r \sin M \frac{\Delta v_y}{v} \tag{18}$$

$$\Delta \dot{r} = 2\, \Delta v_x \sin M + \Delta v_y \cos M \tag{19}$$

where

r, v = initial circular parameters

Δr_o = initial radial variation

Δv_x = initial tangential velocity variation

Δv_y = initial radial velocity variation

M = mean anomaly between initial and final states

$\Delta r, \Delta \dot{r}$ = final state variations in radius and radial velocity

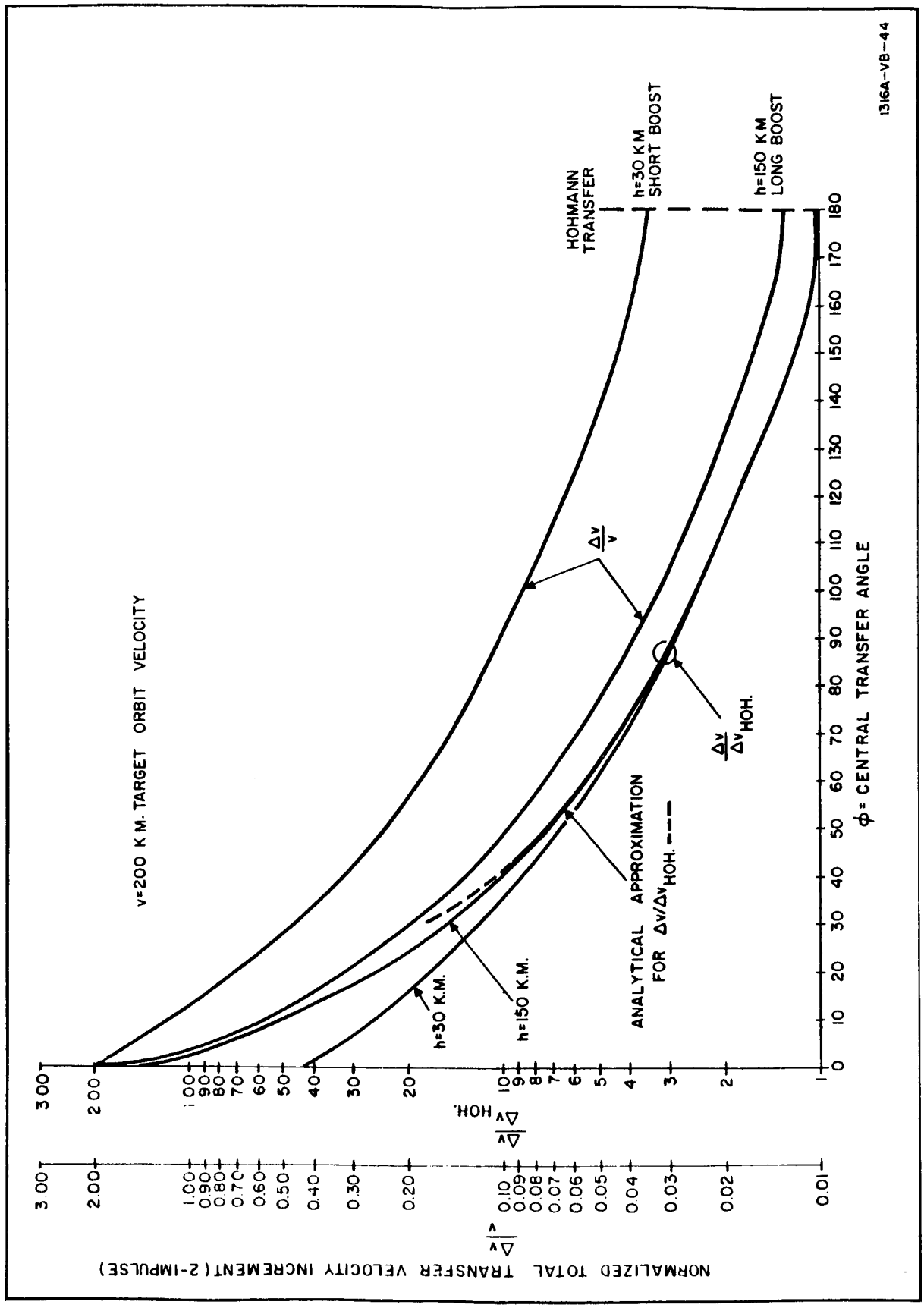

Figure 6. Total Required Velocity Increment for Minimum Energy Circle-to-Circle Transfer

Note that all deviations are relative to a circular orbit. It is therefore expected that transfer trajectories of high eccentricity, obtained from a linear perturbation of a circular orbit should be very inaccurate, i.e., orbits requiring small transfer angles. Since the fuel penalty may be prohibitive at these angles, linearization is justified for the region under consideration.

To find the injection impulse, consider first a perturbation of the parking orbit. Since an initial altitude variation is not relevant $\Delta r_o = 0$, and, for tangential capture at the target orbit $\Delta \dot{r} = 0$. But Δr is constrained as the difference in radii between target and parking orbits, $\Delta r = r_2 - r_1 = \rho$. Substitution of the above into equations 18 and 19 yields,

$$\frac{\rho}{r_1} = 2 (1 - \cos M) \frac{\Delta v_x}{v_p} + \sin M \frac{\Delta v_y}{v_p} \tag{20}$$

$$\frac{\Delta v_y}{\Delta v_x} = -2 \tan M \tag{21}$$

Elimination of Δv_x gives,

$$\frac{\Delta v_y}{v_p} = \frac{\rho}{2 r_1} \frac{1}{1 - \sec M} \tag{22}$$

But Δv_y is simply the normal component of the required injection impulse,

$\Delta v_x = \Delta v_1 \cos \alpha_1$

Also, from 21 $\frac{\Delta_y}{\Delta v_x} = \tan \alpha_1 = -2 \tan M$

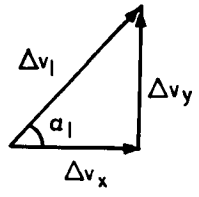

Solving 22 by eliminating α_1 and Δv_y, the initial required impulse is

$$\frac{\Delta v_1}{v_p} = \frac{\rho}{2 r_1} \frac{\sqrt{4 - 3 \cos^2 M}}{1 - \cos M} \tag{23}$$

The final impulse is found by simply reversing the logic, i.e., considering perturbations of the outer orbit. Since the only perturbed quantity is the tangential velocity, equation 18 takes the form,

$$\frac{\rho}{r_2} = 2\left[1 - \cos(-M)\right]\frac{\Delta v_2}{v_t} \tag{24}$$

where

$\Delta v_y = 0$ (orbital contact at apogee)

$\Delta v_2 = v_t - v_2$

$\Delta r_o = 0$

$\Delta r = -(r_1 - r_2) = \rho$

$$\therefore \frac{\Delta v_2}{v_t} = \frac{\rho}{2 r_2}\frac{1}{1 - \cos M} \tag{25}$$

Summing the two normalized impulses,

$$\frac{\Delta v}{v_t} = \frac{\rho}{2(1 - \cos M)}\left[\frac{1}{r_1}\frac{v_p}{v_t}\sqrt{4 - 3\cos^2 M} + \frac{1}{r_2}\right] \tag{26}$$

But, for circular orbits, $v = \sqrt{\frac{\mu}{r}}$

$$\therefore \frac{v_p}{v_t} = \frac{r_2}{r_1}$$

$$\therefore \frac{\Delta v}{v_t} = \frac{\rho}{2 r_2 (1 - \cos M)}\left[\left(\frac{r_2}{r_1}\right)^{3/2}\sqrt{4 - 3\cos^2 M} + 1\right] \tag{27}$$

Normalizing with respect to the Hohmann transfer M = 180°,

$$\frac{\Delta v}{\Delta v_{HOH.}} = \frac{2}{1 - \cos M} \left[\frac{\left(\frac{r_2}{r_1}\right)^{3/2} \sqrt{4 - 3\cos^2 M} + 1}{\left(\frac{r_2}{r_1}\right)^{3/2} + 1} \right] \qquad (28)$$

As a first order approximation, let $r_1 = r_2$. Also, for low eccentricity orbits, take $M \cong \phi_t$. Hence,

$$\frac{\Delta v}{\Delta v_{HOH.}} = \frac{1 + \sqrt{4 - 3\cos^2 \phi_t}}{1 - \cos \phi_t} \qquad (29)$$

Although analytical justification for the above assumptions is not presumed, it is evident from a graphical comparison with the exact results (see figure 6) that the approximate equation is more than adequate in the region under consideration, i.e., transfers over 40 degrees. Since it is a simple matter to calculate Δv for a Hohmann transfer, equation 29 is extremely useful for quick and accurate estimates of the fuel penalty for various central transfer angles.

Figure 6 shows the total velocity requirements as a function of the parking altitude for various central transfer angles. Figure 6 also indicates the inefficiency of small transfer angles between circular orbits. Note that $\Delta v/\Delta v_{HOH.}$ is practically independent of the altitude of the parking orbit for transfers above 40 degrees. The results of figure 6 provide justification for limiting the parking orbit to the lowest possible altitudes if fuel expenditure is the only criterion.

5. PARKING ORBIT TRANSFER CONSIDERATIONS

This section considers the fuel requirements for boost and orbital transfer for the parking ascent phase of the lunar rendezvous.

Referring to figure 7 which provides a measure of the total ascent and transfer fuel requirements, Δv^* is defined as the total velocity impulse required for the minimum fuel ascent and transfer trajectory. This trajectory

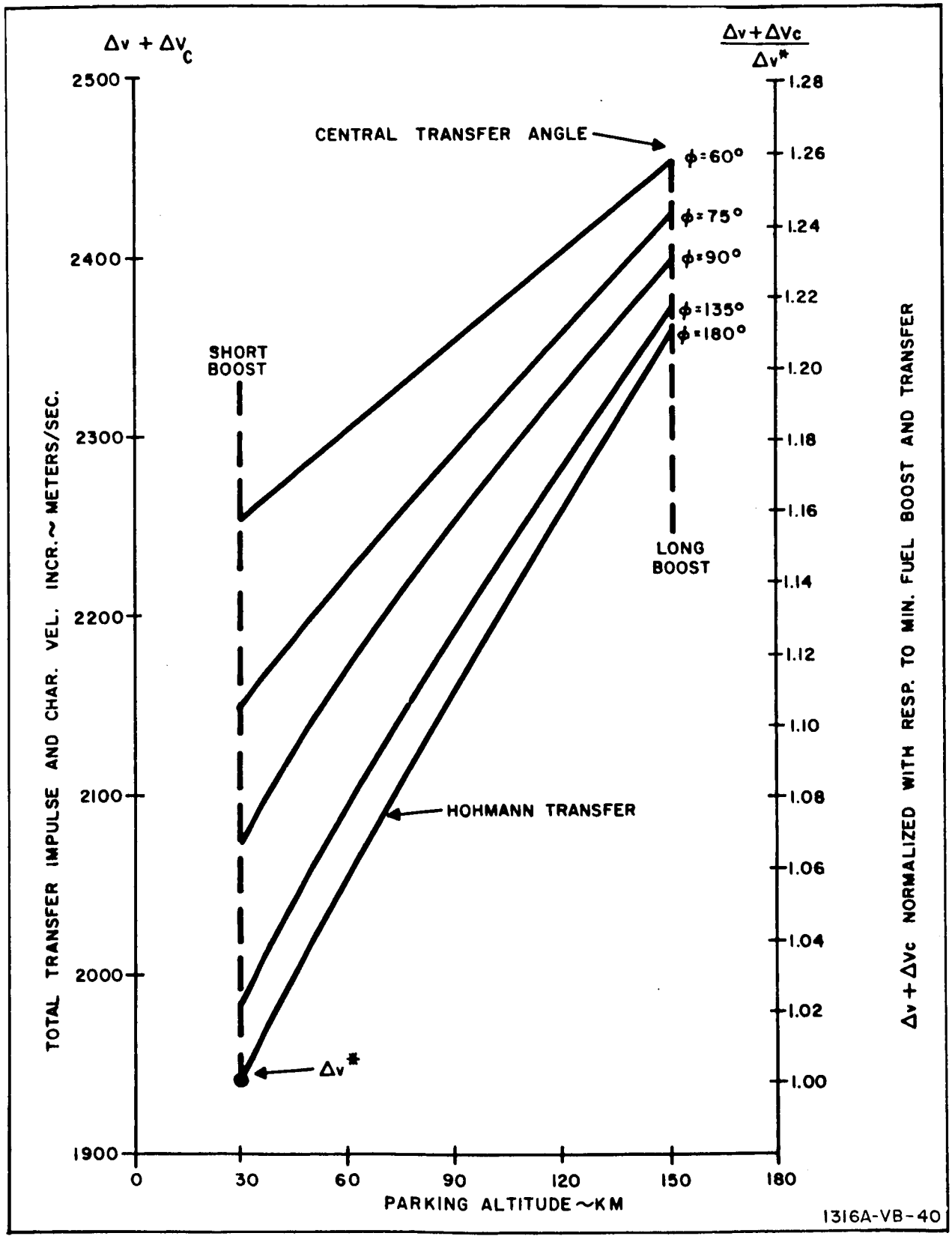

Figure 7. Total Velocity Requirements versus Parking Altitude for Various Central Transfer Angles (200-km Target Orbit)

insures terrain avoidance during parking at 30 km and is followed by a 180 degree Hohmann transfer to 200 km. For a similar transfer but with an initial boost to 150 km, 21 percent more fuel is required; for a 90-degree transfer from 30 to 200 km the fuel penalty is 7 percent, but the time saving is roughly equivalent to one-fourth the period of the target orbit, or 15 minutes. For faster transfers from 30 km the fuel penalty becomes quite significant; i.e., a direct ascent is preferable.

For the high altitude boost, which takes only a few hundred more seconds than the 30-km boost, it is evident that low transfer angles have a significantly lesser effect. The fuel penalty between a 75 degree and Hohmann transfer is only 3 percent for the high altitude, long boost.

For a very quick ascent, time savings close to 25 min can be achieved at a fuel penalty of less than 30 percent compared with the minimum fuel ascent. This fuel difference is equivalent to a Δv of roughly 1/2 km/sec.

Referring to figure 8 which gives the ratio of transfer fuel to the total fuel required, a 6-percent penalty is paid for a 90-degree transfer compared to the Hohmann from 30 km. This penalty is reduced to 1-1/2 percent for the 150-km parking orbit. Obviously, fast transfers from low altitudes may place requirements on the rendezvous scheme which are too stringent; i.e., fuel is wasted in obtaining injection velocity. Figure 9 also substantiates this conclusion.

Figure 10 simply provides the magnitude of the total transfer impulse for various parking orbits and transfer angles. In addition it is relevant to indicate a close approximation to the efficiency of the boost phase by itself. Thus, the difference between the characteristic velocity increment and the parking velocity is plotted versus altitude.

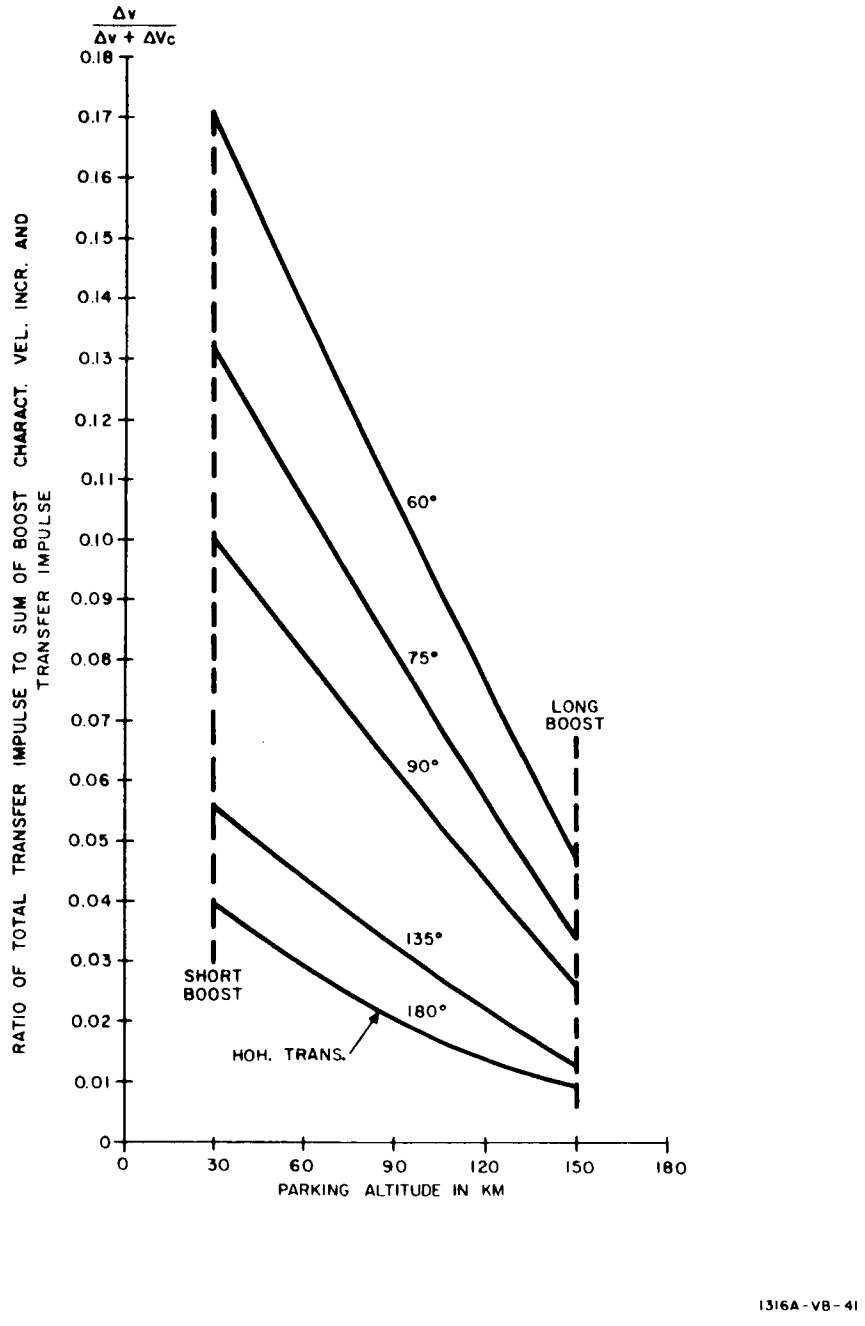

Figure 8. Percentage of Fuel Required for Transfer versus Parking Altitude for Various Central Transfer Angles (200-km Target Orbit)

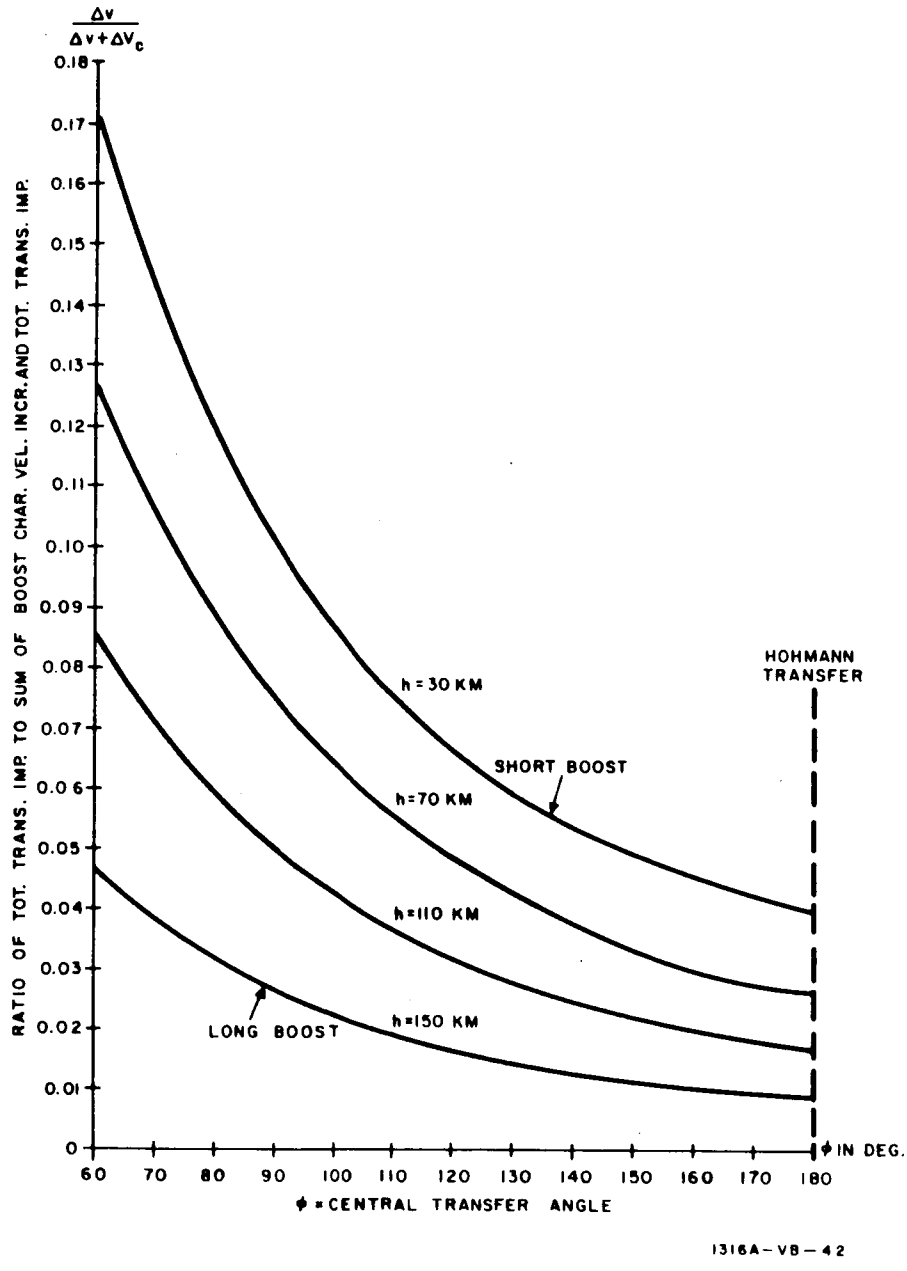

Figure 9. Percentage of Fuel Required for Transfer versus Central Transfer Angle for Various Parking Altitudes (200-km Target Orbit)

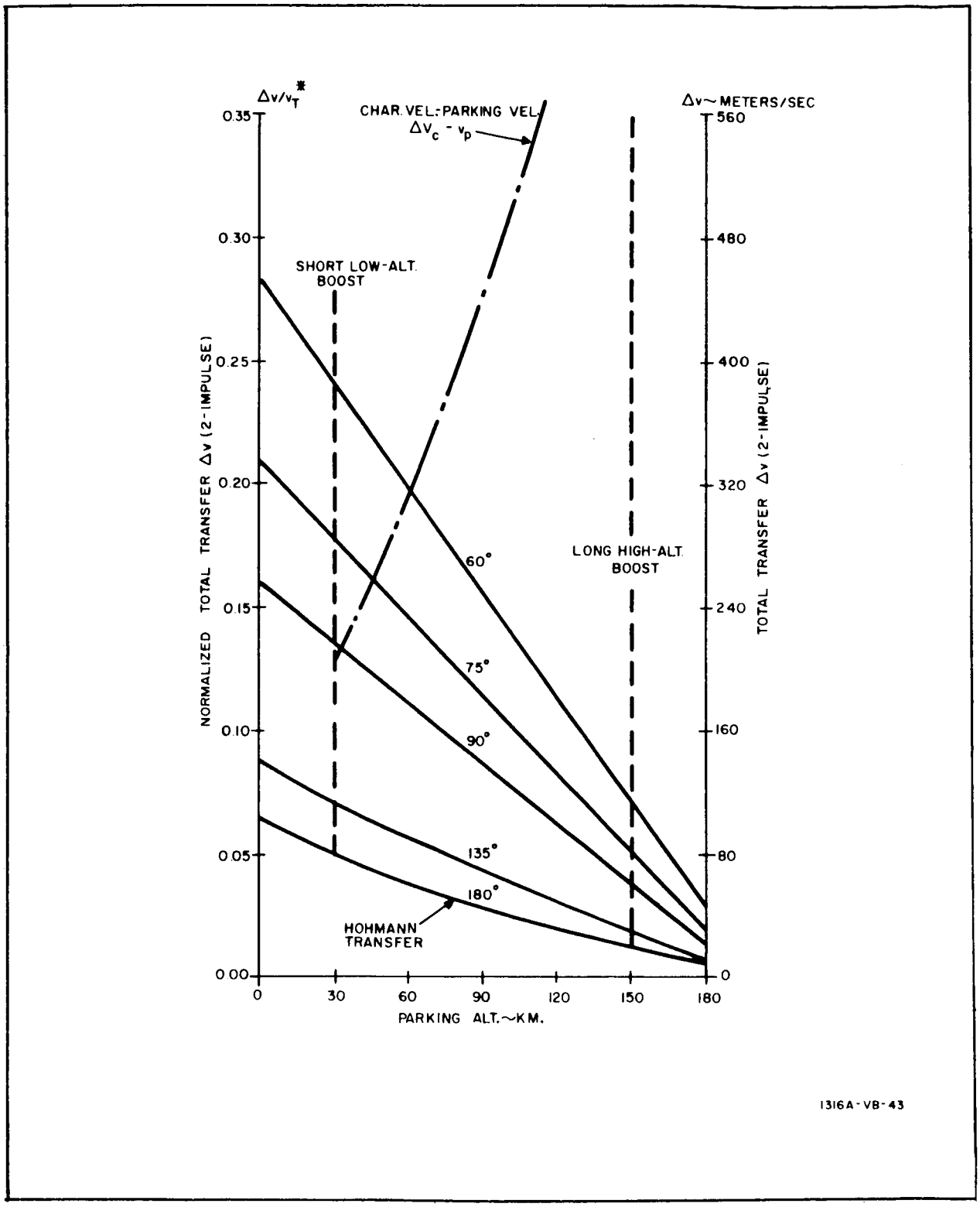

Figure 10. Total Required Transfer Velocity Increment versus Parking Altitude for Various Central Transfer Angles (200-km Target Orbit)

APPENDIX F

LUNAR RENDEZVOUS

SUMMARY OF NOTATION:

a_x	Longitudinal acceleration of chaser due to thrusting
a_z	Normal acceleration of chaser due to thrusting
D	Angle between chaser-to-target range vector and positive x-axis of selenocentric coordinate system
e	Orientation of LOS with respect to an inertial reference
$\dot{e}$	LOS angular rate with respect to inertial space
g	$9.81\ m/sec^2$
h	Altitude of chaser
i	Orbital plane inclination
I_{sp}	Fuel specific impulse
K_1, K_2	Control parameters
K_m	Gravitational constant of moon = $4.90 \times 10^3\ km^3/sec^2$
M_o	Initial mass of chaser
M_p	Mass of propellant consumed by chaser due to rocket firing
R	Chaser-to-target range
$\dot{R}$	Chaser-to-target range rate
R_o	Chaser-to-target range at initiation of active rendezvous
r_m	Radius of moon = 1738 km
R_s	Smoothed value of measured chaser-to-target range
R_l	Range at which longitudinal control of chaser switches from coarse to vernier

R_2	Standoff range at termination of active rendezvous
R_x, R_z	Components of chaser-to-target range in x^1 z^1 system
t	Time
t_F	Amount of time for which chaser rocket is to be fired
t_i	Interval between subsequent data points
ΔV	Velocity increment
ΔV_h	Total velocity increment required to perform a Hohmann transfer
ΔV_1	Velocity increment required for injection of Hohmann transfer
ΔV_2	Velocity increment required during Hohmann transfer to synchronize the chaser with the target
ΔV_I	Deviation from nominal V_1 at injection
V_x, V_z	Relative velocity between target and chaser in x^1 z^1 system
V_{xc}, V_{yc}	Components of chaser velocity in selenocentric coordinates
V_{xc}, V_{yc}	Corrected values of chaser velocity in selenocentric coordinate system
V_{xT}, V_{yT}	Components of target velocity in selenocentric coordinate system
x^1, z^1	Chaser centered coordinate system where x^1 is along the local horizontal and in the direction of motion; z^1 is along the radius vector in the direction of the moon
X_c Y_c	Chaser position coordinates in selenocentric coordinate system
X_c, Y_c	Corrected position coordinates of chaser in selenocentric coordinate system
X_t, Y_t	Target position coordinates in selenocentric coordinate system

1. COMPUTER SIMULATION OF LUNAR RENDEZVOUS TECHNIQUES

The computer program used to simulate the lunar rendezvous is discussed in this Appendix. This program is based on several assumptions

about the orbits of the two vehicles. A nonmaneuvering target vehicle is assumed to be in a circular retrograde orbit about the moon. A maneuverable chaser vehicle is assumed to be initially in a lower altitude circular retrograde parking orbit. The orbits of the two vehicles are assumed to be coplanar and no out-of-plane deviations are considered, thereby reducing the problem to a two-dimensional model.

The nominal case is defined as follows: The altitudes of the target and chaser parking orbits are 200 and 30 km respectively. The initial angle ϕ_I (figure 1) between the two vehicles is defined to be such that a horizontal nominal thrust applied to the chaser at its initial position will cause the chaser to collide with the target exactly 180 degrees later. The program has been arranged so that deviations from this nominal case can be studied. The deviations which have been considered are a deviation in the altitude of the chaser parking orbit, a deviation from a nominal incremental velocity vector in both magnitude and direction, and a deviation from the nominal central angle between the two vehicles.

1.1 Initial Positioning of Target and Chaser

The initial relative positioning of the target and chaser vehicles depends upon a set of deviations from nominal which are inputs to the program. The chaser vehicle has arbitrarily been placed on the positive axis at the time when the injection into the ascent ellipse is made. The deviation from nominal thrust level is specified by an initial velocity increment Δv_I. Thus the position and velocity vectors defining the ascent ellipse of the chaser are:

$$X_e = X_p$$
$$Y_e = 0$$
$$v_{xe} = V_I \sin \gamma$$
$$v_{ye} = v_{yp} + \Delta v_l + \Delta v_I \cos \gamma$$

where:

x_p, v_{yp} = position and velocity of chaser in parking orbit of specified altitude

Δv_n = velocity increment due to nominal thrust

γ = deviation from nominal thrust angle (See figure 1)

A set of orbital elements for the chaser is calculated from this position and velocity vector by the method described in paragraph 1.7.2. The target vehicle is placed in a 200km circular orbit and positioned initially with a specified deviation from the nominal angle ϕ_o (figure 1) between the two vehicles.

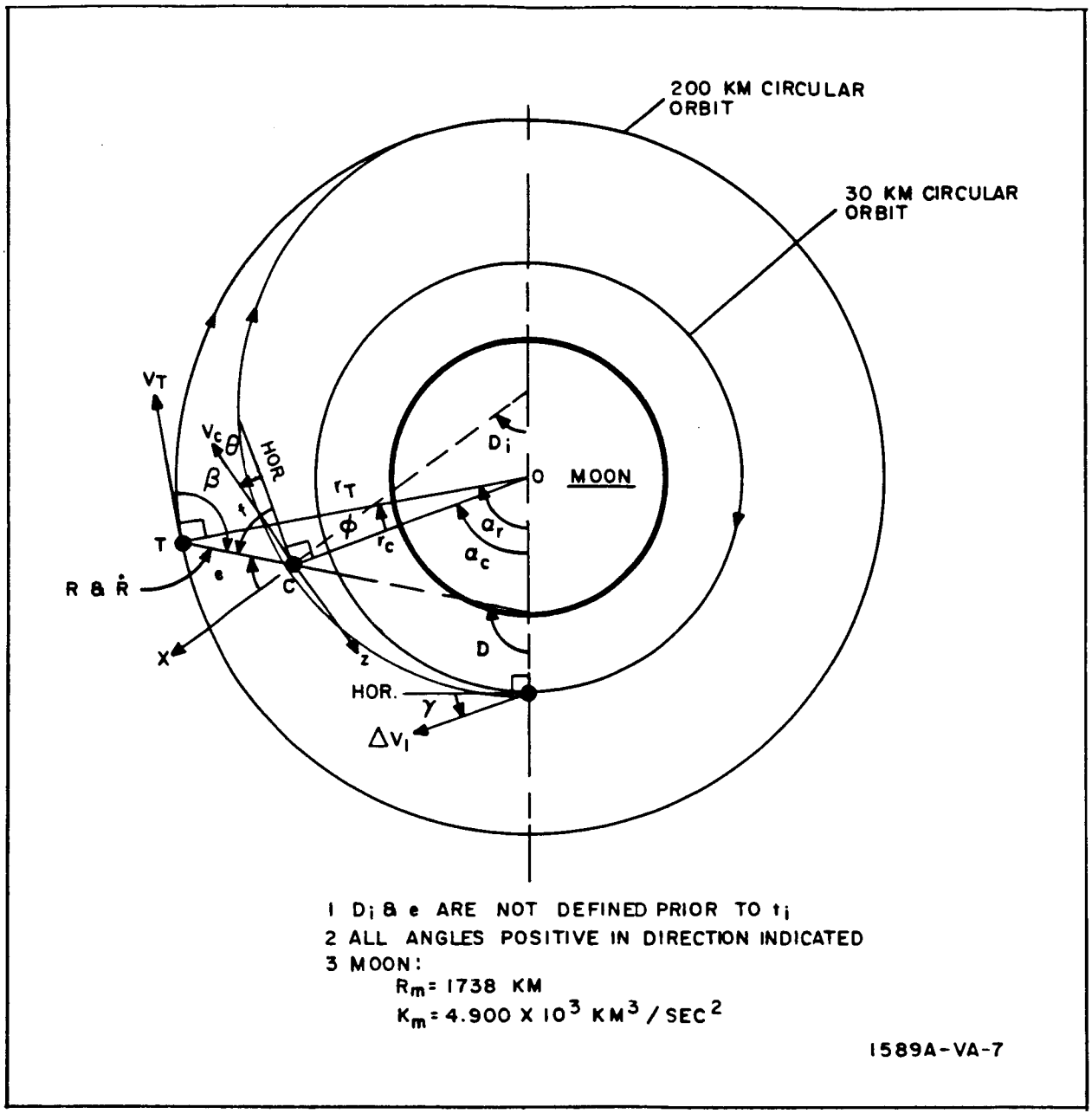

Figure 1. Orbit Diagram - Lunar Orbit Rendezvous

1.2 General Flow of the Program

The program increments time at a specified interval and performs calculations at each time point based on simulated sensor readings to determine when to make rendezvous achieving corrections to the orbit of the chaser vehicle. At each time point the program determines the selenocentric coordinates of both the target and chaser by applying the method described in

paragraph 1.7.1 to the orbital elements of each vehicle. These selenocentric coordinates are then transformed into a local radar oriented x^1 z^1 coordinate system with the origin located at the chaser. The positive x^1 axis lies horizontal to the surface of the moon in the direction of motion and the positive z^1 axis lies along the vertical in the direction of the moon. Thus the local coordinates of the target are represented by a translation and rotation of the selenocentric coordinate system with the angle of rotation λ being the angle the chaser makes with the axis. Thus:

$$\lambda = \tan^{-1}(Y_c/X_c)$$

$$\begin{bmatrix} R_x & V_x \\ R_z & V_z \end{bmatrix} = \begin{bmatrix} \cos\lambda & -\sin\lambda \\ -\sin\lambda & -\cos\lambda \end{bmatrix} \begin{bmatrix} (Y_t - Y_c)(V_{yt} - V_{yc}) \\ (X_t - X_c)(V_{xt} - V_{xc}) \end{bmatrix}$$

where:

R_x, R_z, V_x, V_z = position and velocity of target relative to chaser in x^1z^1 coordinate system

X_t, Y_t, V_{xt}, V_{yt} = position and velocity of target in xy system

X_c, Y_c, V_{xc}, V_{yc} = position and velocity of chaser in xy system

However, due to the rotation of the x^1z^1 system from point to point, it was found that the relative velocity terms, v_x and v_z, were not truly representative of the closing rate between the vehicles. Thus, it became necessary to define closing rates, R_x and R_z, in the x^1z^1 system as the range difference divided by the time interval between two successive points.

The two quantities pertinent to sensor observations are range and elevation defined as the angle between the positive x^1 axis (horizontal) and the line of sight from the chaser to the target (figure 1). Inaccuracies in the sensor measurements are simulated by superimposing random numbers of zero mean and specified standard deviation upon the actual values of range, closing rate, and rate of change of elevation. These observations are resolved into x^1 and z^1 components of range and fed into a smoothing function. The smoothing function performs a least square fit of a specified order on a specified number of points and extrapolates the solution to the next observation point where the smoothed values of R_x, R_z, R_x, and R_z will be used as the control variables in the firing laws.

1.3 Firing Laws

The firing laws described in this subsection serve to control the firing of the chaser rockets which are positioned along the x^1 and z^1 axes.

The firing laws being used in this system require the introduction of several variables. The angle D (figure 1) is defined as the angle between the range vector from chaser to target and the positive X-axis and can be expressed as:

$$D = \tan^{-1}\left(\frac{Y_t - Y_c}{X_t - X_c}\right)$$

where Y_t, X_t, Y_c and X_c are the geocentric coordinates of the target and chaser.

When the target-chaser range has been reduced to 25 km, tne angle D is used as a reference for locking the onboard coordinate system. Let the angle D_i be set equal to D at the time the target-chaser range is 25 km. Then the positive x^1 axis is locked in position at an angle D_i to the x-axis. The positive z^1 axis is perpendicular to the x^1 axis and is in the orbital plane opposite to the direction of motion. The elevation angle e (figure 1) is then defined as the angle between the positive x^1 axis and the range vector from chaser to target.

The variables of control used in the firing laws are the range between the two vehicles R, the closing rate $\dot{R}$, and the rate of change of elevation angle $\dot{e}$. In simulating the firing laws the smoothed values of R, $\dot{R}$, and $\dot{e}$ are always used. The firing laws used in the simulation are designed to hold the elevation angle close to zero by firing along the z^1 axis until the range and range rate can be driven to zero by firing along the x^1-axis.

If the rate of change of elevation angle becomes greater in magnitude than 0.3 milliradian per second for 2 consecutive seconds, an acceleration of the following direction and duration will be applied.

$$t_F = 0.9R\,\frac{\dot{e}}{a_z}$$

$$a_z = -\,a_{zo}\frac{\dot{e}}{|\dot{e}|}$$

$a_{zo} = 0.5$ m/sec^2 (for coarse control)

$= 0.1$ m/sec^2 (for vernier control)

a_{z_o} is the acceleration due to thrust level of z^1 rockets. If

$$|\dot{Re}| > 2.5 \text{ m/sec}$$

the coarse guidance control is used. If $|\dot{Re}| \leq 2.5$ m/sec the vernier guidance control is used. There is a mandatory coasting phase of 3 seconds between all z^1-axis firings.

The x1 axis firings during coarse guidance control are designed to drive R and $\dot{R}$ to zero between the two curves represented by the following inequality:

$$-\sqrt{K_2 |R-R_1|} \leq \dot{R} \leq -\sqrt{K_1 |R-R_1|}$$

$K_2 = 0.70 \text{ m/sec}^2$

$K_1 = 0.35 \text{ m/sec}^2$

R_1 = stand-off range (200 m)

Under conditions of negative acceleration, a_x of -0.5 m/sec^2, the thrust is applied for a time duration of:

$$t_F = \frac{1.7 \left(-\sqrt{K_1 |R - R_1|} + |\dot{R}| \right)}{|a_x|}$$

If $|\dot{R}| < 5$ m/sec, a vernier guidance control is used in the x^1 axis firing. If the chaser is in either quadrant one ($R-R_1 > 0$ and $\dot{R} > 0$) or quadrant three ($R-R_1 < 0$ and $\dot{R} < 0$) the range is opening from the rendezvous point. The firing time is computed as:

$$t_F = \frac{0.9 \left(\sqrt{K_1 |R - R_1|} + |\dot{R}| \right)}{|a_x|}$$

If the chaser is in quadrant two ($R-R_1 < 0$ and $\dot{R} < 0$) or quadrant four ($R-R_1 < 0$ and $\dot{R} < 0$) and if the closure is too rapid (i.e., $|\dot{R}| > \sqrt{K_2 |R-R_1|}$) the firing time is computed as:

$$t_F = \frac{1.75 \left(-\sqrt{K_1 |R-R_1|} + |\dot{R}| \right)}{|a_x|}$$

If the chaser is in quadrant two or quadrant four and the closing rate is too slow (i.e., $|\dot{R}| < \sqrt{K_1 |R - R_1|}$) the firing time is

$$t_F = \frac{0.9 \left(\sqrt{K_1 |R - R_1|} - |\dot{R}| \right)}{|a_x|}$$

When the vernier guidance control is incorporated, the above equations use the following constants:

$K_1 = 0.07 \text{ m/sec}^2$

$K_2 = 0.14 \text{ m/sec}^2$

$|a_x| = 0.1 \text{ m/sec}^2$

R_2 is substituted for R_1

$R_2 = 50$ m (stand-off)

During both coarse and vernier firing control the firing duration must be at least 2 seconds before the thrust is actuated. Also, a coasting time of at least 3 seconds is set between x^1-axis firings.

The rendezvous maneuver is considered to be complete if:

$$R = 50 \pm 10 \text{ meters}$$

and $|\dot{R}| \leq 0.5$ m/sec.

1.4 Corrections to Chaser Orbit for Firing

During periods of firing, corrections must be made to the orbit of the chaser vehicle. These corrections are made by superimposing the effects of firing over a short time period (one second or less) on the position and velocity vectors of the chaser. The effects of firing must first be transformed back into the selenocentric coordinate system and then added to the chaser position and velocity vectors. This operation can be represented by the following matrix equation.

$$\begin{bmatrix} \hat{X}_c & \hat{V}_{xc} \\ \hat{Y}_c & \hat{V}_{yc} \end{bmatrix} = \begin{bmatrix} X_c & V_{xc} \\ Y_c & V_{yc} \end{bmatrix} + \begin{bmatrix} -\sin\lambda - \cos\lambda \\ \cos\lambda - \sin\lambda \end{bmatrix} \cdot \begin{bmatrix} 1/2\, a_x\, \Delta t^2 & a_x\, \Delta t \\ 1/2\, a_z\, \Delta t^2 & a_z\, \Delta t \end{bmatrix}$$

where:

$\hat{X}_c$, $\hat{Y}_c$, $\hat{V}_{xc}$, $\hat{V}_{yc}$ = corrected position and velocity components of chaser
Δt = time interval over which correction is made

The corrected position and velocity vectors of the chaser are used to calculate a new set of orbital elements by the method described in paragraph 1.7.2. The new orbital elements are used for subsequent positioning of the chaser.

1.5 Noise Generation and Smoothing

The program has been planned to provide a specified order N, of least squares smoothing for a specified number of points, M. The smoothed values of R_x and R_z are saved for the previous M time points. At each new time point (intervals of one second are taken when program is in noise generating mode) the blocks of smooth ranges are updated by adding the new values and dropping the values associated with the oldest time point.

It is desired to fit a function of the following form to the observed data.

$$a_o + a_1 t + a_2 t^2 + - - - + a_n t^N = R$$

If we express the observed data at each of the M points in an equation of this form we obtain the matrix equation:

$$\begin{bmatrix} 1 & t_1 & t_1^2 \cdots & t_1^N \\ 1 & t_2 & t_2^2 \cdots & t_2^N \\ \vdots & \vdots & \vdots & \\ 1 & t_M & t_M^2 \cdots & t_M^N \end{bmatrix} \begin{bmatrix} a_o \\ a_1 \\ \vdots \\ a_N \end{bmatrix} = \begin{bmatrix} R_1 \\ R_2 \\ \vdots \\ R_N \end{bmatrix}$$

or in the matrix form:

$$[T] \cdot [A] = [R]$$

When the least squares technique is applied to this system of equations, a solution for the coefficient matrix $[A]$ is obtained in the following form.

$$A = \left([T]^T \cdot [T] \right)^{-1} \cdot [T]^T \cdot [R]$$

The smoothed value of range can now be found at the next time point by substituting the time of the next observation into the general equation.

$$R_n = a_o + a_1 t_n + a_2 t_n^2 - - - + a_n t_n^N$$

where:

t_n = time of the next observation

R_n = smoothed value of range at time t_n

Since the onboard computer system cannot instantaneously perform the smoothing operation the smoothed values have been projected ahead to the next time point so that they can be used as the control variables in the firing laws while the present observations are being smoothed.

1.6 Corrections to Smoother Input for Firing

During periods when the control rockets of the chaser are firing, the acceleration of the chaser due to the firing is much greater than the acceleration due to orbital motion. This extra acceleration would normally tend to cause the smoother output to lag behind the actual values. However, since the firing laws allow the anticipation of firing from one time point to the next, the smoother input can be corrected to offset the effects of the added acceleration.

The smooth ranges can be adjusted by adding to each of the stored values an increment equal to the effects of the added acceleration applied over a time period from the projected time point to the time point associated with each stored value. Thus, if the subscript 1 represented the oldest time point and the subscript M represented the most recent time point then the adjustment can be expressed as:

$$R_{ic} = R_i + (M - i + 1/2)\, a\, \Delta t^2 \qquad 1 \leq i \leq M$$

where:

R_{ic} = adjusted value of smooth range

R_i = uncorrected value of smooth range

a = acceleration due to rockets being fired

Δt = sample interval

These corrections are made to each of the components of range.

Similar adjustments are made to the smoothed values of range rate, $\dot{R}$, and elevation rate, $\dot{e}$. Using a similar notation as found in the case of

range, the range rate adjustment can be expressed as:

$$\dot{R}_{ic} = \dot{R}_i + a\Delta t$$

and the elevation rate adjustment can be expressed as

$$\dot{e}_{ic} = \dot{e}_i + \frac{a\Delta t}{R_i}$$

where:

$\dot{R}_{ic}$ = adjusted value of smooth range rate

$\dot{R}_i$ = uncorrected value of smooth range rate

$\dot{e}_{ic}$ = adjusted value of smooth elevation rate

$\dot{e}_i$ = uncorrected value of smooth elevation rate

a = acceleration due to rockets being fired

Δt = sample time interval

1.7 Transformations between Selenocentric Coordinates and Orbital Elements[1/]

Under the following subheadings methods are discussed for transforming selenocentric coordinates to orbital elements and vice versa. Symbols used in the following subheadings are defined as follows:

Z_1, Z_2, Z_3 = selenocentric position components

$\dot{Z}_1$, $\dot{Z}_2$, $\dot{Z}_3$ = selenocentric velocity components

The following six parameters are referred to as the orbital elements.

a = the length of the semi-major axis

e = the eccentricity of the ellipse

1/ Paragraphs 1.7.1, 1.7.2, and 1.7.3 of this subsection are extracted from Ref 1.

Ref. 1 Davenport, P. B., Coordinate Systems and Transformation for Earth Satellite Prediction, Westinghouse Electric Corp., Report No. AA-2547-61, December 1961.

Ω = right ascension of ascending node (the ascending node is the point where the satellite crosses the $Z_1 - Z_2$ plane, equator, from south to north) $0 \leq \Omega < 2\pi$

i = inclination of the plane of the orbit to the $Z_1 - Z_2$ plane ($0 \leq i \leq \pi$)

ω = argument of the perigee, the angle from the ascending node to the point of perigee ($0 \leq \omega < 2\pi$)

T_o = epoch for the coordinate system and the time perigee occurred.

The following auxiliary parameters are also often used.

P = period of the orbit

n = mean angular motion of the satellite in the plane of the orbit

T_n = time of ascending node

1.7.1 Selenocentric Rectangular Coordinates from Orbital Elements

The selenocentric position, Z, and velocity $\dot{Z}$, are obtained from the elements a, e, Ω, i, ω, and T_o (figure 2) at time t by the following:

$$N = a^{-3/2}$$

$$M = N(t - T_o)$$

the quantity M is known as the mean anomaly.

$$E = M + e \sin E$$

The equation above is Kepler's equation and must be solved for the eccentric anomaly E (paragraph 1.7.3). Once E has been obtained, the sine and cosine of the true anomaly, u, (figure ≤) and the length of radius vector r are given by:

$$\sin u = \frac{\sqrt{1 - e^2} \sin E}{1 - e \cos E}$$

$$\cos u = \frac{\cos E - e}{1 - e \cos E}$$

$$r = a(1 - e \cos E)$$

Let

$$C_1 = \cos\Omega \cos(\omega + u) - \sin\Omega \cos i \sin(\omega + u)$$

$$C_2 = \sin\Omega \cos(\omega + u) + \cos\Omega \cos i \sin(\omega + u)$$

$$C_3 = \sin i \sin(\omega + u)$$

(these are the direction cosines of the satellite)

where

$$\sin(\omega + u) = \sin\omega \cos u + \cos\omega \sin u$$

$$\cos(\omega + u) = \cos\omega \cos u - \sin\omega \sin u$$

then

$$Z_i = r\, C_i \qquad (i = 1, 2, 3)$$

The Z_i are differentiated to yield the geocentric velocity components.

$$Z_i = \sqrt{Gm_e}\ \frac{\sqrt{a}}{r}\ b_i \qquad (i = 1, 2\ 3)\underline{2/}$$

where

$$b_1 = C_1 e \sin E - \sqrt{1 - e^2}\ \cos\Omega \sin(\omega + u) + \sin\Omega \cos i \cos(\omega + u)$$

$$b_2 = C_2 e \sin E - \sqrt{1 - e^2}\ \sin\Omega \sin(\omega + u) - \cos\Omega \cos i \cos(\omega + u)$$

$$b_3 = C_3 e \sin E + \sqrt{1 - e^2}\ \sin i \cos(\omega + u)$$

Alternate expressions for the rates in terms of total velocity, V, but requiring further calculation are given below:

$$V = \frac{\sqrt{a}}{r} \qquad \sqrt{1 - e^2 \cos^2 E}$$

$$S_i = \frac{b_i}{\sqrt{1 - e^2 \cos^2 E}} \qquad (i = 1, 2, 3)$$

2/ In the system of units used for this program, the magnitude of the gravitational parameter, Gm_e is set equal to one. The dimensions have the form of $\frac{(\text{Length})^3}{(\text{Time})^2}$

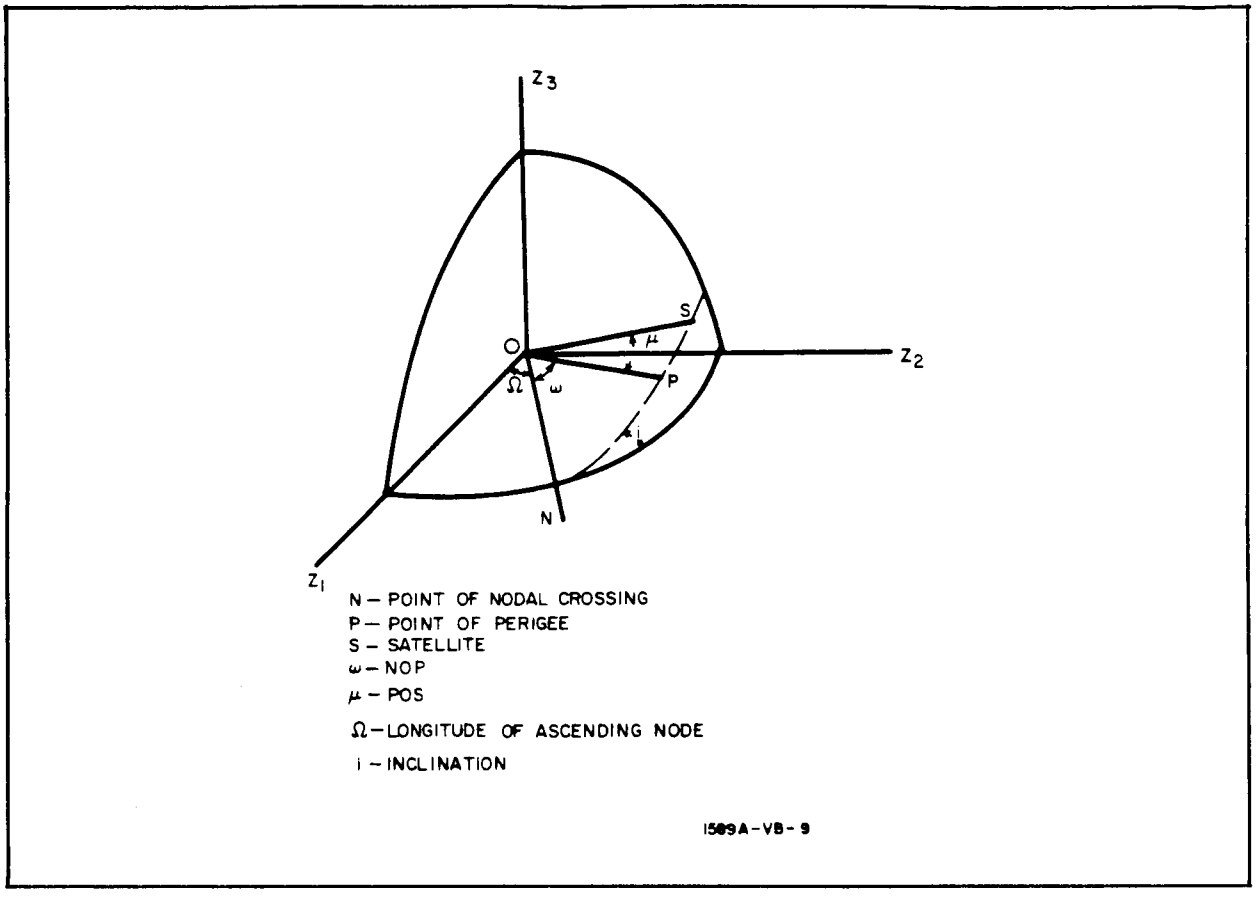

Figure 2. Orientation of the Orbital Plane

(the S_i are direction cosines of the velocity vector)

$$\dot{Z}_i = VS_i \qquad (i = 1, 2, 3)$$

In some instances the period, P, or mean motion, n, may be given as an element instead of length of the semi-major axis, a. In either case, a, can be obtained by one or both of the following relationships:

$$n = \frac{2\pi}{P}$$

$$a = n^{-2/3}$$

The element T_n (time of ascending node) is often given rather than T_o (time of perigee). In this case T_o is obtained by the following relations:

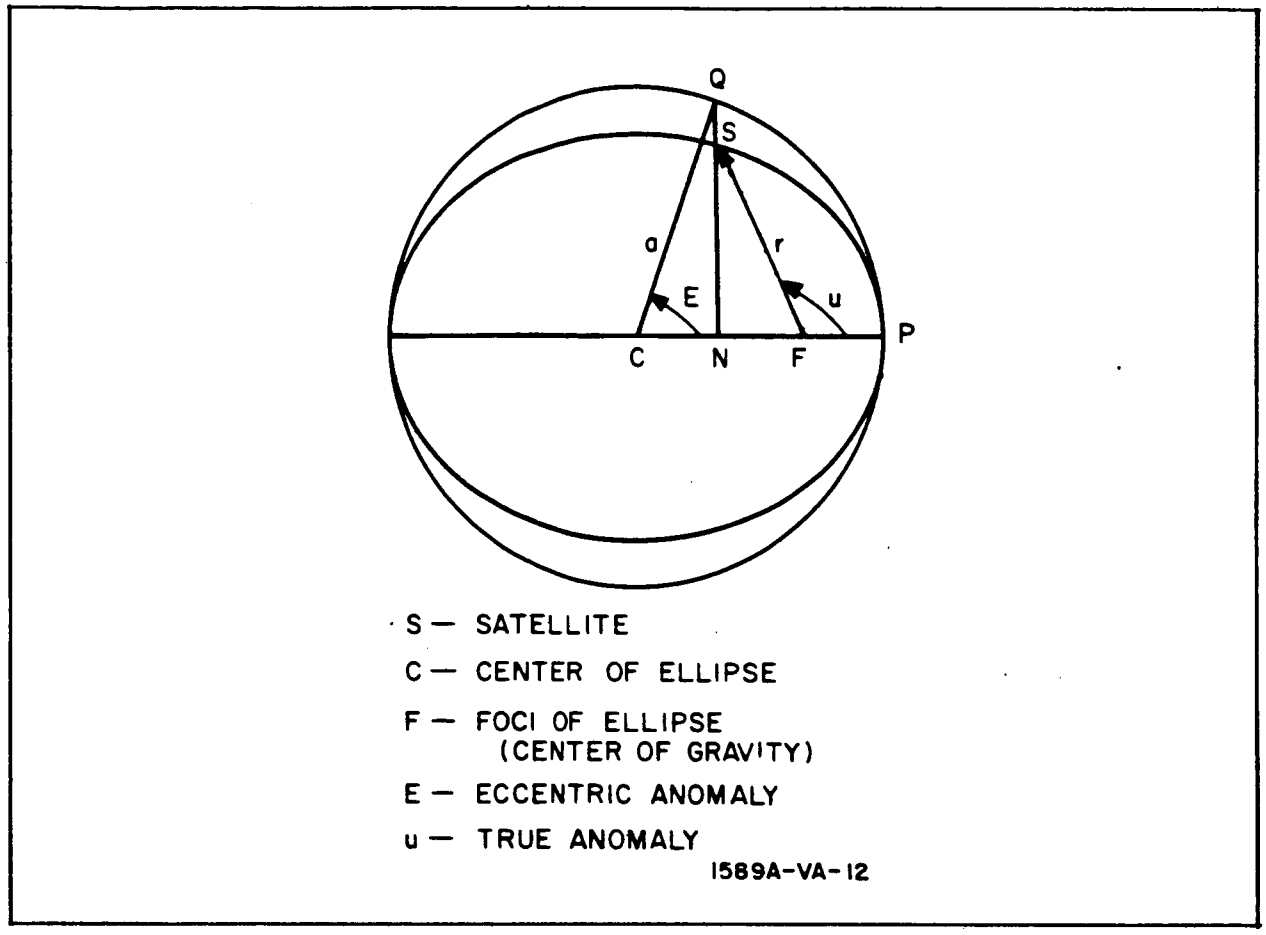

Figure 3. Eccentric Anomaly and Focal Polar Coordinates

$$E_\omega = \tan^{-1}\left(\frac{-\sin\omega\sqrt{1-e^2}}{e+\cos\omega}\right)$$

$$\sin E_\omega \quad \frac{-\sin\omega\sqrt{1-e^2}}{1+e\cos\omega}$$

$$T_o = T_n - \left(\frac{e_\omega - e\sin E_\omega}{n}\right)$$

If E_ω is in the third or fourth quadrant then it should be changed to a negative angle to make the time between T_n and T_o a minimum.

1.7.2 Orbital Elements from Selenocentric Rectangular Coordinates

$$\Omega = \tan^{-1}\left[(Z_2\dot{Z}_3 - Z_3\dot{Z}_2)/(Z_1\dot{Z}_3 - Z_3\dot{Z}_1)\right]$$

$$i = \tan^{-1}\left[Z_3/(Z_2\cos\Omega - Z_1\sin\Omega)\right]$$

$$\epsilon = \omega + u = \tan^{-1}\left[Z_3/\sin i\,(Z_1\cos\Omega + Z_2\sin\Omega)\right]$$

$$r\dot{r} = Z_1\dot{Z}_1 + Z_2\dot{Z}_2 \quad Z_3\dot{Z}_3$$

$$r^2 = Z_1^2 + Z_2^2 + Z_3^2$$

$$V^2 = \dot{Z}_1^2 + \dot{Z}_2^2 + \dot{Z}_3^2$$

$$a = \frac{1}{2/r - V^2}$$

$$e = 1/a\sqrt{a\,(r\dot{r})^2 + (a - r)^2}$$

If $e = 0$ then $\omega = 0$ and $M = E = u = \epsilon$

otherwise:

$$E = \tan^{-1}\left[\sqrt{a}\,r\dot{r}/(a - r)\right]$$

$$u = \tan^{-1}\left[\sqrt{1 - e^2}\sin E/(\cos E - e)\right]$$

$$\dot{M} = E - e\sin E$$

$$\omega = \epsilon - u$$

In either case T_o is found by the fomulas:

$$n = a^{-3/2}$$

$$T_o = t - \frac{M}{n}$$

Additional Relations

$$p = a(1 - e^2) \quad \text{(known as orbit parameter)}$$

$$r = \frac{p}{1 + e\cos u}$$

$$\dot{r} = \frac{\sqrt{a}\ e \sin E}{r} = \frac{a\ e\ n \sin E}{1 - e \cos E}$$

$$\sin u = \frac{\sqrt{a}\ \dot{r}\ (1 - e^2)^{3/2}}{e}$$

$$\cos u = \frac{p - r}{er}$$

$$\tan(u/2) = \sqrt{\frac{1 + e}{1 - e}} \tan (E/2) = \sqrt{\frac{1 - \cos u}{1 + \cos u}}$$

$$u = \tan^{-1} \left[\sqrt{1 - e^2} \sin E/(\cos E - e) \right]$$

$$\dot{u} = \frac{\sqrt{a}\sqrt{1 - e^2}}{r^2} = \frac{n\sqrt{1 - e^2}}{(1 - e \cos E)^2}$$

$$\sin E = \frac{\sqrt{1 - e^2} \sin u}{1 + e \cos u} = \frac{r\ \dot{r}}{\sqrt{a}\ e}$$

$$\cos E = \frac{e + \cos u}{1 + e \cos u} = \frac{a - r}{a\ e}$$

$$\dot{E} = \frac{1}{r\sqrt{a}} = \frac{n}{1 - e \cos E}$$

$$\frac{dr}{du} = \frac{r\ e \sin E}{\sqrt{1 - e^2}}$$

$$V = \sqrt{r^2 \dot{u}^2 + \dot{r}^2} = \sqrt{2/r - 1/a}$$

$$Z_1 \dot{Z}_2 - Z_2 \dot{Z}_1 = \sqrt{a}\sqrt{1 - e^2} \cos i$$

$$Z_2 \dot{Z}_3 - Z_3 \dot{Z}_2 = \sqrt{a}\sqrt{1 - e^2} \sin \Omega \sin i$$

$$Z_1 \dot{Z}_3 - Z_3 \dot{Z}_1 = \sqrt{a}\sqrt{1 - E^2} \cos \Omega \sin i$$

$$e = \sqrt{\frac{a - p}{a}}$$

1.7.3 Solution of Kepler's Equation

$$E = M + e \sin E$$

Let

$$E_o = M + e \sin M \quad (1 + e \cos M)$$

$$\Delta E = \frac{M - E_o + e \sin E_o}{1 - e \cos E_o}$$

$$E_1 = E_o + \Delta E$$

If E_1 and E_o agree to the accuracy wanted then E_1 is the desired approximation to E. If they do not agree, then replace E_o by E_1 and compute a new E_1.

If the calculations are being done by hand, the above process becomes more laborious as e approaches 1. In this case a better value of E_o can be obtained by plotting the two curves:

$$y = \sin E$$

and

$$y = 1/e \, (E - M)$$

as a function of E. The abscissa of their point of intersection is the value of E satisfying the equation.

Another iteration which is simpler than the one above, but requiring more iterations for the same accuracy is: $E_{i+1} = M + e \sin E_i$.

2. INPUTS FOR ANALYSIS OF LUNAR ASCENT TO RENDEZVOUS

The inputs used for the analysis in paragraph 5.3.2.1 of Volume III are obtained from an analysis of lunar rendezvous which is not part of this report but is essentially similar to the lunar rendezvous analysis of Section 6.0 of Volume III except for the guidance and control scheme used. The guidance and control method is not considered representative of typical rendezvous procedure primarily because of excessive fuel requirements. For this reason, the analysis is not included.

The results of the analysis pertaining to injection sensors are listed in table 1 below to serve as a reference for paragraph 5.3.2.1 of Volume III.

TABLE 1

INJECTION SENSOR REQUIREMENTS

Symbol	Quantity	Required Sensor Accuracy (3σ)	State of the Art Accuracy (3σ)
δr	altitude	1.4 km(4.7% of R)	30 m (0.1% of R)*
δv	velocity	1.5 m/sec	0.3 m/sec
$\delta\gamma$	pitch attitude	2.0 deg	0.3 deg
$\delta\psi$	yaw attitude	22.2 deg	0.3 deg
$\delta\phi$	central angle	0.28 deg	--
δR	range	2.0% of R	0.1% of R
δt	timing	40.6 sec	3 sec
δi	inclination	0.8 deg	0.1 deg